LABORATÓRIO NACIONAL
DE ENGENHARIA CIVIL

BINGO PROJECT: IMPACTS OF CLIMATE CHANGE IN GROUNDWATER IN THE LOWER TAGUS

Coupling outputs from climate and recharge models with aquifer modelling

Lisbon • July 2020

R&D HYDRAULICS AND ENVIRONMENT

REPORT 245/**2020 – DHA/NRE**

Title

BINGO PROJECT: IMPACTS OF CLIMATE CHANGE IN GROUNDWATER IN THE LOWER TAGUS
Coupling outputs from climate and recharge models with aquifer modelling

Authors

HYDRAULICS AND ENVIRONMENT DEPARTMENT
Maria Emília Novo
Assistant Researcher, Water Resources and Hydraulic Structures Unit
Tiago Martins
Research Fellow, Water Resources and Hydraulic Structures Unit
Maria José Henriques
Senior Technician, Water Resources and Hydraulic Structures Unit

BINGO PROJECT: IMPACTS OF CLIMATE CHANGE IN GROUNDWATER IN THE LOWER TAGUS

Coupling outputs from climate and recharge models with aquifer modelling

Abstract

The BINGO Project is a Horizon 2020 project, with the goal of evaluating climate change and its impacts on the water cycle in the short range (2015 to 2024). Such evaluation is the basis for risk analysis and this analysis supports the creation of an actionable adaptation actions' portfolio, able to be replicated in other areas beyond those of the 6 case studies belonging to this project. The whole hydrological cycle was analysed for climate change impacts and, in the Portuguese case study issues as floods, surface waters, reservoirs, estuarine water bodies and groundwater were analysed. This report presents the development of a mathematical model to assess the impacts of climate change on Lower Tagus aquifers and the ensuing results.

Keywords: Climate change / Impacts on groundwater / Groundwater modelling / Lower Tagus aquifers

PROJETO BINGO: IMPACTOS DAS ALTERAÇÕES CLIMÁTICAS NAS ÁGUAS SUBTERRÂNEAS NO TEJO INFERIOR

Conjugação dos resultados de modelos climáticos e de recarga com a modelação de aquíferos

Resumo

BINGO é um projeto Horizon 2020, que teve por objetivo analisar as alterações climáticas e respetivos impactos no ciclo da água a curto prazo (2015 a 2024), com vista a fundamentar a análise de risco, a qual, por sua vez, fundamentou a criação de um portefólio de ações de adaptação. O objetivo deste portefólio é fornecer ferramentas de adaptação que possam ser replicadas noutros locais que não apenas os dos 6 casos de estudo do projeto. A totalidade do ciclo da água foi analisada em termos dos potenciais impactos devidos às alterações climáticas e, no caso de estudo português foram analisados os aspetos das cheias, águas superficiais, reservatórios, zonas estuarinas e águas subterrâneas. Este relatório apresenta o desenvolvimento de um modelo matemático para avaliar o impacto das alterações climáticas sobre os aquíferos do Baixo Tejo e respetivos resultados.

Palavras-chave: Alterações climáticas / Impactos das alterações climáticas nas águas subterrâneas / Modelação matemática / Aquíferos do Baixo Tejo

Executive summary

Climate change impacts the water cycle and, although less visible but nevertheless important, is its groundwater component. Climate change impacts on groundwater are due to recharge changes (quantity impacts), saltwater intrusion due to sea level rise and impacts due to changes in dissolved CO_2 concentrations (quality impacts). This latest quality impact (dissolved CO_2 concentrations) is significant in karst aquifers as for instance Ota-Alenquer aquifer system. Besides these natural effects, adaptation can also lead to groundwater quantity and quality issues, due to higher water demands or pollution loads due to changes in new and/or altered pesticides cycles in agriculture.

Adaptation is then required to avoid the worst of these impacts. However, in spite of climate changes being an incremental phenomenon, and so its impacts are felt on the medium to long range (e.g. climate today is behaving a bit different from that of 1980'ies but not so much different from the 2000'ths), politicians think on a short term framework and have a difficulty to deal with data for time spans of 30 years or larger time periods.

BINGO Project (a Horizon 2020 project) was developed to overcome this difficulty and give climate change impacts analysis and ensuing adaptation policies based on short range analysis (2015-2024) tailored for stakeholders and decision-makers.

The Portuguese case study under BINGO Project analyses several distinct components of the water cycle and water management in the Lower Tagus basin, of which the groundwater component is presented in this report. The data used were the climate simulation results of the model MiKlip developed by FUB (Freie Universität Berlin), which were required by BALSEQ_MOD for recharge estimation (cf. Oliveira, 2019). Recharge was an input data of the groundwater flow model FEFLOW. Other input data (topography, hydraulic properties, etc.) were obtained in Tagus Watershed Plans and bibliography.

From the 10 climate simulations, 10 recharge scenarios were derived and, of these, 3 of them were chosen – the extremes of the recharge range and the ensembles of all recharge scenarios – for groundwater modelling once they represent the recharge average and the recharge variation limits for these 10 climate simulations, all equally likely to occur. Those scenarios were R1 = higher recharge (recharge higher than historical period's recharge); R2 = lowest recharge (recharge lower than historical period's recharge); R1_10 = ensembles recharge (actually not very different from the historical period's recharge).

Groundwater modelling was then performed for these 3 recharge scenarios and for 4 drought scenarios. Drought scenarios, not being simulated by MiKlip, were performed for the recharge of year 2004/5 (a severe drought year). These scenarios are: (1) permanent drought scenario (simulated a radical climate change where average recharge would change to about half of the historical period); (2) transient 1 year drought; (3) transient 3 years drought; (4) transient 5 years drought.

The water levels under these scenarios behaved as it was generally expected: rising for the high recharge scenario (R1), remaining more or less the same as the historical period's levels in the

ensembles scenario (R1_10), and lowering for the low recharge scenario (R3). For the drought's scenarios the water level lowered, as expected, and quite dramatically for the permanent state scenario.

Due to the large storage capacity of the aquifers (modelled as one single very large aquifer), the water level's changes are in general moderate, with rises (in R1 scenario) between 2 and 5 m (with some specific, high hydraulic gradient areas showing changes of up to 10 m, or (in R3 scenario) drawdowns between 2 to > 10 m, although, once again, the areas of the larger drawdowns are very circumscribed to specific topographic/high hydraulic gradients. For the ensembles scenario (R1_10), where recharge is quite similar to the historical period, water level changes are almost negligible.

As for droughts, in the permanent state (average recharge for the whole period 2015-2024) would be half of the historical values – a highly unlikely scenario – drawdowns would range from 10 to 60 m, although values of 40 to 60 m occur only in the same areas that previously showed the largest water levels' changes. For drought episodes of 1, 3 and 5 years' length, the drawdowns would range from less than 0.5 m to 1 (1 year drought), less than 1 to 2 m (3 years drought) and less than 2 to 3 m (5 years drought), with the high gradient areas sowing respectively changes of 1 to 5 m, 3 to 5 m and 3 to a little more than 5 m.

From these results emerges the picture of a large inertial system with a small response to climate changes in the short range. Although some issues can be improved on the groundwater flow model, this suggests that at least for high inertial systems, as very large aquifers, the short range framework of climate change adaptation, which is tailored to meet the short range agenda of policymakers, is of reduced value. Climate change requires a long term vision of the future. And this demand a paradigm shift where actions should not be focused on the short range results (elections cycle) but, at least for high inertial systems, should be focused on actions today to bear results on the decades ahead. Which means to act today, based on the results of the long range climate change projections, to bear results on the long range future.

Table of contents

List of figures

List of tables

1 | Introduction

1

This document was developed under BINGO (Bringing INnovation to onGOing water management – a better future under climate change) project, sponsored by the European Union's Horizon 2020 Research and Innovation programme, under the Grant Agreement number 641739. It deals with the mathematical flow modelling of the groundwater component of the water cycle in the Portuguese case-study, which encompasses the aquifers of Aluviões do Tejo, Bacia do Tejo/Sado – Margem Direita and Bacia do Tejo/Sado – Margem Esquerda.

1 | Introduction

2 | BINGO in a nutshell – the groundwater component

The need for a sustainable development requires the wise exploitation of natural resources, and, therefore, the sustainability of all activities impacting water bodies, thereby securing the availability of good-quality water for rational and equitable water use, as is the goal of the European policies concerning water and environment.

Drinking water supply, energy production, agriculture, services and industry demand a reliable supply of water in quantity and quality. However, water abstraction for these activities, coupled with demographic evolution, pollution and urbanisation expansion are a growing pressure to water resources, surface and groundwater, on its quantitative and qualitative aspects.

Adding to the impacts of sectorial policies that do not have a holistic approach of the water cycle and its issues, there is the new, global and powerful threat of climate change. Changes in greenhouse gases concentrations increase atmospheric temperature, which sets in motion a succession of modifications that ultimately affect the water cycle (Figure 2.1), from an increase in atmospheric moisture and ocean's temperatures (generating amongst other changes an increase in evaporation), to a speeding of the hydrological cycle and a shift in the location of the wet and dry regions of the Globe, thus presenting new challenges for water management and protection.

Global sea level rise is another consequence of climate change and although at a local level it might evolve in particular fashions that do not always follow the global rising trend, its evolution impacts the water cycle, in particular groundwater quality in coastal areas. The impacts on surface water quality are also of major concern and capable of a severe impact upon coastal and riverine/estuarine activities, from fishing and urbanization to agriculture and, above all, water supply.

BINGO Project is a European project under the Horizon 2020 that aims to extend the knowledge and awareness of key sectors about climate change impacts on the water cycle and identify reliable adaptation strategies for the short to medium time range, in particular as water resources protection and sustainable exploitation are concerned. To achieve this aim, a set of case-studies, encompassing a wide variety of water issues and realities across the European territory were studied. Groundwater is often the forgotten part of the water cycle, natural or urban, but is in fact an important water resource, used by agriculture activities, industry and water supply. It is also an important ecological services' provider, including the support of groundwater dependent ecosystems and the regulating mechanism for base flow in rivers, which results in an increased resilience of riverine ecosystems and increased surface water resources. Even in the cases were groundwater is managed as a strategic resource, and so, not exploited until hydrological extreme situations (as for instance a severe drought), often the reality in the field shows that it is readily exploited for farming activities and water supply to small urban areas.
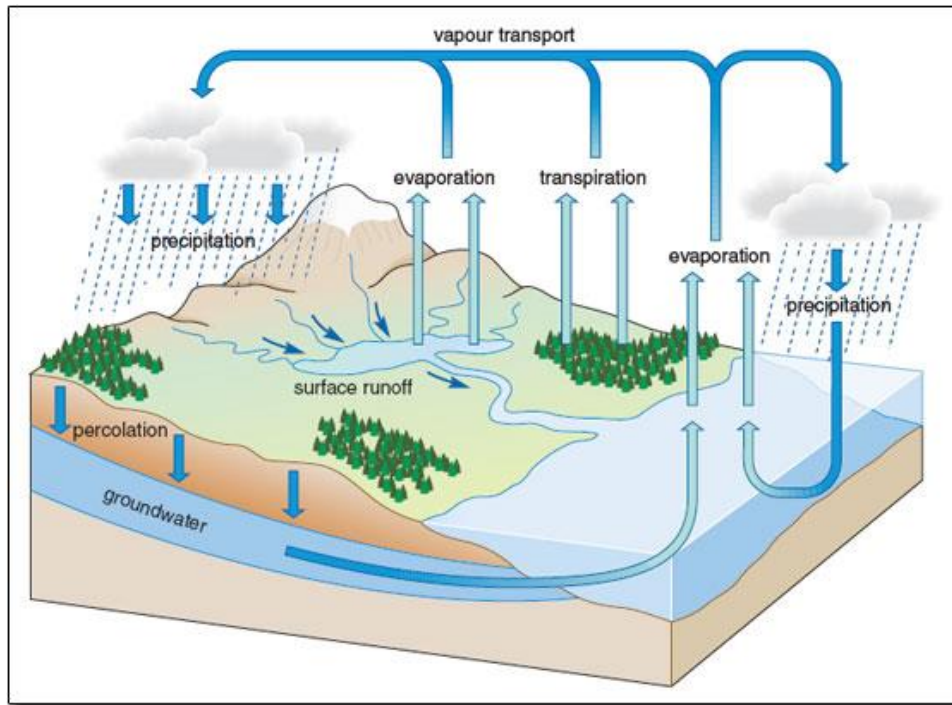
Figure 2.1 – Natural water cycle

Source: https://earthzine.org/2013/05/07/how-weather-stations-can-be-used-to-measure-evaporation/

Groundwater is, as above illustrated, an important component of the water cycle, from storage to regulating surface water bodies, interactions with the ocean at coastal areas and support of ecosystems, not to mention human activities (Figure 2.2). In some European areas groundwater issues are particularly relevant and for this reason, groundwater is one of the water cycle's components studied in BINGO, in three of its six case-study sites: Netherlands, Cyprus and Portugal.

In the Netherlands, the focus is on the impacts of climate change on ecosystems functioning. In Cyprus, the focus is on the allocation strategies and sustainable exploitation of groundwater resources. In Portugal the focus is mainly on the impacts of climate change on water resources availability and the potential risks posed by such impacts on water supply.

In the Portuguese case study, the water systems under analysis are those of the Lower Tagus river basin and, as far as groundwater is concerned, the aquifers under scrutiny are: Ota-Alenquer, Aluviões do Tejo, Tejo/Sado – Margem Direita, Tejo/Sado – Margem Esquerda. In Ota-Alenquer the analysis of climate change impacts concerned just the changes in recharge, while for the remaining aquifers changes in recharge and the ensuing head changes were analysed. Equally important for groundwater availability, although not studied in BINGO, are the water quality impacts of climate change.
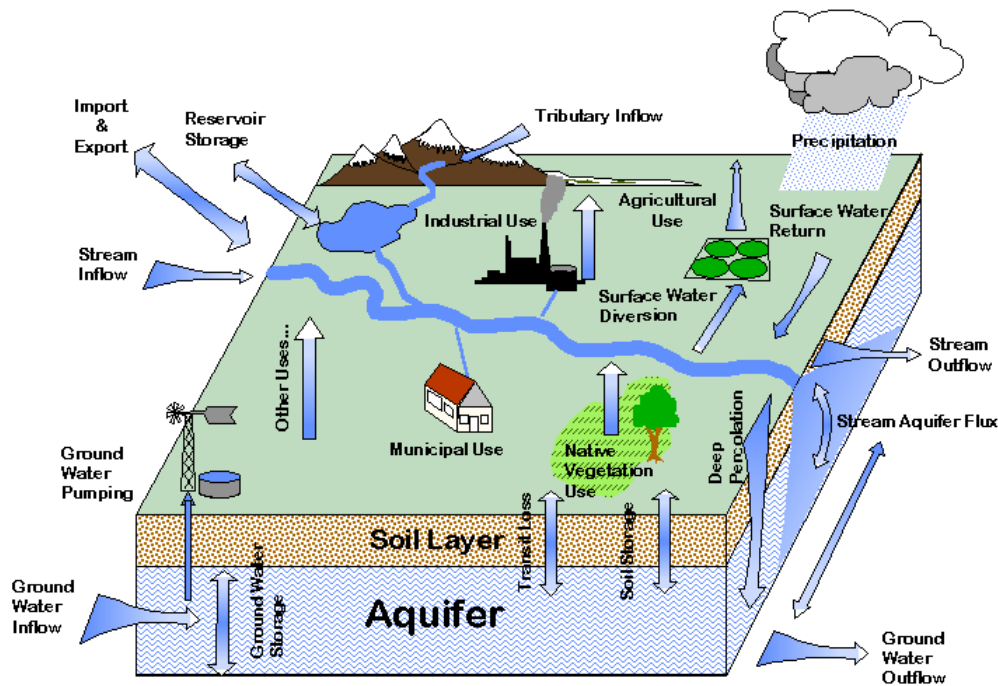
Figure 2.2 – Role of groundwater in surface water systems and human activities

Source : http://zebu.uoregon.edu/1999/es202/l2.html

Water supply and agriculture, although largely supported by surface waters (particularly in the Tagus right margin region), are still strong competitors for groundwater supplies, in a setting that combines a history of serious riverine and estuarine floods and droughts, and the potential for salt water intrusion from the Tagus estuary.

Although floods do, at most, pose a threat to groundwater quality if hazardous wastes get infiltrated and reach the saturated zone, the droughts impacts are felt at both groundwater's quantity and quality. In fact, significant water level's drawdowns might lead to the burning of the water pumps and the abandonment of the wells, at least temporarily. Such events compound an already difficult situation when water demand is at its highest due to the water scarcity in the other supply sources. Often, to avert such situations, the abstraction systems must be changed, pumps with higher capacity to abstract water at greater depths must be bought and installed (as has been reported in 2017 drought), or even the wells themselves must be drilled to lower depths, burdening the costs of the supply, regardless if that happens to a private farming or a local municipal water supply wells.

Besides the natural stresses to groundwater resources, other pressures like domestic sewage, agriculture, livestock activities, forest fires (cf. Lobo Ferreira et al., 2009) and industry also take a toll on the quality and/or quantity of the resource. For instance, changes in land cover and even in the texture and hydraulic properties of the soils due to forest fires can locally change the infiltration rates and, in consequence, the recharge of aquifers (cf. Shakesby e Doerr, 2006). Fires are expected to increase in frequency and severity due to climate change in the Mediterranean area.

It is expected that climate change, coupled with changes in demography and socio-economic developments, will exacerbate some of these pressures. For instance, the expected increase in drought

events, as well as its length and severity, is expected to have a more protracted impact on groundwater recharge and interactions between surface water bodies and aquifers than in present-day conditions. However, the increase of intense rain events might not be translated in groundwater recharge increase but instead in higher erosion with impacts on surface waters' quality and possible discharge changes between streams and the underground environment, due to possible changes in the sediments deposited at the bottom of the stream's canal. Such changes in rain distribution are expected to have impacts on natural vegetation and agricultural activities. Changes in natural vegetation will have impacts on recharge, not to mention the functioning of the surface water systems. But climate change will also prompt agricultural activities to adapt and this adaptation might range from a change in seed/sow calendar to a partial or even total change in the type of cultivars chosen by farmers. This in turn will bring changes to evapotranspiration, runoff and recharge, including the recharge due to irrigation losses by infiltration, and, above all, the water demand for farming, thus affecting groundwater availability.

Sea level rise due to climate change also affects groundwater, as far as its quality is concerned. Although such impacts are only felt in coastal areas, they are nevertheless very important in particular if we take into account the demographic density and water demand of those areas, which is usually supplied by local aquifers. Sea level rise pushes the saltwater/freshwater interface inland, with saltwater encroaching progressively more inland (which is known as saltwater intrusion), and so the wells in these encroached areas must be abandoned due to increasing water salinization. Demographic rises in coastal/estuarine areas require an increased supply of water, adding stress to aquifers already facing saltwater intrusion and possible recharge reductions due to climate change (which promotes further saltwater intrusion). Exploiting estuarine/coastal groundwater resources under such pressures while protecting the water requirements of the coastal ecosystems – often with a valuable role in safeguarding these same areas from erosion – is in itself a challenge, requiring a deep knowledge of the groundwater system and its interactions with sea and rivers. Drought situations will compound the problem not only due to increased water abstraction but also due to lower amounts of groundwater reaching the coastal/estuarine areas (stemming from lower recharge). Both may increase saltwater intrusion, at least while the drought occurs. But even when the saltwater intrusion retreats after the drought, a significant amount of salts usually remains in the structure of the aquifers and will degrade the water that will reach them during the early stages of after-drought period.

As can be seen from the above, groundwater is not an isolated water reservoir but it is one with connections (Figure 2.3) and significant roles in regularizing surface water bodies, particularly within minor rivers and creeks, providing for groundwater dependent ecosystems. It also has a very dynamic role with the ocean and some studies even suggest that water abstraction might also be contributing to sea level rise (cf. Wada et al., 2010; Wada et al. 2016). Groundwater is, in the Tagus case study-area of BINGO Project, defined as a strategic resource, something to be relied on when the normal supply sources are no longer effective. However, it also has an important role on providing water to all human activities on a daily basis at least in the southern region of the Lower Tagus basin. Any negative impacts on this resource will then be felt by farmers, industries and urban areas in that region.
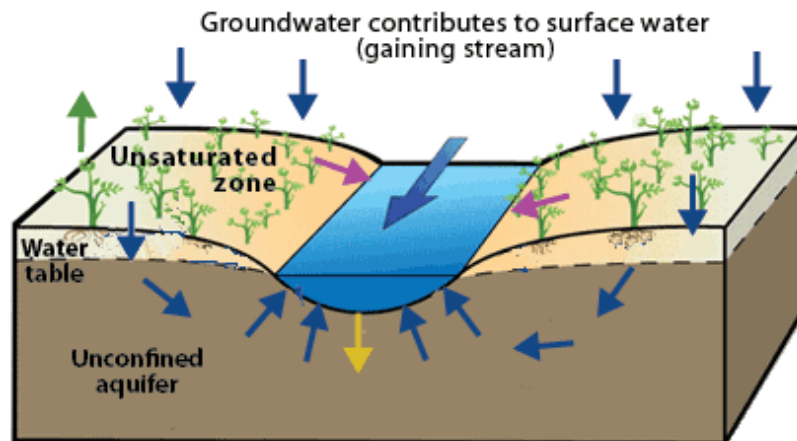
Figure 2.3 – Connections between surface waters and groundwater

Source: https://water.usgs.gov/edu/rivers-contain-groundwater.html

The impacts of climate change on this resource must be understood and aquifer modelling is an important tool for such comprehension. Modelling is also helpful to inform on risk analysis. Furthermore, once groundwater is not an isolated water system but is connected to the other water bodies in the area, inputs from river and estuarine data/modelling should be integrated in the groundwater model, although this has been proved difficult.

In the following chapters the groundwater modelling work and results are presented. Chapter 3 is a general description of the relevant aspects for the conceptual and mathematical models. Chapter 4 describes the perceived threats of climate change on groundwater systems. Chapter 5 describes the conceptual model of the aquifer, the data required for the construction of the mathematical model and the structure of the mathematical model. Chapter 6 presents the results of the model simulations and Chapter 7 the conclusions. Chapter 8 presents suggestions for further studies.

3 | Description of the case study area

Tagus case study area spans from Zêzere's basin, a tributary of Tagus River, to the estuary area (Figure 3.1), comprising rivers, artificial reservoirs, estuarine water bodies and aquifers. Excluding the estuarine waters, all the other water bodies are water supply sources varyingly vulnerable to weather extremes and changes in the average weather behaviour, namely precipitation. The threats to these water systems revolve around floods (riverine and estuarine), droughts, pollution and local overexploitation of aquifers. Droughts in particular may increase the threat of saltwater intrusion both in surface water and groundwater, at least on a temporary basis. Besides the above issues, diffuse pollution – mainly due to farming and livestock activities – is also a major threat to aquifers, a situation that has already prompted the definition of Tagus Vulnerable Area (Nitrates Directive) for Aluviões do Tejo and part of Tejo-Sado/Margem Esquerda aquifers.
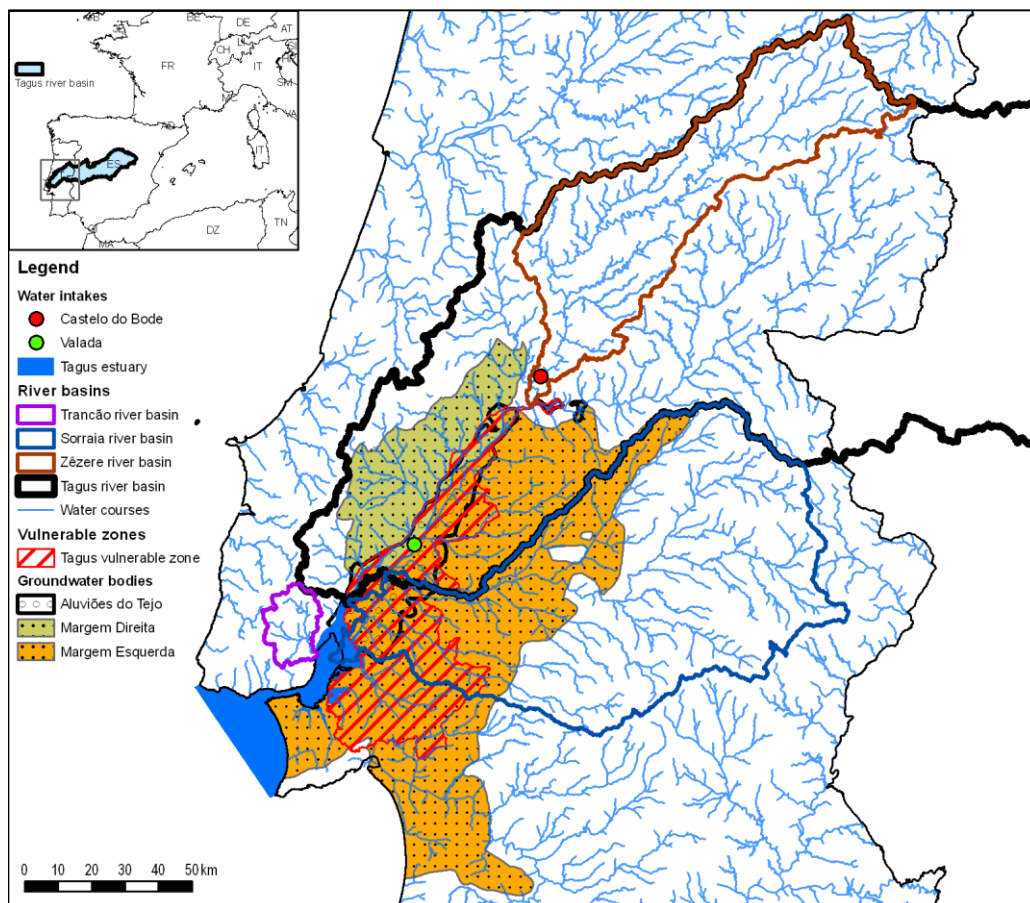
Figure 3.1 – Sites of the Tagus case-study area

Source: Adapted from Alphen et al. (2016) and SNIRH (https://snirh.apambiente.pt/index.php?idMain=4&idItem=3&idlSubtem=link4d)

In the case-study area, groundwater systems **Aluviões do Tejo**, **Ota / Alenquer**, **Tejo-Sado/Margem Direita** and **Tejo-Sado/Margem Esquerda (**Figure 3.1 green and orange coloured areas) are not

isolated from the surface water bodies. Besides the general flow towards the Tagus itself, aquifers discharge into Tagus tributaries through subsurface groundwater flow, often increasing the time span of their seasonal flowing regime (Oliveira, 2009). On the other hand, Tagus is known to influence the quality and evolution of hydraulic heads in its vicinity. The same influence, at least in groundwater quality, is identified in several studies (Simões, 1998; Zeferino, 2016) along the interface Tagus estuary/Tejo/Sado – Margem Esquerda aquifer. Aquifers can also be a main source for some Tagus tributaries' springs. For instance, Ota/Alenquer aquifer is the main water source for Ota stream springs. As such, the analysis of climate change impacts on water systems' must integrate groundwater.

The aquifers under study have large variations in dimension, geology and functioning, reflecting the major groundwater environments of the Lower Tagus. **Ota-Alenquer** is a small karstic system that feeds the Ota and Alenquer karst springs. These springs, besides feeding the Ota River, have been (together with the water wells located in their vicinity) an important water supply source to Lisbon, supplementing water supply sub-systems of Alviela and Tejo exploited by EPAL. **Aluviões do Tejo**, **Tejo/Sado – Margem Direita** and   are 3 large aquifers developed in the wide sedimentary basin of the Lower Tagus. They are partially interconnected by low permeability units (aquitards). Aluviões do Tejo, Tejo/Sado – Margem Direita aquifers constitute an important strategic water resource for Lisbon and Tagus right margin counties, and a water supply source for some farming, livestock and smaller urban centres in that margin. Tejo/Sado – Margem Esquerda is the almost single water supply source for all the socio-economic activities of the Tagus left margin counties. It is also a complementary water supply to Lisbon, through the wells exploiting it beneath Aluviões do Tejo.

3.1   Climatology

The climate of the case-study area during the historical period set for BINGO project (1/10/1979 to 30/09/2009) shows Mediterranean characteristics, with July and August being the driest months. By the Köppen classification it is a temperate mesotermal with dry hot summers. APA (2012), using the Thornthwaite classification, identifies a sub-humid to dry sub-humid climate for Tagus right margin region, while for Aluviões do Tejo and Tagus left margin regions climate is moist sub-humid to dry sub-humid. In Table 3.1 the average climate parameters are presented for the historical period above mentioned.

Table 3.1 – Average climate parameters in the historical period

Climate average parameters (historical period 1/10/1979 – 30/9/2009)		Values
Temperature		16 ºC
Precipitation	Average year	675 mm/year
	Wet year	935 mm/year (≈138% of a normal year)
	Dry year	455 mm/year (≈67% of a normal year)
Moisture (at 9:00 a.m.)		65% to 87%
Evaporation		1 283 mm/year
Evapotranspiration		500 to 800 mm/year
Solar radiation (whole basin)		5276 and 5769 MJ/m^2 *
Winds (average)		5 to 20 m/h (the higher values from coastal areas) with prevalence of north-westerly winds

* July and August being the months with highest radiation

Source: APA (2012)

3.2 River network

The river network in the aquifers' area develops over a wide alluvial plain whose borders loosely follow the north and east borders of Tejo/Sado – Margem Esquerda aquifer, western border of Tejo/Sado – Margem Direita aquifer and beyond the southern border of Margem Esquerda aquifer up to the Alentejo's plains, defining an area oriented NE-SW (cf. Figure 3.1). Sorraia river is the main tributary of Tejo's left margin (watershed = 7 611 km^2), followed by the much smaller rivers of Muge, Ribeira de Ulme/Vala de Alpiarça (watershed circa 430 km^2) and Ribeira de Magos (watershed = 70 km^2). On the right margin, the northern tip of Tejo/Sado – Margem Direita aquifer is occupied by the downstream area of Zêzere river (the most important tributary on Tagus right margin, with a basin area = 5 029 km^2), Almonda and Alviela rivers (watersheds of 167 and 274 km^2, respectively). Downstream, the main tributaries are: Rio Maior (watershed = 922 Km^2), Rio Alenquer (watershed = 286 km^2) e Rio Trancão (watershed = 279 km^2).

These right margin tributaries (Alviela, Almonda, Maior and Alenquer) are fed by large springs at the border of Maciço Calcário Estremenho aquifer – a large limestone structure of 800 km^2 area (Crispim, 2010) which means that a substantial amount of water reaching Tagus is transferred from this limestone aquifer through these rivers (APA, 2012). Amongst these springs are especially noteworthy the Olhos d'Água do Alviela, which are the source of Alviela River and was the main water supply to Lisbon for most of 20th century. Besides this link between Tagus river, its right margin tributaries and Maciço

Calcário Estremenho aquifer (located outside the case study area), other connections between aquifers and river network in the case-study area are known, namely the discharges from aquifers into the river network or rivers recharging the aquifers in specific areas, (e.g. where heads have been severely depressed near Tagus river due to water exploitation). Temporary streams typically function as aquifers' discharge areas, mainly to aquifer's local flows (Oliveira, 2009). Water availability for surface waters is given in Figure 3.2 (APA, 2012).

Figure 3.2 – Water availability under natural regime for the whole Portuguese area of Tagus basin

Source: APA (2012)

3.3 Estuary and coastal areas

The estuary and its surrounding region have an area of 1.6 km^2 (APA, 2012a). Along its margins several important cities are located (e.g. Seixal, Almada), including the largest urban centre of Portugal (Lisbon). Agriculture is a very important activity of the estuary region, in particular in its northern upstream border (along Aluviões do Tejo and large parts of Tejo/Sado – Margem Esquerda aquifers), while industry is strongly concentrated in its southern margin, in particular in Seixal area and in the northern area of Vila Franca de Xira/Alverca. There is also important harbour activity on both north and south margins of the estuary, in particular Lisbon and Almada/Trafaria areas. These activities beget significant pollution loads for the soils and the estuary and important groundwater abstractions to satisfy the demand. Farming activities, urban areas on the south margin and industry rely strongly on groundwater supply and this can lead to saltwater intrusion in the aquifers, if the right set of pumping volumes and hydrogeological conditions exists. Besides saltwater intrusion due to water abstraction, pollution due to these activities – in particular agriculture – is discharged both in estuary and soils. Groundwater pollution then occurs due to recharge in polluted soils and interactions with estuary waters.

Tagus estuary is a mesotidal estuary (APA, 2012) and its dynamics control water salinity (and up to a certain point, aquifer saltwater intrusion) as well as the transport of pollutants from its entry sources up to the ocean or the surrounding aquifer. Maximum flow velocities inside the estuary reach 2 m/s at its mouth, lowering to 1 m/s along its main channels, slowing further upstream, while tides are amplified inside the estuary due to depth reduction (APA, 2012). Such high speed flows allow for tides to travel up to 15 km upstream (APA, 2012), which might influence the extension of the areas prone to aquifer's saltwater intrusion.

Besides the estuarine region, the dynamic processes on the coastal area (from Trafaria to Cabo Espichel) can also have an impact on Tejo/Sado – Margem Esquerda aquifer along Península de Setúbal's seaside. This 30 km sandy beach seashore, backed by a fossil cliff, is located south of Tagus mouth and has an arched shape: its northern sector opens W-SW, its central area opens to W and its southern stretch to W-NW (Pinto et al., 2007 in APA, 2012). The coastal dynamics, controlled by the sheltering conditions of Cabo Raso and Cabo da Roca, the prevailing SW incident wave, bathymetry and tidal currents (Freitas et al., 1993), coupled with sea level change, are the main factors controlling seashore retreat due to erosion, coastal flooding and possible seawater intrusion in this region. Nowadays there are some, inconclusive, hints from geophysical surveys of possible saltwater intrusion (in Praia do Pescador) although the same surveying campaign also identified, along other areas of the coast, possible upward flows along NW-SE fractures from the (lower) Miocene aquifer that seem to bring fresh water to the upper aquifer's coastal region (Ferreira, 2012). If that is the case, saltwater intrusion might be attenuated in the future due to this upwelling of fresh water in the coastal area. Nevertheless, mathematical modelling done by the same author for a climate scenario of 1.5 m sea level rise, precipitation decrease of 42% and the same present-day water abstraction rates, projects a 20 m inland encroachment of saltwater intrusion (Ferreira, 2012).

Another example of the interaction sea/surface-water/groundwater in the case study area is Lagoa de Albufeira, also located in Tejo/Sado – Margem Esquerda aquifer. This SW-NE elongated coastal lagoon

with 1.3 km^2, oblique to the sea shore, has a maximum depth of 15 m and is isolated from the ocean by a coarse sand barrier of 1200 m under constant oceanic reshaping (APA, 2012). This sand barrier must periodically be opened to renovate lagoon's waters, once the southward transport of sands along the coast reconstructs the barrier, closing the lagoon sometime after its opening (Cruces et al., 2002 in APA, 2012). Draining a 106 km^2 basin, Ribeira da Apostiça flows into Lagoa de Albufeira, which also receives inflows from several minor streams located in lagoon's southern border (APA, 2012). Pollution reaches Lagoa de Albufeira through Ribeira da Apostiça and the south border creeks but also from groundwater discharges, which bring in significant pollution loads. This process is identified by the chemical evolution of lagoon's water and the aquifer's NE flow occurring south of the lagoon (Duarte, 2012). In fact, although the lagoon's water composition is the result of sea water, river flows and groundwater, the main sources of contamination (nitrates and sulphates) are groundwater discharges, as suggested by the isotopic and hydrochemical studies (Duarte, 2012). This author identified strong pollution (nitrates and sulphates) in the aquifer area south of the lagoon, due to old septic tanks and farming activities, with water in some wells not complying with the quality standards for human consumption.

3.4   Geology and hydrogeology

The case-study area includes the large sedimentary basin of Tejo, spreading from near Tomar to the estuary region, where the 3 large aquifers Aluviões do Tejo, Tejo/Sado – Margem Direita and Tejo/Sado – Margem Esquerda are located (cf. Figure 3.1; Figure 3.3). Ota/Alenquer aquifer is located at the outskirts of this basin.
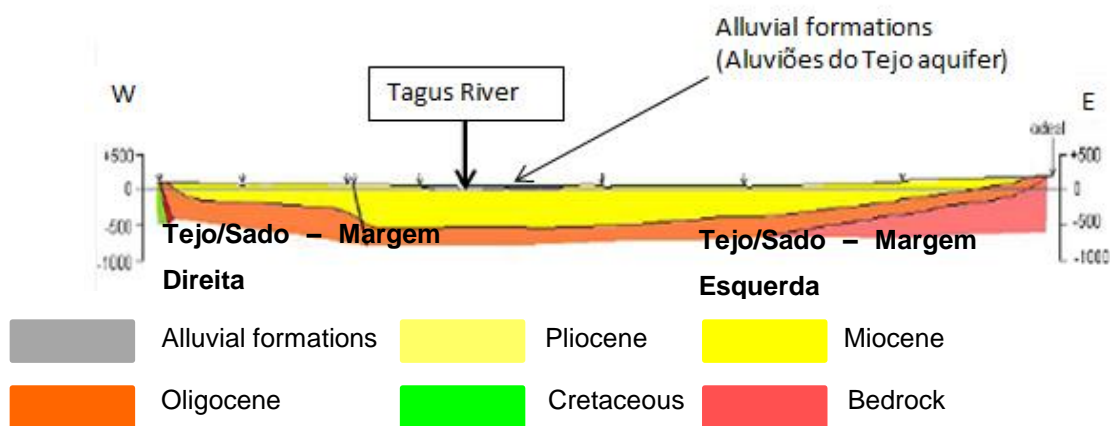
Figure 3.3 – Cross section of Tagus sedimentary basin showing the location of the Aluviões do Tejo aquifer and the formations of Tejo/Sado underlying aquifers

Source: http://www.arhtejo.pt/c/document_library/get_file?uuid=e5a4e269-88f5-440c-88d3-28cf40c218b7&_groupId=10225

Ota-Alenquer karstic aquifer (area = 9.38 km^2) lies at the SW border of the large Tejo/Sado Margem Direita aquifer. It is developed on Jurassic detritic and reef limestones with a moderate karstification, topped by sandstone deposits. It has a dome-like structure (Figure 3.4) and thickness of up to 200 m. A large number of faults intersect the aquifer, functioning as preferential directions for karst development and groundwater circulation.

This is a poorly known aquifer. Heads and most hydraulic properties' data are lacking, and this is the reason why no mathematical flow modelling was performed. Instead, only recharge estimations were done, using recharge model BALSEQ_MOD. There are only few transmissivity data, ranging from 1 000 to 14 000 m^2/day (Paradela & Zbyszewski, 1971; *in* Almeida *et al.*, 2000), which is normal for karstic systems. As for direct recharge from the outcropping area estimations range from 1.8 hm^3/year (Oliveira et al., 2000) to 4 hm^3/year (Almeida et al., 2000) for the historical period. However, the discharges of Ota and Alenquer springs and the well abstraction volumes (which remain under sustainable regime) suggest a much higher recharge, on the range of 25 hm³/year, of which 21 hm³/year are assumed to come from the neighbouring karstic area of Serra de Montejunto. This suggests an underground connection between the aquifer and Serra de Montejunto, which is further backed up by the results of tritium studies (Almeida et al., 2000). If that is so, then there is a general NW to SE flow, from Montejunto up to Ota and Alenquer springs, located at Ota/Alenquer aquifer's downstream area.
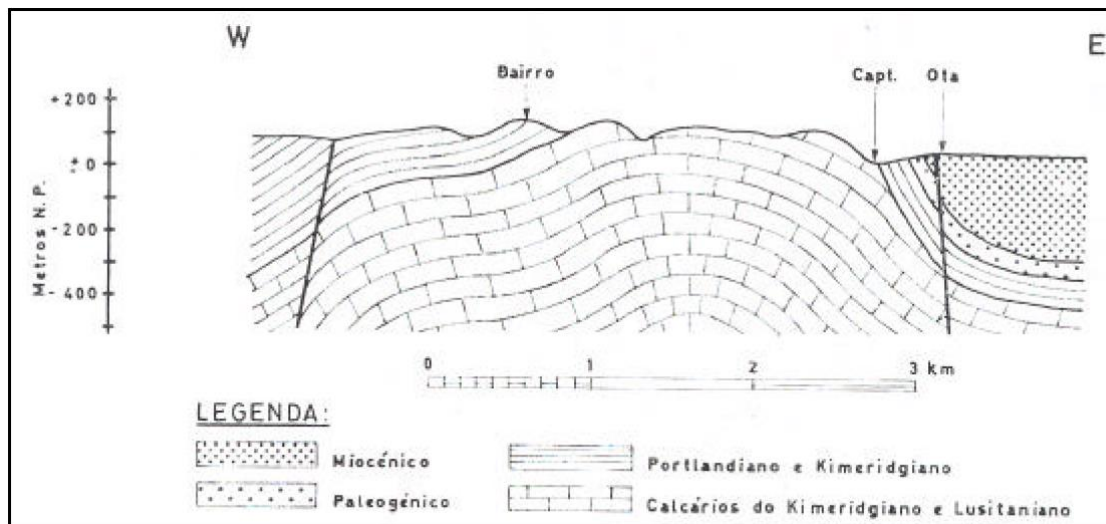
Figure 3.4 – Cross-section of Ota/Alenquer aquifer near EPAL wells in Ota

Source: Paradela & Zbyszewski (1971, *in* Almeida *et al.*, 2000)

Aquifer's natural discharge is made through the karstic springs of Ota and Alenquer, which become the source of Ota and Alenquer streams, two Tagus tributaries (Almeida et al., 2000). These springs have a markedly temporary behaviour and there is a significant lack of data concerning their discharge volumes.

Well abstraction for water supply was between 17 e 26 hm³/year until 1996 (Cavaco & Benoliel, 1997). Water abstraction volumes for agriculture are unknown but should be quite low, due to the characteristics of the area. The main pressures affecting this aquifer, while moderate, are basically from farming activities and, locally, from sewage discharges of small urban areas.

Aluviões do Tejo aquifer is a multilayer, essentially unconfined porous aquifer developed in alluvial and terrace Pleistocene and Holocene deposits, covering an NE-SW elongated area of 1 113.20 km² (Almeida et al., 2000; Figure 3.5). It straddles over the contact area of Tejo/Sado – Margem Direita and Tejo/Sado-Margem Esquerda aquifers and is in direct connection with Tagus River (cf. Figure 3.3). Its

thickness ranges from 7 to 74 m for the alluvial formations and from 8 to 42 m for the terraces, increasing towards its SW border, leading to a maximum measured thickness of circa 90 m (Lobo Ferreira et al., 2011; Figure 3.5). The alluvial deposits encompass sands, silts and clays, while the terrace formations are composed of gravels, sands, conglomerates and clays; a unit of conglomerates rests at the base of the alluvial deposits and the terraces sit at its top. These deposits have a complex internal geometry of superimposed intermingled lenticular units, often bearing signs of paleo-erosions. This gives rise to a wide variation of hydraulic properties both horizontally and vertically (Almeida et al., 2000; Oliveira et al., 2000; Mendonça et al., 1982; Zbyszewski, 1953; Zbyszewski et al., 1971). The same authors identified a subtle tendency towards larger clay contents at the right side of the aquifer. Basal conglomerate's semi-confined conditions were identified at SW area up to the estuary.
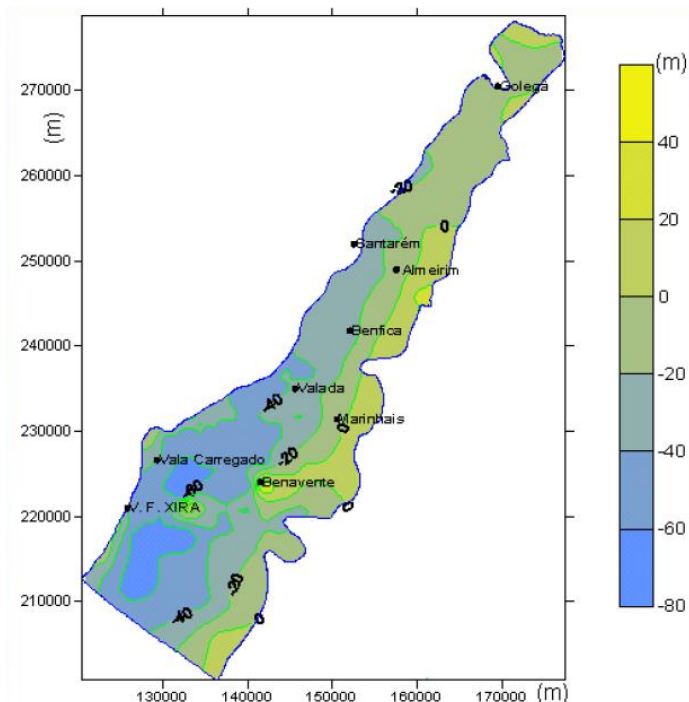
Figure 3.5 – Areal extension of Aluviões do Tejo aquifer and topography of its bottom

Source: http://www.arhtejo.pt/c/document_library/get_file?uuid=e5a4e269-88f5-440c-88d3-28cf40c218b7_&groupId=10225

The hydraulic properties of this aquifer are presented in Table 3.2 and show large spatial variation. For instance, transmissivity increases upstream and towards the central aquifer area, being in general larger in terrace formations; productivity has an increasing trend towards the centre and upstream areas of the aquifer and also changes temporally, locally becoming very low in summer. Due to this, the most widely exploited unit is the conglomerate deposits at the base of the alluvial sequence, due to their higher and more temporally reliable productivity.

Table 3.2 – Hydraulic properties of Aluviões do Tejo aquifer

Hydraulic properties	Formations	Values
Hydraulic conductivity	Alluvial formations	1,1 to 464 m/day (average = 140 m/day)
	Terrace formations	43 to 229 m/day (average = 136 m/day)
Porosity	Whole aquifer	2 to 35% (average ≈ 20%)
Storage coefficients	Whole formations (alluvial formations have slightly higher values than terraces)	7.1×10^{-5} to 1×10^{-1} (average = 8.4×10^{-3})
Transmissivity	Alluvial formations	6 to 5 575 m^2/day (average ≈ 1 600 m^2/day; most common values = 823 to 2 246 m^2/day)
	Terrace formations	92 to 5 794 m^2/day (average ≈ 2 020 m^2/day)
Productivity	Whole aquifer	1 to 80 l/s (average ≈ 10 l/s)
Specific yield	Alluvial formations	0.2 to 25 l/s/m (average = 6.8 l/s/m)
	Terrace formations	0.03 to 41 l/s/m (average = 6.2 l/s/m)

Sources: Almeida et al. (2000); Oliveira (2009); Mendonça (1990); Paralta et al. (2001); Delgado Rodrigues et al. (1989)

Direct recharge, occurring along the whole outcropping area of the aquifer, has been estimated between 210 up to 220 hm^3/year, which is circa 30% precipitation on average (Oliveira *et al.*, 2009; Almeida *et al.*, 2000; Silva, 2009). However, recharge is not uniform across space and values as low as 15% precipitation have been suggested for some downstream areas (Mendonça, 1990). Permanent storage is estimated at 4 km^3 (Oliveira, 2009).

Recharge from underlying aquifers of Tejo/Sado – Margem Direita and Tejo/Sado – Margem Esquerda, seems also to occur, as it is suggested by the hydrogeochemical characteristics of some locations (Simões, 1998). Recharge from Tagus (as well as some of its tributaries) seems also to occur at local level, particularly in overexploited areas; this hydraulic connection between Tagus and the aquifer is suggested by changes of heads and hydrogeochemistry in some of the areas neighbouring the river (Mendonça, 1990; Mendonça, 2009; Simões, 1998).

On the whole, induced recharge (from rivers + irrigation losses) has been estimated as 5 to 5.5 hm^3/year, which is something like 2.5% direct recharge (Lobo Ferreira et al., 2011). Recharge from the underlying aquifers hasn't so far been estimated.

Rivers, streams and creeks can also function as aquifer's discharge outlets and some of them, as for instance Almonda and Alviela, 2 important Tagus tributaries, can either become sources of recharge or discharge, depending on water levels' fluctuations in the aquifer (http://aquiferural.ist.utl.pt/es/node/109).

Natural discharges of the aquifer amount to 567 421 m³/day, of these being 7% (39 720 m³/day) discharged into the estuary and springs and the remaining 93% corresponding to discharges into the river network (Almeida *et al.*, 2000; Mendonça, 1990). The distribution and nature (concentrated or diffuse) of these discharges is partially controlled by the tectonic fracturing criss-crossing the alluvial basin (Simões, 1998). Discharges due to abstraction from wells has been estimated around 1 hm³/year (Oliveira, 2009), although agriculture abstraction values are poorly known.

Horizontal groundwater flows towards Tagus River, streams and rivers (e.g. Rio Sorraia) of the Tagus River network and towards the estuary, as heads shows (Simões, 1998; Almeida *et al.*, 2000). Saltwater issues reported near the estuary – and also upstream, in Azambuja, Benavente and Vila Franca de Xira – (Oliveira *et al.*, 2000a) are proof of the hydraulic connection between the estuary (and Tagus river) and the aquifer. Vertical flows also occur: (1) upward due to discharges of underlying aquifers, (2) downward from the river network (in the locations were it discharges into the aquifer). Such vertical flows are often controlled by tectonic fracturing (Simões, 1998).

This aquifer is a significant supply source for agricultural irrigation and local water supply. However, the dominant pressures are water-quality related, while the quantity pressures are so far of secondary importance. In fact, although there are pollution hotspots linked to industry, mainly near the estuary (in Vila Franca de Xira and in the upper estuary NE region), nitrates and pesticides leaching from agricultural activities are the main pollution issues. This has led to the definition of a Tagus Vulnerable Area, following the Nitrates Directive, encompassing the whole Aluviões do Tejo aquifer and the surrounding area of Tejo/Sado – Margem Esquerda aquifer (http://www.draplvt.Mamaot.pt/Ordenamento/Ambiente/Zona-Vulneravel-Nitratos/Documents/Zona%20VulneravelA3.pdf). Domestic pollution, as well as agro-industry pollution is also of some importance in Lezíria do Tejo (http://snirh.pt/snirh/download/relatorios/redes_agsub_oeste.pdf).

Tejo/Sado – Margem Direita aquifer is a multilayer, essentially porous, confined to unconfined aquifer, located on Tagus basin's right margin. Developed on Miocene detritic and calcareous formations of sub-horizontal layers often of wide extension, it has an outcropping area of 1629 Km² with a broad tabular-trapezoidal shape (Figure 3.6), limited at its western border by several faults. Its easternmost area dips under Aluviões do Tejo aquifer (Figure 3.6), seemingly contacting with Tejo/Sado – Margem Esquerda aquifer by faults located along the Tagus river canal. Its thickness ranges from circa 200 to more than 600 m (Almeida et al., 2000).

Limestone formations are composed of poorly karstified limestones and marls, interbedded with clays and some sandy lenses. They cover the underlying Miocene sandstone formations throughout most of the aquifer's outcropping area (cf. Figure 3.6). These sandstone formations have a wide lithological variation both vertically and horizontally, with interbedded layers of clay and gravel and conglomerate-like lenses, although the coarser sediment's lenses are less common that those of clay. Due to the fact that limestone formations are less permeable than the sandstone deposits, they make a poorer aquifer, behaving in large part as an aquitard. The hydraulic properties of this aquifer are presented in Table 3.3.

Figure 3.6 – Location and stratigraphic setting of Tejo/Sado – Margem Direita aquifer
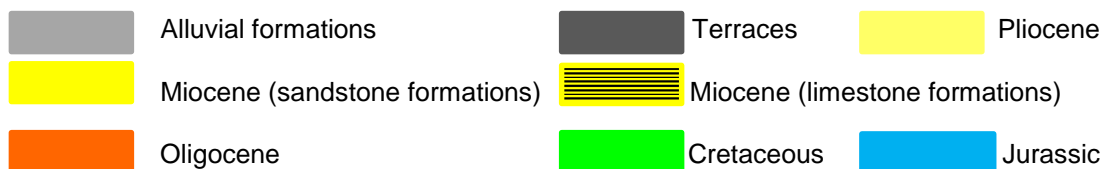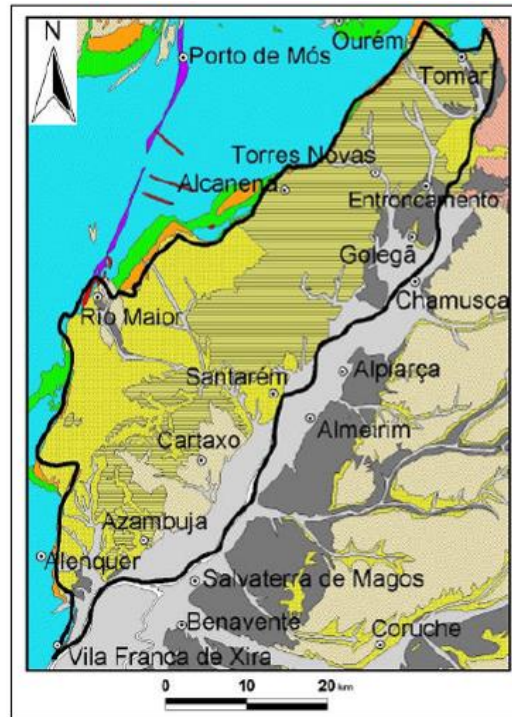
Figure 3.6 – Location and stratigraphic setting of Tejo/Sado – Margem Direita aquifer

Source: Almeida et al. (2000)

Hydraulic conductivity is poorly characterized horizontally and vertically but wide value changes are assumed for vertical conductivity, due to the vertical variations in lithology. Transmissivity shows a wide anisotropy, having a reduction trend towards N of Santarém and its western border (Simões, 1998; Almeida *et al.*, 2000).

Direct recharge has been estimated between 355 and 361 hm^3/year (Oliveira *et al.*, 2000) although other authors give much lower estimates, on the range of 150 to 200 hm³/year (Almeida *et al.*, 2000). Permanent storage is estimated around 10 km^3 (Oliveira, 2009).

Recharge due to infiltration of irrigation and water supply networks' losses, also occurs but its amount is unknown. The same goes for the recharge from streams, in particular those that come from the neighbouring Maciço Calcário Estremenho (e.g. Almonda and Alviela rivers). Diffuse recharge from the most superficial units towards the lower, more productive, units occurs.

Table 3.3 – Hydraulic properties of Tejo/Sado Margem Direita aquifer

Hydraulic properties	Formations	Values
Hydraulic conductivity	Whole aquifer	12.2 to 28.3 m/day
Porosity	Whole aquifer	20% in average
Transmissivity	Limestone formations	10 to 130 m^2/day (most frequent values); highest values = 1 200 m^2/day
	Sandstone formations	20 to 160 m^2/day (most frequent values); highest value estimated = 4 100 m^2/day
	Whole aquifer	14.5 m^2/day (average)
Productivity	Limestone formations	0.1 to 20.8 l/s (average = 7.3 l/s)
	Sandstone formations	0.1 to 75 l/s (average ≈ 15 l/s)
Specific yield	Whole aquifer	0.04 to 1.7 l/s/m (average ≈ 0.5 l/s/m)

Sources: Almeida et al. (2000); Oliveira (2009); Paralta et al. (2001); Simões (1998)

Natural discharges occur to the local river network, springs and Aluviões do Tejo aquifer. The location of such discharges is controlled, at least partially, by the tectonic structures, namely faults (Simões, 1998). Such discharges have not been thoroughly quantified. Abstraction from wells ranges from 118 to 158 hm^3/year[1], which is circa 33 to 45% recharge (Oliveira, 2009). The main abstraction areas are: Valada, Ota, Alenquer, Rio Maior, SW Entroncamento, Qta. das Ladeiras, Torres Novas, Alcanhões, Espadanal, Cartaxo and Golegã.

The general direction of horizontal flow is towards Tagus River (Figure 3.7), as indicated by the heads distribution across the aquifer, but there are local variations to this general trend, with the upper units discharging into Tagus tributaries or towards the estuary (Lobo Ferreira *et al.*, 2008; Oliveira, 2009).

Vertical flows do occur and might partially be controlled by the tectonic settings. These flows are usually upward, towards Aluviões do Tejo, as suggested by field observations, but in areas of overexploitation such upward flows may be inverted and Aluviões do Tejo aquifer discharges then into Tejo/Sado – Margem Direita aquifer (Mendonça, 2009). The volume of the flows between aquifers is unknown. Lateral flows with Tejo/Sado – Margem Esquerda are unknown, being assumed that the poorly known Tagus fault is a potential barrier to flow between Tejo/Sado Margem Direita and Margem Esquerda aquifers (Almeida *et al.*, 2000)

---

[1]   These values are distributed as follows: domestic water supply + industry ranging = 11.5 to 12.5 hm^3/year; agriculture = 106 to 145 hm^3/year.

Figure 3.7 – Flow directions in the aquifer

Source: Oliveira (2009)

This aquifer is a significant water source for agriculture and also for water supply. Nevertheless, and in spite of these quantitative pressures which are not yet worrying (but not to be neglected either), quality pressures are the main issues. Pollution due to agriculture and urban sources is reported, as well as, at a local level, industrial pollution (Simões, 1998). The areas most affected by agricultural pollution are: Rio Maior, Golegã-Chamusca, Santarém, Torres Novas, Cadaval, Entroncamento and Vila Nova da Barquinha (https://dre.pt/application/file/a/611853). Industrial pollution might still be a problem along the industrial region of Vila Franca de Xira – Póvoa de Santa Iria – Moscavide area, directly infiltrating into the aquifer along Póvoa de Santa Iria – Moscavide region and east of Vila Franca de Xira – Póvoa de Santa Iria. In the river bank areas between Forte da Casa – Vila Franca de Xira, covered by alluvial deposits, industrial pollution might reach Tejo/Sado – Margem Direita aquifer through percolation from Alluviões do Tejo aquifer. Some of this industrial pollution is due to abandoned industrial sites. Saltwater intrusion is reported in Azambuja and surrounding areas of the estuary (Simões, 1998).

As with the two previous aquifers, **Tejo/Sado – Margem Esquerda** aquifer is also a multilayer, porous, confined to unconfined aquifer. Located on Tagus basin's left margin, it is developed on Pliocene sandstone formations interbedded with some clay, Miocene sandstones similar to those of Tejo/Sado Margem Direita and, at the bottom, a Miocene marine detritic/calcareous formation of sands, marls and calcareous sandstones (Almeida et al., 2000). With an outcropping irregular trapezoidal shape area of 6876 km², set on a NE-SW elongated depression (Figure 3.8), its westernmost area dips below Aluviões do Tejo aquifer, were it meets Tejo/Sado – Margem Direita aquifer's eastern limit. However, the exact location or nature (e.g. tectonic) of such limit is unknown. It is suspected that, at least in the estuary area and a bit upstream, the contact between Margem Direita and Margem Esquerda is the Tagus fault. Locally graben structures do occur, generating sub-basins inside the main aquifer, and in Península de

Setúbal, the aquifer's structure is controlled by faulting and the large synclinal that at its southern border is limited by the karst terrains of Serra da Arrábida.

⬜	Alluvial formations	⬛	Terraces	🟨	Pliocene
🟨	Miocene (upper sandstone+marine calcareous/sandstone)	🟧	Oligocene
🟩	Cretaceous	🟦	Jurassic	*remaining coloured areas are Hercynian bedrock
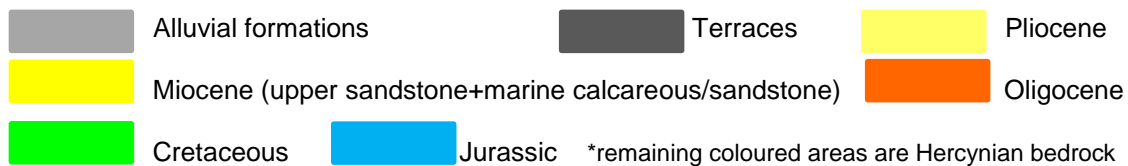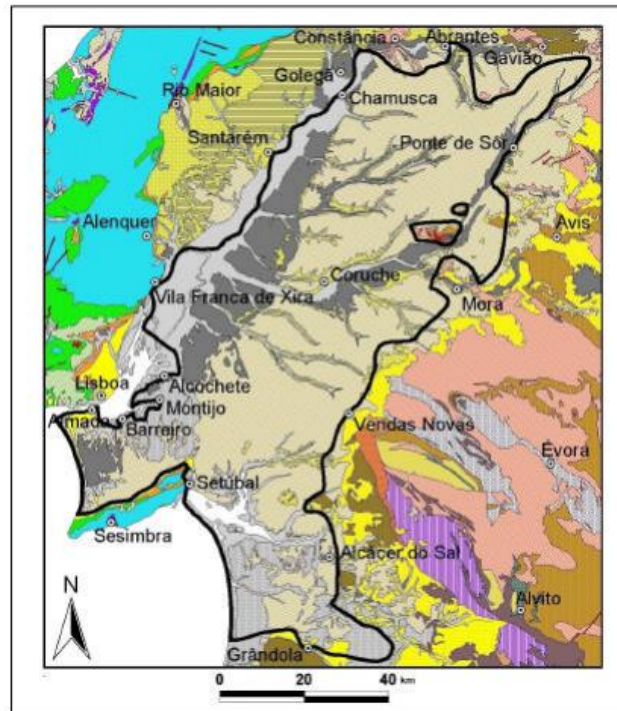
Figure 3.8 – Location and stratigraphic setting of Tejo/Sado – Margem Esquerda aquifer

Source: Almeida et al (2000)

The sediments lie in a complex, mainly sub-horizontal succession, along a wide areal extension. They show a wide range of thicknesses, with a general increasing trend towards the centre of the Tagus basin (westward zone of the aquifer). On average, thickness range from 200 up to 400 m (Victor *et al.*, 1980; Almeida et al., 2000) but locally they can be much higher as is the case of Península de Setúbal, were values of 800 m or even more have been suggested from drilling data (Barreiras et al., 2009; Mendonça *et al.*, 2004). Due to lithological variations of these sediments (mainly cementation and proportion of silt/clay vs. sand and gravel), hydraulic behaviour changes are expected across the aquifer. Lithological differences between the sedimentary deposits originate at least 3 main aquifer bearing units: (1) a topmost mainly free aquifer (Pliocene sandstones); (2) a confined/free aquifer (Miocene sandstones); (3) a confined aquifer (Miocene marine sandy-calcareous formations). Leakage between these 3 aquifers occurs, being dependent on the local hydrogeological settings defining the confining conditions. On Table 3.4 are presented the hydraulic properties of these units.

Table 3.4 – Hydraulic properties of Tejo/Sado Margem Esquerda aquifer

Hydraulic properties	Formations	Values
Hydraulic conductivity	Whole aquifer units	2.5 to 28.5 m/day
	Whole aquitard units	1×10^{-7} to 1×10^{-6} m/day (in Almada and Seixal areas)
Porosity	Whole aquifer	26 to 38%
Effective porosity	Calcareous sandstones	0.5% (average)
	Sandstones	28% (average)
Storage coefficients	Pliocene sandstones	2.2×10^{-3} (average)
	Miocene formations	3×10^{-4} (average)
Transmissivity	Pliocene sandstones	19 to 3000 m^2/day
	Miocene sandstones	3 and 1500 m^2/day (most frequent values: 45 to 179 m^2/day)
	Miocene marine formations	29 to 4100 m^2/day (most frequent values: 127 to 693 m^2/day)
	Whole aquifer	3 to 4100 m^2/day
Productivity	Pliocene sandstones	18.6 l/s (average)
	Miocene sandstones	14.7 l/s (average)
	Miocene marine formations	39.1 l/s (average)
	Whole aquifer	From 0.08 (at a Pliocene well) to 110 l/s (at a Miocene marine well)
Specific yield	Whole aquifer in Península de Setúbal area	0.5 to 25 l/s/m

Sources: Almeida et al. (2000); INAG (1997); Mendonça (1990); Mendonça (1996); (Oliveira et al., 1994); Oliveira (2009); (Oliveira, 2009a); Paralta et al. (2001); Paralta et al. (2009)

Upward flows under natural conditions occurred from the lower towards the upper aquifer units of Aluviões do Tejo (Mendonça *et al.*, 2004), being largely controlled by tectonic structures (Simões, 1998). However, hydraulic heads have shown a general decreasing trend since 2000 (Lobo Ferreira et al., 2011) and overexploitation situations have been reported, generating an inversion of these flows (Mendonça, 1993; Almeida *et al.*, 2000). Such downward flows generate quality issues due saltwater intrusion, particularly if overexploitation occurs in upper Miocene units below areas where Pliocene aquifer already has saltwater intrusion (e.g. Barreiro; cf. Zeferino, 2016). Salinization due to low quality waters ascending from the Miocene marine aquifer into Miocene sandstones' overexploited areas may also occur but it is a very local phenomena (Mendonça, 1993; Almeida *et al.*, 2000; Paralta *et al.*, 2009).

The general horizontal flow is towards the centre of the basin, the estuary and, on the coast side and southernmost part of the basin, the ocean and Sado River, as suggested by the heads distribution (Figure 3.9).

Direct recharge has been estimated from 700 hm^3/year (Almeida *et al.*, 2000) to 1 300 hm^3/year (Oliveira, 2009) for the whole area of the aquifer. Permanent storage was estimated at 43.2 km^3 (Oliveira, 2009). Recharge due to irrigation and urban water/sewage network losses also occur but have not been estimated for the whole aquifer. However, in Península de Setúbal, recharge from irrigation was estimated as 12 hm^3/year and from urban water networks as 19 hm^3/year (HP, 1994). Recharge from the river network is unknown for the whole aquifer but has been estimated for Península de Setúbal as 3.2 hm^3/year from estuary inflows and 1.6 hm^3/year from river inflows (PNUD, 1980). Recharge of the lower formations of leakage from upper aquifers (namely the Pliocene aquifer) hasn't also been evaluated for the whole aquifer. In Península de Setúbal, such recharge has been estimated as 3.96 hm^3/year, while Pliocene recharge from the lower aquifer (Miocene sandstones) was estimated as 0.97 hm^3/year (HP, 1994).

Natural discharges are mainly to rivers, streams, springs, and estuary and, in Península de Setúbal, also the ocean (Figure 3.9). They are poorly known, with just some estimates in Península de Setubal, where discharges into rivers are estimated at 33.5 hm^3/year and discharges into the ocean at 50.0 hm^3/year, while circa 4.7 hm^3/year is discharged into Tejo/Sado estuaries (PNUD, 1980).
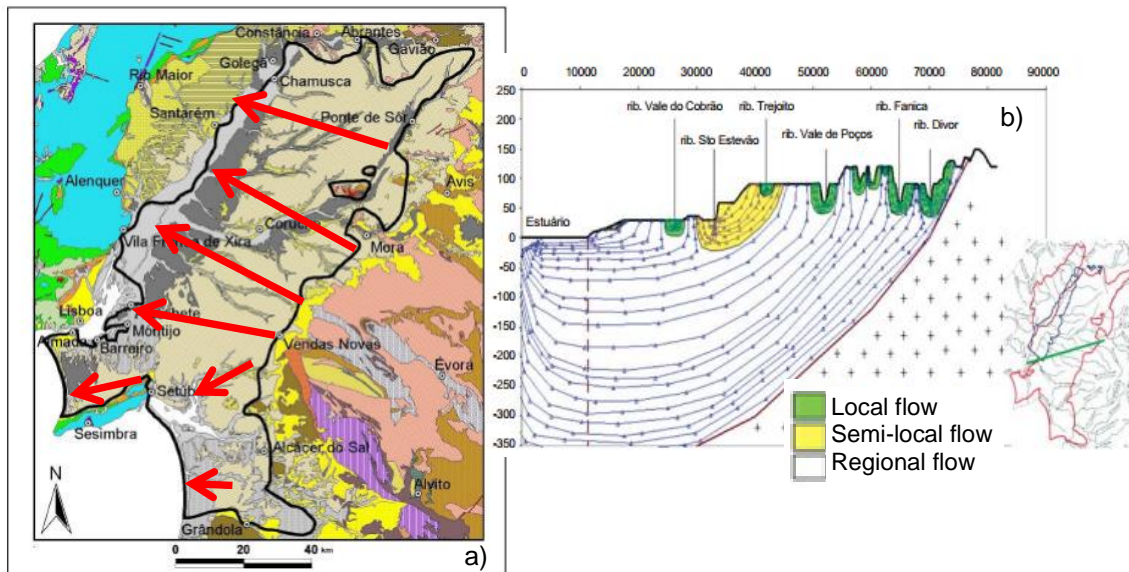
Figure 3.9 – Flow directions in the aquifer a) general directions; b) length of flow

Source: Oliveira (2009)

The total amount of water abstractions range from 426 to 569 hm^3/year for the whole aquifer (Oliveira, 2009), corresponding to 33% up to 42% of recharge (Lobo Ferreira *et al.*, 2008). Farming activities exploit 345 to 479 hm^3/year, industry (self-supply) 13.7 to 17.6 hm^3/year and domestic + industry 67 to 73 hm^3/year (Oliveira, 2009). The main abstraction areas are: Almeirim, Barreiro, Lezíria de Vila Franca de Xira, Mitrena, Montijo, Moita, Setúbal, Palmela, Benfica do Ribatejo, Almada-Seixal (Fialho, 2009).

It must be stated that there is a trend towards higher productivities in the central area of the basin (Almeida et al., 2000), where in fact the aquifer underlies Aluviões do Tejo. Specific yield is poorly known.

The quantitative pressures are essentially related to water supply and at county scale can be significant. However quality pressures are the most important. These pressures are mainly due to agriculture, whence a large part of this aquifer is also included in the Tagus Vulnerable Area (cf. https://dre.pt/application/file/a/611853). Vale do Tejo, Chamusca and the NE area of the estuary are particularly critical, as is the whole downstream area of Chamusca, Montijo and Seixal as far as livestock pollution is concerned (Mendes *et al*., 2006). Along Vale do Tejo, downstream Chamusca up to the estuary, the pollution reaches first the Aluviões do Tejo aquifer and from there it can percolate down to Tejo/Sado – Margem Esquerda upper productive units. Besides agriculture, domestic pollution is also important in Península de Setúbal; in Lezíria do Tejo this type of pollution can eventually reach Tejo/Sado – Margem Esquerda aquifer due to percolation from Aluviões do Tejo. Industry is also significant, in particular in Península de Setúbal, where in some cases, even the lower aquifer has been affected (Amaral *et al*., 2009). Agro-industrial pollution along Lezíria do Tejo can reach Tejo/Sado – Margem Esquerda aquifer from percolation from Aluviões do Tejo. Saltwater intrusion due to overexploitation along Tagus estuary's coastal areas has been reported in Almada, Cachofarra, Porto Alto, Malhada, Alcochete, Barreiro, Mitrena and Praias do Sado (Mendonça, 1993; Almeida *et al*., 2000; Simões, 1998).

3.5   Ecosystems

Water resources are vital for the ecosystems of the case-study area. Under a possible scenario of dwindling water resources, conflicts, already present, between ecosystem needs and human consumption are expected to increase. This situation will bring extra difficulties to water managers trying to comply with water and environment protection's European legislation (e.g. Water Framework Directive, Groundwater Directive, Directives 92/43/CEE and 79/409/CEE). Aquatic ecosystems in the case-study area are under thereat due to climate change and ensuing heads' changes, fluvial functioning modifications and sea level evolution. Riverine, estuarine/coastal and groundwater dependent ecosystems, such as temporary ponds and some coastal lagoons, are affected by such changes. One example is Lagoa de Albufeira coastal lagoon, in Península de Setubal, which is partially dependent of Tejo/Sado – Margem Esquerda aquifer, receiving discharges from its superficial productive units (and groundwater pollution from human activities in the neighbouring area; cf. Duarte, 2012). A scenario of recharge decrease will be translated into smaller water discharges into the lagoon. For groundwater dependent temporary lagoons, the threat posed by temperature increase in recharge reduction scenarios, and longer and more frequent drought periods, will endanger these ecosystem's functioning, once, in such conditions, they will not receive enough groundwater discharges and/or suffer longer dry periods. Longer spells of drought might be especially disruptive, which, joined by an evaporation increase due to higher atmospheric temperatures, might lead to much shorter pond

persistence, threatening for instance the capacity of younger generations to grow up and effectively reproduce.

Besides these issues and competition with human activities for water, aquatic ecosystems, either groundwater dependent or not, are threatened by water pollution. One of the main threats, as far as groundwater dependent systems are concerned, is pollution due to farming activities either by overland flow or by infiltration into the aquifers, being then discharged into these ecosystems. Climate change is expected to impact agricultural pollution either due the arrival of new pests, longer periods during which current pests will be active and also the eventual new needs of new cultivars that farmers might adopt to adapt to climate change.

3.6   Human pressures

Anthropogenic pressures on groundwater, mainly from agriculture, urban centres and industry, result on quality and water availability (quantity) issues. Road network can also be a quality stressor while mismanagement of the coastal area can lead to aquifer saltwater intrusion (cf. sub-chapter 3.3).

3.6.1   Agriculture

Agriculture is the main water consumer in the case-study area. Its sources are both surface waters and groundwater (Figure 3.10) and, as far as the aquifers are concerned, the amounts of water abstracted have been estimated at 351 hm^3/year for an average year and 384 hm^3/year for a dry year (Lobo Ferreira et al., 2011; cf. Table 3.5). Livestock abstracts 2.4 hm^3/year from aquifers (cf. Lobo Ferreira et al., 2011).

Such abstraction volumes can locally bring significant heads' changes. For instance, in intensive farming areas, heads rebounds usually occur after corn harvesting (Inês Matos, oral communication). Consequently, the modification of natural flow regimes either between rivers and aquifers or between distinct aquifers can occur (cf. sub-chapter 3.4), at least temporarily. And although, on the whole, the aquifers under study do accommodate this exploitation, locally the effects of such heads' variations (or even a permanent drawdown in over-exploited areas) can be felt, hindering water abstraction in some wells. These heads/flow modifications also allow for the incoming of lower quality waters into the locally over-exploited areas, which, in coastal zones, might lead to saltwater intrusion or its aggravation (cf. sub-chapter 3.4).

Agriculture can also impact recharge due to changes in agricultural practices and crops. Land cover changes bring about recharge changes, mainly due to evapotranspiration modifications. Changes in crops, and its irrigation demands, are expected to do the same due to irrigation losses. It must be noticed, however that such changes haven't yet been estimated.

Agriculture and livestock activities also have a strong impact on water quality due to its own pollution loads. Usually discharged into soils, where they become available to be carried into the aquifer by recharge, such pollution loads have been estimated by Lobo Ferreira et al. (2011). They are shown in Table 3.6.

MD - Lezíria do Vale do Tejo (right margin)
Private irrigation: mainly using groundwater but also superficial sources

ME - Lezíria do Vale do Tejo (left margin)
Private irrigation: mainly using groundwater but also superficial sources

Valas do Tejo (Public water channel)
Superficial sources

Península de Setúbal:
Mainly groundwater (also for domestic supply)

Lezíria Grande VFX
Public Irrigation Perimeter
Superficial sources

Sorraia Valey:
Public Irrigation Perimeter
Superficial sources

Figure 3.10 – Irrigation sources in the case study area

Source: adapted from BINGO D4.2. report (Freitas et al., 2017)

Table 3.5 – Agriculture water demands supplied by groundwater (hm^3)

Aquifer	Average year (50%)	Dry year (80%)
O26 – Ota-Alenquer	0.089	0.100
T1 – Bacia do Tejo-Sado/ Margem Direita	80.166	88.318
T3 – Bacia do Tejo-Sado/ Margem Esquerda	208.534	227.584
T7 – Aluviões do Tejo	62.463	68.370

Source: adapted from Lobo Ferreira et al. (2011)

Table 3.6 – Pollution loads associated with agriculture, livestock and related activities

Aquifer	Livestock		Agro-industry		Agriculture		Total
	N (t/year)	%	N (t/year)	%	N (t/year)	%	N (t/year)
O26 – Ota-Alenquer	0.0	0.0%	0.0	0.0%	0.2	100.0%	0.2
T1 – Bacia do Tejo-Sado/ Margem Direita	264.4	35.6%	35.0	4.7%	443.0	59.7%	742.3
T3 – Bacia do Tejo-Sado/ Margem Esquerda	1 045.6	58.5%	5.9	0.3%	737.3	41.2%	1788.8
T7 – Aluviões do Tejo	407.2	53.8%	0.3	0.0%	349.9	46.2%	757.5

Source: adapted from Lobo Ferreira et al. (2012)

Under climate change, new crop types are expected to be adopted, most probably less water demanding ones, leading to lesser volumes of irrigation losses. Improving efficiency, a very positive aspect of adaptation, will also decrease irrigation losses. How these changes will affect the overall recharge remains unknown. Assuming they lead to lesser water losses reaching the aquifer and if this is added to the expected recharge reduction due to climate change, coupled with land cover and overall water demand changes from all socio-economic sectors, then hydraulic heads will be depressed, which may lead to low quality water percolating into aquifers. One example of this might be the increase in saltwater intrusion along the coastal areas (ocean and estuary alike), which will add up to the saltwater intrusion due to sea-level rise.

3.6.2   Domestic activities

Domestic supply is another pressure upon aquifers and can generate significant drawdowns. These add up to the already significant impacts of agriculture (cf. sub-chapter 3.6.1). The main domestic water supplier is EPAL, with the following well locations (APA, 2012): Carregado (8 wells), Concelho de Alenquer (3 wells), Quinta do Campo, Concelho de Alenquer (2 wells), Valada (5 wells), Cartaxo (15 wells), Espadanal, Azambuja (2 wells), Lezírias, Vila Franca de Xira (15 wells), Ota, Alenquer (6 wells), Alviela, Alcanena (Olhos de Água spring). Besides EPAL there are also other public water supply companies exploring the lower Tagus aquifers:

- Águas do Ribatejo
- Águas de Santarém
- CM Golegã
- CM Azambuja
- CM Seixal

and other municipal water suppliers, with the following main well locations: Barreiro, Mitrena, Montijo, Moita, Setúbal, Palmela, Benfica do Ribatejo, Almada/Seixal; adding to this, multiple private wells do exists.

EPAL and other domestic suppliers' wells are presented in Figure 3.11.

Estuary & areas prone to saltwater intrusion
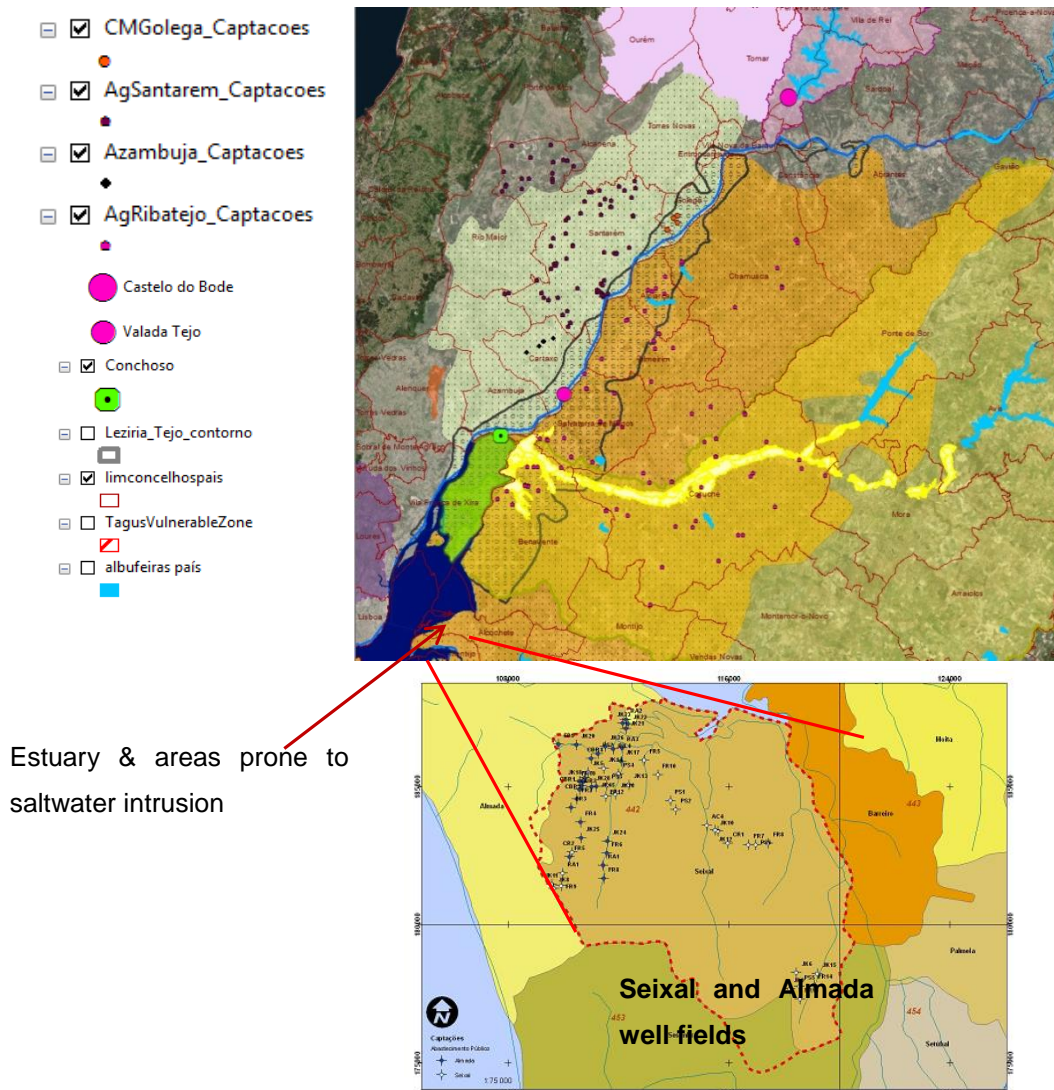
Figure 3.11 – Location of the main well fields for domestic supply in the case study area

Source: adapted from Rocha (2017) and Fialho (2009)

Groundwater abstracted for domestic supply has been estimated at 123.8 hm^3/year (Lobo Ferreira et al., 2011) and the abstraction values by aquifer are presented in Table 3.7.

Domestic activities also generate pollution loads, mainly through septic tanks and eventually some ETAR's discharging into the soil. The problem is particularly relevant in Tejo/Sado – Margem Esquerda aquifer, where several urban areas lack sewage treatment facilities and operational efficiency. The counties most affected are: Almada, Barreiro, Montijo, Seixal and Moita counties (Lobo Ferreira et al., 2011). Aluviões do Tejo also have this problem in Vila Franca de Xira county, from small villages scattered across the agricultural plain. The pollution loads estimated per aquifer are given in Table 3.8 (Lobo Ferreira et al., 2011).

Table 3.7 – Water demands supplied by groundwater (hm^3)

Aquifer	Volume
O26 – Ota-Alenquer	0.490
T1 – Bacia do Tejo-Sado/ Margem Direita	16.936
T3 – Bacia do Tejo-Sado/ Margem Esquerda	89.140
T7 – Aluviões do Tejo	17.194

Source: adapted from Lobo Ferreira et al. (2011)

Table 3.8 – Pollution loads due to domestic sources

Aquifer	N (kg/year)	P (kg/year)	Volume (m^3/year)
O26 – Ota-Alenquer	5	15	680
T1 – Bacia do Tejo-Sado/ Margem Direita	487	1338	60318
T3 – Bacia do Tejo-Sado/ Margem Esquerda	1086	918	44880
T7 – Aluviões do Tejo	33	98	4414

Source: adapted from Lobo Ferreira et al. (2011)

3.6.3   Industry

Although agriculture and domestic activities are the main water stressors in the case study area, industry is not to be discarded. This is particularly true in Tagus left margin and the riverine region from Póvoa de Santa Iria to Vila Franca de Xira, where heavy industry is or used to be located.

Industry in the case-study area often relies on its own private wells for water supply although other supply sources are used as well. Water demands supplied by groundwater have been estimated by Lobo Ferreira et al. (2011) at 20.4 hm^3/year. The amounts abstracted by aquifer are presented in Table 3.9.

These industrial centres have left a significant pollution load that often reached the underlying aquifers. One example is Siderurgia Nacional steel plant site, where groundwater was found contaminated with oils, grease, ammoniacal nitrogen and sulphates (Lobo Ferreira et al., 2011). SPEL (explosives factory) surrounding area is another example. At this site, contamination reached the upper and lower aquifers, apparently without much degradation of contaminants even after 50 years of their disposal in the soil (Amaral et al., 2009). This highlights the possibility that, at least in some sites, pollution can be long term, even after the shutdown of contaminant sources. Some of the most problematic sites in the case-study area are:

- Seixal – former steel plant (Siderurgia Nacional); hydrocarbonates due to harbour and shipyard activities; former explosives factory-SPEL (Lobo Ferreira et al., 2011).
- Barreiro – former CUF chemical plant and remaining industrial area (Zeferino, 2016).

Table 3.9 – Water demands supplied by groundwater (hm^3)

Aquifer	Volume
O26 – Ota-Alenquer	0.067
T1 – Bacia do Tejo-Sado/ Margem Direita	6.354
T3 – Bacia do Tejo-Sado/ Margem Esquerda	10.238
T7 – Aluviões do Tejo	3.721

Source: adapted from Lobo Ferreira et al. (2011)

The most important pollution loads associated with the main industrial centres of the case study area is presented in Table 3.10.

Table 3.10 – Pollution loads associated with industrial activities in the case study area

Aquifer	Industrial centre	Type of residues	Pollutants
T1 – Bacia do Tejo-Sado/ Margem Direita	Alcanena	Sludge (50,000 m^3)	Cr
T3 – Bacia do Tejo-Sado/ Margem Esquerda	Seixal: Steel plant*	Dust and metallic sludge, contaminated soils, oil residues (21,000 tons)	Fe, Zn, Mn, Si, Al, S, CaO_x, Cr, Cu, Ni, Pb, Zn, Hg, As, SO_4, NO_3, hydrocarbons & other organic compounds
	Seixal: SPEL & harbour facilities	Sludge & other dangerous wastes	Hg, Ni, Cr, Fe, Mn, Al, U, NT, DDT, TNT, hydrocarbons & other organic compounds
	Barreiro: CUF & industrial area	Sludge & other dangerous wastes (52,000 tons)	Organic & inorganic compounds, Zn & other heavy metals

Source: adapted from Lobo Ferreira et al. (2011)

On the whole, these aquifers have a large capacity to accommodate the water demands, although locally this might not hold true. Pollution problems due to saltwater intrusion and/or heads drawdown are spatially restrained and due to local overexploitation. Pollution due to agriculture is significant and of a regional nature, having prompted the definition of the Tagus Vulnerable Area due to nitrate contamination. Table 3.11 shows the exploitation rates by aquifer and Figure 3.12 the know wells used for supply of domestic, industrial and agriculture activities.

Table 3.11 – Exploitation rates of the aquifers

Aquifer	Exploitation rate (%)
	Lobo Ferreira et al.
O26 – Ota-Alenquer	86.0
T1 – Bacia do Tejo-Sado/ Margem Direita	37.2
T3 – Bacia do Tejo-Sado/ Margem Esquerda	38.3
T7 – Aluviões do Tejo	0.45%

Source: adapted from Lobo Ferreira et al. (2011)
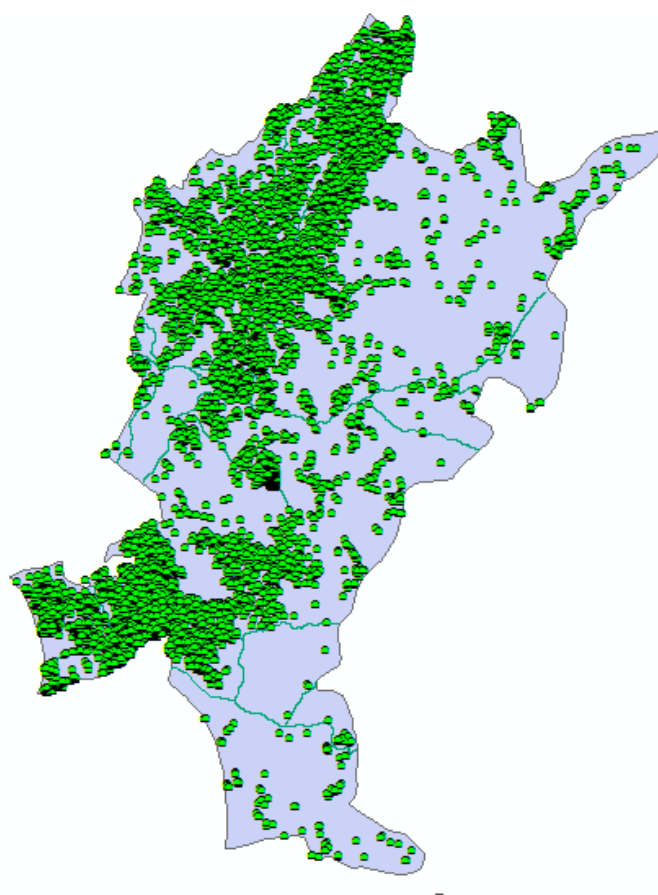
Figure 3.12 – Supply wells for agriculture, domestic uses and industry

4 | Climate change perceived threats in the case study area – the groundwater component

SIAM II study predicts for the long term horizons of 2050 and 2100 a temperature increase in all seasons for the whole Portuguese territory. The largest increases are predicted to occur in summer, ranging from 3ºC in mainland coastal areas to 7º C in inland regions, 1 to 2º C in Azores and 2 to 3º C in Madeira depending on the climate model used (Santos e Miranda, 2006; https://apambiente.pt/index.php?ref=16&subref=81&sub2ref=118&sub3ref=393). SIAM II also predicts a general precipitation decrease, strongest in summer but also in spring and autumn; for winter, some projections point to a significant increase, while others show a mild reducing trend (Santos et Miranda, 2006). The more recent study ClimAdaPT.local predicts an average annual precipitation reduction of 4 to 51% in 2100, with spring reductions between 9 and 66%, summer's up to 88% and autumn's between 6 to 50%; winter is the less predictable, with models' results ranging from a mild 6% increase to a 40% decrease (http://climadapt-local.pt/wp-content/uploads/2016/09/ficha_lisboa.pdf).

Historical observations confirm a rising temperature trend in line with the projections from the climate models of the above cited studies (Figure 4.1). As for historical observation in precipitation, there is no clear trend (Figure 4.1), although there seems to be a slight increasing tendency in autumn (cf. http://portaldoclima.pt/en/#).
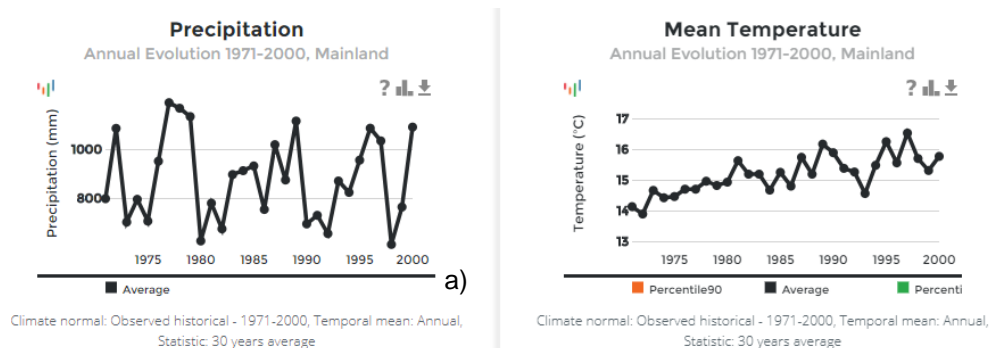
Figure 4.1 – Temperature and precipitation observed evolution on mainland Portugal

Source: IPMA (http://portaldoclima.pt/en/#)

This suggests a future hotter climate, with a slight tendency for autumn precipitation increase, which might lead to more intense autumn precipitation events in the coming years. Such temperature increase and possible precipitation regimes' shifts is bound to impact the water cycle, including its underground component. These impacts can be direct and indirect, and will change recharge, spring and other types of discharge (e.g. towards rivers), heads and water availability. Climate change directly impacts groundwater by three distinct phenomena: (1) changes in precipitation (amounts and time schedules) and temperature, which affect recharge; (2) sea-level rise, which mainly affects water quality in coastal aquifers; (3) recharge/discharge changes due to modifications of water levels/flow periods of surface waters. Indirect impacts are due to vegetation cover that naturally will change due to modifications on

precipitation and temperature – impacting mainly the processes of recharge, evapotranspiration and runoff – and those due to the human reaction to climate change. Human response to climate change, together with natural land cover change, discharges from rivers, etc. generate indirect impacts on groundwater. Such impacts might be positive or adverse for water quantity and quality. Increased temperatures are bound to increase water consumption and most likely groundwater abstraction. Recharge reductions due to precipitation decrease and temperature rise may occur, prompting water availability decreases, coupled in some cases with quality issues (e.g. saltwater intrusion due to sea level rise is increased due to heads' drawdowns). Farming adaptation such as changing cultures and pests will most likely lead to changes in: (1) water demands for present-day or new cultures, (2) crop development, irrigation and phytosanitary calendars and (3) pollution's phytosanitary nature and loads as well as new discharge schedules due to new pests or changes quality. in present-day pests' life cycle. All these changes will impact water abstraction volumes and pollution loads.

One of BINGO Project's aim is to better understand these impacts on water resources in the short term, to substantiate adaptation measures for the water sector. Climate models used in BINGO for the short term project precipitation and temperature increases, which results in recharge increases or decreases, depending on the temperature/precipitation outcomes of the climate models. Such recharge changes will impact water quality at least as far as saltwater intrusion is concerned. Precipitation and temperature changes will also impact river flow and water quality and this will have indirect impacts on groundwater recharge/discharge from/into rivers and its

4.1   Recharge and heads changes

Recharge changes means that the amount of water reaching the aquifer will change accordingly and lead to heads' changes. Such changes can be due to natural weather fluctuations, and then have a relatively short duration or, if due to climate change, they will show a sustained trend over a large period of time.

A sustained recharge decrease means less water reaching aquifers, inducing a hydraulic heads' falling trend. This will affect shallower abstraction wells – with some of them becoming dry, seasonally or permanently – and flows (1) between aquifers and surface water bodies and (2) between aquifers. This impact is more severely felt in small aquifers (once their storage capacity is limited) which react more intensely to recharge changes, in particular if residence times are very short (e.g. well-developed karst aquifers). In large aquifers, as those hereby studied, sustained recharge decreases are not expected to generate significant heads' drawdowns up to 2024. In fact, the recharge reduction to generate a significant drawdown is quite large and recharge projections up to 2024 do not achieve such high recharge losses. Nevertheless, where hydrogeological settings create small superficial aquifers (e.g. terrace deposits) recharge changes are readily expressed by water level changes, with impacts on the shallow wells usually used for local supply and small farming activities. If permanent heads' drawdowns will occur, owners might be forced to relinquish these wells for deeper ones, increasing the costs of water supply for these activities. On the long run (2050, 2100), the situation might become more severe

and then recharge reductions might be significant enough to lead to heads' drawdown trends in large aquifers.

Recharge changes will be due to precipitation changes but also to vegetation cover modifications prompted by climate change and farmers' adaptation strategies such as adoption of new cultivars to cope with the new temperature and precipitation conditions. These are aspects of climate change impacts still needing deeper research.

Abstraction rates, also due to climate change, are expected to increase due to rise of water needs in domestic, farming, livestock and industrial activities. This is due to higher temperatures prompting higher water demands but, in agriculture, such increases may also be due to an increased aridity of climate and a growing mismatch between the vegetative development of cultivars and wet periods. This may force farmers to increasingly rely on groundwater to water their crops. Under lower recharge conditions, this can lead to heads' drawdown trends. Such drawdowns – already observed in the case study area during the main irrigation period and worsening in protracted drought events – will not be uniform across the whole aquifers' area. This is due to the local hydrogeological characteristics and the local amount of abstraction. For this reason, some areas might be particularly prone to water availability and/or water quality problems. For example, in Tagus' estuary margins where abstraction rates are too high (or were high and the aquifers didn't recovered yet from such overexploitation), the ensuing heads' drawdowns created (or aggravated) saltwater intrusion issues (cf. Zeferino, 2016; Magalhães et al., 2013). Significant drawdowns near the main rivers may generate pollution issues due to infiltration from these water courses.

Recharge changes due to climate change for the period 2015-2024 have been computed from the 10 climate change realisations done by MiKlip under BINGO project for the whole area of Tagus lower basin (Oliveira, 2019). Most of these realizations point to a slightly higher precipitation average and a higher temperature which, coupled with the evolution of the other weather parameters influencing recharge, leads to an increased recharge in most realisations, quite large in some realisations as is the case for R1 realisation (Novo et al., 2018; Oliveira 2019). The recharge for the ensembles scenario illustrates this, as can be seen in Figure 4.2, orange bar. Recharge changes for the highest (R1), ensembles (R1_10) and lowest (R3) precipitation realisations are presented in Table 6.2. So, for most MiKlip's realisations, recharge will increase, which leads to higher heads and the possibility of more widespread groundwater floods[2].

---

[2] Groundwater floods = floods due, or exacerbated by, the rising heads due to high or protracted events of rain.
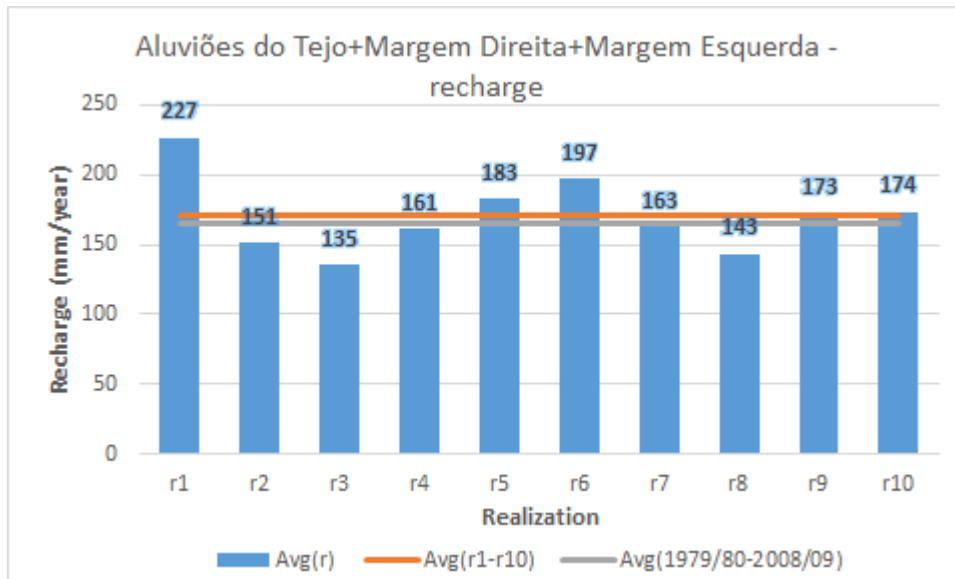
Figure 4.2 – Average recharge values for the 10 realisations of MiKlip

Source: Oliveira (2019)

4.2 Droughts

Droughts are extreme events that although inducing significant drawdowns, which depend on the length and severity of the drought in question, do not impact <u>permanently</u> the aquifer's functioning or its average water levels. By opposition, long term changes of average climate parameters will permanently change the average heads' surface and consequently the functioning of aquifers. This can be particularly expressive in karst aquifers. So, for aquifers, the most important issues concerning climate change are the climate normal changes and not the extreme events. In fact, after a drought, even if a severe one, the aquifers get replenished, more or less thoroughly, depending on the amount, duration and intensity of rains after drought. Nevertheless, if droughts become more frequent and severe, water levels might not reach the normal heights before a new drought sets in. Such situation might lead to a long term heads' drawdown, which will be further compounded by sharp abstraction increases, once the depletion of smaller surface reservoirs may prompt a shift to groundwater supply.

Under climate change scenarios, more frequent and severe droughts are predicted by ClimAdaPT.pt (http://climadapt-local.pt/wp-content/uploads/2016/09/ficha_lisboa.pdf). Similar predictions are made by IPCC (2013). Southern and south-eastern Europe are the most prone regions to drought hazard increase, with projected minimum river flows' reductions of up to 20% in 2020 and up to 40% in 2080 for the Portuguese territory (EEA, 2012). A study from Guerreiro et al. (2017) predicts an intensification of drought conditions in Tagus Basin by the end of the century, although the models disagree on the magnitude of these changes; while some predict a small drought increase, most project the occurrence of multi-year droughts that, in some model runs, can last up to 8 years by 2100. The same study predicts that in average 80% of the basin will experience extreme drought, by the same time horizon. EEA (2017) predicts a large increase in droughts for the Mediterranean region, including Iberia.

Observations of the recent drought evolution, namely the evolution of PSDI index from 1961 to 2000, show an intensification of drought frequency, in particular from February to April (http://www.ipma.pt/pt/oclima/observatorio.secas/pdsi/apresentacao/evolu.historica/) and a general increase in drought severity, in particular between January and April (Figure 4.3).

However, for the near term horizon (= 2024), MiKlip climate model realisations do not show any drought conditions' increase but quite the opposite, as referred in sub-chapter 4.1, the exception being Ota-Alenquer region, were precipitation is projected to decrease circa 10% (Oliveira, 2019). This might seem to fly in the face of recent experience in the Portuguese territory and the trends described on the above paragraph but this might be due to uncertainty problems and to the fact that models are a simplified representation of reality and might not correctly account for climate variability and other climate/land/ocean intricacies of the natural system. The drying trends observed might result from climate's natural variability coupled with climate change or the result of a faster climate evolution than that predicted by climate models. For the 10 years horizon, assuming MiKlip's model projections are correct, an increase in droughts is unlikely. Summers might however become drier, and will be hotter, so this will bear impacts on summer aquifer recharge.

Large aquifers such as those of the case study usually recover well after a drought. But if multi-annual droughts become frequent, a heads' decreasing trend might occur, leading to the abandonment or deepening of the abstraction wells. In aquifers with an already significant exploitation rate this can lead to a significant water budget imbalance and water availability reduction. Deepening the wells can lead to quality problems if they happen to tap into deeper aquifers with lower water quality.

Legend

	0.50 to 0.99: light rain
	0.00 to 0.49: normal (rain)
	0.00 to -0.49: normal (dry)
	-0.50 to -0.99: light drought
	-1.00 to -1.49: weak drought
	-1.50 to -1.99: weak to mild drought
	-2.00 to -2.49: mild drought
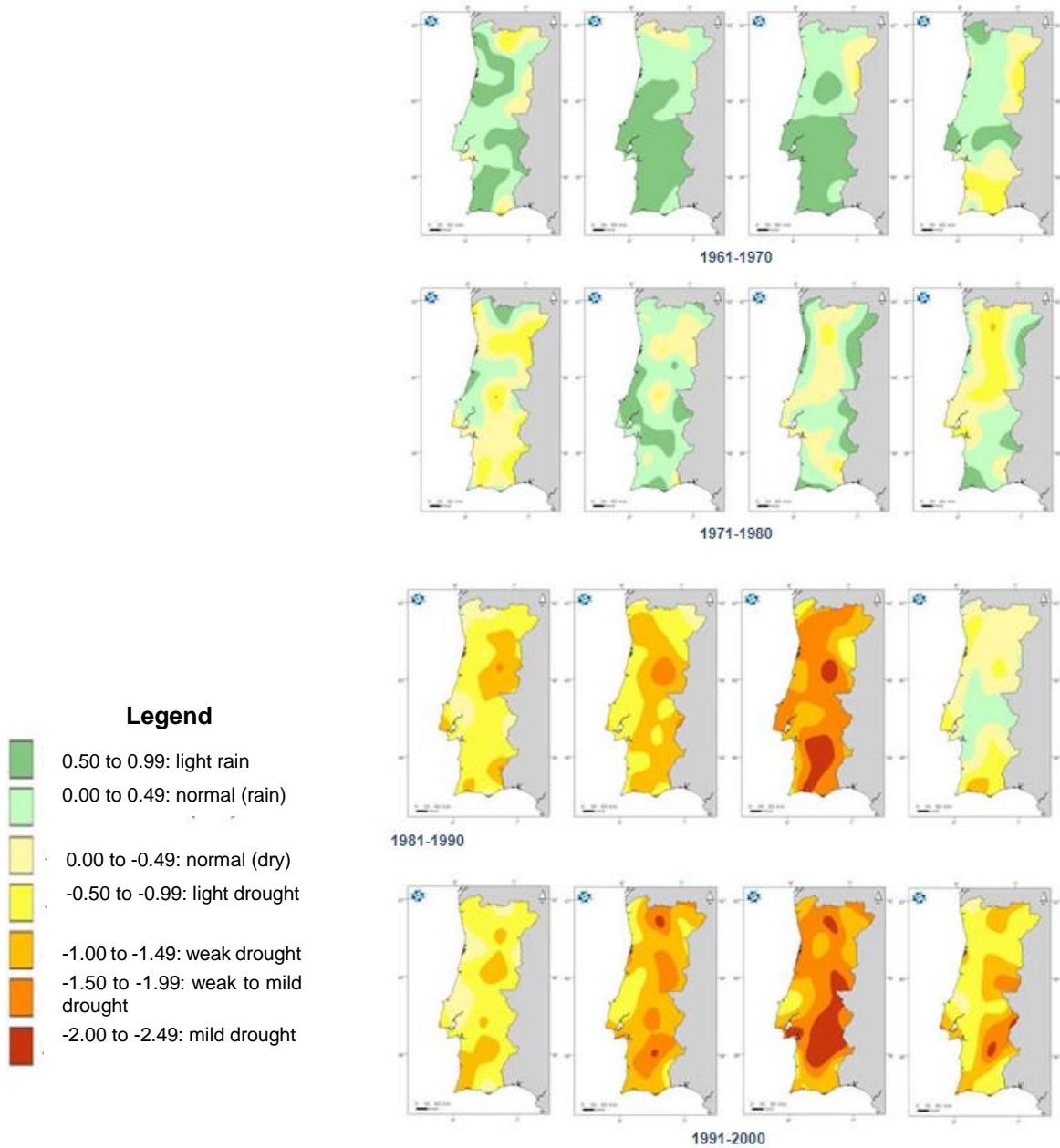
Figure 4.3 – Evolution of drought conditions in Portugal

Source: http://www.ipma.pt/pt/oclima/observatorio.secas/pdsi/apresentacao/evolu.historica/index_link.html?page=os_series_longas.xml

4.3   Floods

Floods generate quantity and quality impacts in shallow aquifers, although this issue has been seldom studied. They are a source of recharge as several studies show (Koeniger & Leibundgut, 2000; Ghazavi et al., 2012; Wang et al., 2015; WisContext, 2016) but at the same time they play a role in groundwater quality changes, either by diluting pollutants in the aquifer (Ghazavi et al., 2012) or by increasing pollution, depending on the local context (Wang et al., 2015; Sun et al., 2016; WisContext, 2016).

As for flood impacts in aquifer recharge, Wang et al. (2015) show that in 2013, in Sanjiang Plain, a groundwater levels' average increase of 1.24 m occurred during a 4-months long flood; the largest water level rises occurred near flooded rivers and shallow low permeability strata (Figure 4.4). This shows that groundwater levels' rise due to floods is a combination of infiltration rates coupled with local hydrogeological conditions. Koeniger & Leibundgut (2000) show a parallel evolution between the water level rise in Rhine river and the surrounding groundwater levels (Figure 4.5); the isotopic data prove that indeed water from the Rhine enters the aquifer during flood periods, while it is known that in non-flood periods the aquifer discharges into the river (1700 m^3/day*km). Ghazavi et al. (2012), in a semi-arid area of Iran, where for 3 years straight a constant heads' drawdown occurred, identified lower drawdowns in a flood spreading area of an ephemeral river that in areas further away.
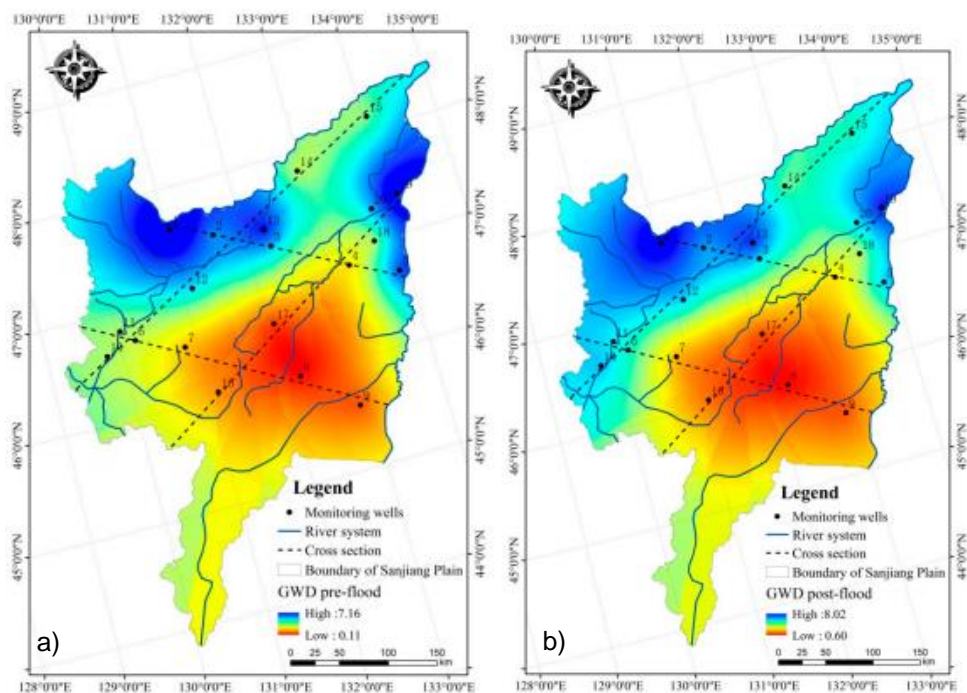
Figure 4.4 – Groundwater level changes due to 2013 flood in Sanjiang Plain, China: a) water levels pre-flood; b) water levels after flood

Source: Wang et al (2015)
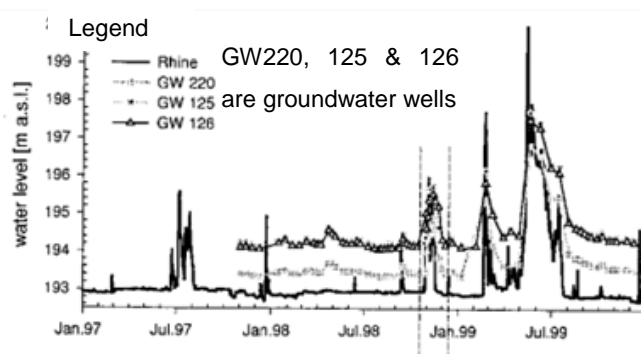
Figure 4.5 – Groundwater and Rhine river levels' changes during floods

Source: Koeniger & Leibundgut (2000)

Due to the relationship between floods and recharge above drawn, it is no surprising that quality issues are also part of floods' impacts on groundwater. For example, in an area near Beijing affected by a flash flood in 2012, floodwater introduced large amounts contaminants, including microbes into the aquifers, so affecting drinking water supply (Sun et al., 2016). Groundwater contamination due to floods is also addressed by WisContext (2016): after the floods of July 2016 in Wisconsin, residents relying on groundwater for private supply were advised that "*contaminants like bacteria and nitrate flow from the surface into groundwater supplies from farms, septic systems, and other sources, aided by rain and simple gravity, like the flash flood that inundated NW Wisconsin on July 10 only speeds up that process [of groundwater pollution]*". WisContext (2016) also warned "*well owners who observe flooding or changes in their water should assume their wells are contaminated, but wells in areas that don't show obvious signs of flooding could be in danger too*".

The detrimental or positive impacts floods may have on groundwater quality depends of a set of factors, of which the local conditions are the most important (cf. Wang et al., 2015). Positive impacts are shown by Ghazavi et al. (2012) who observed a reduction in electrical conductivity, SO_4^-, Cl^- and several other ions in the wells near the flood spreading area, when compared with those wells further away from it. On the detrimental side, flood's infiltration waters can carry into aquifers pollutants already in the soil, which might be particularly relevant in intensive farming areas. Adding to this is the capacity of floods to transfer pollutants to areas where they are not usually present, infiltrating them into aquifers along the way (cf. Chaturongkasumrit et al., 2013). Pollution transfer due to floodwater, in this case microorganisms, which ended up contaminating groundwater for human consumption is also reported by Sun et al. (2016).

Perhaps the most interesting work concerning the impacts of flooding in groundwater quality is that of Wang et al. (2015) which presents a case for the strong control of local conditions on the role (positive or negative) that floods have on groundwater quality. Near the Songhua and Heilong flooded rivers, chlorides and nitrates were reduced after flooding, while further away – which coincidentally is an area of intense agricultural activity, and so where contaminants build up in the soil – these same contaminants increased (Figure 4.6).
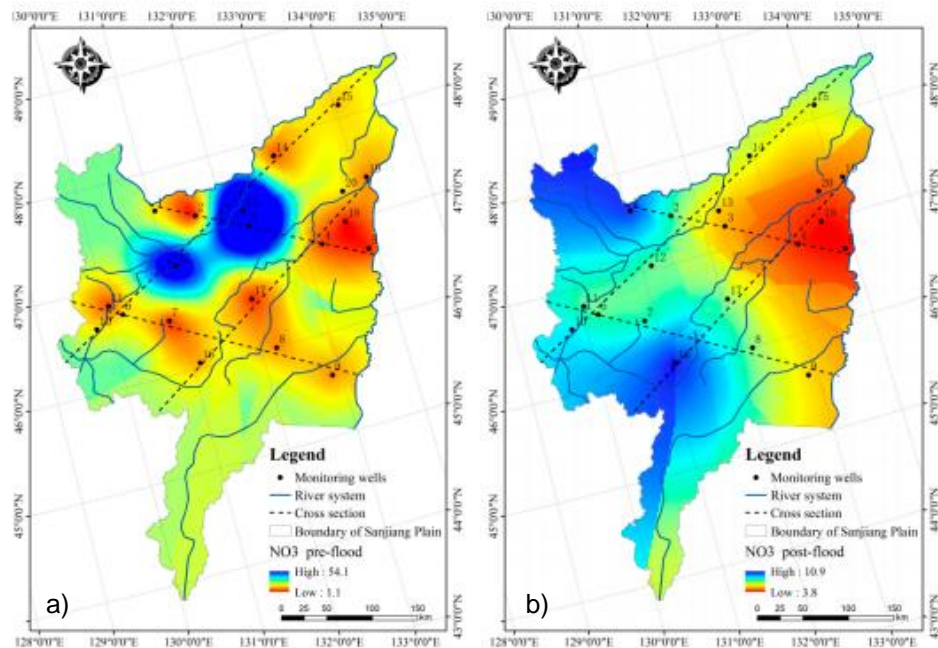
Figure 4.6 – Evolution of nitrates due to 2013 flood in in Sanjiang Plain, China: a) NO⁻₃ pre-flood; b) NO⁻₃ after flood

Source: Wang et al. (2015)

Historical flood trends' in Tagus river are poorly known in spite of the existing water levels' data, some series going back to 1900 (cf. SNIRH database). The long record of floods, particularly in Ribatejo, shows a region prone to floods, to the point that the local population had developed adaptations to cope with the more or less regular floods of the past. These floods can spread through a wide area, as was the case of the 1876 flood (known as the Great Flood) or the 1979 flood, the second largest on record and the largest of the XX century (Loureiro, 2009). Floods of such areal extent can transfer pollutants to areas far away for the pollution sources and this might be particularly important in Ribatejo, which is an intensive farming region, with industrial facilities as well. This might mean that pollutants usually not present in some infiltration areas might reach them through floods and infiltrate into the aquifers. Once quality impacts of floods on groundwater is largely unknown in the area, it is not perceived if pollution loads increase after a flood or if they show an evolution similar to the above described by Wang et al. (2015).

Flood trends under climate change scenarios are now starting to be addressed by adaptation studies such as ClimAdapt.pt or PMAAC-AML (2018). The first study tackling this issue was SIAM I, although it didn't exactly analyse the flood trends but the projected number of days with precipitation above 50 mm, for the temporal horizon in 2100 (Santos et al., 2002). Once daily precipitation shows a high correlation with runoff, flood risk was projected to have an increase or remain as today in Tagus basin (Santos et al., 2002). More recent studies at European scale show somewhat contradictory results, at least for the Iberian region. Kundzewicz et al. (2012) predict a larger recurrence period for the 100-year floods in this region, while EEA (2012) and Feyen et al. (2011) predict either an increase or a decrease of an actual 100-year flood's frequency for 2100 when compared with the reference period 1961-1990, depending on the climate models used. For the 10 years horizon of BINGO project (= year 2024), flood regimes

are not expected to change significantly, which means that its associated aquifer pollution and recharge should remain more or less the same as today. The exception might be flash floods due to more frequent events of intense rain.

Flash floods, due to their ability to destroy infrastructure and high erosional capacity, are particularly prone to quickly carry pollution downstream where it can be available for infiltration if the right infiltration conditions are met. Upstream, where damage has been done, pollution might enter the aquifers from wells and other destroyed structures. Given the increasing trend of this type of flood's frequency in the future throughout Europe (EEA, 2012), flash flood's impacts should increase. However and specifically for the Iberian region, EEA (2017) does not account for any impacts of flash or other types of floods (Figure 4.7). Still, EEA (2019), citing the study of Scocciomarro et al. (2015), states that such study "*suggested that future increases in intense precipitation events will be more pronounced at the sub-daily time scale over Spain and the western European seaboard*". This might point to a future increase in flash flood occurrences in the Iberian Peninsula.
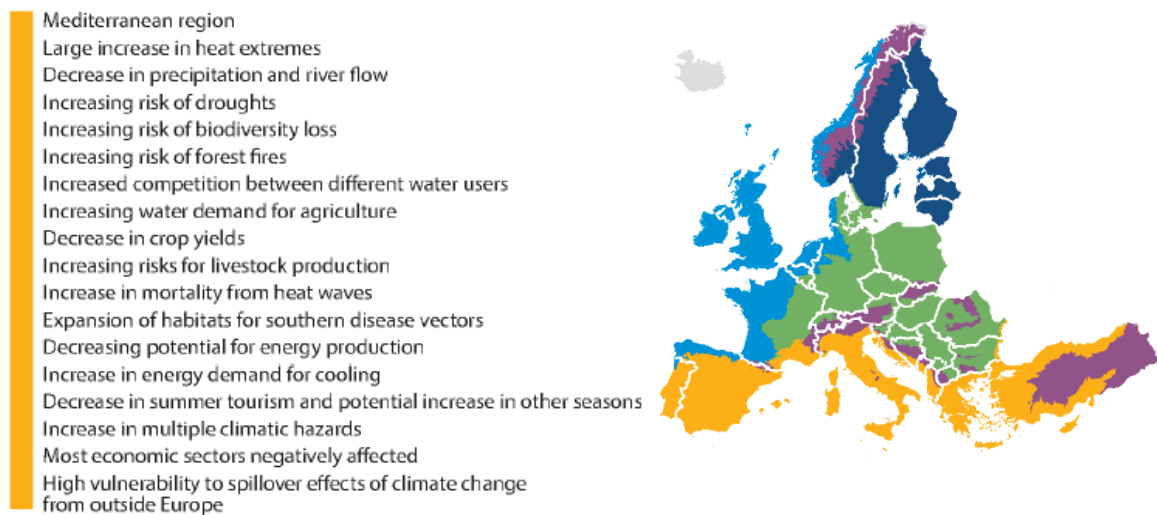
Figure 4.7 – Climate change impacts in the Mediterranean area

Source: EEA (2017)

4.4   Surface water flows and quality changes

Besides aquifer recharge modifications, climate change will also modify river flow regimes. If hydraulic connectivity between rivers and aquifers exists, such connectivity will suffer changes. For instance, if a river usually receives discharges from the aquifer but the hydraulic equilibrium between river and aquifer will change (e.g. due to long sustained decreased recharge, in particular if coupled with water abstraction increases) it may reach a point where the river becomes a recharge source for the aquifer instead of a discharge outlet. In rivers that seasonally alternate between discharge from and recharge into aquifers, climate change may change the length of recharge/discharge period and volume interchanged between river and aquifer. Such hydraulic connections are a migration route for pollution which can travel from river to aquifer and vice-versa. Once climate change also impacts water quality in

rivers and lakes due to the compounded effect of increased temperatures and longer dry periods (and probably also a larger share of farming and/or other pollution discharges), it's easy to understand that where water infiltrates from these water bodies into aquifers, groundwater quality issues might arise, if the vadose zone doesn't have enough capacity to remove pollution.

Increased water abstraction due to climate change can impact the river/aquifer hydraulic connections by sustainably decreasing the groundwater levels. In fact, water abstraction can do it even in absence of significant climate change stressors. For instance, before widespread exploitation of the alluvial aquifer of Tagus River, the aquifers used to discharge into Tagus (Mendonça, 1990; Mendonça, 2009), and they still locally do it into the minor streams of this river network (Oliveira, 2009). However, when aquifer's exploitation depressed enough the groundwater levels, Tagus became a recharge source for the shallow aquifer in the locations where drawdowns where larger. In this way it became another possible route for pollution to reach aquifers, although this process has been poorly studied in the area.

Present day conditions show a decrease of Tagus flow rates, mainly due to management strategies upstream the case-study area, coupled perhaps with present-day climate change effects. If runoff trends will follow the observed lowering trend of the past decades, then water quality issues may occur in rivers, lakes and ponds of the case study area. Water retention increase upstream, recharge reduction and increased water abstraction, will worsen pollution. And once heads are expected to decrease as well, due to reduced recharge and increased water demand, these quality issues will worsen further, once groundwater discharges into rivers will be reduced or even disappear in some cases, curtailing the dilution mechanisms associated with such discharges. Such larger heads' drawdowns, allowing for infiltration from rivers into aquifers, as it seems to be happening in large swaths of lower Tagus (Rodrigues, oral communication, 2017), will expand the vadose zone, which may help to degrade pollutants before reaching the aquifer. However, such thickness increase may not be enough to counteract the incoming pollution, in particular if the surface water bodies have an already larger pollution load, due to increased temperatures and oxygen depletion. The aquifers most prone to bear such adverse impacts are the shallow ones as is the case of Aluviões do Tejo.

Under climate change, a minimum river flow[3] reduction of up to 40% is expected in 2080 for the Portuguese Territory (EEA, 2012; Figure 4.8). SIAM II, although finding mixed trends for annual runoff in 2100, projects a reduction trend in spring, summer and autumn (Santos e Miranda, 2006). Specifically for Tagus, SIAM II projects summer runoff reductions of 5 to almost 75% in 2050, and up to 80% in 2100, depending on the models used.

---

[3] For a 20 years' return period, scenario SRES A1B and control period 1961–1990.

Figure 4.8 – Projected change in minimum river flow (return period of 20 years) in Europe

Source: EEA (2012)

For the BINGO project's time horizon of 2024, small changes in natural runoff are predicted once a slight increase in precipitation is coupled with an increase in temperature (ensembles scenario), promoting a slightly larger evaporation from surface water bodies. If such projections hold true, then adverse impacts will be due to water management upstream and groundwater management, namely near the rivers. These problems will be more acute during summer.

4.5   Sea level rise

The historical records for the 20th century show a mean sea-level rise along the Portuguese coast of 0.15 m (Antunes & Taborda, 2009), which is consistent with the global estimates for mean sea-level rise (Hagedoorn et al., 2007 in Guerreiro et al., 2015).

Sea level rise affect coastal aquifers due to saltwater intrusion generated by higher average sea levels. This affects aquifer functioning (e.g. modifying submarine discharges) and groundwater availability, and the areas where saltwater intrusion is already occurring due to overexploitation are particularly vulnerable. Coastal areas with low to moderate slope, as those of a significant part of Tagus estuary, are potentially more susceptible to this phenomenon.

Saltwater intrusion is further aggravated under aquifer recharge decrease, as projected by the long range climate scenarios, potentially spreading to a larger aquifer area than if sea level rise alone was at work. Under these worsened conditions, and depending on the well density, its distribution along the coastal area of the aquifer and their abstraction rates, the number of wells affected by rising salinization may increase.

To further worsen the problem, water demands are expected to increase under climate change and it is likely that groundwater abstraction might increase as a coping mechanism, particularly for agriculture which is likely to face lower precipitation in Spring and Summer (Santos e Miranda, 2006). Over-exploitation – which will increase due to the combined effect of lower recharge and higher water abstraction – will lead to upconing and saltwater intrusion migrating upwards (Figure 4.9), rendering impossible further exploitation of the affected well.
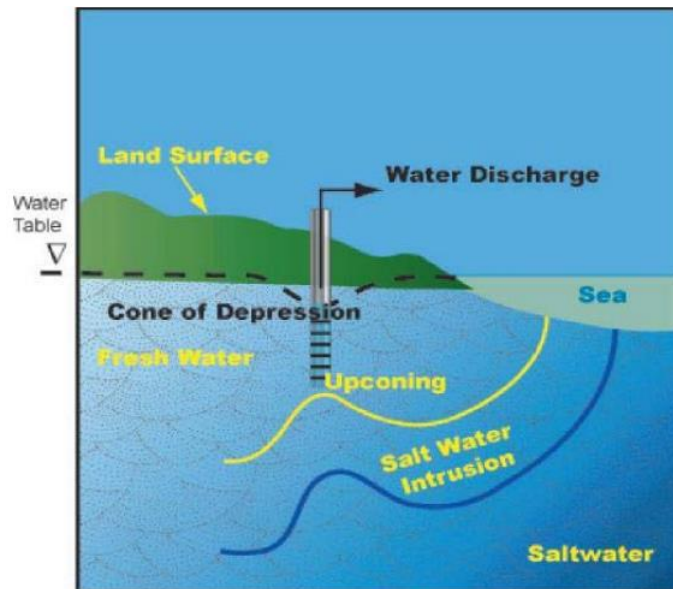
Figure 4.9 – Saltwater intrusion due to upconing

Source: http://www.mae.gov.nl.ca/waterres/training/adww/2015/04_Lynn_Pilgrim.pdf

Tagus estuary coastal region fosters important urban centres and a significant industrial and harbour activity. Such populations and economic activities are mainly supplied by groundwater in the estuary's south margin (cf. Cavaco e Benoliel, 1997; APA, 2012; Zeferino, 2016; PMAAC-AML, 2018) and in some areas such as Industrial Complex of Barreiro, saltwater intrusion is reported (Zeferino, 2016). Suspicions of the same phenomena in Seixal and Moita counties are reported by Simões (1998) and Almeida et al. (2000). In the south margin, where saltwater intrusion seems to be already occurring, the estuary has a wide tidal flat and low inland topography, which makes it highly vulnerable to saltwater intrusion due to sea level rise. The hydraulic connection between Tagus estuary and the upper aquifer and between upper and lower aquifers of Tejo/Sado – Margem Esquerda (Zeferino, 2016) further increases such vulnerability. To compound things further, strong heads' drawdowns in the lower aquifer created heads inversion with the upper aquifer. Due to this, the water from this aquifer (affected by saltwater intrusion) is reaching the deeper one (Zeferino, 2016). As a confirmation of this problem, some wells in the area have been abandoned due to salinization.

Under climate change, estuary functioning may also undergo modifications. Nowadays, the estuary saline tide goes up to 50 km upstream from the estuary mouth, reaching Vila Franca de Xira (Guerreiro et al., 2015). This means that a large shore area of Aluviões do Tejo aquifer is in contact with salt waters. Under climate change, due to sea level rise and particularly the expected Tagus reduced flow, the saline

tides may go further inland, so a larger area of this aquifer may be affected by saltwater intrusion. In fact, if sea level rise on itself will have little impact on salinity distribution along the estuary and upstream areas affected by it up to 2024 (Fortunato, 2018). Unlikely, if there are significant changes in Tagus flows, salinity can reach larger areas upstream (ibidem), exposing the riverine aquifers' areas to saline river waters. BINGO project projections for 2024 do not point to significant runoff changes. If sea level rise will not induce changes in estuary's salinities and runoff modifications due to climate change will be minimal, the Tagus flow reductions will be due to upstream management practices. So, surface water management upstream is perhaps the most important factor on salinity impacts at downstream aquifers' riverine areas.

Sea level at Cascais station has risen 4 mm/year (Antunes & Taborda, 2009), which means a 0.4 m rise in 2100 if there wasn't a sea level rise acceleration. Predictions of global sea-level rise for the 2000-2023 range 11 cm (Nauels et al., 2017 in Fortunato et al., 2018), which is a faster rate than the one observed at Cascais station. Taking into account the observed sea level rise in the Portuguese coast, Guerreiro et al. (2015) assume, for the Tagus estuary, 2 mean seal-level rise scenarios: (1) a 0.5 m sea-level rise (best estimate scenario) and (2) 1.5 m sea-level rise (high end scenario). The best estimate scenario agrees with IPCC (2013) projections of global mean sea-level rise between 0.26 and 0.98 m. As shown by Ferreira (2012) using mathematical modelling, a 1.5 m sea-level rise scenario can significantly increase saltwater intrusion along the narrow coastal area from Trafaria to Cabo Espichel. In that study, a saltwater interface advance of 20 m inland may occur under a climate change scenario of 42% precipitation reduction and 1.5 m sea level rise. No studies have been conducted yet, concerning aquifer's saltwater intrusion along the estuary and the river upstream up to Vila Franca de Xira, for the 1.5 m sea level rise scenario.

Sea-level rise implies more frequent marine floods and, for the Tagus estuary, this will be exacerbated by the increased tidal amplification due to resonance, with maximum water levels projected to increase by 4 to 7 cm, for the high end scenario (Guerreiro et al., 2015). As such and according with Guerreiro et al. (2015), salt-wedge intrusion in the estuary will increase by 2100, and this may further promote aquifer saltwater intrusion. Storm surges – which do not significantly impact the aquifers once these are very short duration phenomena – are not expected to change significantly (Fortunato et al., 2017; 2018; Rodrigues & Fortunato, 2017).

5 | Aquifer model description

To evaluate the impact of climate change on aquifer behaviour and groundwater availability, a mathematical model was developed using FEFLOW, based on a conceptual model that tried to simplify the hydrogeology and the hydraulic connections between surface water bodies and aquifers. Recharge changes and water abstractions were also addressed in the conceptual and the resulting mathematical model.

5.1 Conceptual model

The sedimentary basin were Tagus aquifers are located is a thick, complex succession of sands, silts and clay layers and lenses of Miocene, Pliocene and Holocene age and at the bottom, a mainly sandy-calcareous Miocene sequence (Almeida et al., 2000). This litho-stratigraphic succession is affected by faults and, in Peninsula de Setúbal, a synclinal-like structure associated with Arrábida Hills. A clay impervious layer sets the boundary between recent (alluvial and terraces' units) and Pliocene formations, both of them being sandy deposits interbedded with layers and lenses of silts and clays. Such clay deposits control, to a certain extent, the vertical flow between the different water-bearing units of these formations (Simões, 1998; Mendonça, 1990; 1996). Miocene formations are somewhat separated from the overlying Pliocene by discontinuous clay deposits. This allows some vertical water flow between Miocene and Pliocene aquifers (Simões, 1998). The lower Miocene formations are marine calcareous sands and marls and usually bear lower quality waters. In Peninsula de Setubal this lower calcareous sequence is isolated from the above sandy-silty-clay sequence by tick marl deposits (Almeida et al., 2000).

Due to this geological setting, **the aquifer structure** of the area is a complex spatial succession of water bearing units intertwined with aquitards and impervious deposits. Miocene, Pliocene and Alluvial deposits are separated by aquitard zones and, as far as Miocene is concerned, in at least some areas in the basin, also by an impervious zone between the deeper marine calcareous formations and the shallower sandy units. Figure 5.1 presents a simplified hydrogeological interpretation of the aquifer structure.

Tectonics also play a role in controlling water flow between different aquifer units but the information concerning such role is quite scarce and almost not possible to translate accurately in the mathematical model. This is due to the scarce information about the hydraulic behaviour of these fractures and the difficulty to represent such structures in a regional mathematical model at the scale used for the case-study area. For instance, the Tagus Fault, covered by the alluvial deposits, and said to run underneath Tagus River vestibular area, is assumed to be a frontier between Tejo/Sado – Margem Esquerda and Tejo/Sado – Margem Esquerda (Lobo Ferreira et al., 2011). However, the knowledge of its functioning (as a barrier or otherwise) is extremely scarce. This is the main reason why, in the conceptual and

mathematical models, faults are not considered and Tejo/Sado – Margem Direita and Margem Esquerda aquifers were simulated as one large aquifer, in spite of some differences in their lithological build up.
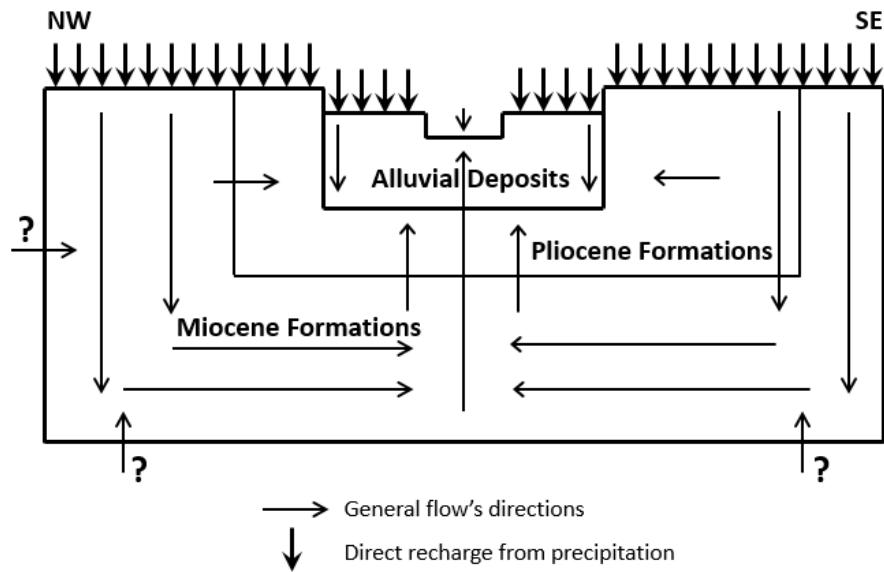
Figure 5.1 – Conceptual model of aquifer behaviour

Source: Mendonça (2009)

Hydraulic connection between river network and the aquifers seems to occur, considering the water budget of the aquifers (Oliveira, 2009; Lobo Ferreira et al., 2011). Under natural conditions Tagus was the main discharge zone for regional flow and the small streams and creeks still function as the main discharge zones for local and semi-local aquifer's flows (cf. Figure 3.9; Oliveira, 2009). Although heads and river water levels provided by SNIRH don't allow an exact identification of the places and volumes of Tagus River and its main tributaries discharges into the aquifers, there is indirect indication that Tagus is truly discharging into them, under todays' aquifers' exploitation. Even if river discharge locations were known, the hydraulic parameters of the riverbed are unknown, which hinders the correct simulation of this process.

The estuary is connected with the aquifers and this is expressed in several saltwater intrusion situations, mainly on the Tejo/Sado – Margem Esquerda aquifer (cf. Zeferino, 2016). The sea/aquifer connection along the coastal area from Trafaria to Cabo Espichel (W border of Peninsula de Setúbal) is less clearly understood, once salinization spots identified there can be due to saltwater intrusion but may also have other explanations (Ferreira, 2012).

Aquifer recharge is mainly direct recharge from precipitation. Recharge from water supply systems leakages in urban areas is also a component of the total recharge but its volumes have not been thoroughly evaluated, except on specific regions of the case-study area. One of these regions is Peninsula de Setúbal, where water recharge from urban water supply losses was estimated at 19 hm³/year (HP, 1994). This is almost certainly an outdated value for present-day reality. Recharge due to irrigation losses, as for urban water supply losses, has not been estimated for the whole case-study

area. Some estimates have been made for Peninsula de Setúbal, giving values of 12 h^3/year (HP, 1994). For the remaining aquifers' areas, recharge due to irrigation or other water sources losses is unknown.

As for **discharges**, 87% of the whole volume of water circulating through Aluviões do Tejo aquifer is discharged into the river network, while 3% is discharged into Tagus estuary and 7% is discharged by springs outside the river network (adapt. Mendonça, 2009).

Water abstraction is presented in Table 5.1, were values refer to the sum of abstractions for each category of water uses (domestic, agriculture, etc.) by aquifer.

Table 5.1 – Recharge, water abstraction and exploitation rates of the case study aquifers

Aquifers	Average recharge (hm^3/year)	Abstraction (hm^3/year)	Exploitation rates (%)
Bacia do Tejo – Sado / Margem Direita	172,65	98,308376	56,94%
Bacia do Tejo – Sado / Margem Esquerda	1090,956749	378,541046	34,70%
T7 - Aluviões do Tejo	220,4167133	124,316	56,40%

Source: adapted from Lobo Ferreira et al. (2011)

After a simplification procedure of the above information to select which knowledge was fundamental and could be translated into the mathematical model, the conceptual model **assumes a hydraulic continuum between Tejo/Sado – Margem Direita and Tejo/Sado – Margem Esquerda aquifers**. This option was chosen once hydraulic data is lacking for Tagus fault, which is assumed to behave as a barrier between the 2 aquifers, making its representation not possible in the mathematical model.

Vertically the 3 aquifers under study can be described **by a 3-layered model**:

- *Layer 1* – Aluviões do Tejo aquifer (alluvial deposits). It is a free aquifer and recharge is direct precipitation.
- *Layer 2* – Pliocene deposits of the Right and Left Margin aquifers. It is an intermediate aquifer, between Aluviões do Tejo (on top) and Miocene deposits (at bottom). It is a free to semi-confined aquifer. Pliocene deposits usually have lower transmissivities and porosities than the alluvial materials (Almeida et al., 2000). Recharge is due to direct precipitation, eventual leakage from the alluvial deposits or, on some over-exploited areas, discharges from Miocene formations (Mendonça, 1993).
- *Layer 3* – Miocene sediments of the Right and Left Margin aquifers. Represents the lower aquifer, which is confined but with unconfined areas (mainly at the border of the sedimentary basin). This aquifer has 2 very distinct regions: an upper detritic, with transmissivities significantly inferior to those of the lower detritic/calcareous marine deposits. Hydrochemistry is also different from the upper detritic and lower marine deposits. Recharge comes from leakage from Pliocene formations but the outcropping areas also supply direct recharge from precipitation.

Horizontally the layers' tops are defined as:

- <u>Layer 1</u> – the Tagus alluvial deposits' outcropping area surface.
- <u>Layer 2</u> – the Pliocene deposits' outcropping area surface and, in the region where these are under the alluvial deposits, the bottom of Layer 1.
- <u>Layer 3</u> – once Miocene deposits are essentially covered by the alluvial and Pliocene deposits, its top is the bottom of Pliocene (and alluvial formations where Miocene directly contacts with them) and, on the areas where these formation outcrop, the topographic surface.

The bottom of the model is the surface defined by the bottom of all the boreholes with known data. **The bottom of each layer** is defined by the bottom of the oldest lithology as recorded in boreholes' logs, for respectively the 3 main formations: alluvial deposits, Pliocene and Miocene. For the alluvial deposits this is the bottom of a conglomerate deposit overlaying a thick clay unit of wide spatial continuity.

The layers are deemed lithologically and hydraulically **heterogeneous**. **The vertical flows between aquifers** are upward or downward depending on over-exploitation conditions. **Such flows leak** through the semi-pervious layers at the bottom of Layer 1 (alluvial formations) and Layer 2 (Pliocene formations). At a regional scale, **the horizontal flows** are from the borders of the basin towards the Tagus River, located at the basin's centre.

The **hydraulic heads** generally follow these rules:

- <u>Aluviões do Tejo</u> (Layer 1), Pliocene and Miocene outcropping areas (in Layer 2 and 3 respectively) – the water levels follow the topography. In the alluvial deposits, water levels range from 1 to 5 m deep but there are locations of confinement in some downstream areas where, before exploitation, artesian behaviour could occur. Pliocene and Miocene outcropping areas show a water level's continuum with alluvial formations.
- <u>Pliocene</u> (Layer 2) - when underneath the alluvial deposits, the Pliocene (intermediate aquifer) becomes confined and such confinement lead to artesianism, with water levels above those of the alluvial deposits, under no abstraction (= natural flow conditions).
- <u>Miocene</u> (Layer 3) – Miocene is mainly confined, and its water levels (under natural flow conditions) were usually higher than those of overlying Pliocene and alluvial aquifers. Miocene has 2 aquifer units: the lower aquifer unit (calcareous formations) has higher water levels than the upper unit (sandy formations). However, and once there is not enough data to characterize the hydraulic heads distribution throughout the basin for the upper and lower Miocene aquifer units, a simplification was used, where both units were deemed (and simulated) as one.
- <u>Tagus basin's central area</u> – this is the area where the alluvial deposits (= Aluviões do Tejo aquifer) are located and is the main discharge area of the whole basin's aquifer system. Under natural conditions the water levels were as follows: alluvial deposits < Pliocene < Miocene. In the remaining areas of the basin, the relationships between water levels are more changeable but, conceptually, it was assumed a tendency for Miocene heads to be higher than those of the Pliocene.

Rivers are in hydraulic connection with the uppermost water bearing unit. This means that river etwork is hydraulically connected with the alluvial deposits and, in Pliocene and Miocene outcropping areas, with their shallower water bearing units. In Pliocene and Miocene outcrop areas, the river network usually receives the aquifers' discharges. Under natural conditions (no abstraction) Aluviões do Tejo discharged into Tagus and Sorraia Rivers (and Valas de Alpiarça and Azambuja). Under the same conditions, Aluviões do Tejo used to receive discharges from Pliocene aquifer, and this aquifer received discharges from Miocene aquifer. Tejo and Sorraia functioned as discharge zones for the whole basin's aquifer system. However, due to overexploitation, this natural flow is modified and, in the overexploited areas, Tagus River discharges into Aluviões do Tejo. Overexploitation also locally inverts the natural flows between Aluviões and Pliocene and between Pliocene and Miocene aquifers.

Aluviões do Tejo and Pliocene aquifers also have **hydraulic connections with the estuary**. This is illustrated by heads' oscillations due to tidal effects. Under natural flow, aquifers' upper units discharge into the estuary. However, overexploitation in southern estuarine border allows for saltwater intrusion (e.g. in Margueira, Cachofarra, Porto Alto, Malhada, Alcochete, Barreiro, Mitrena and Praias do Sado; cf. Mendonça, 1993; Simões, 1998; Almeida *et al.*, 2000; Ferreira, 2012; Zeferino, 2016).

Aquifer recharge was considered as only the direct recharge due to precipitation. This is due to the lack of good quantification of other types of recharge, in particular as its areal distribution variation is concerned.

5.2   Mathematical model

Mathematical modelling was used to assess the impacts of climate change upon aquifers' water levels and flow. The type of mathematical modelling chosen was finite-elements once this type of model is able to simulate water flow and pollutants propagation where density differences between pollutants and groundwater play a major role in their propagation. For BINGO case study, it was initially expected that saltwater intrusion would be simulated along the estuarine border – where some of these problems already occur – and upstream up to where tidal salinity influence was observed in Tagus River. Density differences between groundwater and saltwater from the estuary are a major driver of saltwater intrusion.

FEFLOW is a finite-element computer program from DHI-WASY GmbH, able to simulate regional problems with a high number of elements. It can simulate interactions between rivers and aquifers, saltwater intrusion, saturated and unsaturated flow, multi-species mass transport (pollution problems) and transport controlled by fluids' density effects and chemical kinetics, amongst other groundwater issues. For this reasons, it was chosen for modelling BINGO case study.

5.2.1   From conceptual to mathematical models

The conceptual model is translated into the mathematical model in a step-by-step procedure, were increasing complexity is added once the model has performed well in the more simplified conditions. In the present case, the evolution of the model follows the following steps:

- **Step 1: Geometrical data input into the model and construction of the mesh** –topography data, aquifer limits, depth and thickness of the layers and river network are introduced into the model. These data are used by the model to generate the mesh. These must be in accordance with the conceptual model.

- **Step 2: Hydraulic, recharge and boundary conditions set up** – after mesh generation, vertical and horizontal hydraulic parameters and recharge data are input into the model. Boundary conditions are also input into the model. Head boundary conditions h = 0 m (representing present day sea level) were defined for the coastal area and h = topography for rivers, once there was not enough data to set a fluid transfer boundary condition. Aquifer limits, where eventual hydraulic connections with the surrounding lithologies are suspected to occur, were represented by fluid flux boundary conditions. At least a head boundary condition must be defined, otherwise the model will not run. Observation points, required for model calibration, should also be input at this stage.

- **Step 3: Steady state flow model, natural conditions** – the model has no pumping wells, recharge remains constant throughout the whole simulation period. If unknown head relationships between rivers and aquifers, such interactions can be approximately simulated by boundary conditions h = constant = topographic height at each mesh node representing the rivers.

- **Step 4: Model calibration** – the model is run and for the first tests it might be possible it will not converge. Refinement of the mesh – horizontally (adding more mesh elements) and vertically (subdividing the initial layers into a larger set of thinner layers) – might be required. Eventually, boundary conditions may also need revision. When the model converges, the error between observed and simulated heads is most likely to be large. This error must be reduced by modifying the hydraulic parameters and recharge estimates until achieving the best fit possible between observed and simulated heads.

- **Step 5: Wells data input** – once the model is calibrated for permanent state, natural conditions (= no groundwater abstraction), data concerning the pumping wells (average flow rates and, whenever known, water abstraction depths) are input into the model, using wells boundary condition; well depths, screening depths (if these are unknown, a full penetrating well must be set up) and pumping rates are mandatory. It might be required to aggregate wells once the model only allows for 1 well per mesh element. For the case study, the average pumping rates for the 1979-2009 (historical period) were used.

- **Step 6: Steady state flow model, pumping conditions** – all the data to simulate the historical conditions are now set in place and although the model has been calibrated for natural flow, after the introduction of these new stressors (= pumping wells), it might require new calibration or even might not be able to converge and crash. In any case, the model will need to be recalibrated. Flow models are the basis to understand aquifer response to any stressors and any transport models are built upon the flow models.

- **Step 7: Recalibration of the model** – if the model will not converge, refinement of the mesh and/or changes in the hydraulic properties, at least in problematic areas, might be necessary. If

the model does converge but the error of observed vs. simulated heads is large, then hydraulic properties must be modified at least in the most problematic areas until a fair agreement between observed and simulated heads is achieved.

- **Step 8: Running for climate change scenarios** (permanent flow) – once the model was calibrated, it was run for 3 scenarios: a high recharge (R1), average (R1_R10) and low recharge (R3). Comparing the heads under historical period pumping conditions with those of each recharge scenario, which is associated with specific climate projections, illustrates the impacts of climate change upon the aquifers.

- **Step 9: Transient flow model** – the model should by now be running with monthly recharge and pumping rates for the 1979-2009 period. However, from the lack of monthly data concerning pumping, the model had to run in a "semi-transient" fashion, where constant pumping rates and recharge were set for specific time periods (1, 3 and 5 years). Lack of data concerning monthly average river stages also further hindered the development of "full-transient" simulations.

- **Step 10: Running for drought scenarios** – this was done for 3 drought scenarios: 1, 3- and 5-years' drought length, which average conditions were those of the 2004/2005 drought (a severe protracted historical drought). Comparing the heads for the pumping conditions in the historical period (permanent state model) with those for each drought length identified the impacts of drought across the whole aquifers' extension.

- **Step 11: Recalibration of the model** – this wasn't necessary for the present case study.

- **Step 12: Transport data input** – at this stage, data concerning the type and number of pollutants, location of the pollution sources, concentration and pollutants' densities should be input. These are the basic data to run transport models.

- **Step 13: Transport model** – originally this was planned to simulate saltwater intrusion in the aquifers, due to sea level rise and recharge changes. A steady state approach would be developed simulating first the 1979-2009 historical period, after model calibration. Then, the model would run for sea level rise at the end of 2024. Comparing the results of both simulations, saltwater intrusion evolution can be analysed. However, due to very scarce groundwater salinity data along the coastal areas for the historical period, this model could not be implemented.

The data required to build the mathematical model has different typologies and must be arranged into a congruent package that the mathematical model can work with. Topography, layers' top and bottoms and river network data were input as shapefiles. Hydraulic properties and recharge can be input also by shapefiles or manually, thorough the definition of distinct areas, each one with constant values set up manually. Hydraulic heads can be defined by shapefiles, or by single values input manually for each layer or for different uniform areas manually defined in the model. Wells data (location, depth, pumping rates) can be input by Excel or shapefiles. Observation points can be input manually or by shapefile. Boundary conditions were input manually for each node where such conditions occurred. Temporal variations of recharge and pumping rates where unknown, so they were not used. Transport parameters were manually input as single values.

5.2.2   Data requirements

Data used to build the mathematical FEFLOW model are:

1. **For model geometry**:
   - *Coordinate System* – the coordinate system used for all georeferenced data is ETS89.
   - *DTM* – defines the upper boundary of the model (aquifer top). MDT shapefile was obtained from the 2011 Tagus Watershed Management Plan database.
   - *Horizontal limits of the model/aquifers* – result from the reworking of the shapefiles with the geographical delimitations of the 3 aquifers under study (Aluviões do Tejo, Tejo/Sado – Margem Direita and Tejo/Sado – Margem Esquerda). The shapefiles were obtained from 2011 Tagus Watershed Management Plan database.
   - *River network* – defines the set of nodes in the model where boundary conditions for rivers (= their interactions with aquifers) are defined. Shapefile obtained from 2011 Tagus Watershed Management Plan database and further treated by BINGO team for error correction.
   - *Top and Bottom of aquifer layers* – they result from the interpretation of boreholes' data from Simões (1998) and data collected for 2011 Tagus Watershed Management Plan, partially presented in Lobo Ferreira et al. (2011). The analysis of this data led to the identification of certain lithological units as the basal formation for each of the 3 layers of the conceptual model: Alluvial deposits (Layer 1), Pliocene (Layer 2) and Miocene (Layer 3). How this interpretation was translated into the mathematical model is explained in chapter 5.3.2.

2. **For hydraulic parameters**:
   - *Hydraulic conductivity, Porosity, Specific storage* – initial shapefiles for these parameters were generated with values from 2011 Tagus Watershed Management Plan (APA, 2012) and related bibliography (Lobo Ferreira et al. 2011; Heat, 1983). These were subsequently manually modified during model calibration.

3. **For heads and recharge**:

   Recharge – the shapefile for <u>historical recharge</u> was produced for 2011 Tagus Watershed Management Plan using model BALSEQ_MOD (Lobo Ferreira et al., 2011). During calibration procedures, the historical period recharge was reduced to half of its original estimation. <u>Recharge under climate change scenarios</u> was calculated for the 2015-2024 period using BALSEQ_MOD and precipitation as well as other climate normals (required for evapotranspiration estimation) produced by MiKlip climate model. The analysis of climatological data produced by MiKlip and recharge estimation for the different climate projections generated by MiKlip is reported in Oliveira (2019). The data required for recharge evaluation, were:

   - *Precipitation* (daily values): (1) for Aluviões do Tejo and Margem Direita aquifers, the precipitation series period was 1/10/1979 - 30/09/2009; (2) for Margem Esquerda aquifer it was a 1/10/1980 - 30/09/2009 series.

- ▪ *Evapotranspiration* (reference evapotranspiration): monthly values defined for 1/10/1979 - 30/09/1998 time series for Aluviões do Tejo and Margem Direita aquifers; for Margem Esquerda time series period was 1/10/1980 - 30/09/2009. From 1988 up to 2009, the monthly values were assumed as equal to the average values for the respective month in 1/10/1959 - 31/9/1988 series.
- *Initial heads* – these were plain single values, one for each hydrogeological unit (Alluvial deposits, Pliocene, Miocene), directly input into the model and no shapefiles were required. The values used are given in Table 5.2.

4. **For water abstraction and model calibration**:

- *Observation wells* – these are required for model calibration and were input into the model by shapefile. It includes well location and observed heads in each well, from 2011 Tagus Watershed Management Plan and CCDR-LVT databases. Observed heads' report to 1980-2009's period.
- *Abstraction wells* – the shapefile was built from wells' reports in APA databases (collected for 2011 Tagus Watershed Management Plan), INSAAR, EPAL and CCDR-LVT[4] databases.

5. **For sea level**:

- *Average sea level* – the data is a numerical value, set up at each node of the estuary and sea boundaries of the model. The data is from the work performed by Fortunato et al. (2018) and Antunes & Taborda (2009). For the historical period it is set at 0 m, and for 2024 (sea level rise impact analysis) is set as the sea level predicted by these authors for that year, taking into account the sea level rise rates.

6. **Transport parameters**:

- *Dispersivity, Molecular diffusion* – due to the lack of data for these parameters, average values were those found in bibliography (Schulze-Makuch, 2005; Bjerg, 2008; DHI, 2014), for the average hydrogeological characteristics of the alluvial, Pliocene and Miocene deposits.
- *Density ratio* – value is given by model bibliography (DHI, 2014).

7. **Salinities**:

- *Initial concentration* – aquifer salinities' data should come from monitoring data but these are quite scarce, which hindered the development of the transport model. Sea water salinity is given by bibliography and estuary salinity distributions were defined by Fortunato et al. (2018).

Table 5.2 presents the data types and their respective input files, as required by the model.

---

[4] Database on licensed abstraction wells

Table 5.2 – Data and its respective input files for FEFLOW model

Data type				File /Data
MDT = top of the model				Slice 1.shp
Horizontal limits of the model				limite_modelo 3b.shp
River network				Rios_principais9C.shp
Aluviões do Tejo (Layer 1) bottom				Slice 2.shp
Pliocene bottom				Slice 3.shp
Miocene bottom = bottom of the model				Slice 4.shp
Hydraulic conductivity				Camadas_K (initial file).shp
Porosity				Porosidade (initial file).shp
Specific storage				specific_Storage (initial file).shp
Recharge	Historical	Annual		REC_BINGOsemO26.shp
	Climate change scenarios	Annual	Drought	REC_PGRHTejo2004_5.shp
			Realisation 1 to 10	REC_BINGOsemO26.shp
Initial heads	Alluvium			0 m
	Pliocene			5 m
	Miocene			10 m
Observation wells				piezo_pocos_sem_lixo44.shp
Abstraction wells				vertices_malha_elevation_top_bottom_semBC_Vol_capt4_comEPAL_DISTOHUB_Stats_v4.shp
Average sea level rise				4 cm (in 2024)
Dispersivity	Longitudinal	Alluvium		5 (initial value)
		Pliocene		3 (initial value)
		Miocene		1 (initial value)
	Transverse	Alluvium		0.5 (initial value)

Data type		File /Data
	Pliocene	0.3 (initial value)
	Miocene	0.1 (initial value)
Molecular diffusion		8.64×10^{-5} m^2/day
Henry constant		0
Decay rate		0 day^{-1}
Density ratio		0.0245 for the ocean shores; for the estuary values are not yet determined
Initial concentration		35000 mg/l (NaCl) for the ocean shores; for the estuary the values and their spatial distributions in the mesh borders are those of Fortunato et al. (2018) as shown in Figure 6.58; for the aquifer, values are very scarce

5.3   Description of the mathematical model

The build-up of the mathematical model starts with the input of the topography, river network, and wells' distribution. The mesh is then automatically generated by the model using all these structures, automatically refining the mesh in the location where these structures are located. This process is followed by the input of the lithological units as model layers (top and bottom of each layer represented by model slices) and the eventual subdivision of such layers into thinner ones. Such subdivision usually occurs during calibration. The model automatically builds the mesh to encompass the layers, after these (or more exactly their top and bottoms) had been input into the model. Once the geometric structure of the model is defined, it is time to input the essential hydraulic properties required to run a flow model. Then, after model calibration, the model is run for the historical period and climate change scenarios. Once the flow model is calibrated, the transport model – for impacts analysis of sea level rise on saltwater intrusion – can be built upon it.

5.3.1   The Supermesh and the Mesh

The mesh is the basis of any finite element mathematical model. It is set by a spatial arrangement of nodes and elements describing the basic geometry of the aquifers under study. In FEFLOW, the mesh is generated from an initial supermesh, where the fundamental aspects of the area to be modelled are defined. Amongst these are the limits of the aquifers, river network, location of the abstraction/injection wells, location and geometry of pollution sources, channels and other important hydraulic structures that might impact the aquifer. So, to generate a good supermesh and ensuing mesh, it is advisable to have all this information already available and input into the model. Pumping wells can be introduced after mesh generation but the model discretization will not be as good as if these have been input before supermesh generation, even if mesh refinement is done around the wells after their input. Extra care must be exerted for data consistency among the shapefiles required to build the supermesh.

In the present case study model, the **supermesh** was generated from aquifer borders and river network shapefiles. For the river network it is advisable to have a simplified shapefile because if too many river segments are represented, the model will not generate the supermesh or, if it does, it will lead to a mesh with too large number of elements, which will slow the future model runs. The Supermesh of the case study model is composed of 1 polygon, 35 lines, 36 elements and 4065 nodes.

The **mesh** is the real network of elements and nodes defining the simulation domain and in FEFLOW there are 2 distinct possibilities for mesh generation:

(1) *structured mesh* – each layer must spread throughout the whole model area;

(2) *unstructured mesh* – with this mesh, different domains can be defined, which means layers are not mandatorily spreading throughout the whole model area; due to this, very complex aquifer geometries can be built, coupled or not with complex natural (e.g. fault systems) or human structures (e.g. mining structures). Besides simulating flow under such geometrically complex settings, flow along the borders of such structures can also be simulated. The unstructured mesh drawback is the demand of larger computational resources.

In the case study, and once the hydrogeological structure could be plainly represented by 3 tabular layers, the structured mesh was chosen. After supermesh and ensuing mesh generation. the case study regional model sports a mesh with **a total of 677 170 nodes and 1 274 500 triangular prismatic elements**, representing an **area of 8.58x 10^9 m^2 and a volume of 1.57x10^{12} m**^{3}. Each slice has 26 045 nodes and 50 980 elements.

At the time of supermesh/mesh development, the abstraction wells' shapefile was not yet available. Therefore, these wells were introduced later on (using Multilayer wells boundary conditions), which meant that the mesh refinement around the wells is less good than if they would have they been introduced at the supermesh development. So, modelling the processes near the wells is less accurate. For a regional model like this, that may not be very relevant but for detailed studies of specific wells it will most likely by a handicap. The downside of introducing the wells at the supermesh development stage is that a larger number of nodes and elements is generated, which demands higher computational resources when running the model.

5.3.1.1 Refinement and meeting the quality criteria for the mesh

After mesh generation, some rearrangement of the nodes is most likely required[5] in order to meet a set of criteria that safeguards solving flow (and transport) equations' robustness. Such criteria are:

- *Delaunay criterion* – a Delaunay triangulation of a set of points in a 2-D surface ensures that the circumcircle (circumference circling, in this case, a triangle) associated with each triangle of the mesh has no points in its interior. In practice what this criterion does is to prevent the mesh

---

[5] This is done at the top slice, once the node/elements structure of this slice will be exactly replicated in all the other slices of the model. In a structured mesh the model does not allow for different nodes' configurations on different slices, once this would generate irregular elements.

from having triangles with extremely acute angles and long "flat" shapes, once such sliver triangles can badly interfere with flow and transport equations solving.

- ***Maximum interior angle of triangles*** – the more equilateral are the triangle elements of the mesh, better model convergence and faster flow and transport equations' solving is achieved. This criterion seeks the larger interior angle of each triangle to identify the too obtuse ones. The user should then change the shape of these triangles to make them the more equilateral as possible.

- ***Peclet number[6]*** – criteria required for transport problems only. Usually the finer the mesh the lower should be the Peclet number. Usually the Peclet number is lower than 2.

When generating the mesh, the model tries to meet these criteria for the largest number of elements possible. However, usually, some elements will fall out of one or more criteria. This means the user must check the mesh and change the position of criteria disobeying elements' nodes in a way that the reshaped element with conform to them. The user must reshape the disobeying elements' nodes to conform to all required criteria. It must do it also to any elements that after reshaping of the former disobeying ones are now violating one or more criteria. This means the user must check for criteria violations, modify the violating elements, then recheck the mesh and reshape any new elements that are now criteria violators. This iterative process must also be performed whenever, during calibration (or due to model problems), parts or even the whole mesh are refined. The final mesh of the case study model, after reshaping to conform to Delauney and maximum interior angle of triangles criteria, is shown in Figure 5.2. The general characteristics of the supermesh are given in Table 5.3 and those of the mesh in Table 5.4.
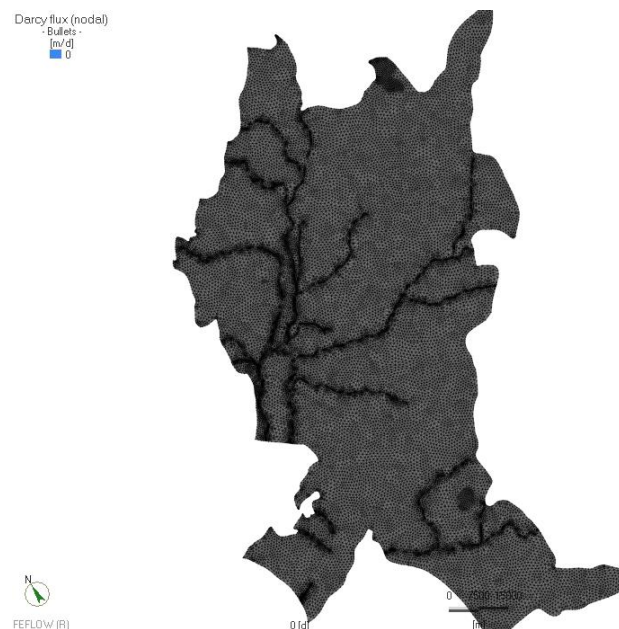
Figure 5.2 – Mesh after the final horizontal refinements (Slice 1, top of the model)

---

6 The Peclet number is the advection ratio of a physical quantity due to flow, divided by the diffusion rate of that quantity driven by an appropriate gradient.

Table 5.3 – Supermesh characteristics

Structure type	Number of elements
Elements	36
Nodes	4065
Polygons	1
Lines	35
Points	0

Table 5.4 – Mesh characteristics

Characteristics		Value	
Dimensions		3D	
Nodes per element		6	
Element type		Triangular prisms	
Number of layers		25	
Number of Slices		26	
Elements per layer		50 980	
Total elements (25 layers)		1 274 500	
Nodes per slice		26 045	
Total nodes (26 slices)		677 170	
Interior holes		0	
Mesh quality	Delauney violation triangles	0%	
	Obtuse angled triangles	> 90º	5.1%
		> 120º	0%

5.3.2   Layers and slices

FEFLOW defines a layer by 2 entities: the slice (2 for each layer) and the layer itself. The slices define the top and bottom of each layer. The layer itself is the vertical space between 2 consecutive slices. Once the conceptual model has 3 hydrogeological units – Alluvium, Pliocene and Miocene – initially the mathematical model had 3 layers (= 4 slices), one layer for each hydrogeological unit:

- **Layer 1** = Alluvium (and so, the Aluviões do Tejo aquifer).
- **Layer 2** = Pliocene (representing the shallow to intermediate water bearing units of Tejo/Sado – Margem Direita and Tejo/Sado – Margem Esquerda aquifers).
- **Layer 3** = Miocene (representing the lower water bearing units of Tejo/Sado – Margem Direita and Tejo/Sado – Margem Esquerda aquifers).

The top slice defines the **top of the model** and is built by FEFLOW from by the DTM shapefile fed into the model before supermesh generation. FEFLOW could then generate slices, given the base of the model domain but this would lead to oversimplification of its vertical structure. To avoid this, the slices (top of layers 2 and 3; bottom of layer 3) were built based on geological information, using ArcGIS®. This procedure guaranteed that thickness changes of the lithological units would be built into the model.

Once a structured mesh was chosen, the 3 units had to spread throughout the model domain (cf. sub-chapter 5.3.1), which is not what happens in reality. To overcome this problem, the bottoms of the 3 layers (generated by 3 shapefiles, one for each layer bottom) were defined with the following rules:

- **Layer 1** – in the alluvial deposits (=Aluviões do Tejo aquifer) outcropping area, the bottom depth of this layer is obtained by subtracting the depth of the alluvial deposits from the DTM topographic surface. For the remaining area of the model domain, this layer was artificially extended over the Pliocene and Miocene outcropping areas. In this artificially extended areas, Layer 1 bottom is 1 m bellow the topographic surface[7].
- **Layer 2** – in the alluvial deposits outcropping area, its bottom is defined by subtracting the base of the Pliocene deposits, as given by boreholes, from Layer 1 bottom. In the remaining model areas, the bottom of Layer 2 is 1 m Layer 1's bottom.
- **Layer 3** – its bottom is the surface defined by boreholes' bottoms, once beyond that depth there is no information. In the areas were boreholes didn't reach the Miocene, if no near boreholes were available to interpolate a more real depth, a 1 m thickness for Miocene was given for such areas, although there might be still Pliocene at that depth.

Once this simplified representation didn't account for the leaky layers between the main hydrogeological units and there were model convergence problems due to so few layers, this 3-layer model was vertically refined to a total of 25 layers and 26 slices. This new vertical refinement allows for a better representation of the vertical hydraulic variations occurring in alluvial, Pliocene

---

[7]   To better simulate the reality in these artificially extended areas, its hydraulic properties are the same as those of the Pliocene deposits for the Pliocene outcropping zones. For the Miocene outcropping areas the hydraulic properties are those of the Miocene deposits.

and Miocene deposits. The final vertical structure of the model is shown in Table 5.5 and Figure 5.3 (which also shows the model's horizontal refinement). FEFLOW refines the mesh vertically dividing the distance between 2 consecutive slices in equal parts. This means that where the model had Pliocene or Miocene deposits with 1 m thickness – and once vertical discretization represents them now with 10 layers – each of these layers have now 10 cm thickness. For Alluvial deposits the thickness of these former 1 m zones is a bit larger, once the Layer 1 (Alluvial deposits) was divided into 3 new layers. This new vertical discretization demands careful definition of the model problem to make it able to deal with a large number of cells becoming dry in the top layers during simulation, due their extremely small thickness in the Pliocene and Miocene outcropping areas.

Table 5.5 – Vertical structure of the mathematical model

Lithological Unit	Lithology & aquifer depiction	Type of units	Slices
Alluvial deposits	*Former layer 1*. Depicts Aluviões do Tejo aquifer	Water bearing units	1, 2, 3
Pliocene	*Former layer 2*. Depicts Tejo-Sado – Margem Direita and Tejo-Sado – Margem Esquerda aquifers Pliocene deposits	Leakey units	4, 5, 6
		Water bearing units	7 to 14
Miocene	*Former layer 3*. Depicts Tejo-Sado – Margem Direita and Tejo-Sado – Margem Esquerda aquifers Miocene deposits	Leakey units	15, 16, 17
		Water bearing units	18 to 26

Slice 1 represents the topographic surface. **Slices, 4, 5 and 6** represent the leaky units at Pliocene top; in this way semi-confinement bellow the alluvial deposits and artesian conditions under natural flow can be simulated. **Slices 15, 16 and 17** represent the leaky units between Pliocene and Miocene, allowing for the simulation of semi-confinement of the Miocene aquifer, when under Pliocene. **Slice 26** is the bottom of the model.
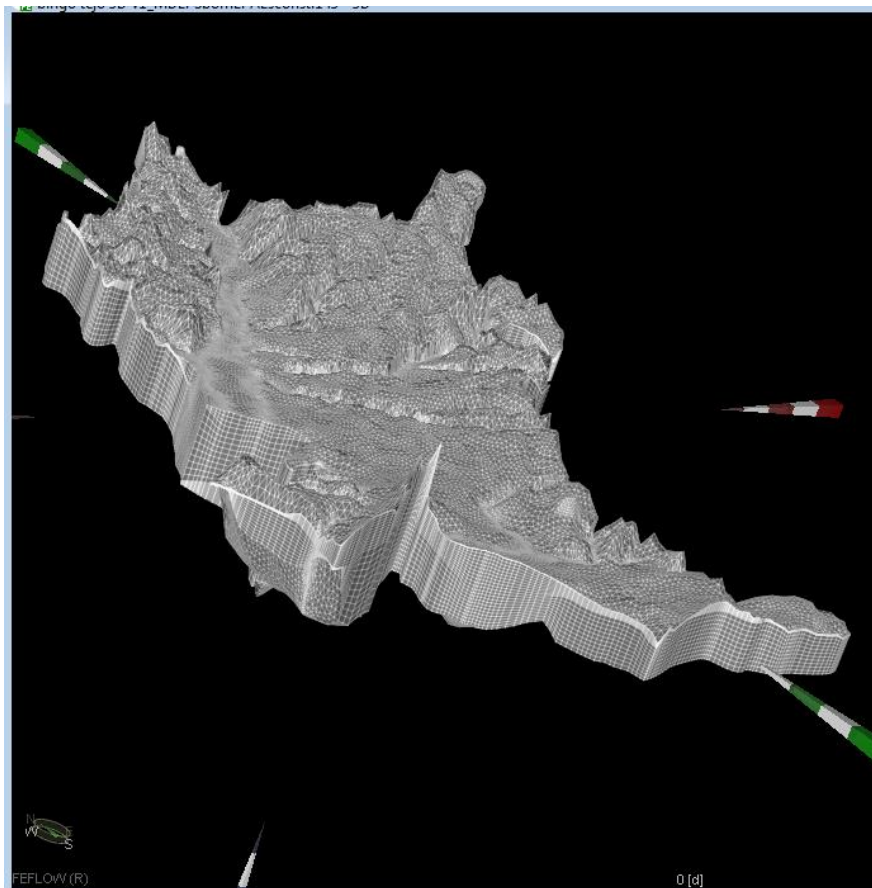
Figure 5.3 – Vertical structure of the model showing the layers and slices

5.3.3   Problem settings

After creating the mesh, the basic characteristics of the mathematical problem must be defined, taking into account the conceptual model. The mathematical model is defined as **3D flow, layered, horizontal and planar**. It starts as **steady state** and, later on, transient models were built from it to simulate transient flow for drought analysis.

Once the conceptual model defines unconfined, semi-confined and confined aquifers, the model is set for **saturated groundwater-flow**, once this is the option allowing the simulation of all such behaviours. In fact, the issue was not to understand the unsaturated zone but the aquifers. In order to simulate these different behaviours, the first layer – between Slice 1 and 2 (= top of Aluviões do Tejo aquifer) – is Phreatic. The layers corresponding to Pliocene and remaining alluvial deposits (Slices 3 to 14) are Dependent to account for the phreatic/semi-confined nature of these layers. The remaining layers (Miocene) are set as Confined once only in the western area of the model, its upper layers can show a phreatic to semi-confined behaviour (Table 5.6). To be able to simulate the phreatic conditions, the model is set as **unconfined**, with the storage of the unconfined layer extended to the water table, and once the model should allow for flooding to assess climate change impacts, the option for **unconstrained heads at the top of the model domain** was chosen.

Although the lithological units are in fact anisotropic, for simplification and lack of fine data on anisotropy, the model started as isotropic, becoming anisotropic during the calibration process. **Anisotropy** orientation **is axis-parallel**, which means the major conductivity directions are parallel to the Cartesian coordinates, reflecting the basic horizontal layering of the model.

The solver chosen was the Standard Iterative **PCG** (Preconditioned conjugate gradient method) and the **preconditioning method** was the **Incomplete factorization**. The main characteristics of the mathematical model are shown in Table 5.6.

<p align="center">Table 5.6 – Model basic characteristics</p>

FEFLOW model characteristics	Description	
Problem type	3D flow, steady state, phreatic	
Flow equations	Standard (saturated, but with unconfined conditions controlled by free-surface settings)	
Unconfined conditions	Unconfined, extended storage of unconfined layer to the water table, unconstrained heads on the top of the model domain	
Layer/slice confinement conditions	Slice 1 (a)	Phreatic
	Slice 2 to 14 (b)	Dependent
	Slice 15 to 26 (c)	Confined
Residual water depth for unconfined layer	0.2 m	
Anisotropy of the hydraulic conductivity	Axis-parallel	
Solver	Standard iterative PCG (Preconditioned conjugate gradient method)	
Preconditioning method	Incomplete factorization	
Error tolerance	0.51×10^{-3} (*)	
Maximum number of iterations	35	
Computing mass matrixes	Consistent mass	

(a) topmost water bearing unit of the Alluvial deposits; (b) remaining alluvial deposits and Pliocene deposits; (c) Miocene deposits; *for severe drought conditions and to allow model convergence this value was raised to 2.31×10^{-3}

5.3.4 Material properties

Material properties are the mandatory hydraulic properties required to solve flow and transport equations. FEFLOW also places recharge under material properties, because layers' hydraulic properties are defined by slice – that is, the data is ascribed not to the elements of the layer but to the nodes of the mesh that tops the layer – and recharge enters the model through the top slice in most of the cases.

Sources and sinks, inflows and outflows from top/bottom of the model and transfers to and from the model, although may occur along any area in the top layer of the model (or any lower slice), are normally set up by the boundary conditions and not by material properties.

For the flow problem, the hydraulic properties considered were conductivity, porosity, specific storage and recharge. For transport problems, dispersivity and molecular diffusion are the basic material properties to run the model. In case of saltwater intrusion, once 2 fluids of different densities are involved (saltwater and groundwater), density ratio is also a mandatory property.

5.3.4.1 Conductivity, porosity, specific storage

Due to the small amount of data concerning their spatial variation, average values given by the bibliography (APA, 2012; Lobo Ferreira et al., 2011) were set up for **porosity** and **specific storage** (in the model acknowledged as drain fillable capacity) according with the lithology by layer. Exceptions to such horizontal isotropy were: (1) Layer 1 (slices 1 to 3) areas beyond the alluvial deposits; (2) Layer 2 (slices 4 to 14) in Miocene outcropping areas. So, in Layer 1 the area corresponding to Pliocene outcrops got the porosity and specific storage of Pliocene lithologies; in Miocene outcropping areas, these parameters were set up in accordance with the Miocene lithologies. A similar reasoning was applied to the other layers.

For the slices 4 to 6 and 15 to 17, representing leaky units, were assigned low the values given by bibliography (http://www.aqtesolv.com/aquifer-tests/aquifer_properties.htm) for semi-pervious deposits. In Pliocene and Miocene outcropping areas, it was assumed that these layers would not be leaky, so porosity and specific storage were respectively those of Pliocene or Miocene.

During calibration these parameters were kept unchanged because the model has low sensibility to these parameter changes and heads are just negligibly affected. Table 5.7 presents the values of the parameters in the model.

Table 5.7 – Model's porosity and specific storage

Lithological Unit	Layer (initial)	Slices	Porosity (%)			Specific storage (1/m)		
			Alluvial area*	Pliocene area*	Miocene area*	Alluvial area*	Pliocene area*	Miocene area*
Alluvial	Layer 1	1 to 3	0.2	0.14	0.12	1.2×10^{-4}	3.97×10^{-4}	5.32×10^{-4}
Pliocene	Layer 2	4 to 6	0.4	0.14	0.12	1×10^{-6}	3.97×10^{-4}	5.32×10^{-4}
		7 to 14		0.14	0.12		3.97×10^{-4}	5.32×10^{-4}
Miocene	Layer 3	15 to 17		0.4	0.12		1×10^{-6}	5.32×10^{-4}
		18 to 26			0.12			5.32×10^{-4}

*these correspond to the real outcropping regions of the formations in the case-study area; in red bold is the values for the leaky layers underneath respectively the alluvial deposits and Pliocene; the grey areas mean that the formation does not exist anymore: in slices 7 to 14, the alluvial area is occupied by Pliocene; in slices 15 to 17 is occupied by the leaky zone between Pliocene and Miocene formations, and in slices 18 to 26, all is Miocene deposits

Conductivity is by nature anisotropic once vertical conductivity is usually 1/10 of the horizontal conductivity. So conductivity was defined as Kyy = Kxx and Kzz = Kxx/10. The values for Kxx were given by bibliography (APA, 2012; Lobo Ferreira et al., 2011). In outcropping Pliocene and Miocene areas, the conductivities were those of respectively Pliocene and Miocene lithologies. Although for the alluvial deposits the bibliography refers a conductivity increase towards central and upstream zones of these deposits, the lack of quantitative data concerning such variations hindered their representation in the model. Only after calibration, it was possible to have a crude representation of such horizontal variations.

Slices 4 to 6 and 15 to 17 were defined as leaky and their conductivities were defined by bibliography values (http://www.aqtesolv.com/aquifer-tests/aquifer_proper ties.htm) for semi-pervious deposits. This allowed the simulation of the semi-confined areas and its respective artesian behaviour.

When calibrating the model, the conductivity values were found to be quite high. So they were progressively changed in the 3 directions in accordance with Kxx = Kyy = Kzz * 10 rule until the error of simulated vs. observed heads was the least as possible. Table 5.8 presents the horizontal conductivities for each slice.

Table 5.8 – Model's horizontal conductivities

Lithological Unit	Layer (initial)	Slices	Conductivity ranges (m/d)		
			Alluvial area	Pliocene area	Miocene area
Alluvial	Layer 1	1 to 3	100 to 460	50 to 0.01; in south area 200 to 50	20 to 0.05; locally 40 or 70 (alluvial areas)
Pliocene	Layer 2	4 to 6	1x10^-6	50 to 0.0; in south area 100 to 0.3 in Slice 4; 20 to 0.3 in Slice 5 to 14	10 to 0.05; locally 20 or 40 (in intensely fractured areas)
		7 to 14			
Miocene	Layer 3	15 to 17		1x10^-6	
		18 to 26			

5.3.4.2   Diffusivity, dispersivity, density ratio, decay rate

Although saltwater intrusion simulations were not performed, the basic parameters for this type of transport simulation were defined as:

- **Diffusivity** – the initial values were set at 8.64 x 10^-5 m²/day, in accordance with DHI (2014) saltwater intrusion example, once no diffusivity data was found in the literature.

- **Dispersivity** – transversal dispersivity is usually at least an order of magnitude smaller than longitudinal dispersivity (http://www2.nau.edu/~doetqp-p/courses/env303a/lec36/_lec36.htm). Dispersivity values for Pliocene and Miocene were those from Schulze-Makuch (2005) and Bjerg (2008). For the alluvial deposits, the default value given by FEFLOW was adopted because it is a value well in the range of those given for sandy sediments by the bibliography. The dispersivity values are presented in Table 5.9

- **Density ratio** – the value 0.0245 was adopted for the sea-shore areas, once fresh groundwater has negligible NaCl concentrations when compared with sea average salinity (35 000 mg/l). This value is the one that DHI (2014) recommends for simulating saltwater intrusion, starting from a non-saltwater situation. Saltwater intrusion occur around Melides (Diamantino, 2001), Barreiro (Zeferino, 2016) and possibly other areas along Tagus estuary's shoreline and maybe in some areas of Costa da Caparica's coastline (Ferreira, 2012). Such areas, which would require a different density ratio once groundwater is at least brackish, are not large enough to have an expression at the model scale. Tagus estuary coastal areas would also require different density ratios once estuary salinities range from 35.7 to 1 ppt (Fortunato et al., 2018). Such variation illustrates a salinity gradient from the typical ocean water to upstream Tagus (cf. Figure 6.58). So, along the estuary coastline a gradually changing density ratio should be defined.

- **Henry constant** and **decay rate** – are set at 0 once NaCl does not dissolve in gaseous phases (and so Henry constant does not apply) and being a conservative species, it suffers no decay rates.

Table 5.9 – Model's dispersivities

Lithological Unit	Layer (initial)	Slices	Dispersivity (m)			
			Dispersivity direction	Alluvial area	Pliocene area	Miocene area
Alluvial	Layer 1	1 to 3	Longitudinal	5 m	3	1
			Transverse	0.5 m	0.3	0.1
Pliocene	Layer 2	4 to 6	Longitudinal	0.5	3	1
			Transverse	0.05	0.3	0.1
		7 to 14	Longitudinal		3	1
			Transverse		0.3	0.1
Miocene	Layer 3	15 to 17	Longitudinal		0.5	1
			Transverse		0.05	0.1
		18 to 26	Longitudinal			1
			Transverse			0.1

5.3.4.3   Recharge

In a 3D model, recharge is an area-related property. This means recharge values are attributed to the elements of the mesh on the top slice, so recharge is defined through in/out flow on top/bottom option, which describes the net infiltration from the top of model domain. The recharge values for the historical period (1979/2009) were those of 2011 Tagus Management Plan (APA, 2012; Lobo Ferreira et al., 2011) in shapefile format. During calibration, recharge values were reduced to ½. Induced recharge due to irrigation losses or other types of water losses (e.g. urban) were not considered due to the general lack of representative data, recent or otherwise. After calibration, values range from 0 m/day (in impervious deposits) to 8.15×10^{-4} m/day. The large majority of recharge values ranges from 1 to 4.89×10^{-4} m/day.

For climate change scenarios, recharge was calculated from MiKlip climate model results for the time horizon of 2024 using BALSEQ_MOD water budget model (Oliveira, 2019). MiKlip results were given for 10 climate realisations. Recharge computed for each realisation and subsequent analysis presented in Oliveira (2019) lead to the choice of 3 scenarios:

- **High recharge** – associated with climate realisation R1
- **Low recharge** – associated with climate realisation R3
- **Average recharge** – associated with the ensemble of the 10 climate realisations R1_10

To *assess climate change impacts*, the recharge for each of these scenarios replaces the historical values in the flow model. These scenario recharges were also reduced by half for congruence with the historical recharge after calibration. Steady state conditions were adopted for this analysis.

To *assess drought impacts under climate change*, recharge for the extreme drought period of 2004-2005, estimated also by BALSEQ_MOD, was used (Oliveira, 2019). Steady state conditions were used to simulate the extreme scenario of permanent severe drought. Transient state conditions were used for 1, 3 and 5 year's length droughts. The recharge scenarios were:

- **1 year drought** – transient state
- **3 year's drought** – transient state
- **5 year's drought** – transient state
- **Permanent drought** – steady state

5.3.5 Boundary conditions

Boundary conditions are used to define the model areas were water exchanges occurs with the surrounding systems. These are the interfaces between aquifer and ocean, rivers, lakes, other reservoirs or other aquifers. In the case-study area, the aquifer interacts with the river network, the estuary, the seashore (at the western border of Península de Setúbal), Arrábida limestone "aquifer" and, at the southern tip, with Bacia de Alvalade. All these interfaces are represented in the model by boundary conditions. FEFLOW has specific boundary conditions to represent abstraction/injection wells: (1) Wells and (2) Multilayer wells. These should not be mistaken with Observation Points, which can be piezometers or wells, but are used by the model just to determine the error between the observed and the calculated variable (heads and/or pollutants concentrations). Well boundary conditions are used in 2D models only. It basically represents very superficial wells. Multilayer wells are used in 3D models and can reach any depth up to the model's bottom. These wells can be fully penetrating or be assigned with distinct screening zones at different depths. The sets of boundary conditions differ, depending on the problem being solved. FEFLOW can solve the following problems: (1) flux, (2) transport, (3) age, (4) heat transport. **For flow** (used in the case study to assess impacts of climate change and droughts) the boundary conditions available are:

- *Hydraulic head* (Dirichlet condition) – nodal-defined boundary condition were hydraulic head is set at a constant value (at a node or nodes) defined by the user. It is used to model constant water levels at certain locations (e.g. sea/aquifer border, if considering a static average sea-level). This boundary condition was applied just to the 1st slice for: (1) river network, (2) seashores, (3) most of estuary coastline, anywhere where topographic height was > 3 m present day average sea-level, once it was assumed that up to 2024, sea level rise would be far below such threshold. For river network the boundary condition is h = ground height; this means it changes from node to node throughout the length of the river, in agreement with topography. For seashore and estuary areas the boundary condition is h = 0 m, including cliff coastlines bases. During calibration, in very local areas of steep topographic gradients h = ground height. This was due because in such areas the size of the elements didn't allow a more realistic

representation of the hydraulic gradients. In fact, in such cases, before boundary conditions, the model would simulate a flooding situation that in reality does not occur. The model distribution of this boundary condition is presented in Figure 5.4.
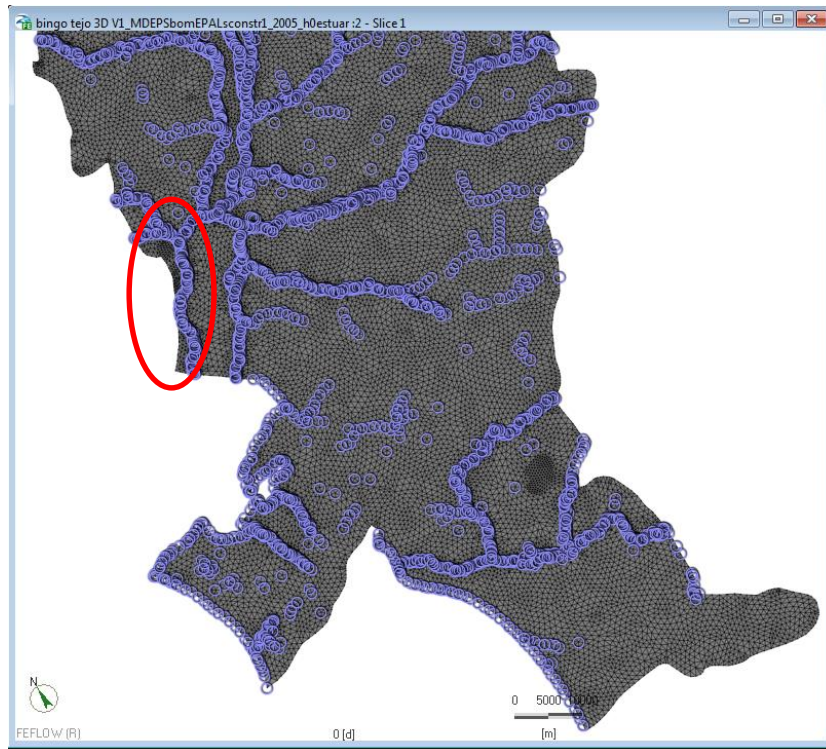
Figure 5.4 – Hydraulic heads BC at central-estuary area of the model

- **_Fluid Flux_** (Neumann condition) – it defines a fixed flux (inflow or outflow) occurring at the border of the aquifer. This type of boundary condition is used to define flow zones between hydraulically connected aquifers (or aquifer/reservoirs). On a 3D model it is an area-defined (the section across which flow occurs) boundary condition and values are assigned to the nodes of that area. Unlike hydraulic head boundary condition, which can be assigned to nodes just in one slice, in fluid-flux, the consecutive nodes of 2 adjacent slices must be selected. Values are negative if water enters the model and positive if it goes out. In the case study, model this boundary condition was applied to nodes in Slices 1 and 2 only, along aquifer borders where contact with other aquifers or locally significant water bearing units occur and significant flows to/from the aquifer can be expected. Such areas are: (1) 2 small local areas at the northern border with locally important water bearing units, (2) at the extreme NE border with locally important water bearing units, (3) Arrábida Hills border, (4) SW border with Sines aquifer, (5) SE border with Bacia de Alvalade aquifer. All values were positive except for Arrábida border, were it is assumed water enters the aquifer (Table 5.10). Fluid flux boundary conditions' locations are shown in Figure 5.5.

Table 5.10 – Flow model's boundary conditions

Boundary condition type (time constant)	Total n. of nodes	Issue modelled	Location (1)	Values*
Hydraulic head	4372	River network	Throughout the model	h = ground height
		Coastal area	W border Peninsula Setúbal	h = 0 m
			W border, south from Peninsula Setúbal	h = 0 m
		Tagus estuary	W border, central	h = 0 m
Flow — Fluid flux	256	Border of the model with other aquifers	Arrábida border	-0.5 m/d
			N border	0.5 to 5 (W part)
				4 (E part)
			NE border	0.7 to 5
			SW border	4.5 (W part); 1.7 m/d (E part)
			SE border	0.7 (N & S part); 1.3 (E part)
Multilayer wells	2247	Abstraction wells	Throughout the model	Average volumes of abstraction

*the values given are after model calibration; (1) Locations are given in Figure 5.4 and Figure 5.5

- **_Fluid transfer_** (Cauchy condition) – simulates hydraulic connections (leaky) between rivers and aquifers. Water stage in the river is the value assigned by node (once the model will determine the hydraulic properties of the riverbed from the material properties in the area surrounding the nodes). In a 2D model, it is a linear structure but, in a 3D model, it is an area-defined boundary condition. Due to lack of data this boundary condition was not applied to the case study model.

- **_Wells_** – this condition applies to 2D models although it can be used in 3D if the wells are only in the top layer of the model (=very shallow wells). This is a nodal boundary condition, so the wells' abstraction/injection rate is assigned by node. The well(s) must be fully penetrating and cannot intercept more than 1 layer. Positive values simulate pumping while negative simulate injection.
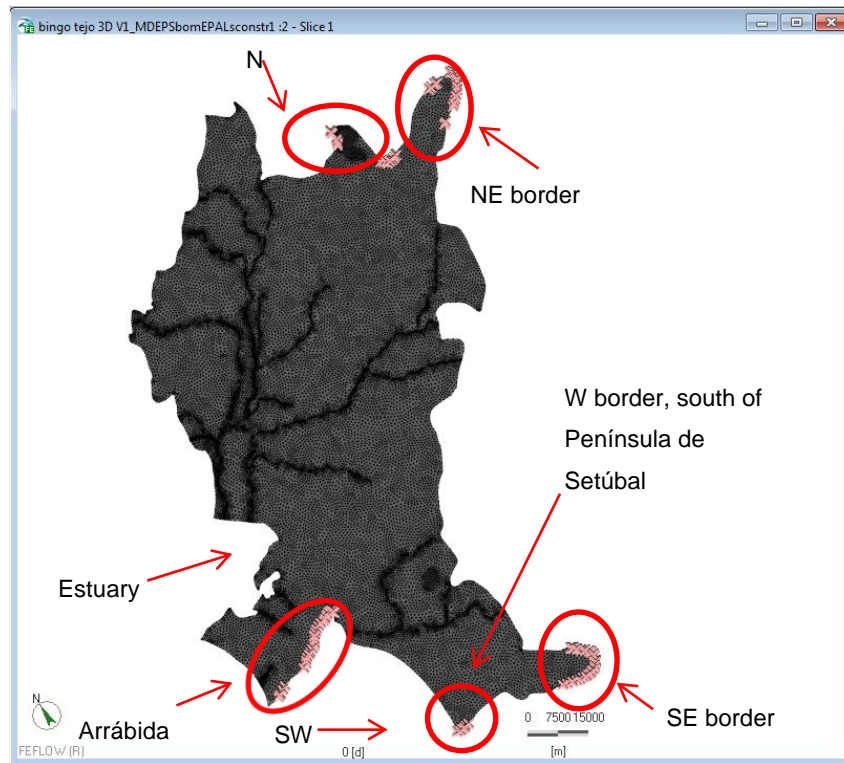
Figure 5.5 – Fluid flux boundary conditions of the model

- **_Multilayer wells_** – this boundary condition applies only to 3D models. It allows for wells to intersect several layers. They can be fully penetrating or have non-continuous screening areas. This is an edge-defined boundary condition, meaning that it is applied along the edge of the element were the well is located. This means the model location of the well might be a little different from its location in the real world. Only one well per element can be assigned and positive values identify abstraction, while negative identify injection. If the Supermesh has not accounted for wells[8] (and generated the mesh accordingly) and there are large elements and/or a high density of wells, an element might have several wells in it. In this case, for any element in such situation, a mandatory aggregation of the original wells into one single-representative well is required. Positive values represent abstractions and negative values injections. In the case study, model wells were set up by this boundary, after aggregation, because they intersect several layers. Well aggregation was accomplished using ArcGIS and flow rates of each "new" well are the sum of all the wells that have been aggregated into it. Flow rates were average annual values, so truly transient conditions could not be simulated. The depth of the wells must be input for the model to define which layers are intersected by each well. The depths of the "new" wells are the average of the individual wells it aggregates. However, due to layer bottoms' and topographic surface unevenness, the depth of each "new" well was compared with the bottom layer depth at well location. If it was deeper than the layer bottom, well depth was set equal to bottom layer. The same reasoning was applied to "new" wells' tops, so if the well top

---

[8] As is the case when wells enter the model after mesh generation.

was above the topographic surface (= Slice 1) the topographic elevation would be given to the well. Figure 5.6 shows the locations of this boundary condition.
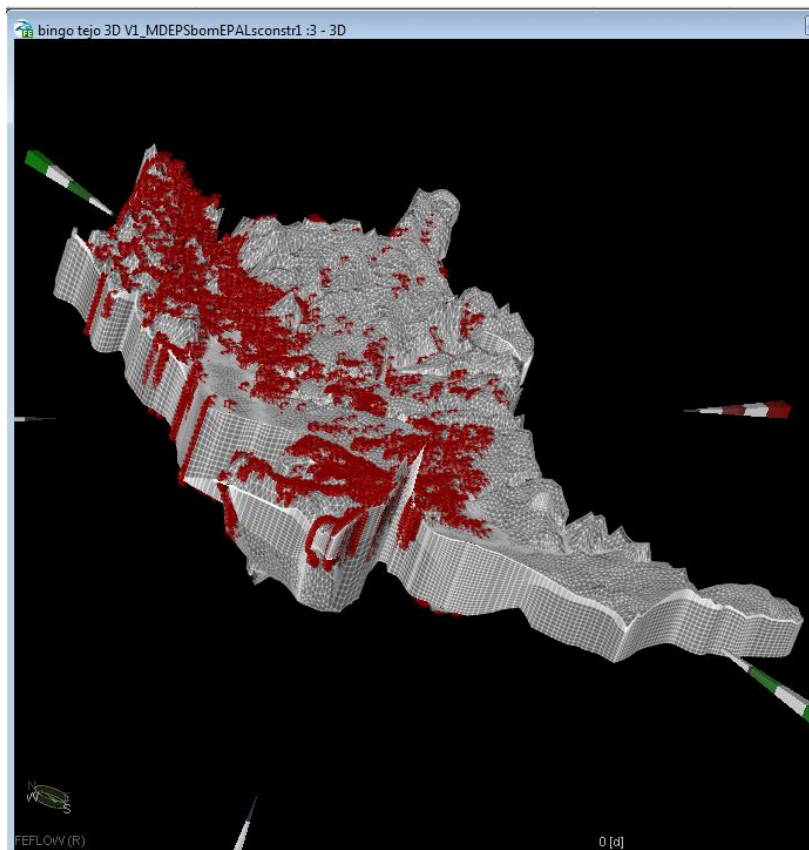
Figure 5.6 – Multilayer wells boundary conditions in the model

For transport (for sea level rise impacts on saltwater intrusion simulations) there are 4 types of boundary conditions:

- *Mass concentration* – this nodal-defined boundary condition simulates pollution point-sources with constant pollutants concentrations (at least in each time step). The known concentration is assigned to the source representing node. The model will not calculate concentrations for such nodes. This can lead to a mass inflow when neighbouring nodes have a lower concentration or to an outflow on the opposite case.

- *Mass flux* – it represents known pollutant inflows or outflows (typically in a fluid flux boundary condition) of known concentration(s). In 2D models it is a nodal boundary condition defined along a line. In 3D models it is an area boundary condition, so it must be assigned to the nodes of the area where pollutant(s) flow occurs.

- *Mass transfer* – it represents pollution transport across leaky zones (e.g. through a river bed). In 2D models it is a nodal boundary condition defined along a line. In 3D is an area-defined boundary condition, so it must be assigned to the nodes of the leaky area(s). A predefined

reference concentration must be applied to line(s)[9] or surface(s)[10] nodes of the boundary condition. Conductance (= transfer rate) is assigned by the model from the material properties of the leaky area (or line).

- **Mass nodal sink/source** – it represents pollution injection or abstraction wells with known pollutant(s) injection/abstraction concentration rate(s). It is a nodal boundary condition, so it is assigned to the node(s) where pollutant(s) inflows/outflows occur.

5.3.6   Process variables

Process variables for **flow models** are required to run the model. They include initial hydraulic heads, ressure, PDarcy flux and rate budgets but initial hydraulic heads are the only process variable of mandatory input. These initial heads might not accurately represent reality and they may be input by shapefiles (for large models), node by node (for very simple and small models) or just one value for each model's slice. In **transport models** pollutant(s)', the process variables are the initial mass concentration(s) and pollutant(s)' rate budgets but the initial mass concentration(s) (one value or a spatial distribution of values) is the only process variable of mandatory input. The process variables must be defined for each of the model's slice(s).

The **initial hydraulic heads used to run the flow model** are given in Table 5.11. These values obeyed the following relationship: Miocene heads > Pliocene heads > alluvial deposits heads, as defined in the conceptual model from field observations in the case study's central area.

The **initial concentrations to run the transport model**, were set at 0 mg/l NaCl for most of the aquifer domain and 35 000 mg/l NaCl in the ocean domain. These values were chosen because it was assumed that, at an initial stage, the water in the aquifer domain is freshwater, so with very low chloride concentration; 35 000 mg/l NaCl is the average concentration for sea water.

Table 5.11 – Model's initial hydraulic heads

Lithological Unit	Slices	Head values (m)
Alluvial	1 to 3	0
Pliocene	4 to 14	5
Miocene	15 to 26	10

---

[9] In 2D models.

[10] In 3D models.

5.3.7   Observation points

Observation wells, identified in the model as Observation points, are required for model calibration. Once they are not abstraction (or injection) wells, they are treated differently from abstraction/injection wells, even if they are located in the same mesh element. Observation points do not influence the simulation run and are used by the model only to compute observed vs. simulated error (heads and/or concentrations) in each observation well, taking into account a threshold error (identified as Confidence Interval) given by the user. In the present case study, the confidence interval is equal to 3 m. The sum of the errors gives the global simulation error. When the error observed vs. simulated error is below the confidence interval, the model can be assumed as calibrated at the points where this occurs. Observation points are defined by location, the respective observed head and/or concentration. Unlike pumping wells, which are node or edge-defined entities, observation points can be located anywhere in the model: an edge, a node or inside an element. The case-study flow model has 504 Observation points and their areal distribution is shown in Figure 5.7.
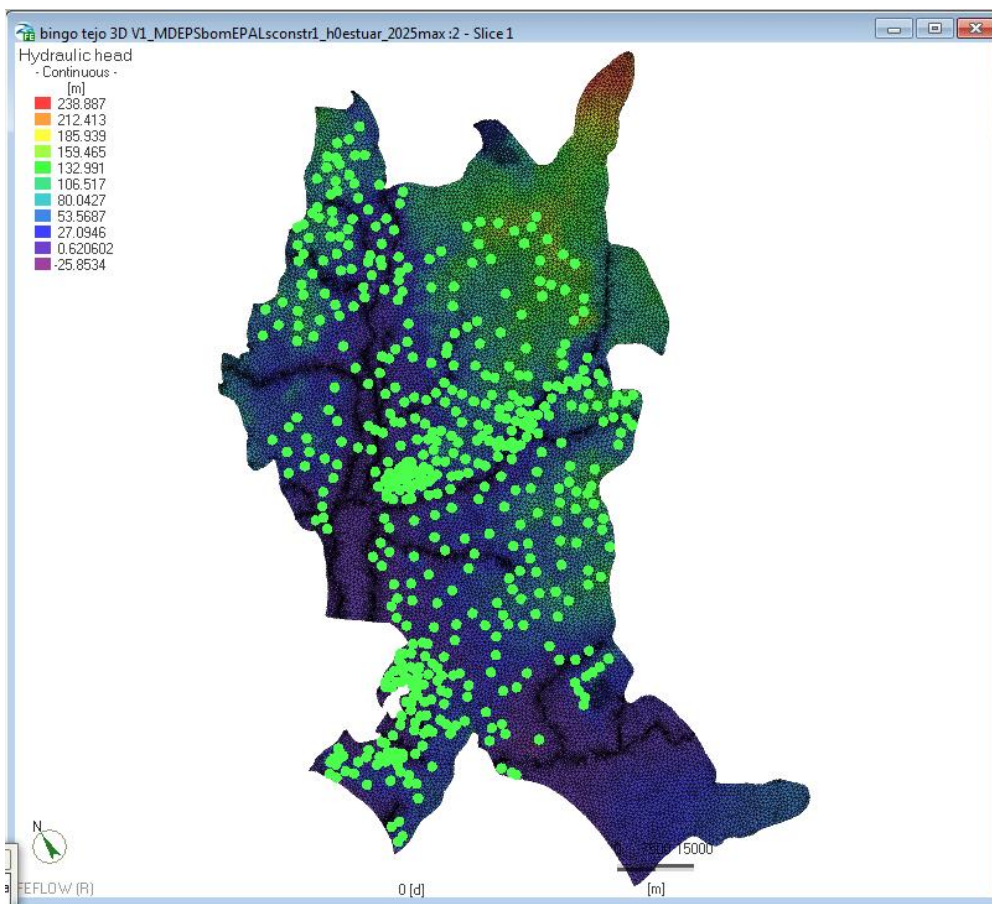
Figure 5.7 – Observation points in the model

Observed heads in the Observation points were assigned at the topmost layer of the model. Heads per Observation point are single values, which were the only ones known. No heads per water bearing unit were available. The data for the Observation points was assembled from several sources (see chapter 5.2.2.) and analysed for discrepancies and errors before being fed into the model. For saltwater intrusion analysis (by transport model), and once there are very few locations were salinity concentrations are

known, very few Observation points could be defined. Due to this, transport model calibration would be not possible.

5.4   Calibrating the model

Besides heads in Observation points, a set of premises based on the conceptual model and field observations from former studies were used to calibrate the model:

- Hydraulic heads in the alluvial deposits are usually at 1 to 5 m deep.
- Hydraulic heads in alluvial deposits < heads in Pliocene < heads in Miocene in the central area of the model, under natural (no pumping) conditions.
- Hydraulic heads follow the topographic surface at the topmost slice, being at least 1 m bellow the topographic height in each node of the mesh.
- No flooded areas were allowed, except in very low terrain were marshes are known to occur.

Once the observation points give the heads at the topmost slice and the model calculates heads for each slice of the model, the way to check if Miocene and Pliocene heads behaved according with the conceptual model was to check from the topmost Pliocene and Miocene slices below the respective leaky layers (Slice 7 and Slice 18 respectively) if, in the central model's area, Miocene's heads were higher than Pliocene's. Outside this area, Pliocene and Miocene heads' relationships are in general poorly characterized, so *Pliocene heads < Miocene heads* was not considered a mandatory condition.

To identify areas where heads were above or too much below the topographic surface, a set of comparison tools was developed in FEFLOW "Auxiliary Data" package. In this package the user can create any set of tools to better check the calibration process. The only tool already present in this package is "**$error_norm_flow**". This tool identifies areas were the model might need local mesh refinement.

The tools developed for the case study identified the mesh nodes where flooding occurred and the differences between head and topographic surfaces, to assess it they obeyed the required premises above presented. One of the tools created was the **elev-piezo**, which evaluates the difference between the topographic height and the simulated head in each point of the mesh; negative values identify flooded areas while large positive values identify model flaws requiring reworking and calibration.

To precisely pinpoint flooded areas – which should not exist under natural and pumping conditions – **error elev vs head** tool was developed. This tool evaluates the significance of the elev-piezo values under a threshold of ±1 m. If, in any one node, heads - topographic height is < +1 m, the node is assumed as not flooded; so flooding with less than 1 m deep is ignored. If heads - topographic height is > +1 m, the node is assumed as flooded and calibration is required. ±1 m threshold was chosen because it is inferior to the user defined observed vs. simulated error = 3 m, allowing for a narrower error between heads and topographic heights.

Flow model's calibration was performed through conductivity changes (in values and spatial distribution), once this was the parameter to which the model was most sensitive.

5.4.1   Troubles and roadblocks

The data to run the model was assumed to be representative of the historical period (1979-2009). For underlined observed heads this assumption may be a bit stretched, once in most observation points, the data reports only to the date of wells' development. This means there are no long term head series for a representative heads' average for the historical period and, if considering natural conditions, the observation values are almost surely affected by neighbouring wells already installed in the area. Calibration is then hindered by a lack of representative data for the historical period and very few data for natural conditions (prior to the historical period). Similar shortcomings affect pumping rates and salinity data.

There are large areas of the model domain where hydraulic (and transport) properties are missing or scarce. Bibliography data was used as a starting point for model calibration.

Due to the lack of sound heads' and pumping rates' time series, true transient state modelling was not possible. The option, for droughts, was to simulate – after flow model calibration in steady state – with the same recharges and pumping rates for different time periods, in what could be called a "semi-transient" condition. Lack of true transient state modelling could be a major roadblock for saltwater intrusion analysis. However, and although it is a transient problem, saltwater intrusion can be tackled by a 2-step steady state approach:

- Building and calibration of an **initial state transport model** – built from the calibrated flow model in steady state. This initial state transport model simulates present day conditions and the sea/aquifer shoreline is defined by boundary condition h = 0 m and the mass concentration boundary condition = 35 000 mg/l.

- **Simulate sea-level scenarios** – the initial state transport model, is run for recharge and sea level conditions in 2024. Head boundary condition is set _h = constant = new sea level_ at sea/aquifer interface. Mass concentration boundary condition is still = 35 000 mg/l at this interface. The model will run with recharge values for 2024.

- **Comparing results** – comparing the saltwater intrusion interface's differences between the initial and sea-level scenarios will give its evolution due to sea level rise and recharge changes caused by climate change. It can also allow for the comparison between the initial condition and, separately, sea level rise and recharge changes, if simulations for only recharge changes or only sea level rise are performed.

5.4.2   Average annual values of the historical period under natural conditions

Calibration for steady state natural conditions – no pumping wells active – followed 5 steps: (1) Initial Stage, (2) South region calibration, (3) Tejo/Sado – Margem Direita aquifer calibration, (4) Tejo/Sado – Margem Esquerda aquifer calibration, (5) Peninsula de Setúbal calibration.

5.4.2.1   Initial Stage

The initial model had a set of 3 layers and 4 slices, representing the alluvial deposits, Pliocene and Miocene. A single value of conductivity, porosity and specific storage were assigned to each layer according with its lithological characteristics. These values are given in Table 5.12. This early state didn't give the head differences between these hydrogeological units observed in the central area of the model. The results also demanded a vertical refinement of the mesh. Some horizontal refinement was also required in problematic areas.

Table 5.12 – Hydraulic conductivity values before model's vertical refinement

Slices	Alluvial deposits	Pliocene	Miocene
Slice 1	150 m/d	80 m/d	100 m/d
Slice 2		80 m/d	100 m/d
Slice 3			100 m/d

So, after **vertical mesh refinement**, the model had 24 slices (later on increased to 26). Alluvial deposits were still defined by Slices 1 and 2, and Pliocene and Miocene by a set of 11 and 12 slices respectively (cf. Table 5.5, Table 5.13). **Horizontal refinement** was made around rivers and any areas where the error-norm flow > 0. This new layering allowed the **introduction of semi-pervious layers** between alluvial, Pliocene and Miocene formations. The new distribution of conductivities, still homogeneous across each formation, is given in Table 5.13 and the associated heads surface after the model run is shown in Figure 5.8 for Slice 1.

Table 5.13 – Hydraulic conductivities (Kxx) after the final vertical refinement

Slices	Alluvial deposits	Semi pervious deposits	Pliocene deposits	Semi pervious deposits	Miocene deposits
Slice 1, 2, 3	150 m/d		80 m/d		100 m/d
Slices 4, 5, 6		10^{-6} m/d	80 m/d		100 m/d
Slice 7 to 14			80 m/d		100 m/d
Slices 15, 16, 17				10^{-6} m/d	100 m/d
Slices 18 to 26					100 m/d
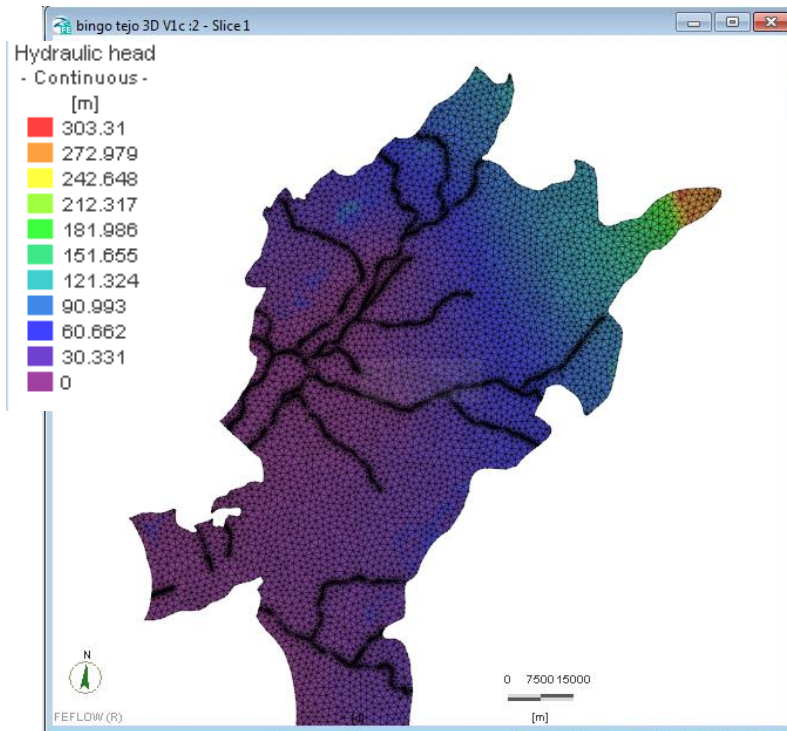
Figure 5.8 – Hydraulic heads in Slice 1, for model version bingo Tejo 3D V1c

The model still performed rather poorly after mesh refinement. Heads in several places were above the topographic surface. Typically these areas were located where the model required further horizontal refinement (where norm flow > 0), as shown in Figure 5.9.
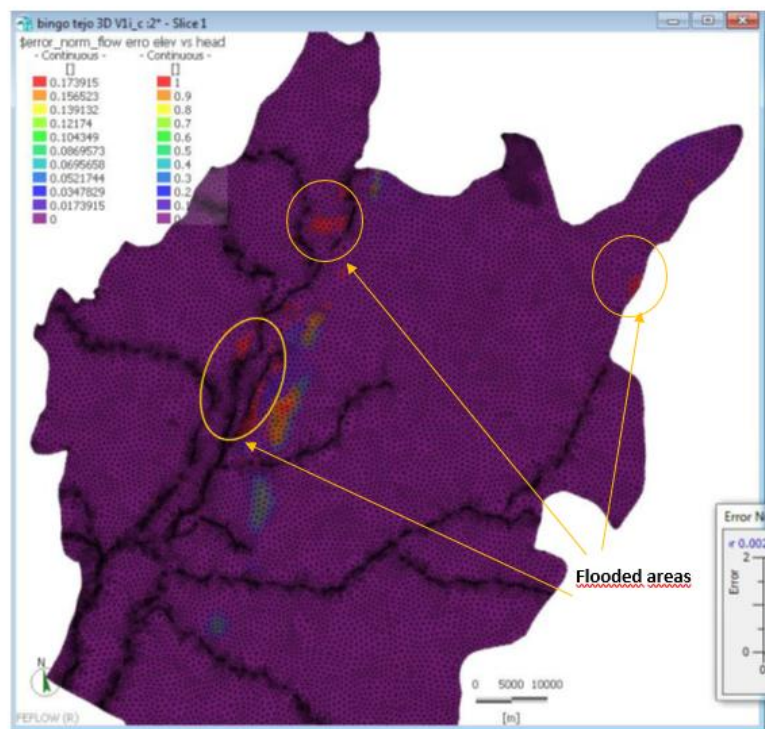
Figure 5.9 – Areas of model flooding (in orange) and model misbehaviour (in multicolour) demanding further refinement of the mesh

Its imbalance was 25 000 m³/day, which is a quite large value although not too exaggerated when considering the water volumes involved. Although the model was finally able to simulate the relationship *h alluvial deposits < h Pliocene < h Miocene* in the central area of the model, in agreement with the conceptual model, it still had oscillation problems.

After the **horizontal refinement in the problematic areas of the model**, the next step was to **reduce the recharge values** to half **in the largest flooded areas**. This reduction to half was done once there is the indication, from other studies, that BALSEQ_MOD often over-calculate recharge and the usual best fit result is a 50% recharge reduction. After such changes, less flooded areas where generated by the model and those had smaller water heights.

Setting **boundary condition h = constant = topographic level** in the second order rivers and **increased conductivity** in the upstream area of the alluvial deposits to 250 m/d made flooded areas disappear. Water residuals were increased to 0.2 m and error tolerance decreased to 1.25 x 10⁻³ (it was initially set at 5 x10⁻²). This lead to other model results' improvements:

(1) Head surfaces for Slice 1 had a better agreement with the topography. Nevertheless, there were still large discrepancies in some model areas, which also happened to be the hydraulically least know areas (e.g.: NE tip of the model, where heads were way below the topographic surface).

(2) Relationship $h_{alluvial\ deposits} < h_{Pliocene} < h_{Miocene}$ is upheld in the central area of the model (where in fact it was identified by field observation).

(3) Oscillation problems reduced to less than 2 m.

(4) Imbalance (= budget error) decreased to circa 10³ m³/day, which is less than the 1% error when considering the whole volume of water.

The heads for these new conditions are given in Figure 5.10. Nevertheless, in spite of the model improvements, there were still significant errors between the observed and the simulated heads in the observation points (besides Slice 1's heads were too much below the topographic surface in some regions of the model). To overcome this, **changes in the vertical conductivity** were made. So, conductivity changed from an initial isotropic Kxx = Kyy = Kzz (see the values in Table 5.12) to Kxx = Kyy = Kzz * 10 in each layer. New conductivity values Kxx = Kyy = 10 and 20 m/d were attributed for Miocene and Pliocene respectively. This reduced the observed vs. simulated heads error in the observation points and, with an error tolerance set at 2.75x10⁻³, the model's oscillation problems disappeared. However, several areas flooded again and the imbalance grew to 16 091 m³/day.

To eliminate the new flooded areas, **recharge for the whole model domain was reduced** by 50%. This strongly reduced the number of flooded areas and their floods' depth. The imbalance came out as 6 000 m³/day. Error tolerance could be reduced to 1x10⁻³ and oscillation problems were reduced to just 1 m. However, the observed vs. simulated heads error was still quite high.
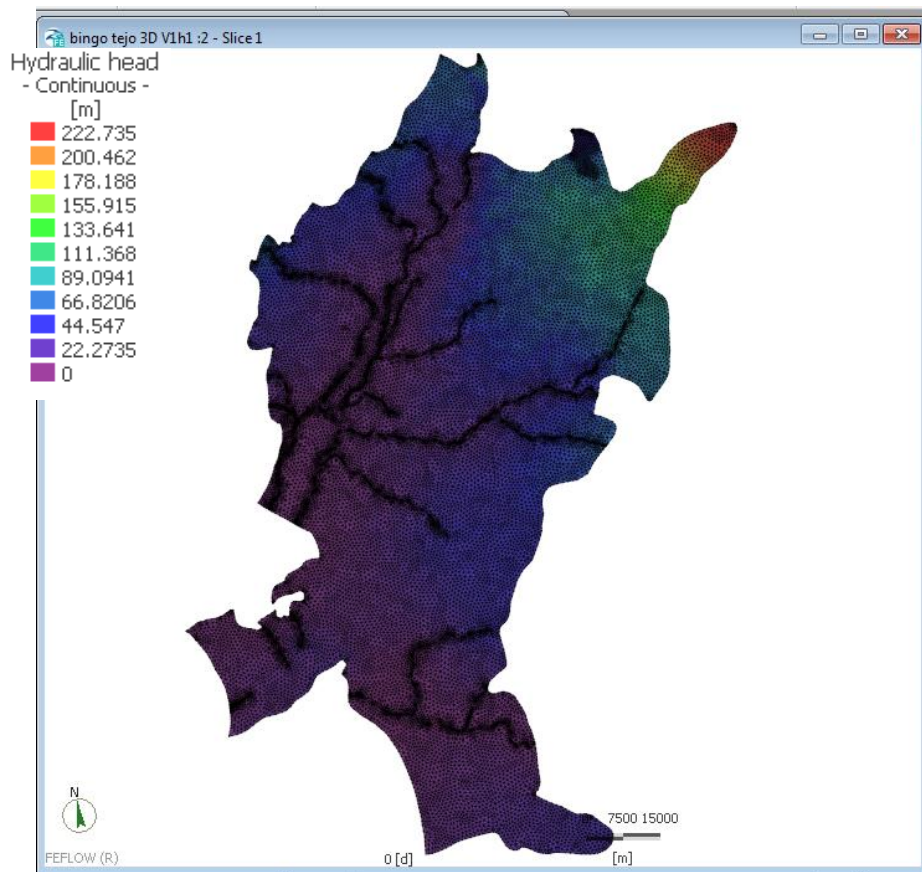
Figure 5.10 – Hydraulic heads in Slice 1, for model version bingo Tejo 3D V1h1

5.4.2.2 Calibration of the model southernmost region (Tejo/Sado – Margem Esquerda aquifer)

To further reduce the high observed vs. simulated heads error on the southern area of the model, **fluid-flux boundary conditions** were set up at Slices 1 and 2 in some parts of the model's border (Figure 5.11) to better simulate outflows towards adjacent areas, some of them aquifers on their own right. **Pliocene conductivities were changed** to Kxx = Kyy (Figure 5.12), in accordance with its horizontal variations in sandy sediments.

The flooded areas almost disappeared in this model area, with the exception on very small areas and a large low zone around Sado's mouth. This is a marshy region and flood was assumed as reflecting its real conditions. Observed vs. simulated heads error for the whole model decreased, but was still quite high: E = 30.56; RMS = 40.8; σ = 40.82. So, calibration for the remaining model areas was performed next, on a region by region basis.
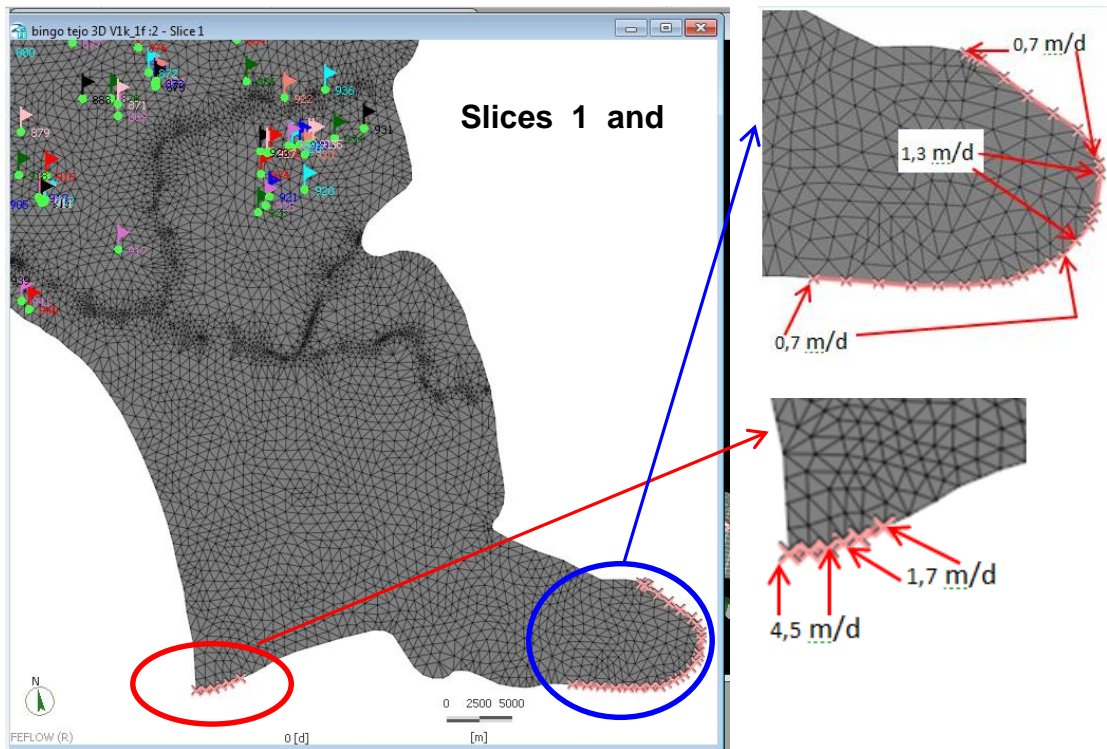
Figure 5.11 – Fluid-flux boundary conditions in the South border of the model (nodes in pink crosses)
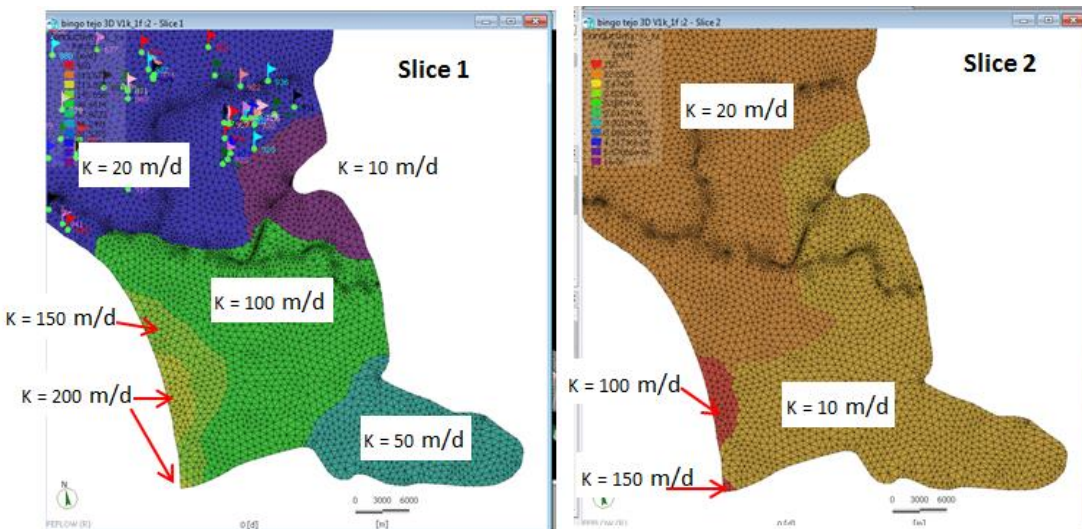
Figure 5.12 – Hydraulic conductivity for Slices 1 and 2 in the south sector of the model

5.4.2.3   Calibration of Tejo/Sado – Margem Direita aquifer

To calibrate this area, **conductivities were changed in an iterative basis**. No attempts were made to change porosity, once the model wasn't sensitive to such changes as far as heads were concerned. After changing conductivities, in the spots where observed vs. simulated errors at observation points were high, model outputs showed:

(1) Heads' surface in Slice 1 follows the topographic surface. Flooded areas disappeared in this region.

(2) Observed vs. simulated errors at observation points ranges from < 1 m to 3 m (locally some points might have errors up to 5 m).

(3) Imbalance = -233 m^3/day.

(4) Observed vs. simulated error for the whole model domain is: E = 11.09; RMS = 16.45; σ = 16.47.

(5) Relationship $h_{alluvial\ deposits} < h_{Pliocene} < h_{Miocene}$ is upheld in the central area of the model.

(6) Model oscillation still occurs. Head differences between simulations were set at 2 m. The error tolerance was set at 5.3 x 10^{-3}.

Calibration at the Tejo/Sado – Margem Esquerda and Alluvial aquifers were the next steps once they had large observed vs. simulated errors at the observation points. Several punctual flooded areas also occur there.

5.4.2.4   Calibration of Tejo/Sado – Margem Esquerda and Alluvial aquifers

The first step for the Aluviões do Tejo aquifer's calibration was to **refine the vertical mesh**. In this final refinement, the first layer – defined by Slices 1 and 2 – was divided into 3 layers, defined by Slices 1, 2 and 3, with Slice 4 defining the top of the leaky layer between the alluvial deposits and Pliocene. The final vertical refinement is presented in Table 5.13. This was used for better representation of vertical conductivity variations in the alluvial deposits. For the Margem Esquerda aquifer, n**ew Fluid-flux boundary conditions** were set up at NE border to better simulate water discharges towards surrounding areas. **Conductivities changes**, performed in an iterative process, were also introduced.

A good agreement between simulated vs. observed heads at observation points and, in Slice 1, with the topographic surface was achieved for Margem Direita, Aluviões and Margem Esquerda aquifers, up to Sorraia River. The amount of flooded areas reduced sharply. Observed vs. simulated heads error for the whole model domain was: E = 4.9, RMS = 8.8; σ = 8.8. Imbalance (budget error) decreased to 130 m^3/day. South of Sorraia River and Peninsula de Setúbal, the model was still performing poorly and presented several small flooded areas.

5.4.2.5   Calibration of Tejo/Sado – Margem Esquerda (Península de Setúbal)

To calibrate Península de Setúbal, a **fluid-flux boundary condition was set at the border of the aquifer with Arrábida Hills** (Figure 5.13). Due to information from other projects, an inflow from the calcareous Arrábida Hills into Margem Esquerda aquifer was assumed and this boundary condition was set at Slices 1 and 2. **Boundary condition h = 0 m** was set for all the nodes defining the southern border of the estuary and the sea-shore of Trafaria-Arrábida. **Boundary condition h = topographic height** was set for 3rd order rivers. **Conductivity changes**, performed in an iterative process of change/simulate/change similar to that used for Margem Direita and Aluviões do Tejo calibration, were also done.
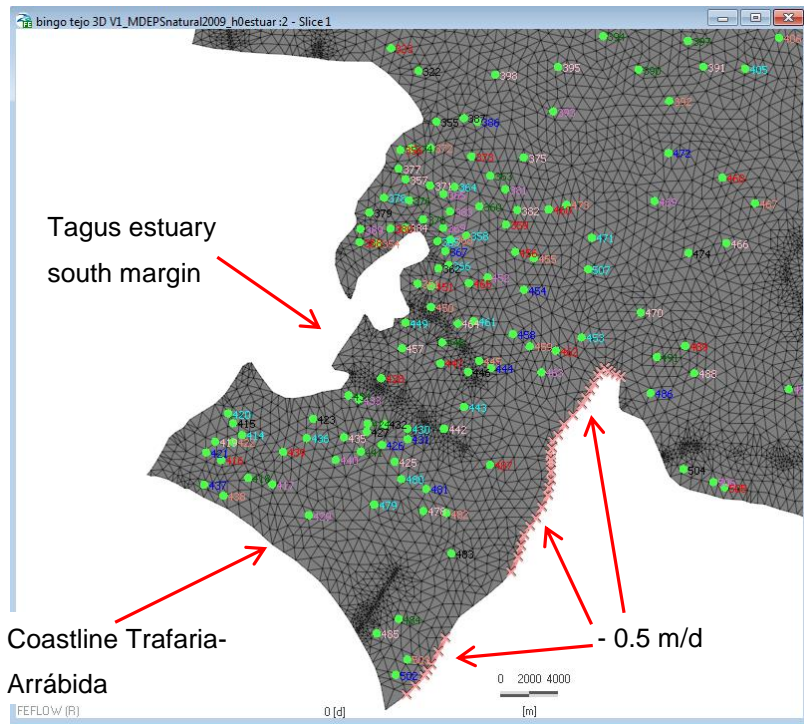
Figure 5.13 – Fluid-flux boundary conditions at the border with Arrábida Hills (nodes in pink crosses)
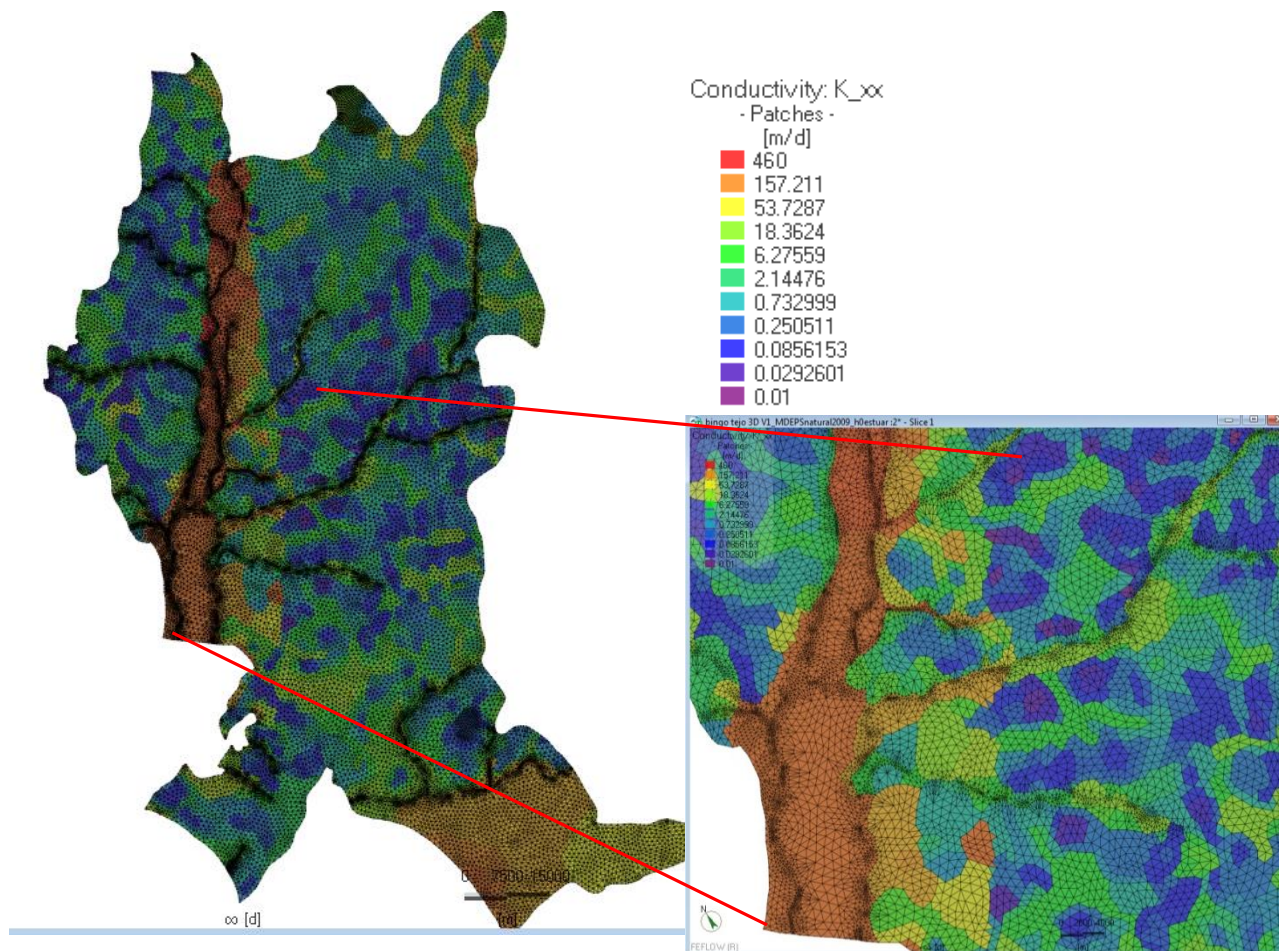
Figure 5.14 – Conductivity's distribution (Kxx = Kyy = 10 * Kzz) for Slice 1

At the end of this process, model outputs showed:

(1) No flooded areas (besides the one assumed to be so at the mouth of Sado River).

(2) Heads in Slice 1 follow pretty well the topographic surface.

(3) Observed vs. simulated heads' error for the whole domains reduced to E = 2.67, RMS = 3.88; σ = 3.88

(4) Imbalance = -768.67 m^3/day. Error tolerance had to be increased to 8.6 x 10^{-3}.

The model was then assumed **calibrated for steady state conditions**. Final conductivities' distribution is shown in Figure 5.14 to Figure 5.18. Heads for the Alluvial aquifer, Pliocene and Miocene formations are shown in Figure 5.19 for Slice 1. Some observation points with their respective heads observed vs. simulated error are shown in Figure 5.20.
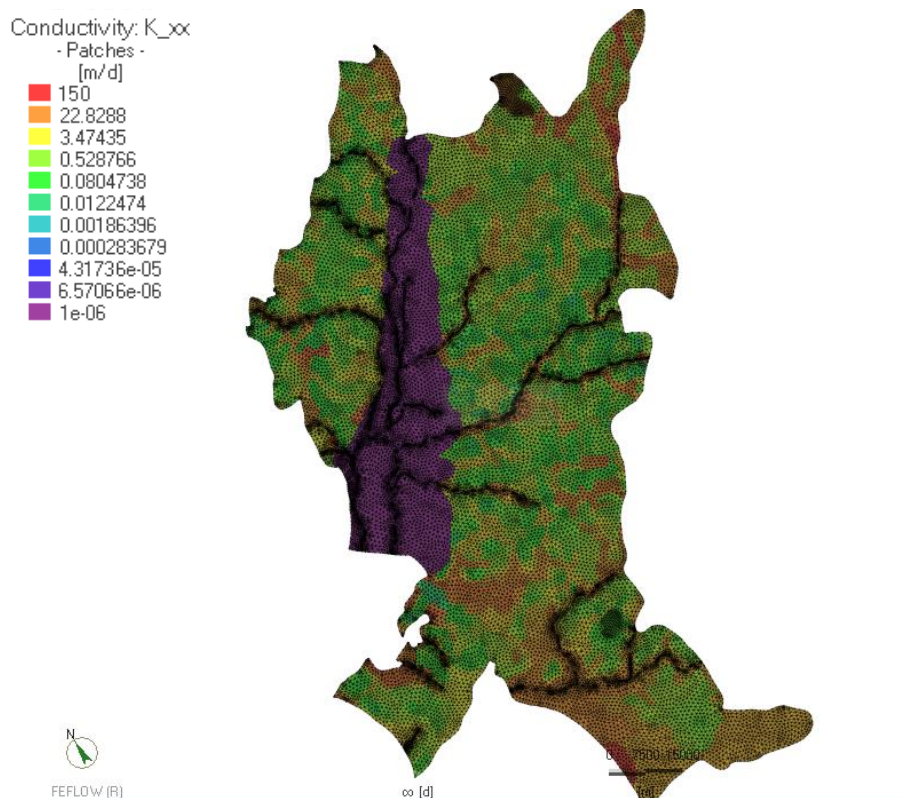
Figure 5.15 – Conductivity's distribution (Kxx = Kyy = 10 * Kzz) for Slice 4 (top of leaky layers between Alluvial and Pliocene deposits)
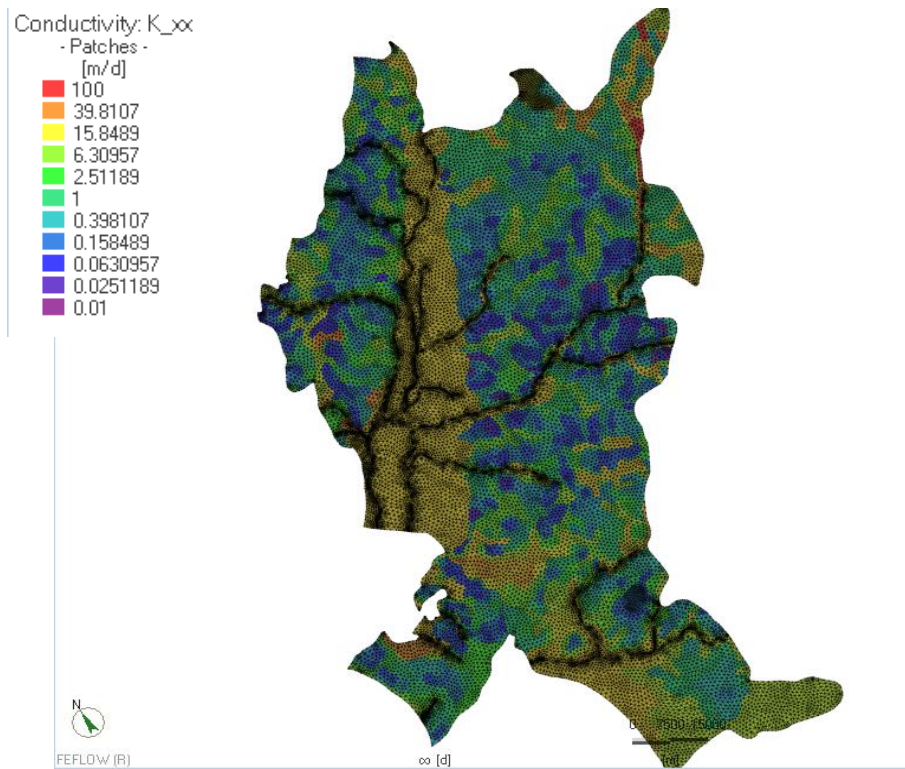
Figure 5.16 – Conductivity's distribution (Kxx = Kyy = 10 * Kzz) for Slice 7 (top of Pliocene deposits)
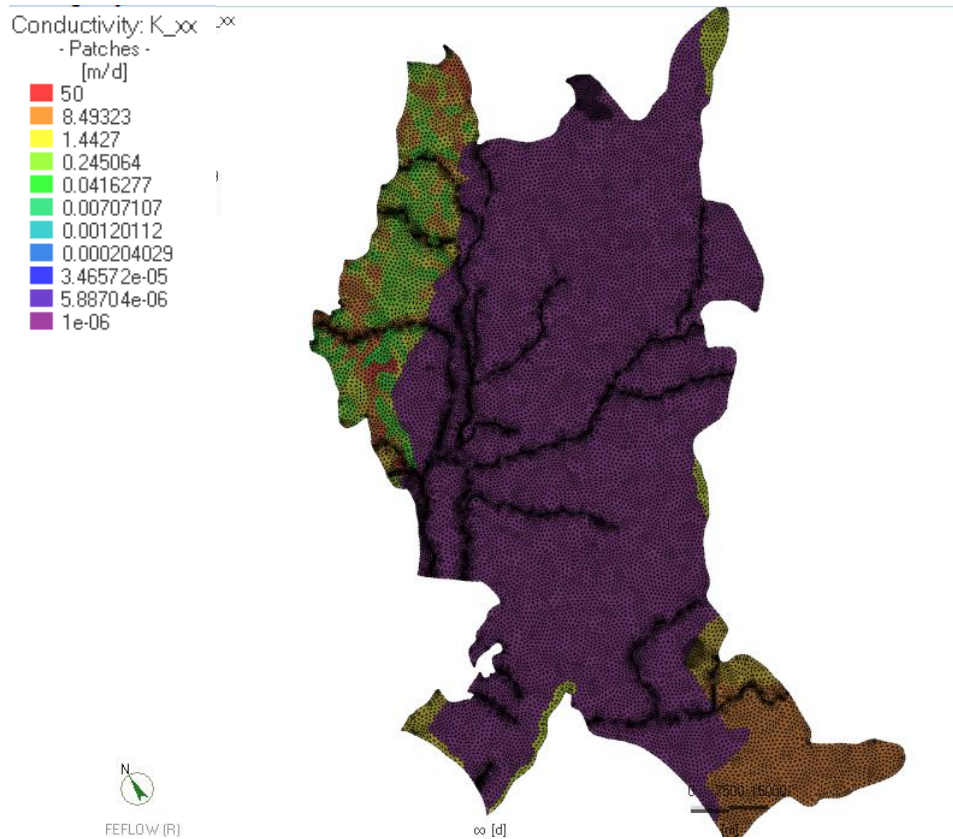
Figure 5.17 – Conductivity's distribution (Kxx = Kyy = 10 * Kzz) for Slice 15 (top of the leaky layers between Pliocene and Miocene deposits)
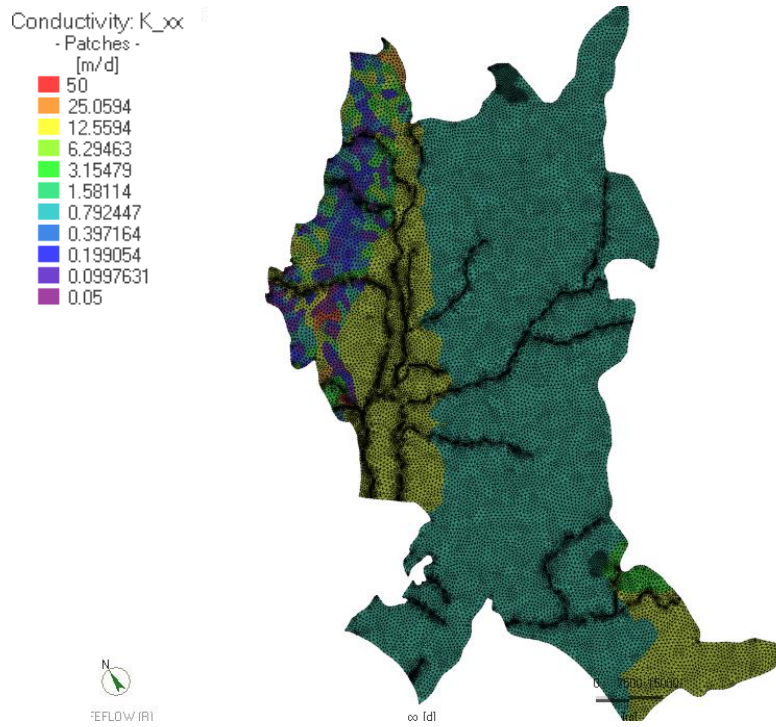
Figure 5.18 – Conductivity's distribution (Kxx = Kyy = 10 * Kzz) for Slice 18 (top of Miocene deposits)
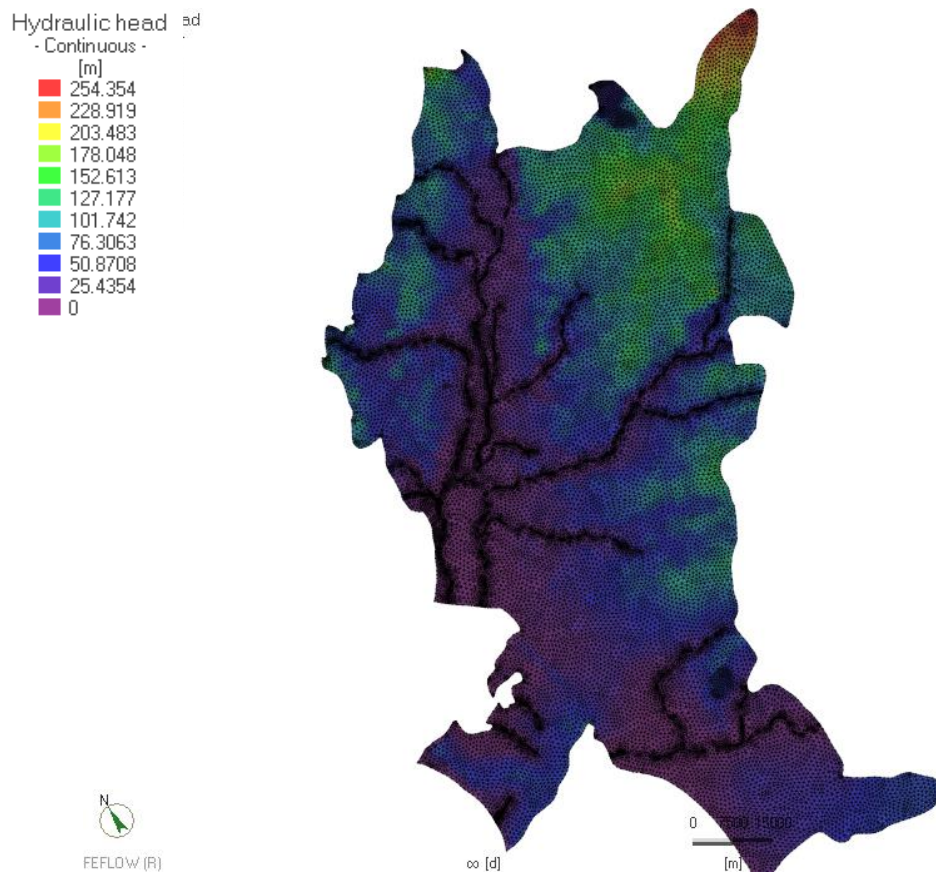
Figure 5.19 – Heads' surface for Slice 1 (steady state natural conditions calibrated model)
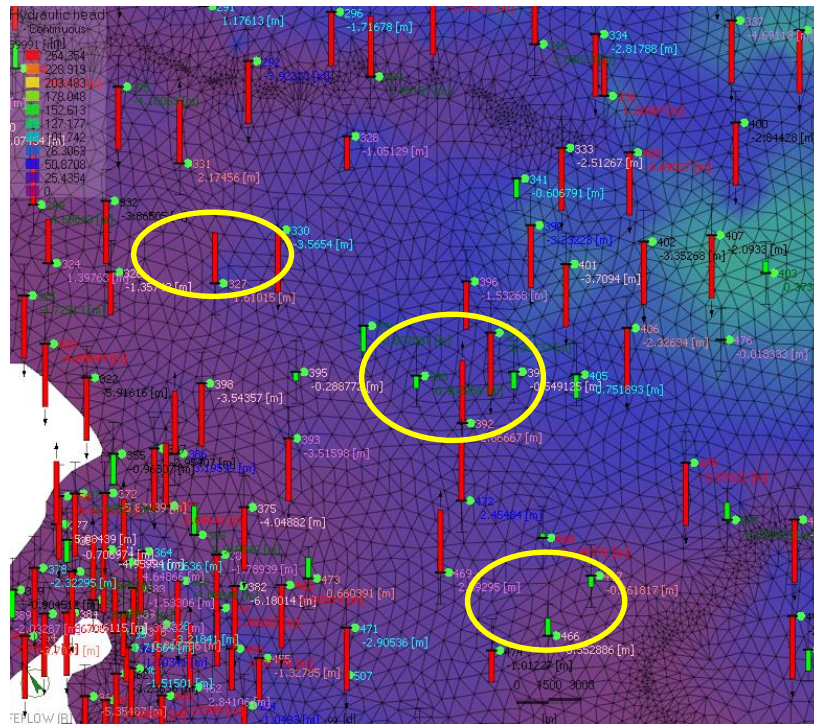
Figure 5.20 – Representation of observed vs. simulated heads' error at observation points in Slice 1 (red: error > 1 m; green: error < 1m)

5.4.3 Average annual values of the historical period with water abstractions

Once the model is calibrated for the natural conditions (no pumping), pumping wells (with constant pumping rates) were introduced into the model. This demanded recalibration, which was done by locally readjusting conductivity values. After recalibration:

- Imbalance = 369.7 m^3/day.
- Error tolerance = 2.28x10^{-3}.
- Observed vs. simulated heads error for the whole model domain: E = 3.496, RMS = 4.8275; σ = 4.832.

In these new conditions, some depression in heads' surfaces is observed, with some points showing up to 15 m drawdowns, when compared with the original conditions for Slice 1 (in the alluvial aquifer). Lowland areas of Sado River mouth show a marked decrease in the flooded/ swampy zone, which agrees with observed trends in the field. All this illustrates the influence of pumping regimes on heads surfaces. Heads for Slice 1 under pumping conditions are shown in Figure 5.21. Figure 5.22 shows the observed vs. simulated heads error in several observation points. Drawdowns due to pumping can be obtained comparing the points (marked in yellow) in Figure 5.20 and Figure 5.22. For a better understanding of what has been done during model calibration, the main steps of the calibration process are shortly described in Table 5.14.
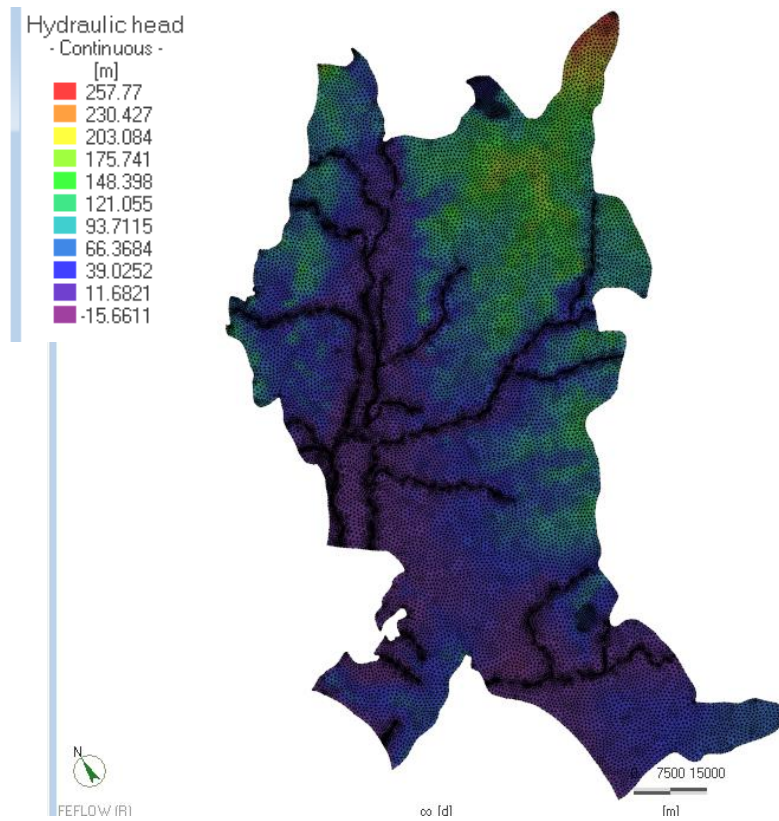
Figure 5.21 – Heads' surface for Slice 1 under pumping steady state conditions for the historical period
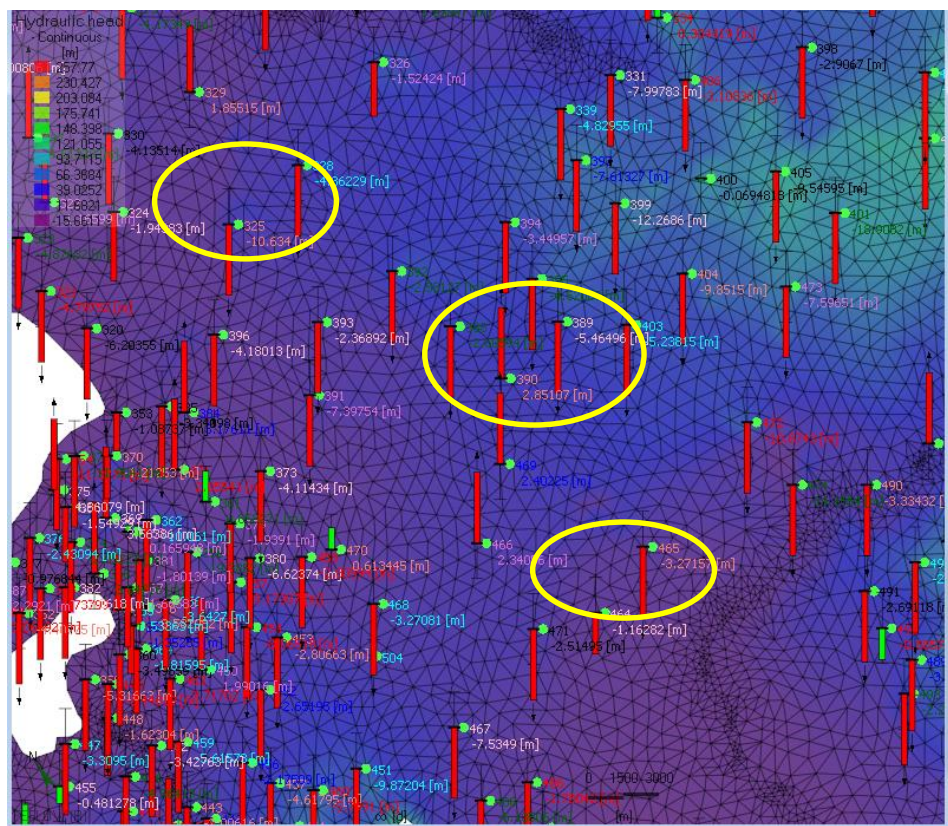
Figure 5.22 – Observed vs. simulated heads error at observation points (steady state pumping conditions)

Table 5.14 – Model calibration's progress

Development step	What was done	What improvements achieved	What was wrong
Phase 1: Model construction	Mesh generation, with rivers; 1 single slice	Start of model build-up	Is a 2D model for a 3D problem
	Layers (3 layers) generation with uniform thickness	A 3D model was obtained	The model does not reproduce real layers' thickness variations
	Real thicknesses are input into the model	Thickness variations are represented in model	Geometric incongruences
Phase 2: Model construction	Geometric incongruences solved by surface interpolation, elimination of crossing surfaces & surface smoothing	Model has good & realistic representation of aquifer geometry (defined in conceptual model)	Model does not have yet the definition of the problem, hydraulic properties, recharge, boundary conditions
	Type of modelling problem & hydraulic properties were input	The model problem has been set up	Recharge and boundary conditions are not yet defined
	Input of recharge and boundary conditions h = 0 m for the coastal area	All basic requirements for running the model are now input	The model runs but it does not converge
	Error tolerance changed from default value (1×10^{-3}) to 3×10^{-3}; Number of iterations increased to 35	The model runs and converges	Heads for the 3 layers are the same; the model domain is completely flooded
	Hydraulic conductivities changed: Alluvial deposits = 150 m/day; Pliocene = 80 m/day; Miocene = 100 m/day (50 m/day as Kzz)	Most of the model is no longer flooded	Flooding still occurs along Tejo, Sorraia and other major tributaries' valleys
Phase 3: Model construction	Boundary condition h = 0 m defined for rivers in the flooded areas; 1st Layer (Alluvium) is set as Phreatic, 2nd layer (Pliocene) as dependent and 3rd layer (Miocene) as confined; error tolerance set at 2×10^{-2}	Flood disappears from valleys but still occurs in the NE tip of the model	NE tip of model flooded; h Miocene < h Alluvial deposits & h Pliocene; Imbalance still very high
	The 3 layer model becomes a 23 layer model (24 slices)	No improvement	Heads & flood problems & very high imbalance remain
	Boundary condition h = topographic height applied to each river node, including 3rd order rivers	Very local flooding: at some rivers' nodes & small areas across the model	Heads' problems and very high imbalance remains
Phase 4: Model construction	Erroneous river nodes corrected; horizontal refinement of the mesh in flooded areas; boundary condition h = 0 m set at flooded nodes where sharp topographic gradients with neighbouring nodes occur	Flooded areas disappear	Imbalance still very high; model oscillation problems still occur; heads basically the same for all slices

Development step	What was done	What improvements achieved	What was wrong
	Error tolerance reduced to 0.2 x 10^{-3}; Residual water depth for unconfined layers changed from 0.00101 to 0.1	Imbalance is strongly reduced	Model oscillation still occurs but is reduced to 1 m; heads at all layers are basically the same
	Fluid flux boundary conditions set at model borders contacting with outside water bearing units; Error tolerance set at 0.3 x 10^{-3}	Model oscillations disappear	Heads are basically the same in all slices
Phase 5: Pre-calibration	Conductivities across horizontal directions, with Kxx = Kyy, specific storage & porosities are different for alluvial deposits, Pliocene & Miocene; vertical conductivities Kzz = Kxx; Impervious layers set between alluvial deposits, Pliocene and Miocene (Kxx = Kyy = 1 x 10^{-6}); error tolerance set at 3.6 x 10^{-3}	Distinct heads for alluvial, Pliocene & Miocene formations in alluvial area (crudely following the conceptual model) are now simulated	Flooded areas have returned and located in areas of poor mesh quality; oscillation problems have returned; error_norm_flow problems show up, mainly in spots in the central area
	Mesh geometry improvement; Recharge reduction to half in larger flooded areas; error tolerance set at 2 x 10^{-3}	Distinct heads for alluvial, Pliocene & Miocene deposits; Most flooded areas disappear; flood height reduced in those still flooded nodes	Some flooded areas remain; model oscillations rise to 7 m; imbalance under the 1% threshold but still high
	Conductivity increase of upstream alluvial deposits to Kxx = Kyy = 250 m/day; error tolerance set at 2 x 10^{-3}; boundary condition h = topographic height set at nodes still flooded, where sharp topographic gradients with neighbouring nodes occur (NE area)	Flooded areas disappear; distinct heads for alluvial, Pliocene & Miocene deposits in most part of the alluvial deposits; Imbalance at 16 900 m^3/day	Model oscillations reduced to 4 m; Alluvial, Pliocene & Miocene heads locally disagree with conceptual model
Phase 6: Pre-calibration	Residual water set 0.2; error tolerance = 1.25 x 10^{-3}	No flooded areas; heads follow the conceptual model; model oscillations = 2 m; Imbalance = 4 000 m^3/day	Model still oscillates
Phase 7: Calibration Right Margin aquifer	Observation points added to the model	Errors between observed and simulated values can be observed & analysed	Observed vs. simulated heads' errors are large, the simulated heads usually being much higher; in the alluvial area the errors are lower (usually < 10 m); in several areas this might be due to the presence of small suspended aquifers (impossible to simulate)
	Kzz is now = Kxx/10	Imbalance reduced to 1 039 m^3/day	Flooded areas return (very small, all located downstream, near rivers); flooded heights ≤ 1 m; observed vs. simulated heads' errors didn't improve
	Conductivities are (Kxx = Kyy): Miocene = 10 m/day, Pliocene = 20 m/day; Alluvial deposits= unchanged error tolerance = 2.75x10^{-3}	No model oscillation; observed vs. simulated heads' errors reduced; heads obey the conceptual model (central area); Pliocene heads bellow Miocene's in Margem Direita and Margem Esquerda south part	Observed vs. simulated heads' errors are still very high; Imbalance raises to 16 091 m^3/day after Pliocene conductivities were changed; several flooded areas return, mainly in NW & NE areas of the model and Península de Setúbal
	Recharge reduced to half in the whole model domain; Error tolerance = 1x10^{-3}	Imbalance decreases to 1000 m^3/day; number of flooded areas strongly decrease and flood height decreases are particularly sharp	Flooded areas still occur; observed vs. simulated heads' errors increased
	Boundary condition h = 0 m removed at coastal border; Pliocene conductivity Kxx = Kyy= 100 m/d in southern model area (slices 1 to 4 only); error tolerance = 0.8 x10^{-3}	Flooded areas significantly reduced; observed vs. simulated heads' error lightly reduced	Imbalance = 8 000 m^3/day; model oscillation = 1 m; flooded areas still occur; observed vs. simulated heads' error still very high

Development step	What was done	What improvements achieved	What was wrong
	Fluid Flux boundary condition set 4.5 m/day & 0.7 to 1.3 m/day at SW (=) and SE model borders respectively; Conductivities (slices 1 to 4) at coastal area S of Sado river = 200 to 300 m/day, SE model zone = 100 m/day and remaining model's S area = 50 m/day	Flooded areas disappeared from model's S part, except in Sado estuary's lowlands; observed vs. simulated heads' error decreased slightly	Imbalance = 8 000 m³/day; flooded areas still occur at: Península de Setúbal seashore, NE & NW model tips & point areas scattered throughout the model; observed vs. simulated heads' error still very high
	Observation points topography corrections; duplicated observation points removed; conductivities changed on a zonal basis, to calibrate Margem Direita area; error tolerance = 5.3 x 10⁻³	Top layer heads start to follow the topography; observed vs. simulated heads' error significantly reduced	Observed vs. simulated heads' error still very high; Imbalance rises to 35 031 m³/day; flooded areas strongly reduced but still occurring at Left Margin, Right Margin (very local) and Península de Setúbal
	Conductivities changed on a zonal basis, to reduce head errors in Margem Esquerda area; Fluid Flux boundary condition set at NE tip of the model; error tolerance = 5.5 x 10⁻³	Observed vs. simulated heads' error reduced (E = 30.56; RMS = 40.8; σ = 40.82); top layer heads with better agreement with topography	Flooded areas still occur but its number and area are significantly reduced although there are still many in Left Margin and Península de Setúbal areas
	Conductivities changed on a zonal basis to better calibrate Margem Direita area; eror tolerance = 5.3 x 10⁻³	**Margem Direita calibrated**; Margem Direita top layer's heads follow topography; flooded areas disappeared in Margem Direita; observed vs. simulated heads' error strongly reduced (E = 11.088; RMS = 16.45; σ = 16.47) and ranges from <1 m to > 3 m (locally 5 m) at observation points; Imbalance reduces to – 223 m³/day	Model oscillates (2 m); flooded areas occur on Margem Esquerda and Península de Setúbal
Phase 8: Calibration Left Margin & Alluvial aquifer	Conductivities changed in Left Margin (Miocene Kxx = reduced from 10 to 1 Slices 16 to 24; Kyy & Kzz unchanged); error tolerance = 5.1 x 10⁻³	Heads obey the rule – alluvial < Pliocene < Miocene heads – set by the conceptual model	Heads at the upper slices and the amount of flooded areas unchanged; observed vs. simulated heads' error rises to: E = 12.117; RMS = 19.1626; σ = 19.18
	Conductivities changed in Left Margin aquifer (Miocene Kxx = Kyy = 1; Kzz = 0.1 m/day) on a zonal basis at its N sector; fluid-flux boundary conditions at model's NE tip of range from 0.7 to 5 m/day	Heads obey the rule – alluvial < Pliocene < Miocene heads – set by the conceptual model	Flooded areas reduction; observed vs. simulated heads' error shows slight decrease
	Conductivities zonally changed in Alluvial aquifer; vertical discretization refinment (alluvial aquifer has 3 slices & whole model 26 Slices; slices 4, 5, 6 & 15, 16, 17 are impervious layers between respectively alluvium & Pliocene, Pliocene & Miocene); error tolerance rises to 6.5x10⁻³	**Alluvial aquifer calibrated;** imbalance = 130; no model oscillation; observed vs. simulated heads' error: E = 7.1; RMS = 11.1; σ = 11.11; top layer heads following topography areas expand; flooded areas decrease	Flooded areas still occur (at Left Margin & Península de Setúbal); some flooded areas had to be forced by BC h = topographic height to disappear (areas of steep topographic gradients between adjacent nodes)
	Conductivities are changed on a zonal basis (except at Península de Setúbal) for adjustment with observed values on Margem Esquerda aquifer; Error tolerance has risen to 6.7 x 10⁻³	**Margem Direita, Alluvial & Margem Esquerda up to Sorraia calibrated**; Imbalance remains = 130 m³/day; observed vs. simulated heads' error reduction (E = 4.9; RMS = 8.8; σ = 8.8); top layer heads follows topography on a wider area; less flooded areas (all south of Sorraia)	Several flooded points remain, south of Sorraia; Península de Setubal's coastline flooding still occurs; several areas have error_norm_flow
Phase 9: Horizontal mesh refinement	Mesh refinement in the error_norm_flow areas	Lower number of error_norm_flow areas	Error_norm_flow problems do not disappear; number of flooded areas (and flood depths) increases
Phase 10: Calibration of Left Margin south of Sorraia River	Boundary condition h = 0 at estuary & sea shores where topography ≤ 3 m; conductivities zonally changed in Margem Esquerda south of Sorraia and in Península de Setúbal; error tolerance rise to 8.6 x 10⁻³	Flooded areas disappeared except in some Peninsula de Setubal's coastline nodes; top layer's heads better follows topography ; observed vs. simulated heads' error is : E = 2.65; RMS = 3.85; σ = 3.85	Imbalance = -817.8 m³/day; flooded points at the with flood heights of ≈1m; Error_norm_ flow problems do not disappear

Development step	What was done	What improvements achieved	What was wrong
	Boundary condition h = 0 is set to the whole coastal and estuary border (except the N border) regardless of nodes' topographic height	**Model calibrated for steady state natural conditions**; Imbalance = -768.59 m^3/day	Observed vs. simulated heads' error slightly increases (E = 2.67; RMS = 3.87; σ = 3.878); Error_norm_flow problems remain
Phase 11: Modelling natural conditions (steady state)	Steady state simulation with average recharge for 1979-2009 (original BALSEQ_MOD's results halved); no pumping	Imbalance = -768.59 m^3/day; observed vs. simulated heads' error: E = 2.67; RMS = 3.875; σ = 3.879	Pumping wells not yet input
Phase 12: Calibrating with pumping wells	Input of agriculture and some industry pumping wells; wells aggregation to obey the one well per mesh element rule; error tolerance = 4 x 10^{-3}	The model is now simulating pumping conditions	Observed vs. simulated heads' error: E = 4.259; RMS = 9.504; σ = 9.513; flooded areas show up again; Imbalance = 15 311 m^3/day; anomalous heads on 5 nodes of Slices 5 & 6 at central area (didn't exist before); Error_norm_flow problems remain
	Conductivities zonally changed in flooded areas; slices 5 & 6 (leaky layers) conductivities changed from 10^{-6} to 1 m/d in the anomalous heads area; error tolerance = 2.2 x 10^{-3}	Imbalance = 15 280 m^3/day; observed vs. simulated heads' error: E = 3.6499; RMS = 5.2215; σ = 5.2266; head outliers at flooded areas disappear; less & smaller flooded areas; top layer's heads follow topography again, in most of the model domain	Still several flooded areas; heads' issues in slices 5 & 6 remain; observed vs. simulated heads' error increased in some observation points and this occurs in previously flooded areas after wells' input; Error_norm_flow problems remain
	Conductivities zonally changed in flooded areas	Flooded areas in Península de Setúbal, S area and Margem Direita (disperse dots); observed vs. simulated heads' error: E = 3.359; RMS = 4.577; σ = 4.581	Imbalance = 17 824 m^3/day; heads' issues in slices 5 & 6 Error_norm_flow problems remain
	Input of domestic supply (EPAL wells); constraints applied to the wells and non-constraints runs and its outputs compared; error tolerance = 2.28x10^{-3}	Imbalance = 369.7 m^3/day; flooded areas occur at S border and 2 areas in Península de Setúbal; setting up constraints does not improve on the results	Observed vs. simulated heads' error: E = 3.494; RMS = 4.827; σ = 4.83; heads' issues in slices 5 & 6 and Error_norm_flow problems remain
	Boundary condition h = 0 m reset along estuary and coastal shorelines; error tolerance = 2.28x10^{-3}	Flooded area at S border reduced to its SE tip; flooded area at Setubal estuary's lowlands strongly reduced; just 3 nodes flooded in Península de Setúbal; model does not oscillate; Imbalance = 369.79 m^3/day; **model is calibrated for steady state pumping conditions**	heads' issues in slices 5 & 6 and Error_norm_flow problems remain; observed vs. simulated heads' error: E = 3.496; RMS = 4.828; σ = 4.832
Phase 13: Modelling no recharge (steady state)	Recharge = 0 mm/year; pumping conditions as before	Imbalance = -81.678 m^3/day; no flooded areas; **The model reacts correctly to recharge changes**	Observed vs. simulated heads' error: E = 17.668; RMS = 24.18; σ = 24.207

5.5   Model issues and shortcomings

Model limitations can be due to calibration or data restrictions, which can hinder the quality of model results and its prediction capacity. Data quality and lack of reliable time-series data were the main issues associated with possible model prediction capacity's limitations. The data & model issues and their ensuing impacts on model reliability are:

- **Estuary's coastline** – at the upstream border of the estuary there are discrepancies between the real coastline and the aquifers' limits defined in Almeida et al. (2000) and Lei da Água. These discrepancies occur because the aquifer's limits were defined by the limit where land is permanently above estuary waters and water abstraction occurs. This ignores the area where groundwater quality is brackish and the tidal flats and marshy areas of Tagus Estuary Natural Reserve[11]. In fact, these are not aquifer areas, once water exploitation is impossible there (due to brackish waters and low permeability) or is not economically practicable. In normal <u>flow simulations</u> such areas can effectively be ignored due to the above stated characteristics, but in <u>saltwater intrusion,</u> simulations of the correct freshwater/saltwater interface's location must be defined. If this area "in between limits" is ignored, the model's interface location will not be correct, hindering the rightful simulation of saltwater intrusion's evolution. This problem might be minimized by expanding the model to encompass such "in between limits" area.

- **Representation of small suspended water bearing units** – small suspended water bearing units located in terrace deposits and interfluvial zones were not represented in the model due to their small areas and lacking data concerning their thickness/bottom elevation and hydraulic conductivity. Due to this, the hydraulic properties of the surrounding aquifer were attributed to them. As such, the model didn't simulate these regions well and large observed vs. simulated errors occurred at observation points. To reduce such errors, the hydraulic conductivities' changes performed during calibration almost certainly do not represent the real values. This generates some local erroneously large drawdowns and error_nor_flow issues when climate change scenarios are simulated. To overcome this issue, reliable data of location, thickness and conductivity must be obtained for these specific areas (which demands field work).

- **River network** – for simplification purposes and saving computational effort, only the 1st and 2nd order rivers were defined in the mesh. Some 3rd order rivers were later on defined by boundary conditions. At the local level, this might not give a very accurate flow and heads simulation but, at regional level, the results conform to the general observation data. Besides, being a regional model, hydraulic parameters' variations of river's sediments can't exactly be represented and locally the observed vs. simulated heads error can be significant. However, the main problem was the boundary condition set up for rivers (see river network boundary conditions below).

---

[11]   An important natural sanctuary at the European level, being classified as a Ramsar site (cf. http://www2 .icnf.pt/ portal/pn/biodiversidade/ei/ramsar).

- **Hydraulic data**: *Hydraulic conductivity, Porosity, Specific storage* – only average values were available, in most cases from bibliography, which means their spatial variations across the aquifers could not be properly represented but only approximated by calibration. For instance, vertical conductivity's variations, which are bound to occur due to interstratification, couldn't be properly represented because data are scarce. The same goes for horizontal conductivity variations, which calibration partly sorted out, although the final outcome might be different from reality at least in some interfluvial areas, in spite of a good observed vs. simulated heads' agreement. This may hinder the reliability of model results in specific regions (e.g. where drawdowns are too high). To overcome this, field data on such spatial variations are required as well as information on bottom elevation/thickness of the layers in such problematic areas (identified in calibration and climate scenarios simulations).

- **Transport properties**: *Dispersivity, Molecular diffusion* – usually these parameters are not known from field data and are normally defined from bibliography values for each type of sedimentary formation; calibration further improves on their spatial distribution and values. However, observed salinity data are scarce, which hinders calibration and compromise model results. This was one of the reasons why saltwater intrusion model wasn't further developed. To overcome this situation, a set of monitoring points and associated geophysical surveys should be implemented to track: (1) where saltwater intrusion is nowadays, (2) salt concentrations vs. observation depth in each observation well to pinpoint saltwater interface's shape and depth.

- **River network boundary conditions (constant heads)** – due to lack of data to set it as fluid-transfer boundary condition, rivers were simulated as constant-head = topographic elevation at each river's node. Such boundary condition will not correctly simulate the aquifer heads' near rivers nor the water changes river/aquifer. This could account for the very low heads' changes along the valleys, as observed in scenarios simulations, in spite of good agreement between simulated and observed values at the end of the calibration. To overcome this, reliable river stages along the 1st, 2nd and 3rd order rivers are required.

- **Aquifers' land borders boundary conditions (fluid flow)** – at some parts of aquifers' borders, aquifer outflows or inflows occur. This is due either to aquifers' and geological limits mismatch, because of productivity considerations, or both limits match but flows from outside formations occur (e.g. Arrábida Hills' limits). These inflows/outflows' locations and respective flow values were defined by calibration and represented by <u>fluid-flux boundary conditions</u>. However, the real flow values along these borders are unknown so it was impossible to validate the values defined by calibration. Also, in most of these areas, there are no observation points to clearly assess the true heads, so the condition "*head surface follows the topographic surface along Slice 1*" was the only one we could use. Although the model replicates well this condition in these boundary conditions' areas, this does not necessarily mean that the real heads and flows are accurately, or rightfully, simulated. Climate scenarios simulation results in those areas seem to indicate local mismatches between real and simulated flow. To better simulate the hydraulic behaviour of those areas, inflow/outflow field data (or at least heads data) at these borders is required.

- **Ocean and estuary/land border boundary conditions (constant head)** – this should be simulated without boundary conditions, to account for sea level rise impacts. However, sea level rise in 2024 is projected to be = 0.15 m for the 1.5 m (in 2100) sea level rise scenario, which was the scenario used in BINGO (cf. Guerreiro et al., 2015; Antunes & Taborda, 2009). Due to this, sea level rise was assumed as negligible in 2024 and ocean/land border was simulated by constant head boundary condition h = 0 m. However, for saltwater intrusion simulations, in particular for longer time horizons, such boundary condition should not be used. Instead the freshwater/salt water interface should be accurately defined and h = sea level in 2024. In this way, saltwater intrusion present-day location, observation wells to follow its advance and hydraulic properties' data are required.

- **Observation data** – there are no reliable head averages data for 1980-2009 time period, required for steady state simulations. What exists is often a single head value from when abstraction wells were being developed. To calibrate natural conditions, heads from the period before aquifer's exploitation should be known. This hinders calibration and compromises scenarios simulations' reliability. When considering transient conditions, heads' time series from the SNIRH observation network are scarce and full of hiatuses, some of them quite long, while WISE network observation points are too far-between to support model calibration. This means there are no reliable heads' time series to confidently simulate transient conditions and perform model validation. Large model areas lacking observation points also compromise calibration. Salinity data faces similar issues and the lack of observation points further hindered the development of the transport model. Installation of observation points (for heads and salinity) in areas where they simply do not exist would help overcome some of these issues. For heads' time series, krigging could be used to generate heads surfaces, from which heads could be extracted where observation hiatuses occur.

- **Pumping data** – pumping data available are the maximum recommended pumping rates at the time of well development (and not all wells were developed at the same time) instead of average pumping rates for 1980-2009 period (historical series). This means pumping rates can overshoot the average true values in some wells, while the opposite might happen in others. This hinders model calibration and may lead to hydraulic parameters' values and distributions not in agreement with reality, at the local level. In spite of the high number of pumping wells in the model, a larger number of wells do exist but couldn't be incorporated, either because they are old large wells with unknown pumping rates, are illegally active wells or the databases are not comprehensive, at least as far as farm, domestic and industrial wells' pumping rates are concerned. So, the real abstracted volumes must be larger than the simulated ones. Another model limitation is the obligation of ascribing just one well per element of the mesh, while in reality several wells often occur in each element. The solution is the aggregation of wells (taking into account wells' pumping rates and depths) but this leads to pumping rates' distribution somewhat different from reality. At the local level, this most likely lead to mismatches between observed vs. simulated heads and flow paths. The lack of pumping rates' time series prevent true transient state simulations and model validation once seasonal and annual pumping rates' variations are unknown. Periodical surveys should be performed to assess real pumping rates and seasonal pumping rate variations.

Such data would not solve the 1980-2009 period issues above cited but would give reliable data for present day conditions.

- **Well screening** – once wells' screening depths are for the most part unknown, a significant number of wells had to be set up as multi-layer fully penetrating. Due to this, flow occurred throughout the whole well depth instead of occurring at the right screening depths. Consequently, flow at different model slices may not faithfully mirror the real flow conditions there. To improve the model, the exact wells that are fully penetrating and the screening depths of those that are not must be known. For wells exploiting just the most superficial water bearing layers, its defining boundary condition should then be changed from *multi-layer well* to *well*.

- **Other model's issues** – the occurrence of non-zero error_norm_flow areas (although small) is most likely related with the distribution of hydraulic conductivity values. Although the values are small, ranging from 10^{-2} to 10^{-3}, this might be the cause of heads anomalies in 2 nodes of Slices 5 and 6 (in steady state simulations) and very low heads in 4 nodes (in transient simulations). The usual way to solve this is to refine the mesh in the problematic areas but after doing it, no improvement of error_norm_flow occurred but instead there was now a sharp increase in computational time. The most likely solution for this problem may be a recalibration of hydraulic conductivity if new data on hydraulic parameters will be obtained. Once calibration was made by changing hydraulic conductivity distributions without any real values to frame it, overfitting might occur in these problematic areas.

6 | Simulations and results

In BINGO project, flow models were the only ones developed, while the transport model was not fully developed due to the reasons presented in previous chapters. Flow models (cf. Beek et al., 2017; Beek et al., 2018) and transport models (planed but not developed) have the following constraints:

- **Flow models** (for heads evolution) – pumping rates in 2024 were assumed as equal to those of the historical series (1979-2009) because socio-economic scenarios do predict significant no-change to very slight water use increase of 2% in groundwater supply (cf. Iacovides et al., 2016; APA, 2012). The simulated conditions were:
    - o **Steady state natural conditions** – zero pumping rates and 1979-2009 average recharges from 2011 Tagus Watershed Management Plan (Lobo Ferreira et al., 2011; APA, 2012). Simulates the aquifer as if under natural (no pumping) conditions.
    - o **Steady state pumping conditions** – present day pumping rates and 1979-2009 average recharge. Simulates present day abstraction rates and heads. Pumping data may not give the real abstraction volumes once these are from pumping rates at well development stage and there are also many supply wells for which there are no data.
    - o **Steady state 2024's maximum recharge scenario** – average recharge from climate model MiKlip Realisation 1 for 2015-2024 (cf. Oliveira, 2019); present day pumping rates. Simulates hydraulic heads for the highest recharge scenario of the 10 MiKlip realisations, assuming no significant groundwater demand increases.
    - o **Steady state 2024's minimum recharge scenario** – average recharge from climate model MiKlip Realisation 3 for 2015-2024 (cf. Oliveira, 2019); present day pumping rates. Simulates hydraulic heads for the lowest recharge of the 10 MiKlip realisations, assuming no significant groundwater demand increases.
    - o **Steady state 2024's ensembles' recharge scenario** – average recharge from climate model MiKlip ensemble of the 10 realisations simulated; present day pumping rates. Simulates hydraulic heads for what might be the most likely conditions in 2024. These are very similar to present day conditions, recharge being only slightly higher.
    - o **Steady state drought conditions (no recharge)** – recharge = 0 mm/year for 2015-2024 period; present day pumping rates. This extreme drought scenario isn't expected to occur, but was used to evaluate the lower heads' limits under drought conditions.
    - o **Steady state 2005 drought conditions** – 2005 severe drought conditions' recharge; present day pumping rates. Simulates 2005 recharge conditions as if they became the new normal in 2024; groundwater abstraction remains constant, assuming other sources would provide supply. This is very unlikely, once ensembles scenario shows a small difference from present day recharge and if such "permanent drought" would occur, groundwater demand would certainly increase. However, abstraction data in 2005 are scarce, so the option was to simulate with present day pumping rates.

- o **Semi-transient state 2005 drought conditions for 1, 3 and 5 years drought** – uses 2005's recharge and present day pumping rates. It simulates severe multi-annual drought events, whose lengths are 1, 3 and 5 years.
- **Transport models (saltwater intrusion)** – although not developed, the basic files for future development were nevertheless generated from the flow model. As said before, data limitations imposed a steady state approach. Comparing the results between a "present day model" with the results of a "scenario model" would give the saltwater intrusion's evolution. The conditions that would be simulated are:
  - o *Saltwater intrusion under natural conditions* – built from the flow model simulating natural conditions: no pumping, recharge of the reference period (1979-2009). Sea level = 0 m and present day's salinities at sea and estuary as in a normal year.
  - o *Saltwater intrusion under present day conditions* – built from the flow model simulating present day recharge (reference period 1979-2009) and pumping conditions. Sea level = 0 m and present day's salinities at sea and estuary as in a normal year.
  - o *Saltwater intrusion under maximum recharge scenario in 2024* – built from the flow model simulating MiKlip realisation 1: recharge for 2015-2024, present day pumping conditions. Sea-level and salinities projected for 2024 under realisation 1 conditions.
  - o *Saltwater intrusion under minimum recharge scenario in 2024* – built from the flow model simulating MiKlip realisation 3: recharge for 2015-2024, present day pumping conditions. Sea-level and salinities projected for 2024 under realisation 3 conditions.
  - o *Saltwater intrusion under extreme drought conditions (no recharge)* – built from the flow model simulating a 0 mm/year recharge and present day pumping conditions. Sea-level and salinities are those projected for 2024 under realization 3. Used to set an upper limit (most adverse) to saltwater conditions.
  - o *Saltwater intrusion under 2005's drought conditions* – built from the flow model simulating 2005's severe drought and present day pumping conditions. Sea-level and salinities are those projected for 2024 under realization 3. Saltwater intrusion for 1, 3 and 5 years droughts can also be developed.

In Table 6.1 are presented the file names of these models, respective situation being simulated and if steady state or transient.

Table 6.1 – Scenario conditions and its respective saltwater intrusion models

Model's name (a)	Type of simulation	
	Condition simulated	Simulation type
bingo tejo 3D V1_MDEPSnatural 2009_h0estuar	Natural conditions (no pumping) with average recharge from 1979-2009	
bingo tejo 3D V1_MDEPSbomEPAL sconstr1_h0estuar_new	Present-day pumping rates & average recharge from 1979-2009	
bingo tejo 3D V1_MDEPSbomEPAL sconstr1_h0estuar_2025R3	Present-day pumping rates in low recharge scenario (MiKlip realisation 3)	
bingo tejo 3D V1_MDEPSbomEPAL sconstr1_h0estuar_2025R1_10	Present-day pumping rates in average recharge (ensemble of all MiKlip realisations scenario)	Steady state
bingo tejo 3D V1_MDEPSbomEPAL sconstr1_h0estuar_2025R1	Present day-pumping rates in high recharge scenario (MiKlip realisation 1)	
bingo tejo 3D V1_MDEPSbomEPAL constr1_2005sRAQ	Pumping rates without recharge (extreme drought scenario)	
bingo tejo 3D V1_MDEPSbomEPAL sconstr1_2005	Present-day pumping rates & recharge from 2005 drought year	
bingo tejo 3D V1_MDEPSbomEPAL sconstr1_h0estuar_2005trans_ano1	Present-day pumping rates & recharge from 2005 drought year, for 1 to 5 years	Semi-transient state
bingo tejo 3D V1_MDEPSbomEPAL sconstr1_salt_natural	Natural saltwater intrusion conditions: average recharge & salinity from 1979-2009, sea level = 0 m, no pumping	Saltwater intrusion steady state
bingo tejo 3D V1_MDEPSbomEPAL sconstr1_salt_actual	Present-day pumping rates, average recharge & salinity from 1979-2009, sea level = 0 m	Saltwater intrusion steady state
bingo tejo 3D V1_MDEPSbomEPAL sconstr1_salt_2025R1	Sea level change in 2024, recharge from realisation 1	Saltwater intrusion steady state
bingo tejo 3D V1_MDEPSbomEPAL sconstr1_salt_2025R3	Sea level change in 2024, recharge from realisation 3	Saltwater intrusion steady state
bingo tejo 3D V1_MDEPSbomEPAL sconstr1_salt_sRAQ	Sea level change in 2024, no recharge	Saltwater intrusion steady state
bingo tejo 3D V1_MDEPSbomEPAL sconstr1_salt_2025_2005	Sea level change in 2024, 2005 drought's recharge	Saltwater intrusion steady state

(a) All models who do not simulate saltwater intrusion have h = ct. = 0 m at the boundary with the estuary

6.1 Flow models' results

Results for steady state and semi-transient state concern: (1) historical period (natural and present day conditions); (2) climate change scenarios; (3) drought scenarios. The results are shown as head's maps and contour maps. The latter illustrates head's changes from the historical conditions (1979-2009's period) to those of climate and drought scenarios. Although FEFLOW generated heads maps for each of the 26 slices, only those of slices 1, 7 and 18 are shown, once they represent:

- *Slice 1* – Aluviões do Tejo aquifer's top at model's central area. In the remaining area it represents Pliocene and Miocene outcropping surfaces.

- ***Slice 7*** – Pliocene's confined area's top under Aluviões do Tejo aquifer (model's central area). In the remaining area it represents Pliocene and Miocene outcrops (layers above Slice 7 are here very thin).
- ***Slice 18*** – Miocene's top; in the outcropping areas (layers above Slice 18 is here very thin) it represents the topographic surface. Miocene is confined under alluvial and Pliocene deposits. Pliocene and Miocene are assumed as continuous units between Tejo/Sado – Margem Direita and Margem Esquerda aquifers.

6.1.1 Flow model steady state runs

Natural and present-day conditions, climate change and steady state drought scenarios are presented below. Error tolerance = 2.28×10^{-3}, once it gave the best fit and smallest budget imbalance.

6.1.1.1 Historical period heads

Two situations were set for the historical period:

- ***Natural conditions*** (no pumping) – to ascertain if the model obeys the conceptual heads relationships between Alluvial, Pliocene and Miocene aquifers as known by observation data before pumping became important.
- ***Present-day pumping conditions*** – to ascertain if the model obeys the observation data under pumping conditions. Comparing this situation's heads surface with that of the natural conditions', gives the impact of abstractions on aquifer flows and heads. Present day pumping conditions' heads surfaces (for Slices 1, 7 and 18) are used as **reference surfaces** when analysing climate change impacts.

6.1.1.1.1. Natural conditions

Head surfaces for the Alluvial, Pliocene and Miocene formations are given respectively in Figure 6.1, Figure 6.2 and Figure 6.3. Using Slice 1 heads surface (Figure 6.1) as reference surface, the relationships between Slices 1, 7 and 18 heads are shown in Figure 6.4, Figure 6.5 and Figure 6.6. The yellow and orange points those figures are the wells for the whole model domain, instead of just those abstracting in the slices in question.

As can be seen in Figure 6.4 (Slice 1's vs. Slice 7's heads surface), Pliocene heads in the central area are above those of the alluvial deposits (outcropping alluvial deposits delimited by red line). The same holds true from Miocene's heads (Figure 6.5). Outside the central area, Slice 1's vs. Slice 7's and Slice 1's vs. Slice 18 heads surfaces show Pliocene and Miocene's heads are slightly lower than Slice 1's heads, as it was to be expected, except in some localized problematic zones (Figure 6.5).

Figure 6.6 shows Pliocene vs. Miocene heads relationship. This was obtained comparing head surfaces of Slice 7 vs. Slice 18. In the central area of the model, Miocene heads are above Pliocene heads; outside that area, Miocene heads tend to be equal or above Pliocene heads, except in the problematic areas.

The results are in agreement with the conceptual model, which states that under natural conditions alluvial heads < Pliocene heads < Miocene heads in the central area of the model.
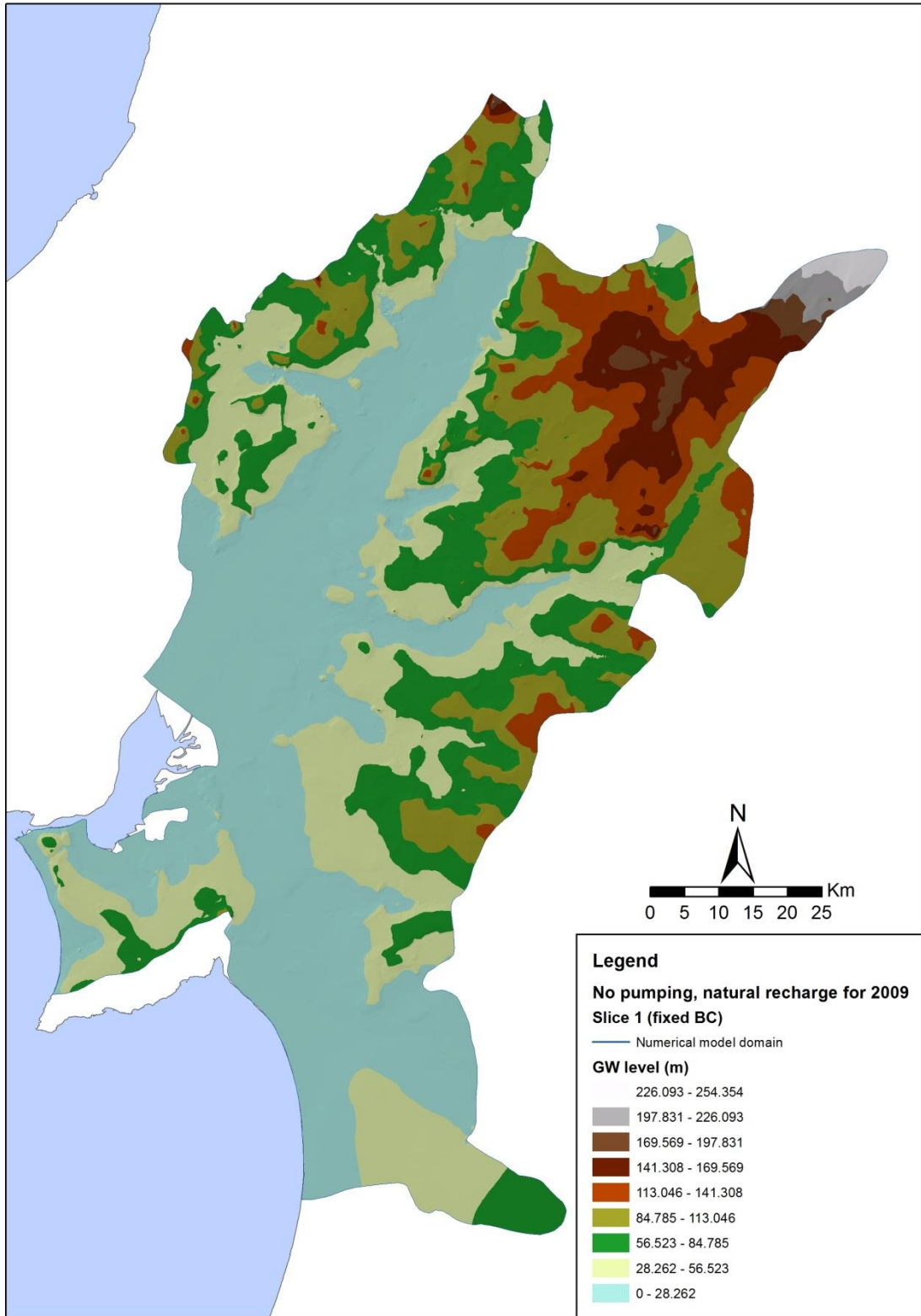
Figure 6.1 – Head surface for alluvial deposits and topmost Pliocene + Miocene water bearing units (Slice 1) under natural conditions for the historical period (1979 – 2009) – annual mean values
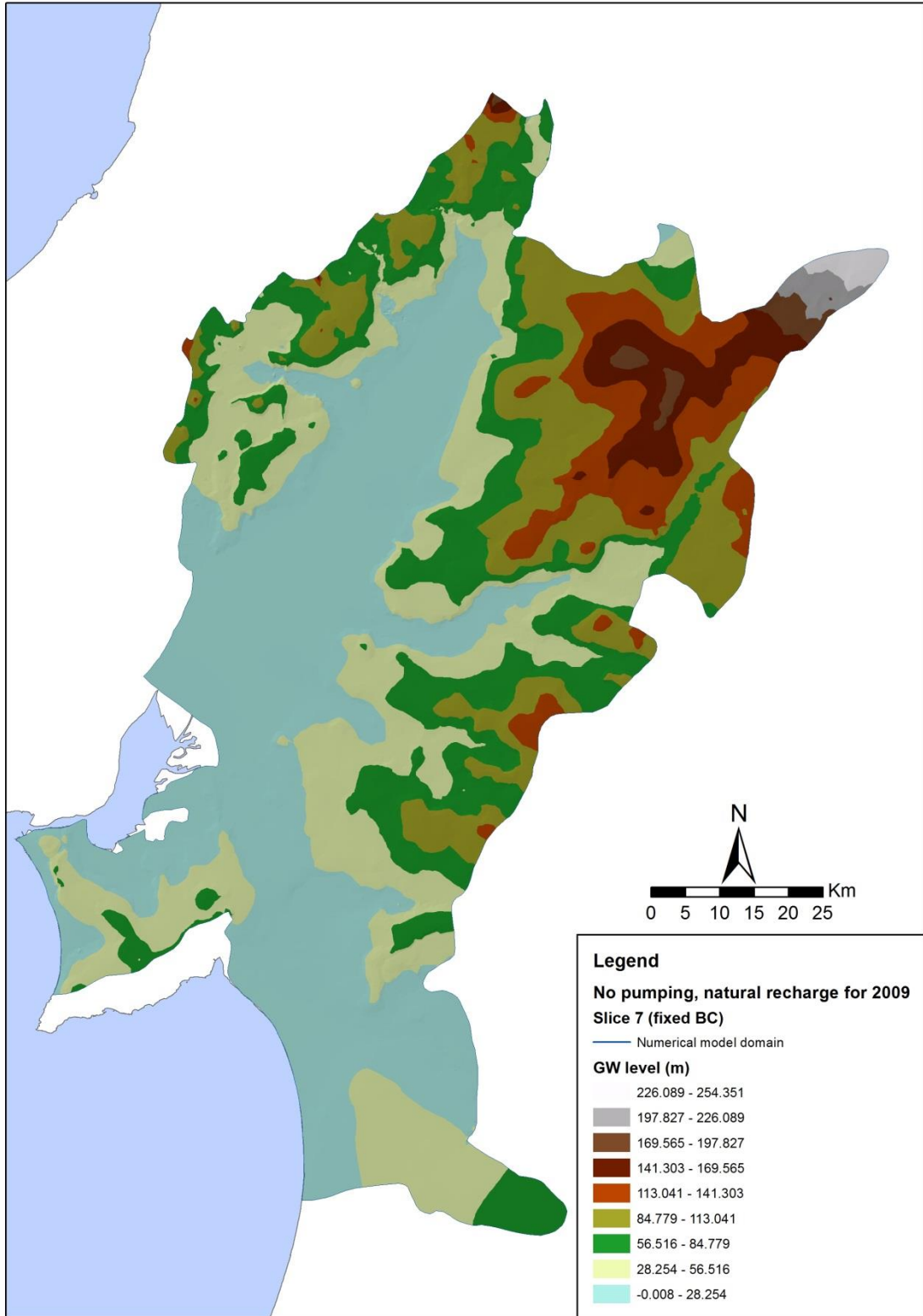
Figure 6.2 – Head surface for Pliocene formations and topmost Miocene water bearing units (Slice 7) under natural conditions for the historical period (1979 – 2009) – annual mean values
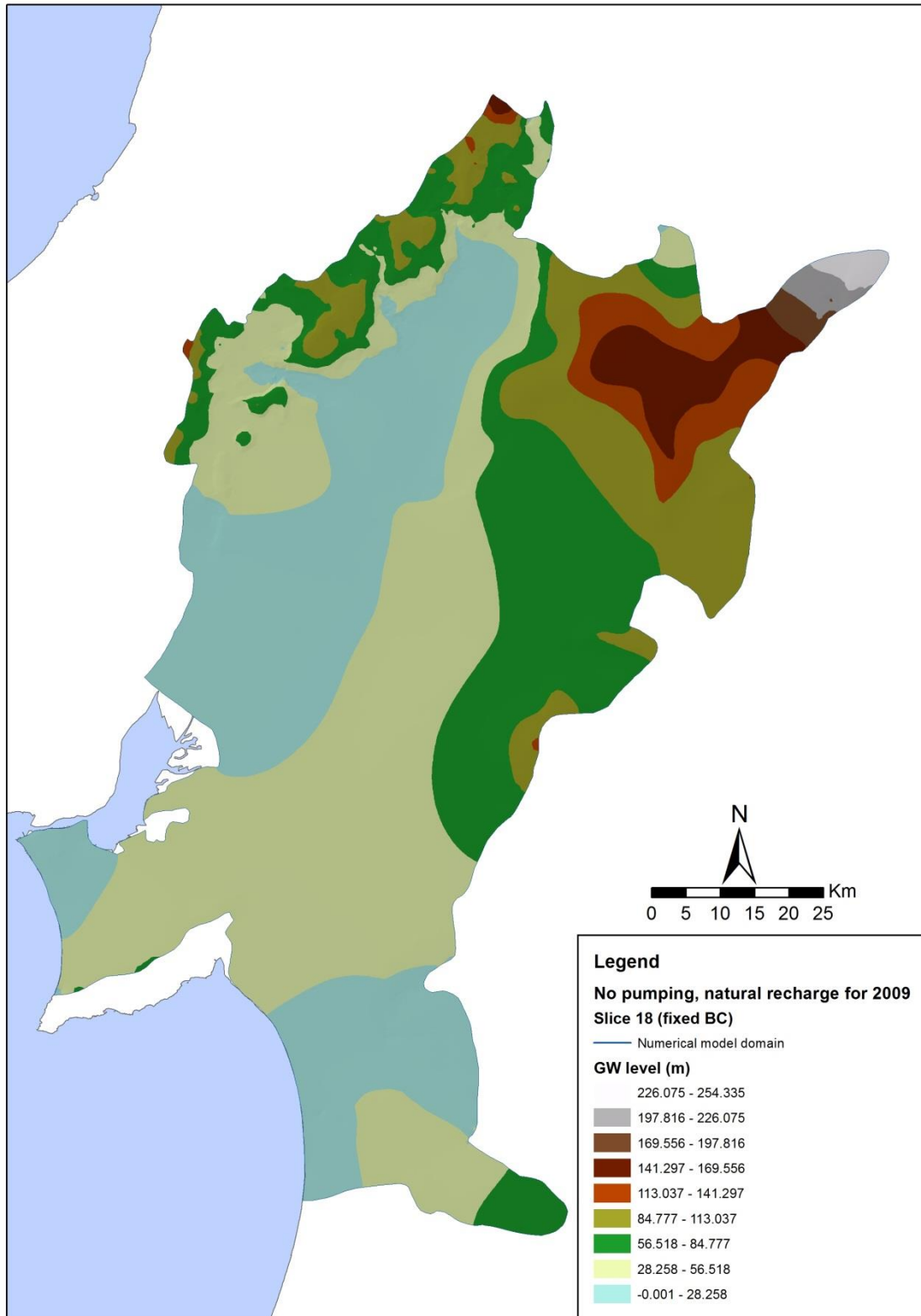
Figure 6.3 – Head surface for Miocene formations (Slice 18) under natural conditions for the historical period (1979 – 2009) – annual mean values
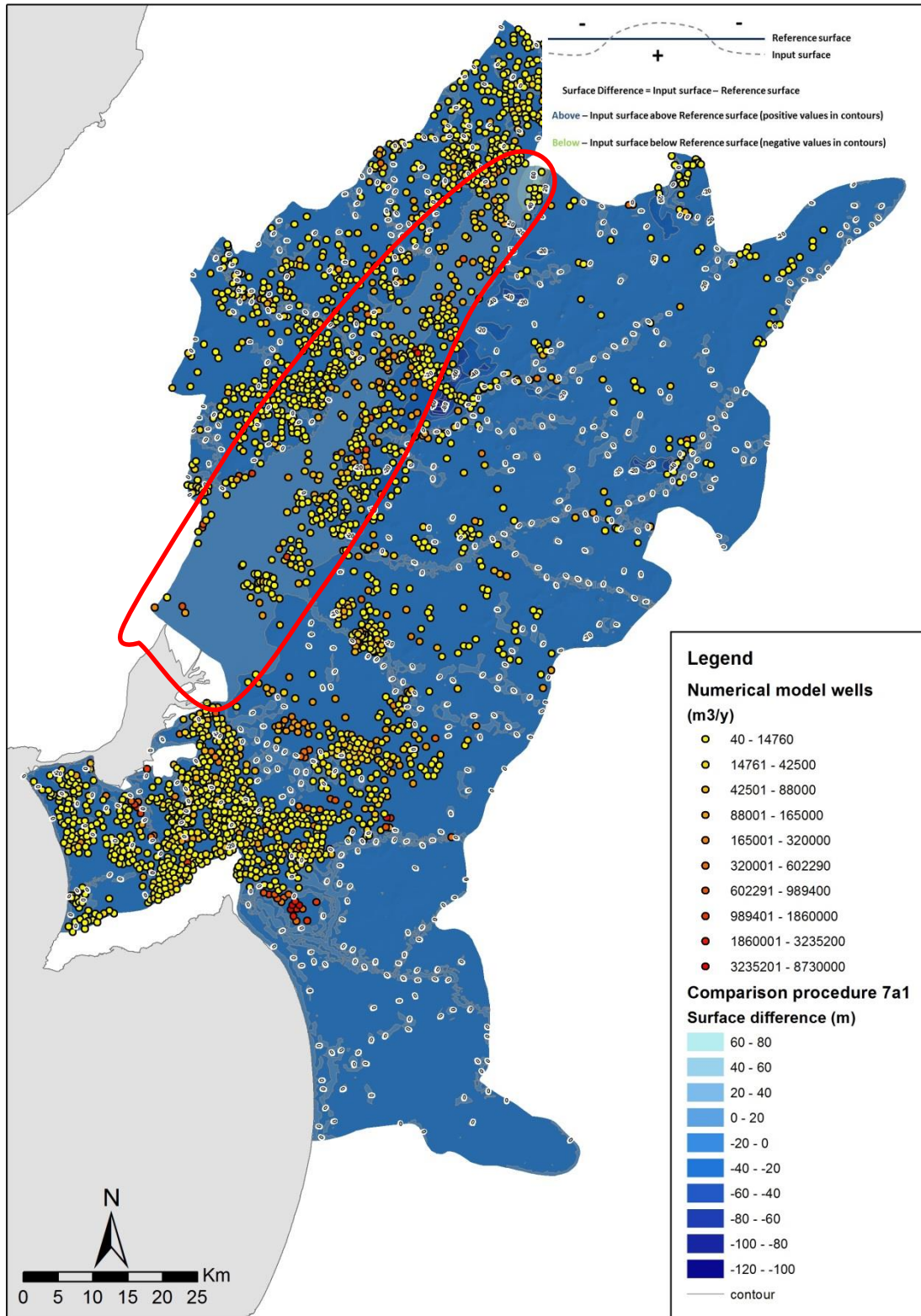
Figure 6.4 – Head differences between Slice 1 and Slice 7 under natural conditions
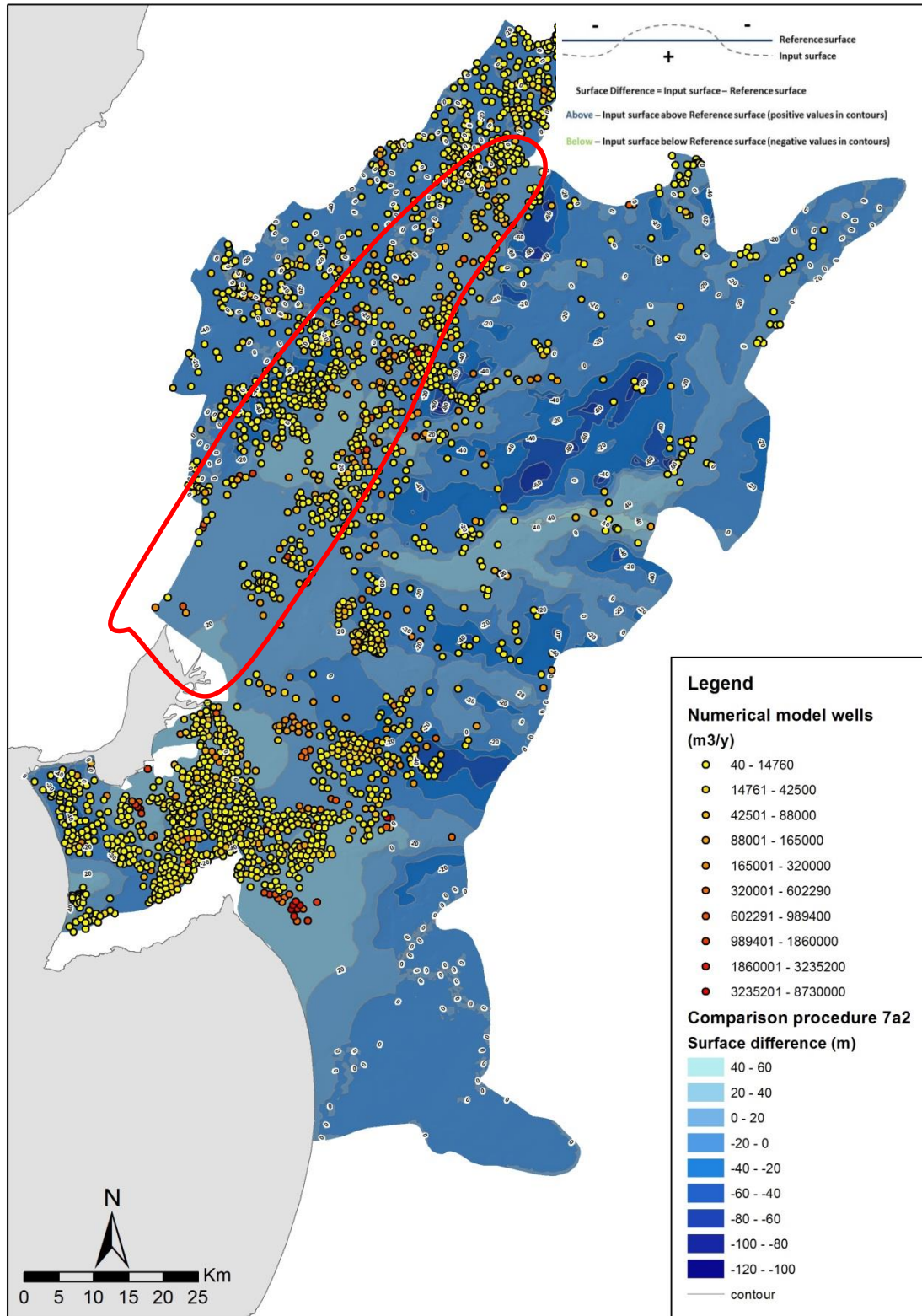
Figure 6.5 – Head differences between Slice 1 and Slice 18 (natural conditions)
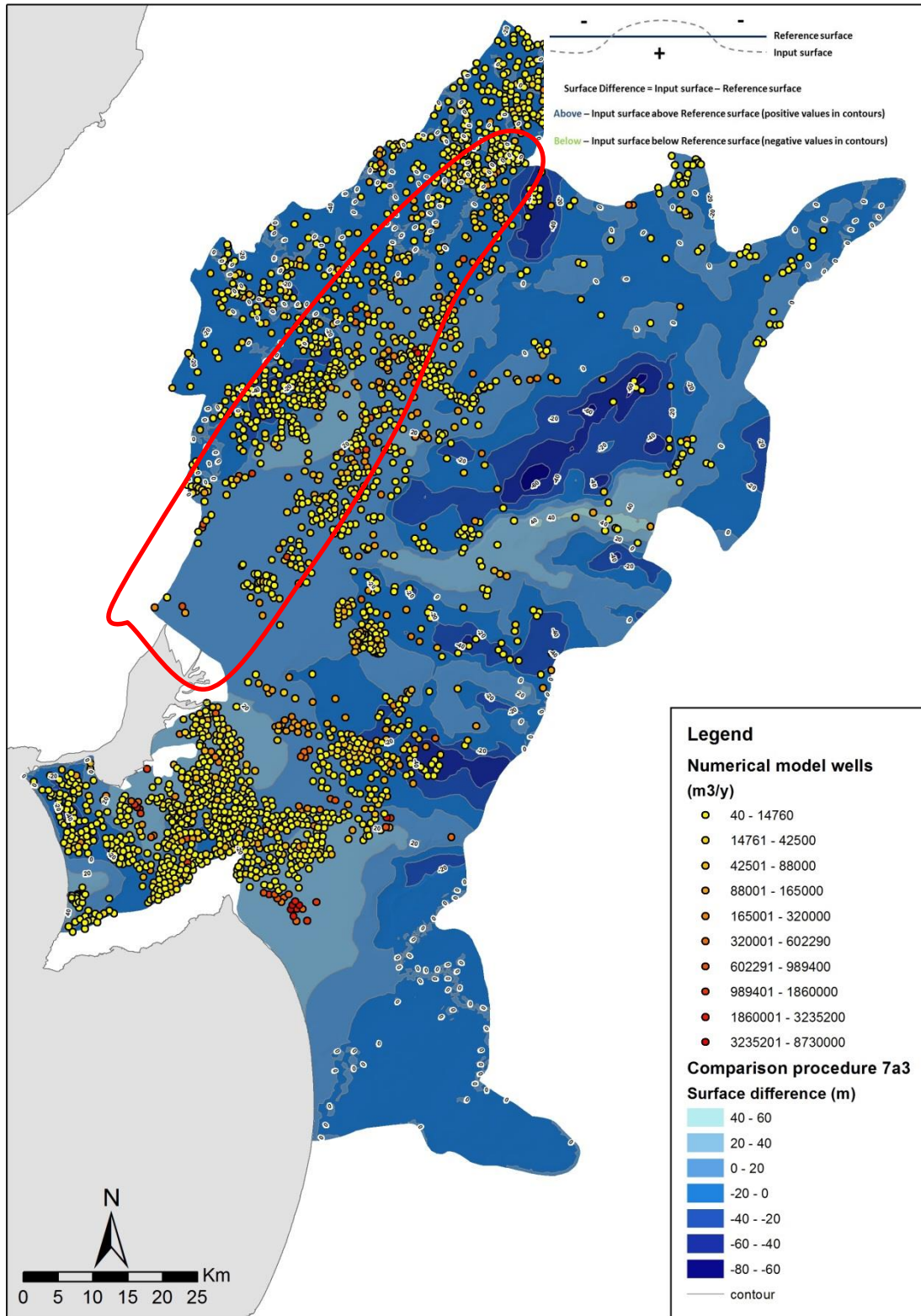
Figure 6.6 – Head differences between Slice 7 and Slice 18 (natural conditions)

6.1.1.1.2. Pumping conditions

Heads surfaces of Slices 1, 7 and 18 are respectively shown by Figure 6.7, Figure 6.8 and Figure 6.9. The differences between natural and pumping heads surfaces for Slices 1, 7 and 18 are respectively shown in Figure 6.10, Figure 6.11 and Figure 6.12. The reference surfaces used to generate such heads' differences are Slices 1, 7 and 18 **head surfaces from reference period natural conditions**, which are compared with the respective Slice 1, 7 and 18's head surfaces under pumping conditions.

Under pumping conditions, **Slice 1's** heads drawdown (Figure 6.10) ranges from 1 to 10 m in most part of the model, when compared with heads from natural conditions, as expected. In areas where anomalous heads are higher than heads under natural conditions, the difference between them is, for most part, lower than 1 m. Once model's Confidence Interval was set at 1 m, these abnormalities are in the range of accepted heads' error.

In **Slice 7** (Figure 6.11), heads drawdown is very small, suggesting a smaller impact of water abstraction. Nevertheless, some of these wells might have large pumping rates and create significant local impacts that can't be discriminated due to the large scale of the model.

In **Slice 18** (Figure 6.12) heads drawdown are also very small (Figure 6.11), except in Península de Setúbal and Sado area, where they can be significant. Coincidentally, these areas have significant abstraction rates from the Miocene formations. So, although there are some areas in the model with anomalous behaviour, in general, the model simulates adequately the impacts of pumping wells.

Figure 6.7 – Heads surface for alluvial aquifer and topmost Pliocene + Miocene water bearing units (Slice 1) under historical period (1979 – 2009) pumping conditions – annual mean values
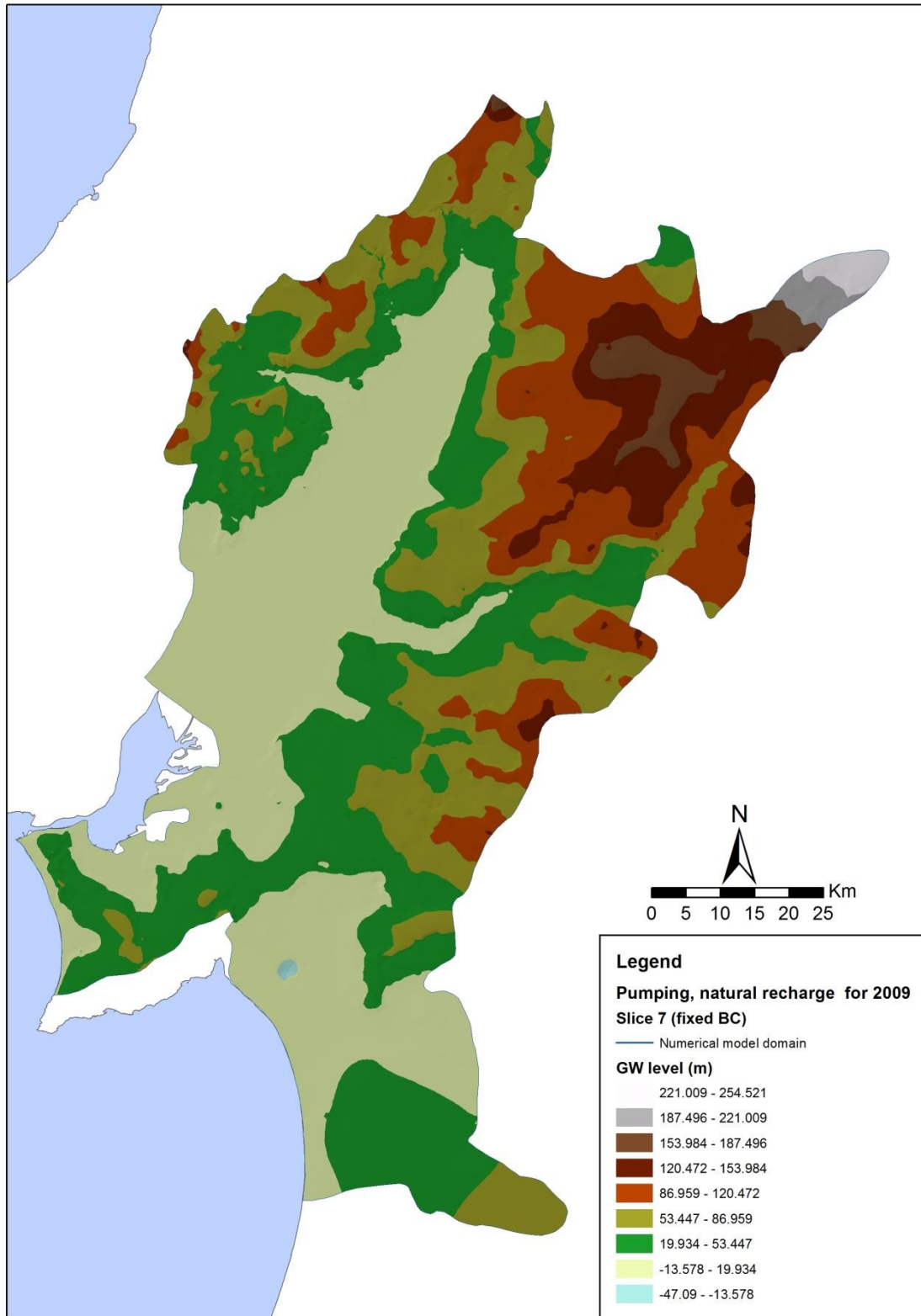
**Figure 6.8 – Heads surface for Pliocene and topmost Miocene water bearing units (Slice 7) under historical period (1979 – 2009) pumping conditions – annual mean values**
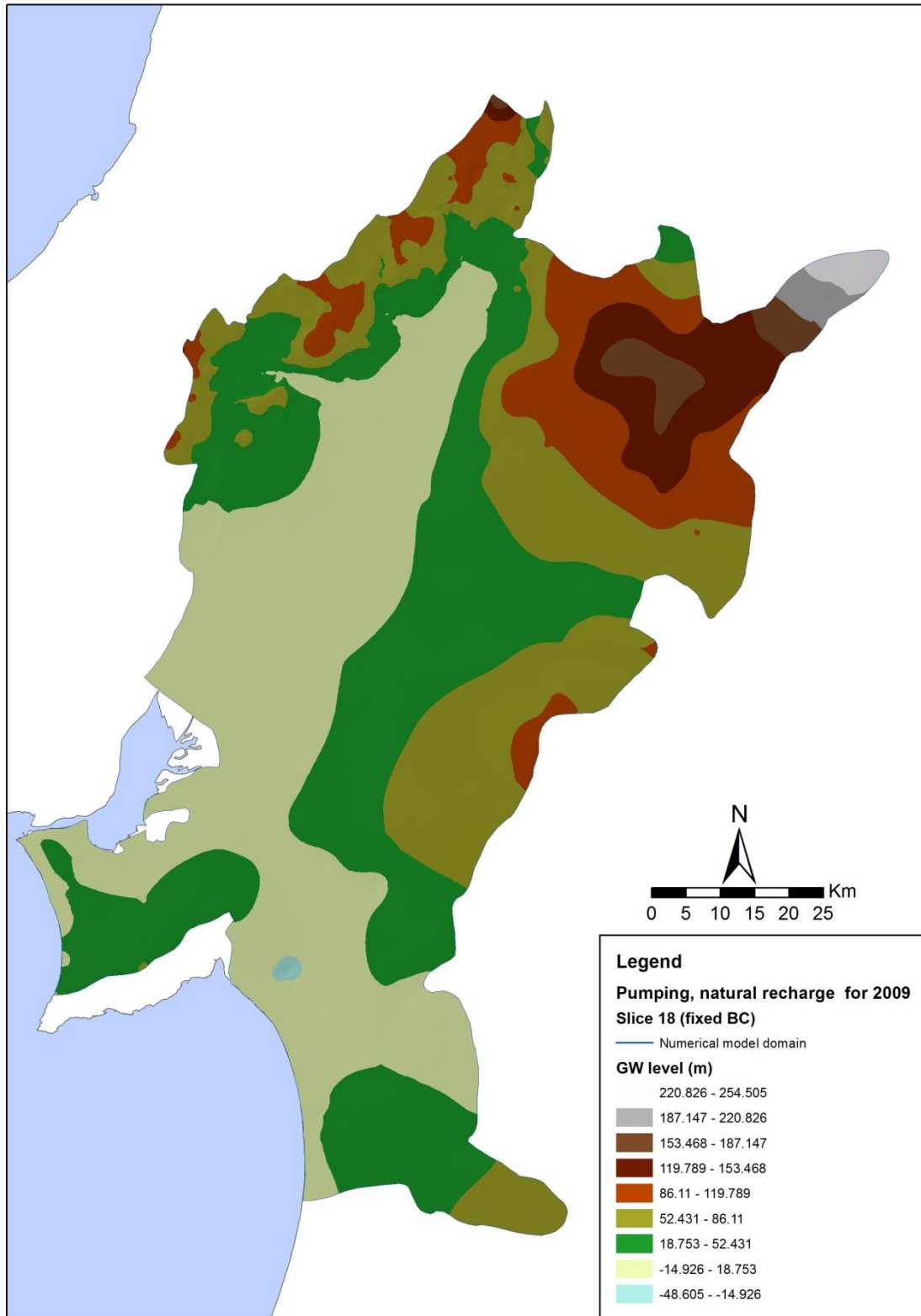
Figure 6.9 – Heads surface for Miocene formations (Slice 7) under historical period (1979 – 2009) pumping conditions – annual mean values
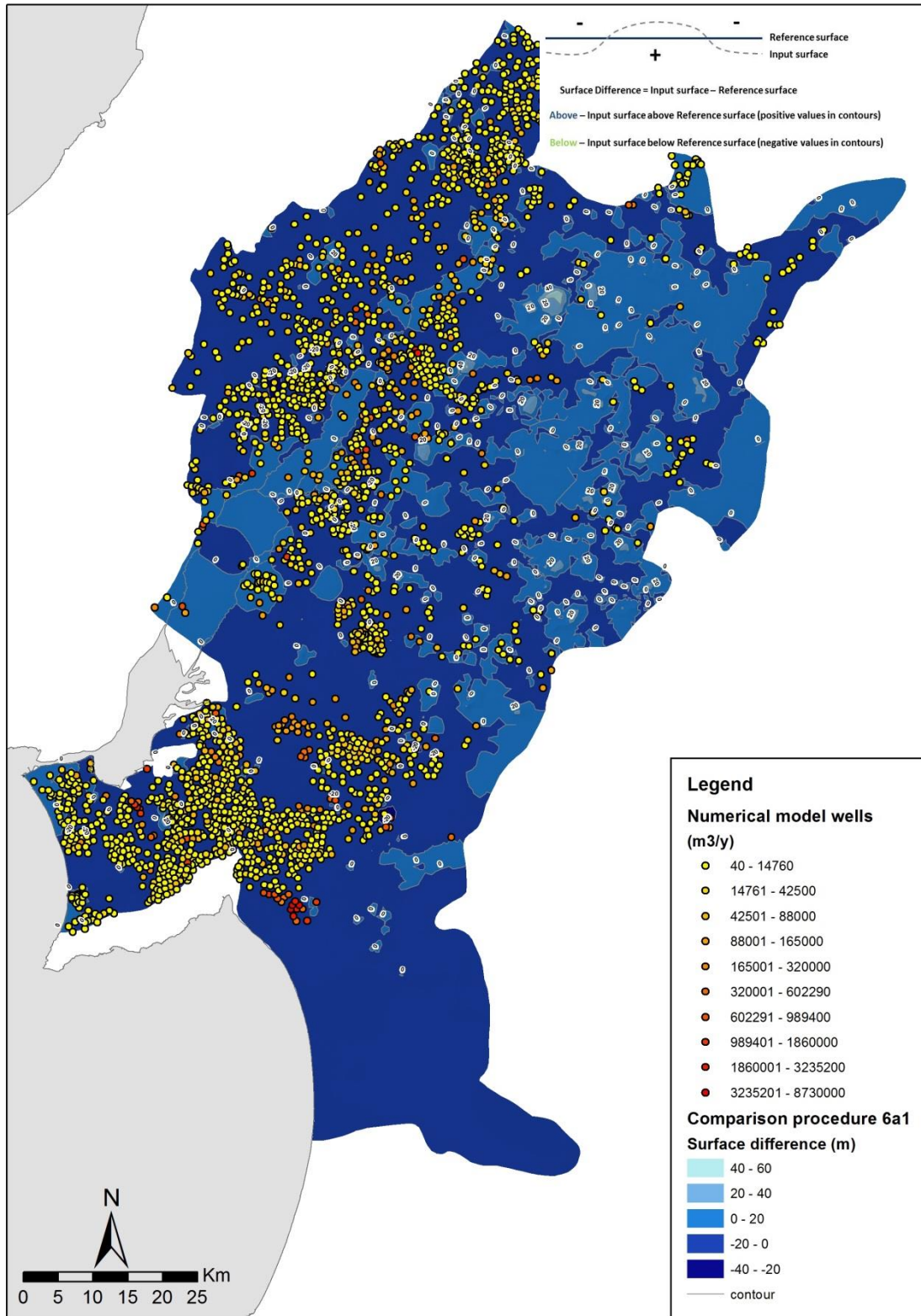
Figure 6.10 – Head differences between natural and historical period (1979-2009) pumping conditions in Slice 1 (annual mean values)
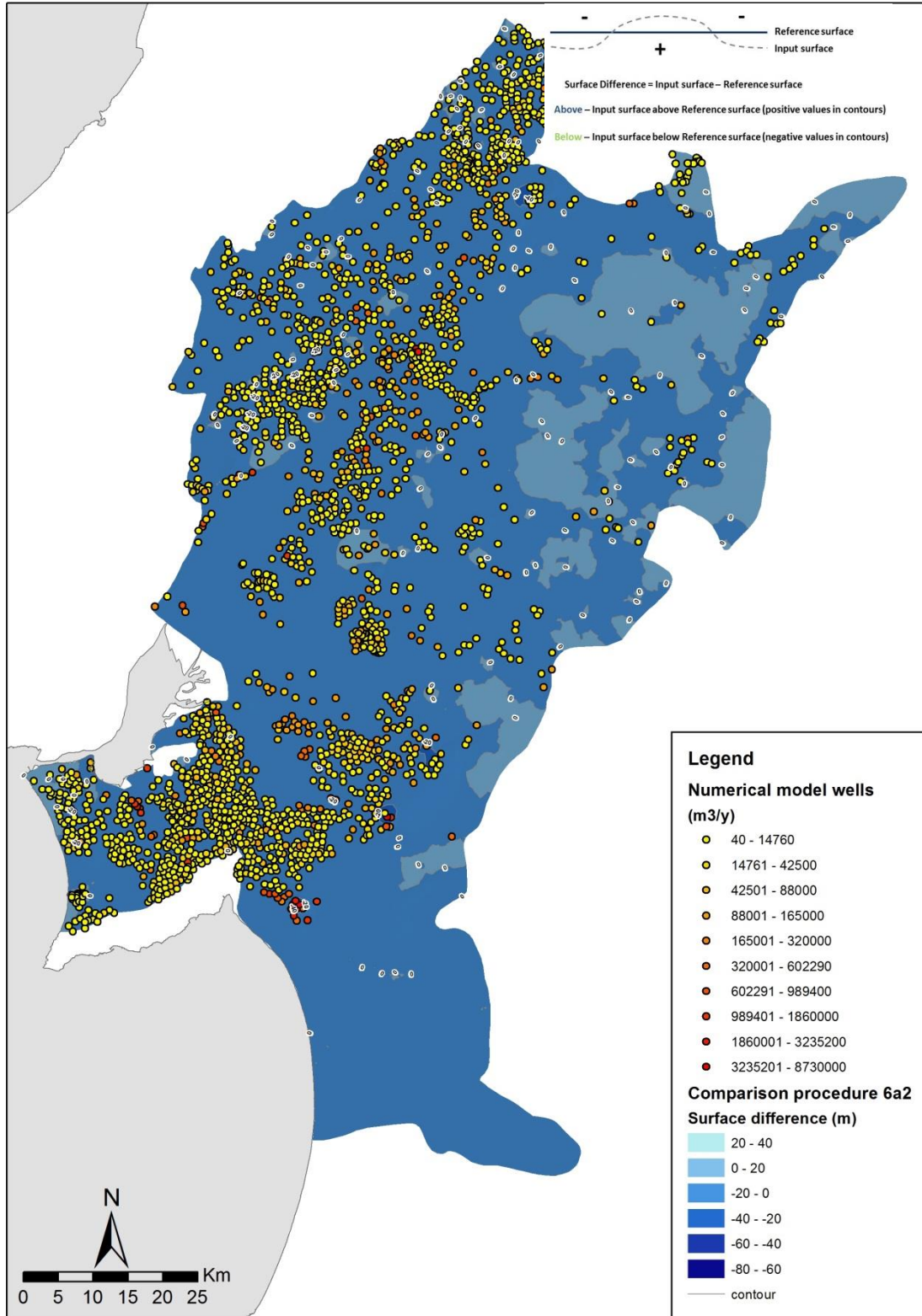
Figure 6.11 – Head differences between natural and historical period (1979-2009) pumping conditions in Slice 7 (annual mean values)
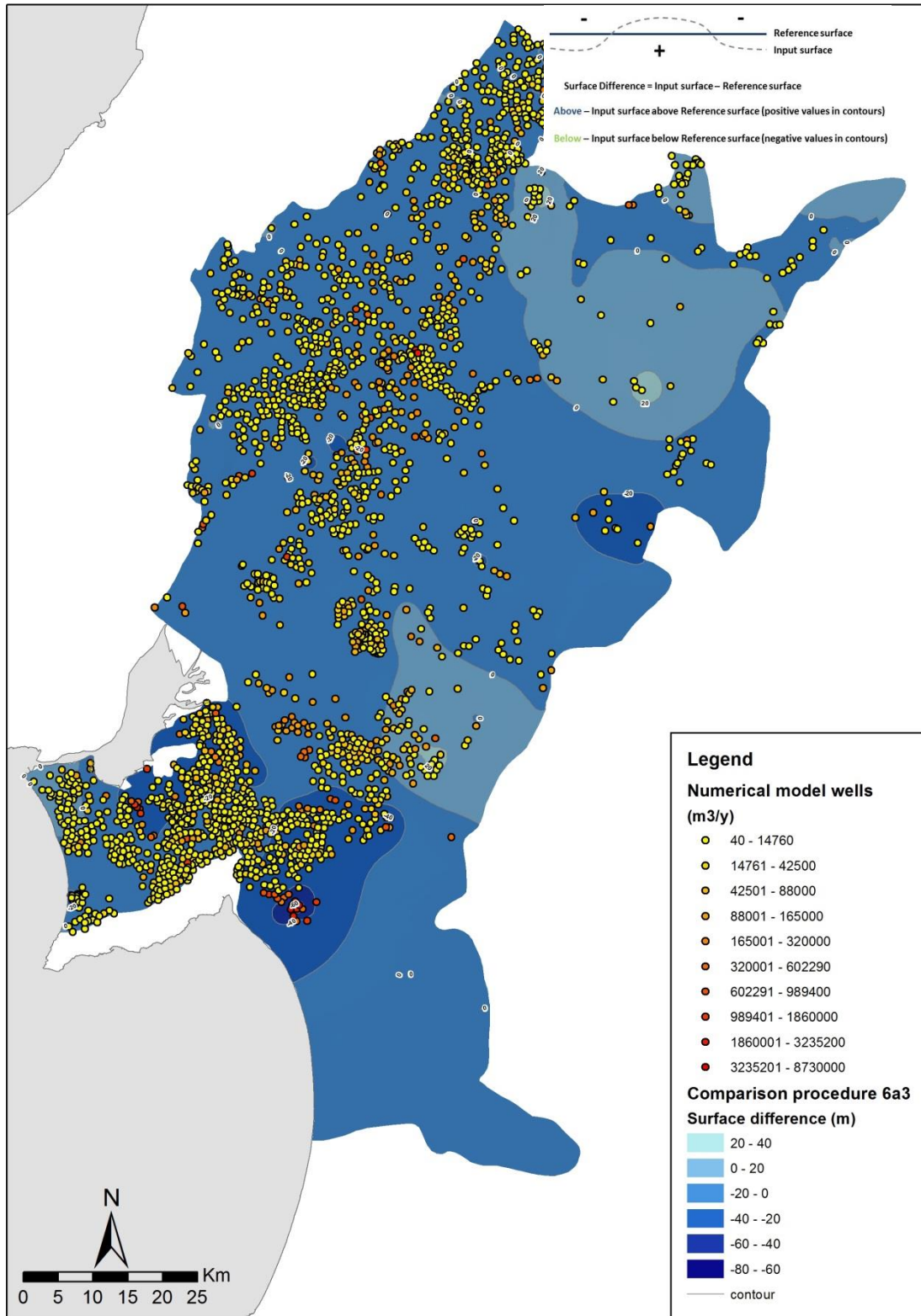
Figure 6.12 – Head differences between natural and historical period (1979-2009) pumping conditions in Slice 18 (annual mean values)

6.1.1.2   Permanent drought heads

The recharge used was that of 2004/2005's severe drought, as given by BALSEQ_MOD (Oliveira, 2019). This was the most severe protracted drought in 60 years, with most of the country enduring severe to extreme drought for 7 to 9 consecutive months and the hottest summer of the previous 75 years (https://www.ipma.pt/resources.www/docs/im.publicacoes/edicoes.online/20081014/KZcwnQrfVHeUZOaTzIth/cli_20050101_20051231_pcl_aa_co_pt.pdf). Due to the lack of reliable data, pumping rates were assumed as equal to those of a normal year, in spite of the fact that they must have been larger.

This scenario simulates a future where average recharge is that of a present day severe drought (corresponding to a 79% decrease from present day average recharge). Such scenario simulates a very dry climate, which is highly unlikely in 2024 or even in 2040. In fact for such conditions to occur, precipitation decreases should be larger than RCP 8.5 emissions scenario's 5.5% precipitation decrease projected for 2040 (http://portaldoclima.pt/en/). So, this scenario was used to **establish the largest possible heads' drawdowns** under known drought and pumping conditions, although in fact drawdowns should be larger once pumping rates in such conditions should be much larger than present day pumping rates.

This scenario's head surfaces are shown in Figure 6.13, Figure 6.14 and Figure 6.15, for respectively Slice 1, Slice 7 and Slice 18. The head changes from the historical period (1979-2009) pumping conditions are shown in Figure 6.16, Figure 6.17 and Figure 6.18. These changes were obtained by comparing this scenario heads surfaces with the head surfaces for the historical period under pumping conditions for respectively the same Slices 1, 7 and 18. So for Slice 1, Figure 6.7's and Figure 6.13's heads surfaces were compared; for Slice 7 the comparison was between Figure 6.8 and Figure 6.14; for Slice 18 between Figure 6.9 and Figure 6.15.

Sharp heads' drawdowns occur in **Slice 1** (Figure 6.16), being on the range of 20 to more than 40 m in Peninsula de Setubal and upstream Sorraia region, while 10 to 15 m drawdowns occur in the alluvial deposits (central area circled in red). Miocene and Pliocene drawdowns are on average between 10 to 20 m, although local drawdowns of 40 to 60 m (green circled areas) can occur; the larger drawdowns occur in areas of sharp conductivity gradients or, locally, in model borders with outside aquifers.

Slice 7's drawdowns (Figure 6.17) are still large: Miocene and Pliocene have drawdowns ≥ 40 m to > 60 m (green circled areas), but with a significant areal reduction in the > 60 m drawdown areas, when compared with Slice 1. In Peninsula de Setubal, drawdowns of ≥ 40 m do not occur.

Slice 18 shows smaller drawdowns (Figure 6.18), usually < 20 m for almost the whole model area; drawdowns of 30 m occur at upstream Sorraia and drawdowns > 40 m (circled green) still occur in areas of sharp conductivity gradients or discharge zones along model borders with outside aquifers.

Such large heads' drawdowns throughout the whole model domain are expected due to the large recharge reduction**.** Drawdowns are larger in upper layers, which might be due to a larger shielding of the deeper layers from evapotranspiration losses.
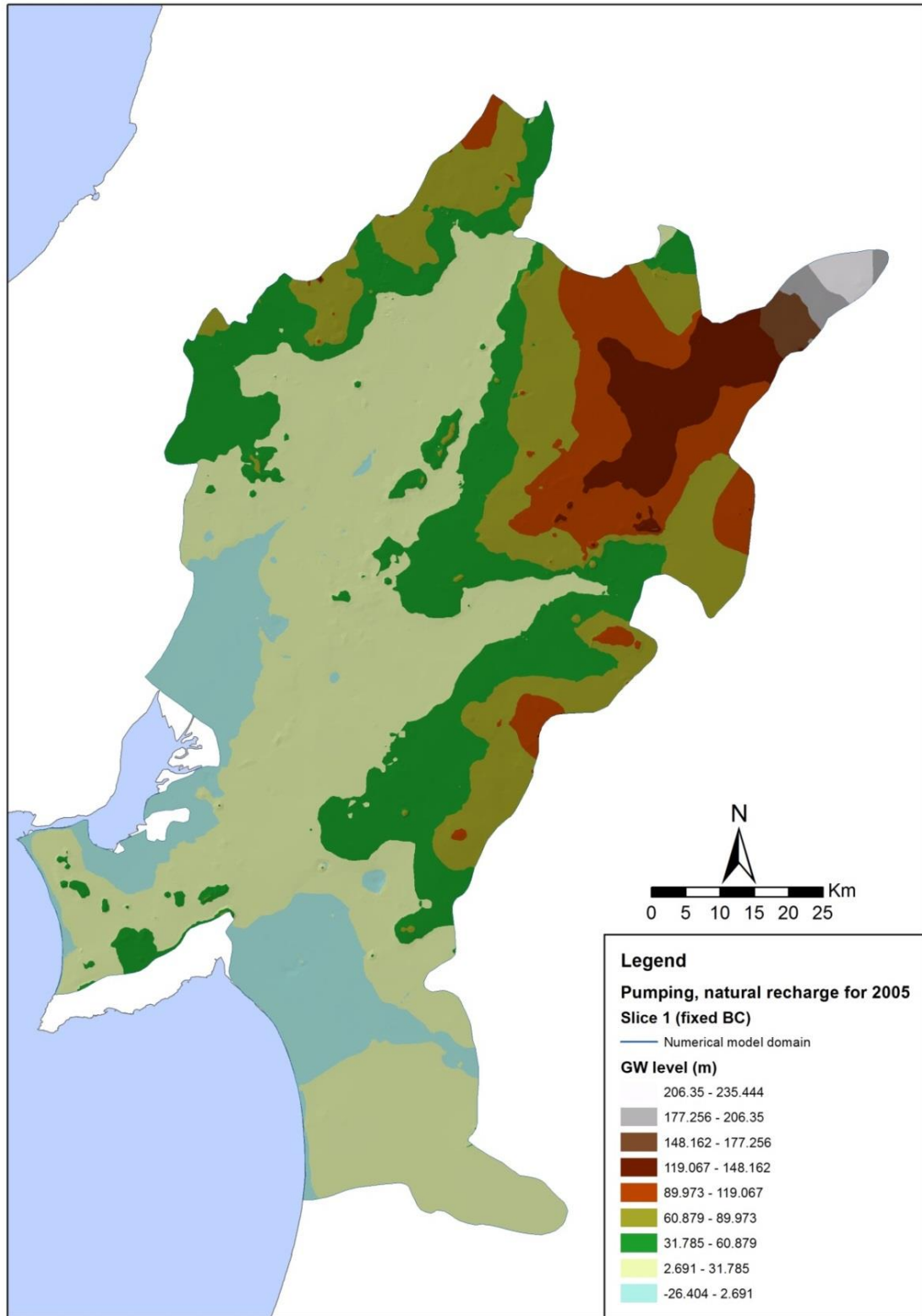
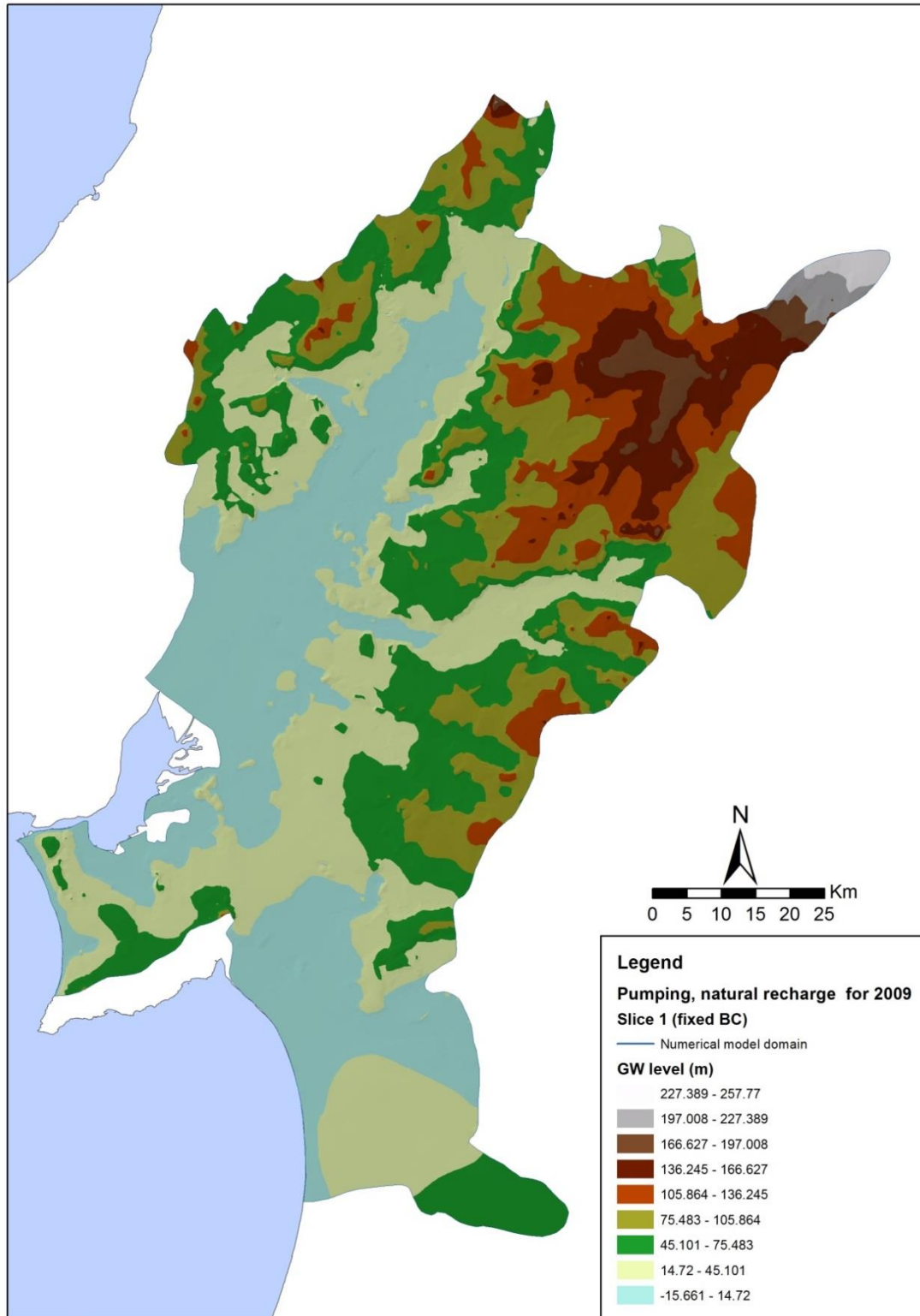**Figure 6.13 – Heads surface for alluvial aquifer and topmost Pliocene + Miocene water bearing units (Slice 1) under severe drought conditions (year 2005) – annual mean values**
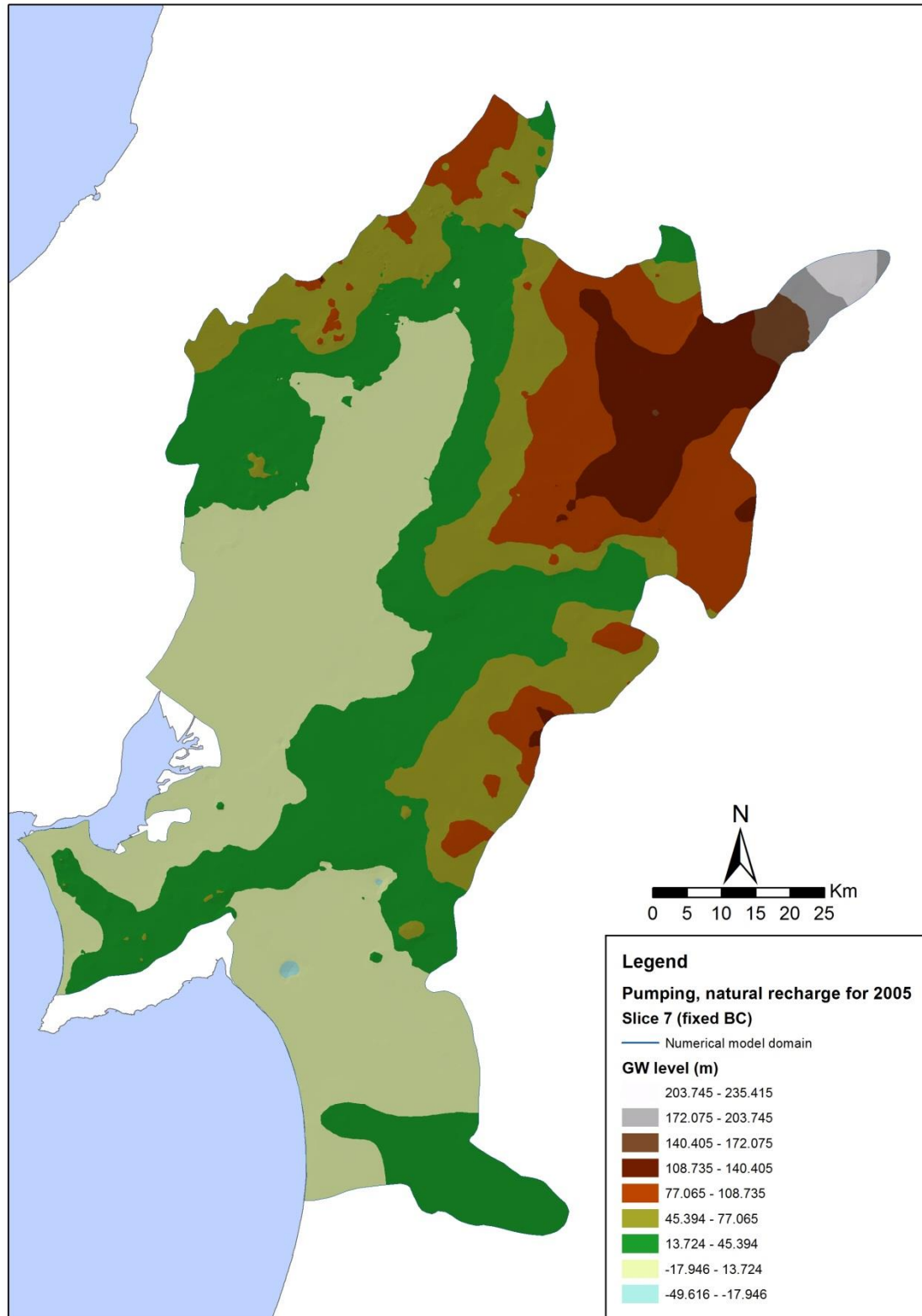
Figure 6.14 – Heads surface for Pliocene formations and topmost Miocene water bearing units (Slice 7) under severe drought conditions (year 2005) – annual mean values
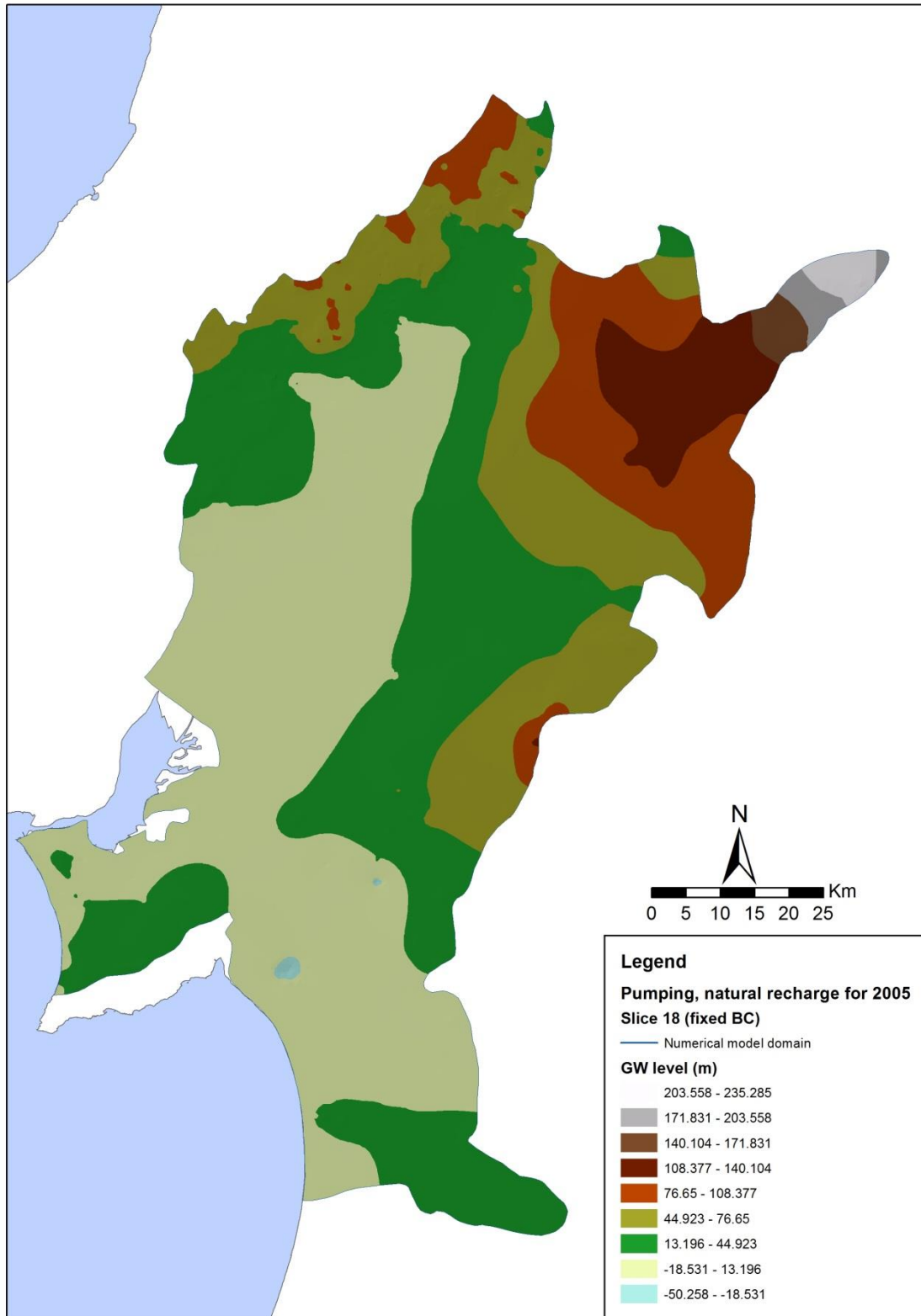
Figure 6.15 – Heads surface for Miocene formations (Slice 18) under severe drought conditions (year 2005) – annual mean values
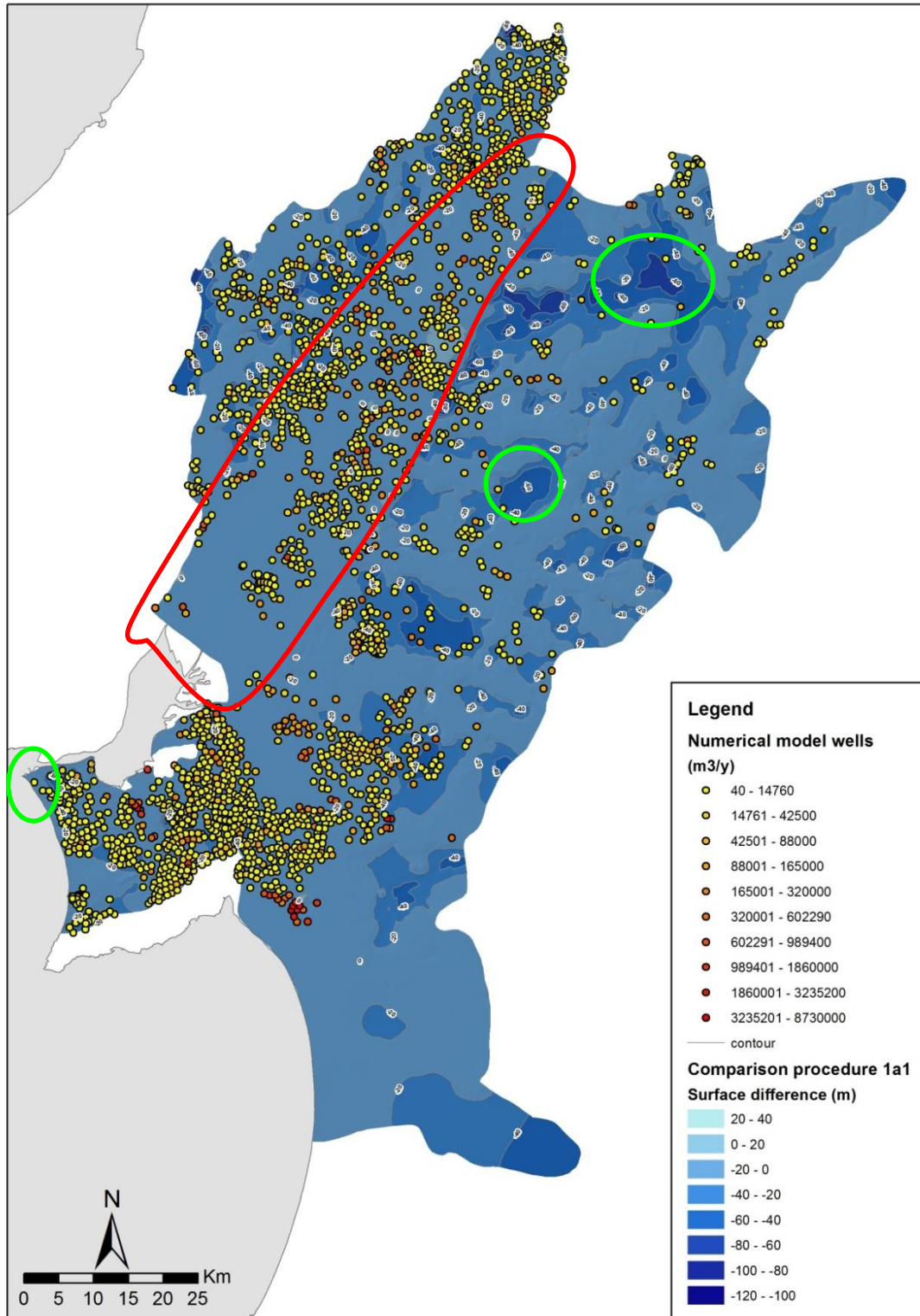
Figure 6.16 – Head differences in Slice 1 between historical period (1979-2009) pumping conditions and 2005 drought scenario (annual mean values)
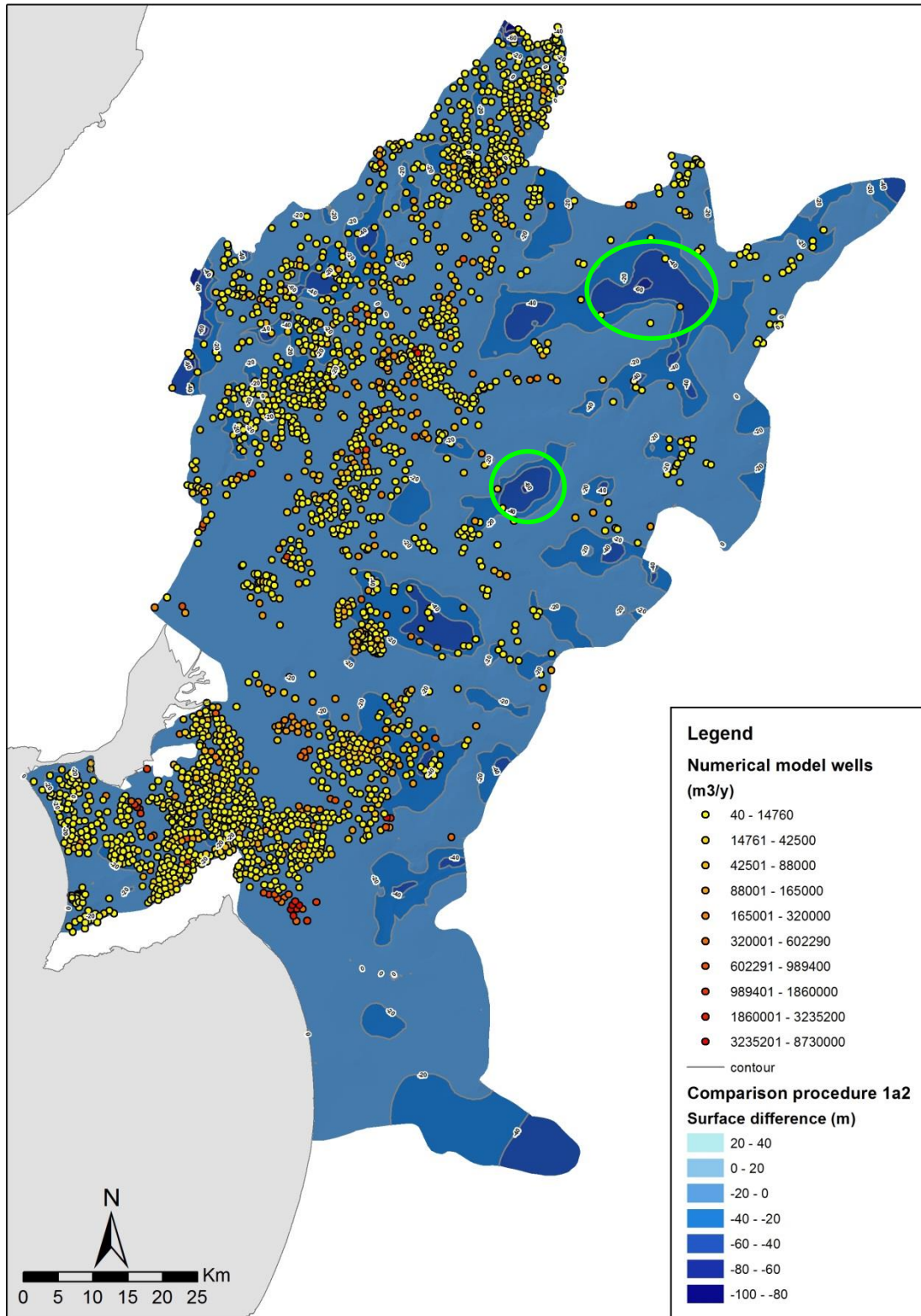
Figure 6.17 – Head differences in Slice 7 between historical period (1979-2009) pumping conditions and 2005 drought scenario (annual mean values)
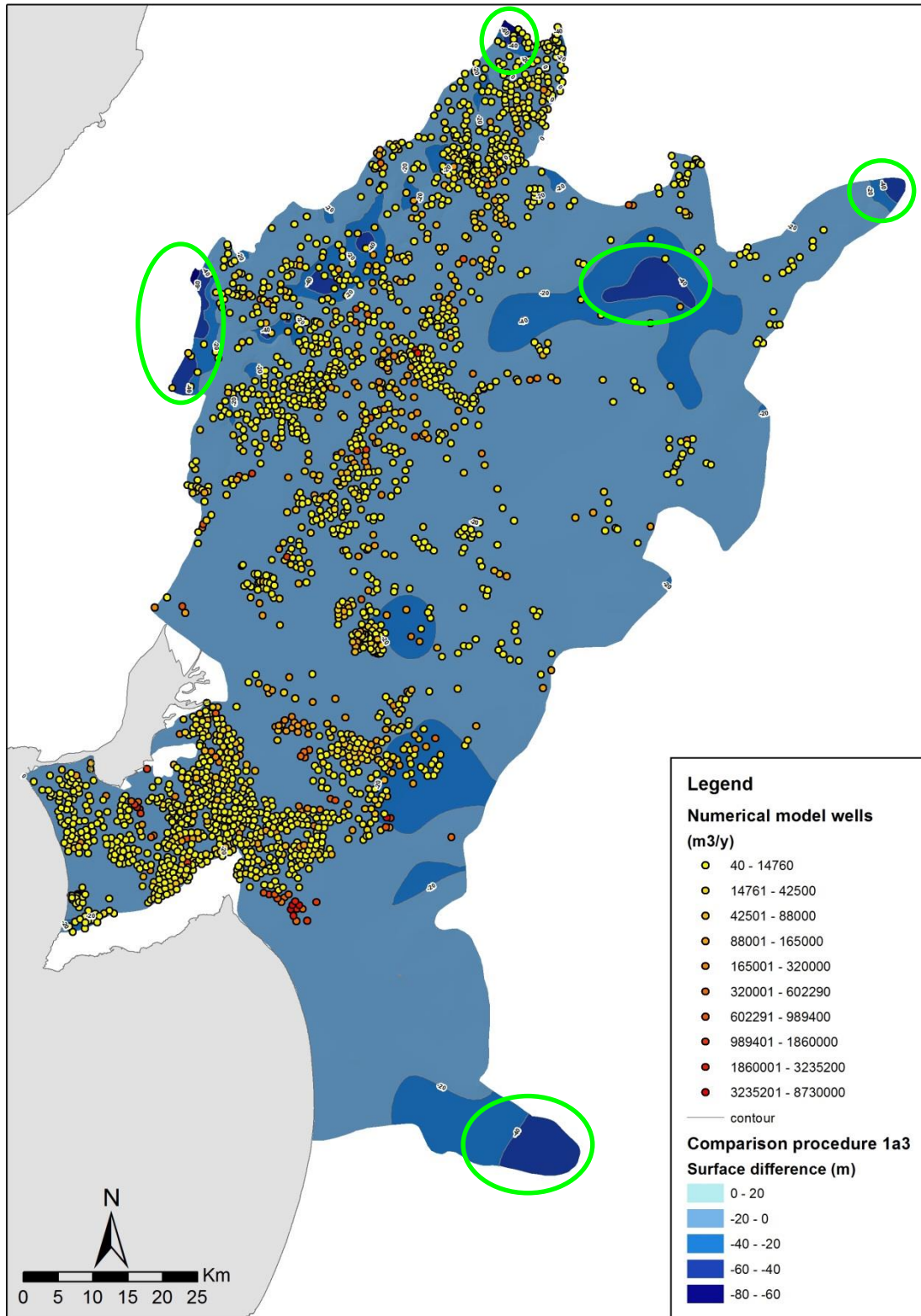
Figure 6.18 – Head differences in Slice 18 between historical period (1979-2009) pumping conditions and 2005 drought scenario (annual mean values)

6.1.1.3   Climate change scenarios' heads

Recharge scenarios for 2015-2024 time horizon where obtained by applying BALSEQ_MOD model to each of the 10 MiKlip climate realisations' outputs (Oliveira, 2019). Of the 10 recharge scenarios (1 for each MiKlip realisation) 3 were chosen, representing climate change realisations' variation spectrum:

- *Realisation R1* – high precipitation scenario. Originates the highest recharge (high recharge scenario R1)
- *Realisation R3* – lowest precipitation. Originates the lowest recharge (low recharge scenario R3)
- *Realisation R1_10* – ensemble of the 10 realisations; it is an average precipitation scenario. Originates an average recharge scenario (ensembles recharge scenario R1_10) for the whole set of 10 climate realisations.

Each recharge scenario is a spatial distribution of average recharge for the whole 2015-2024 period, given in mm/year. It is this distribution that was input into the model to simulate climate change impacts on aquifer's water levels (= heads). Such impacts are identified by comparing **the reference heads surfaces** (1979-2009 period recharge + pumping rates) with those for each recharge scenario, in Slices 1, 7 and 18. This is obtained by subtracting the heads scenario surface from the reference heads surface. Heads' differences between these 3 scenarios illustrate the uncertainty of climate change's impacts on groundwater.

Table 6.2 shows the recharge differences from present day's recharge. Ensembles scenario, the most likely outcome in the near future, has little variation from present day recharge. This suggests that recharge changes for 2024 may not be very significant. Nevertheless, there is also a possibility that either R1 or R3 recharge scenarios might occur, and these show significant recharge variations from present day values.

Concerning socio-economic scenarios (= pumping scenarios), land cover and demographics will not change significantly up to 2024 (APA, 2012), so historical period's pumping rates were adopted.

Table 6.2 – Recharge variation from present day conditions

Aquifer	Realisation R1	Realisation R3	Ensemble of realisations
Aluviões do Tejo	29.39%	-11.62%	0.19%
Margem Esquerda	37.61%	-20.58%	4.20%
Margem Direita	49.07%	-10.40%	5.36%

Source: Oliveira (2019)

6.1.1.3.1 Low recharge scenario

The head surfaces for this scenario (derived from **realisation R3**) are shown in Figure 6.19, Figure 6.20 and Figure 6.21 for Slice 1, Slice 7 and Slice 18 respectively. Head changes from the historical period (1979-2009) are shown in Figure 6.22, Figure 6.23 and Figure 6.24 for Slice 1, Slice 7 and Slice 18, respectively.

Heads drawdowns in **Slice 1** (Figure 6.22) for most part of its area range from 0.5 to 2 m. Valley areas show drawdowns ≤ 2 m while upstream areas have 2 to ≥ 10 m drawdowns. Sharp conductivity gradients' areas show the largest drawdowns usually from 5 to > 10 m.

Heads drawdowns < 5 m occur practically in the whole model for **Slice 7** (Figure 6.23), the location of the largest drawdowns (> 5 m) being under those of Slice 1. However, their areal extent is reduced when compared with Slice 1, in particular the areas with drawdowns > 10 m.

In **Slice 18** (Figure 6.24), drawdowns > 5 m are just localized occurrences and drawdowns > 10 m (red circles) are due to the influence of the fluid-flux boundary condition set in Slice 1 and 2.

As to be expected in this low recharge scenario, there is a general water levels decrease (= heads drawdowns) from historical period's heads, in all slices analysed. This decrease is not very large for most part of the model area. The sharpest decreases occur in Slice 1, being located at some upstream zones and areas with sharp hydraulic conductivity gradients. Drawdowns become smaller and spatially more uniform as the slice depth increases. Flooded areas do not occur.

Figure 6.19 – Heads surfaces for alluvial deposits and topmost Pliocene + Miocene water bearing units (Slice 1) under low recharge scenario (R3 climate realisation's recharge)

Figure 6.20 – Heads surface for Pliocene formations and topmost Miocene water bearing units (Slice 7) under low recharge scenario (R3 climate realisation's recharge)
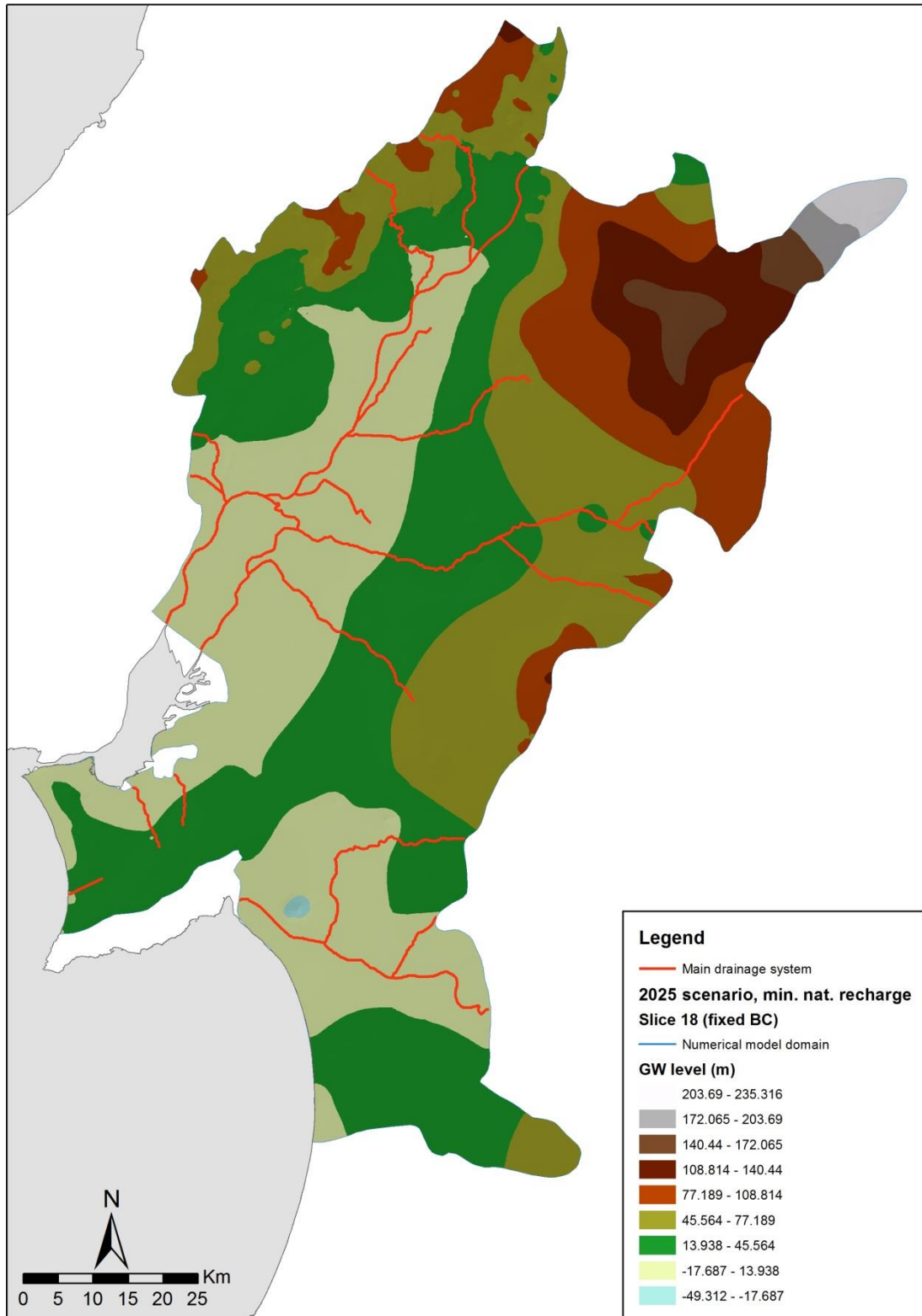
Figure 6.21 – Heads surface for Miocene formations (Slice 18) under low recharge scenario (R3 climate realisation's recharge)

Figure 6.22 – Head differences (annual mean values) between historical period (1979-2009) pumping conditions and R3 realization (minimum recharge scenario) in Slice 1

Figure 6.23 – Head differences (annual mean values) between historical period (1979-2009) pumping conditions and R3 realization (minimum recharge scenario) in Slice 7

Figure 6.24 – Head differences (annual mean values) between historical period (1979-2009) pumping conditions and R3 realization (minimum recharge scenario) in Slice 18

6.1.1.3.2 Ensembles recharge scenario

The ensembles scenario's (R1_R10) head surfaces are shown in Figure 6.25, Figure 6.26 and Figure 6.27 for Slice 1, Slice 7 and Slice 18, respectively. Head changes from the historical period (1979-2009) are shown in Figure 6.28, Figure 6.29 and Figure 6.30, for the same slices respectively.

In **Slice 1** (Figure 6.28) head changes are on average ≈ 0 m for almost the whole model, except in localized areas with significant head decreases from the historical values. Such abnormal values are due to error-norm-flow issues not yet solved. Although error-norm-flow problematic areas are very small, they nevertheless can affect larger areas, in particular if their neighbouring areas have sharp hydraulic conductivity gradients. Similar abnormal behaviour occurs in NW and NE tips of model's border which were set with fluid-flux boundary conditions. This shows the need for further calibration and validation. However, this is not possible at the moment due to lack of data in such areas.

In **Slice 7** (Figure 6.29) head changes are also ≈ 0 m for almost the whole model and the abnormal regions are much more reduced. The abnormal behaviour seen in Slice 1 in the fluid-flux boundary conditions set at the above cited model' border is also observed.

In **Slice 18** (Figure 6.30), head changes are also ≈ 0 m in whole model, the abnormal behaviour areas being strongly reduced in number and extension.

As shown, head changes between the historical period and those of ensembles scenario are minimal. This is expected once recharge changes from the historical period are small (cf. Table 6.2, chapter 6.1.1.3). Notice that although all MiKlip realisations/recharge scenarios have the same probability to occur in 2024, ensembles scenario is assumed as the most likely for adaptation purposes under BINGO Project.
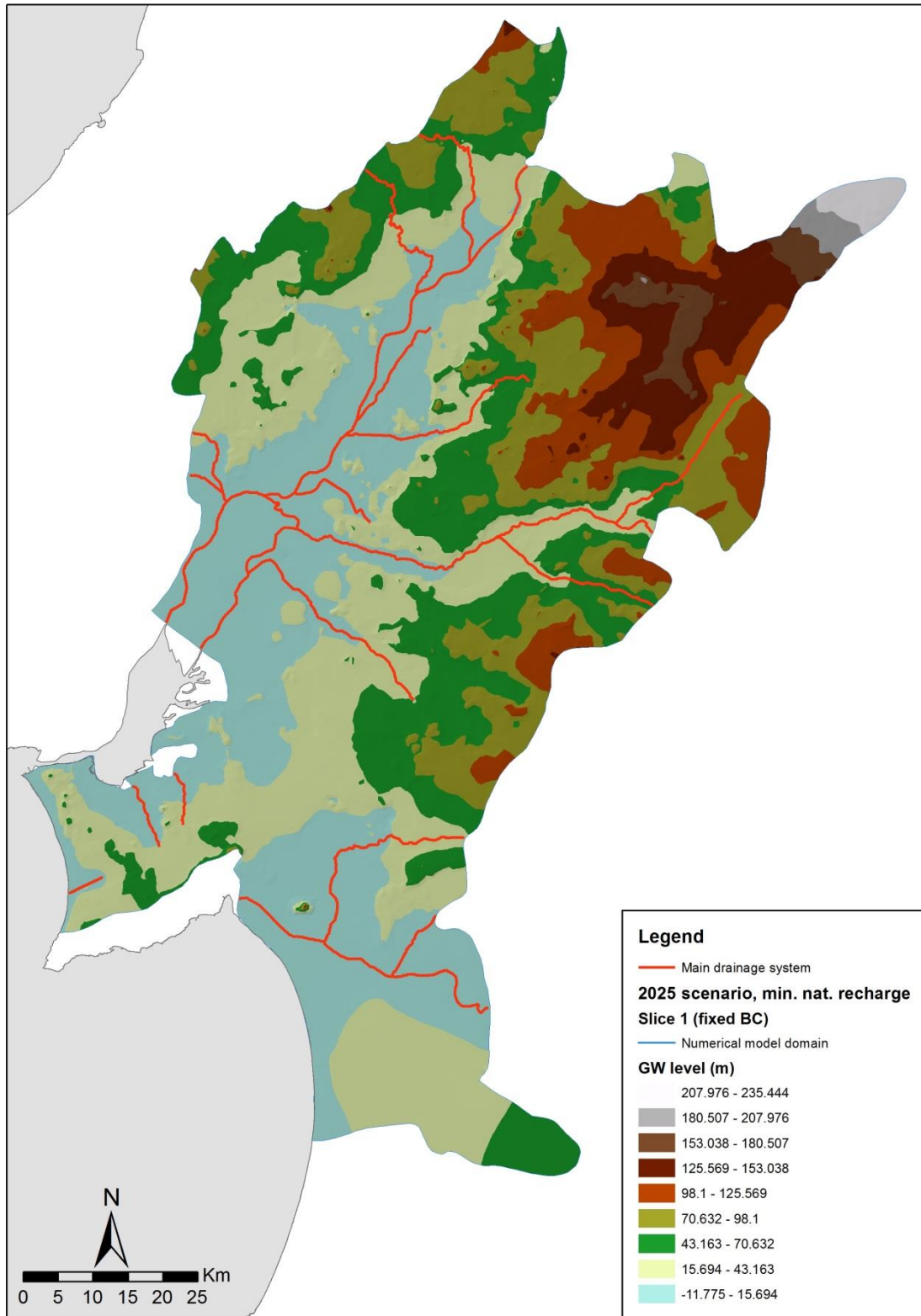
Figure 6.25 – Heads surfaces for alluvial deposits and topmost Pliocene + Miocene water bearing units (Slice 1) under ensembles scenario (average of the 10 MiKlip realizations' recharges R1_10)

Legend

— Main drainage system

2025 Climate change, ave. nat. recharge
Slice 7 (fixed BC)
— Numerical model domain

GW level (m)

	204.449 - 236.007
	172.891 - 204.449
	141.333 - 172.891
	109.775 - 141.333
	78.217 - 109.775
	46.659 - 78.217
	15.101 - 46.659
	-16.457 - 15.101
	-48.015 - -16.457

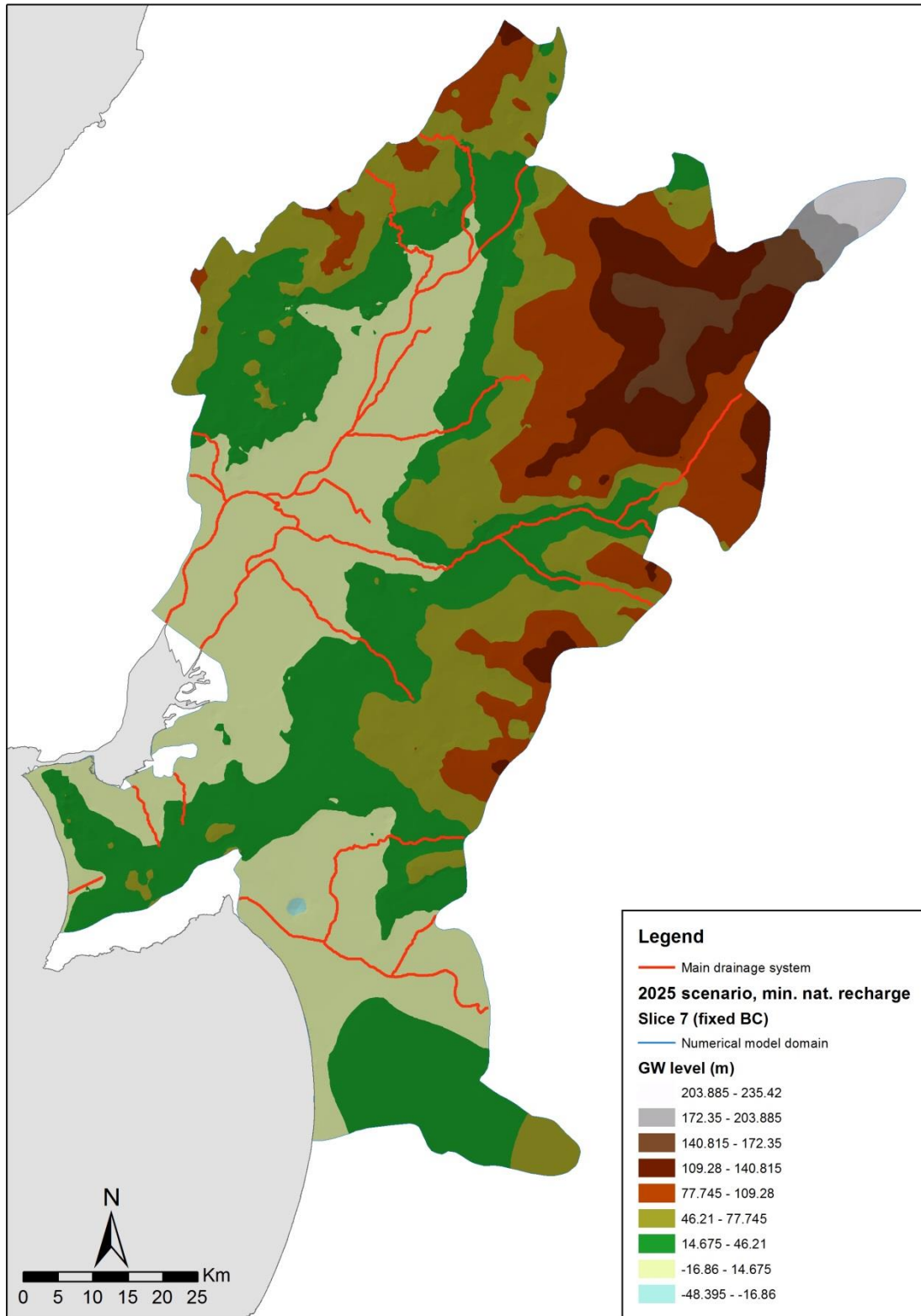**Figure 6.26 – Heads surface for Pliocene formations and topmost Miocene water bearing units (Slice 7) under ensembles scenario (average of the 10 MiKlip realizations' recharges R1_10)**

Legend

— Main drainage system

2025 Climate change, ave. nat. recharge
Slice 18 (fixed BC)

— Numerical model domain

GW level (m)

	203.735 - 235.328
	172.141 - 203.735
	140.548 - 172.141
	108.955 - 140.548
	77.362 - 108.955
	45.769 - 77.362
	14.176 - 45.769
	-17.417 - 14.176
	-49.01 - -17.417
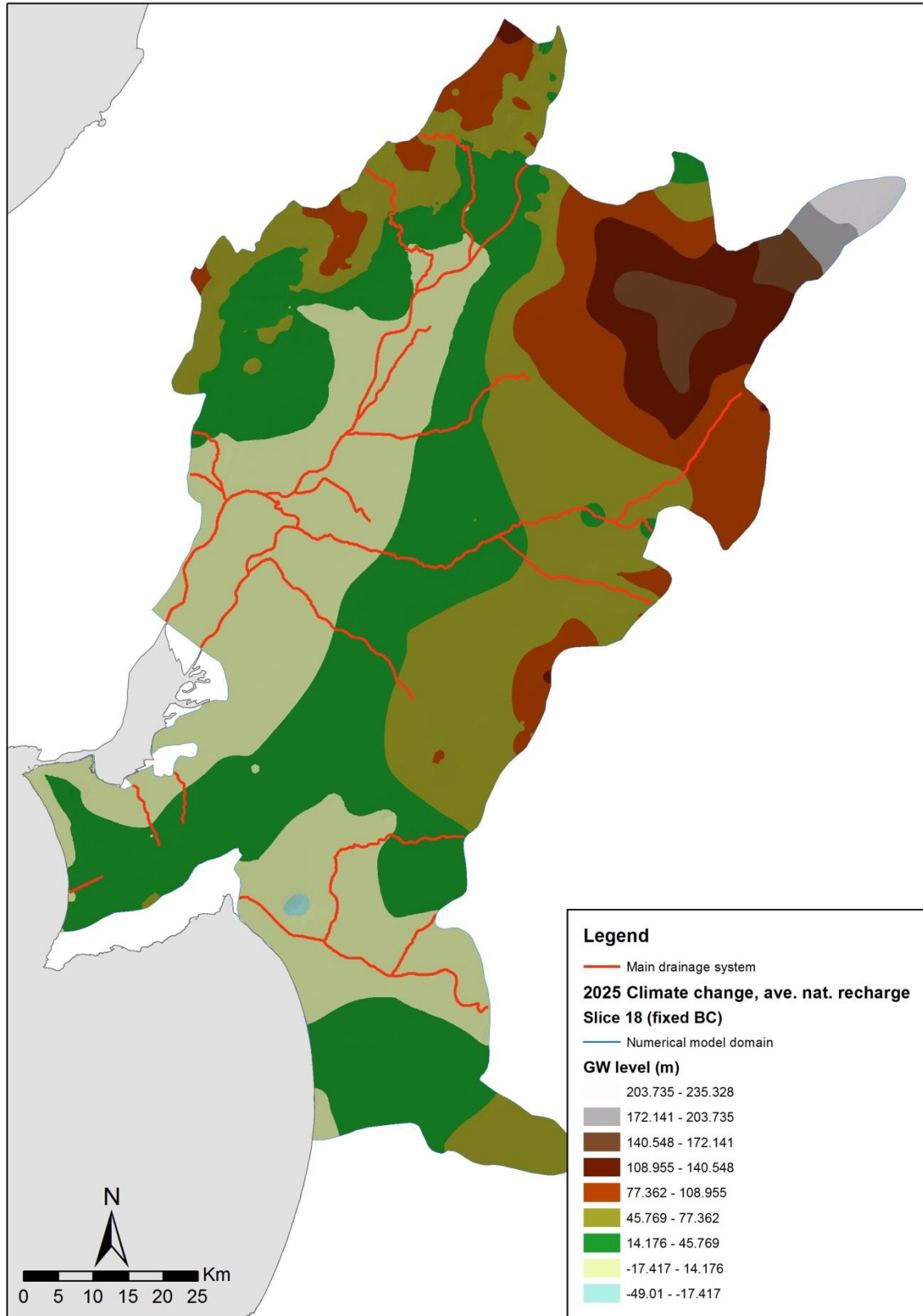
Figure 6.27 – Heads surface for Miocene formations (Slice 18) under ensembles scenario (average of the 10 MiKlip realizations' recharges R1_10)

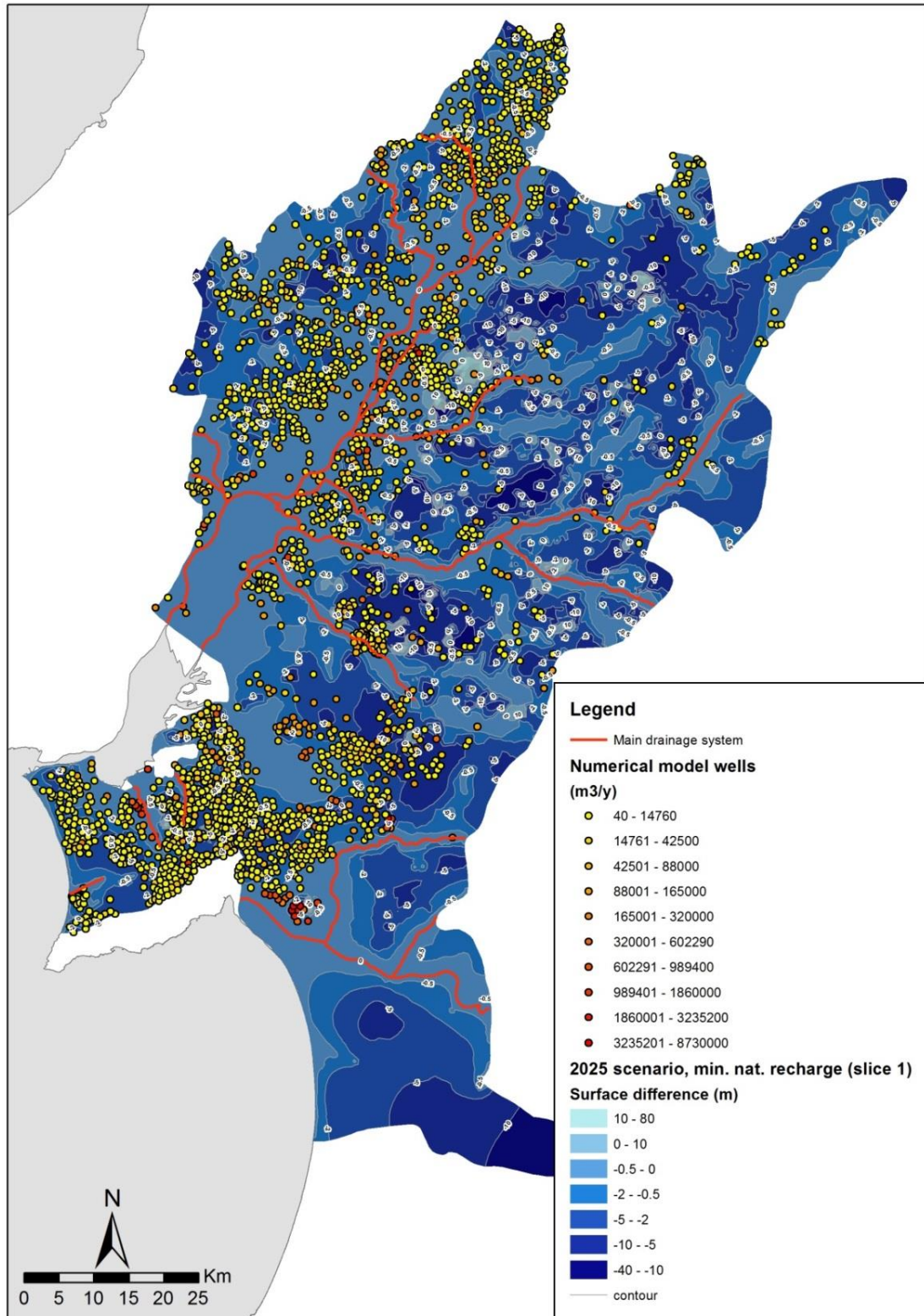**Figure 6.28 – Head differences (annual mean values) between historical period (1979-2009) pumping conditions and ensembles scenario (average of the 10 MiKlip realizations' recharges) in Slice 1**

Legend

— Main drainage system

Numerical model wells
(m3/y)

- ○ 40 - 14760
- ○ 14761 - 42500
- ○ 42501 - 88000
- ○ 88001 - 165000
- ○ 165001 - 320000
- ○ 320001 - 602290
- ● 602291 - 989400
- ● 989401 - 1860000
- ● 1860001 - 3235200
- ● 3235201 - 8730000

2025 ave. nat. recharge (slice 7)
Surface difference (m)

- 20 - 30
- 10 - 20
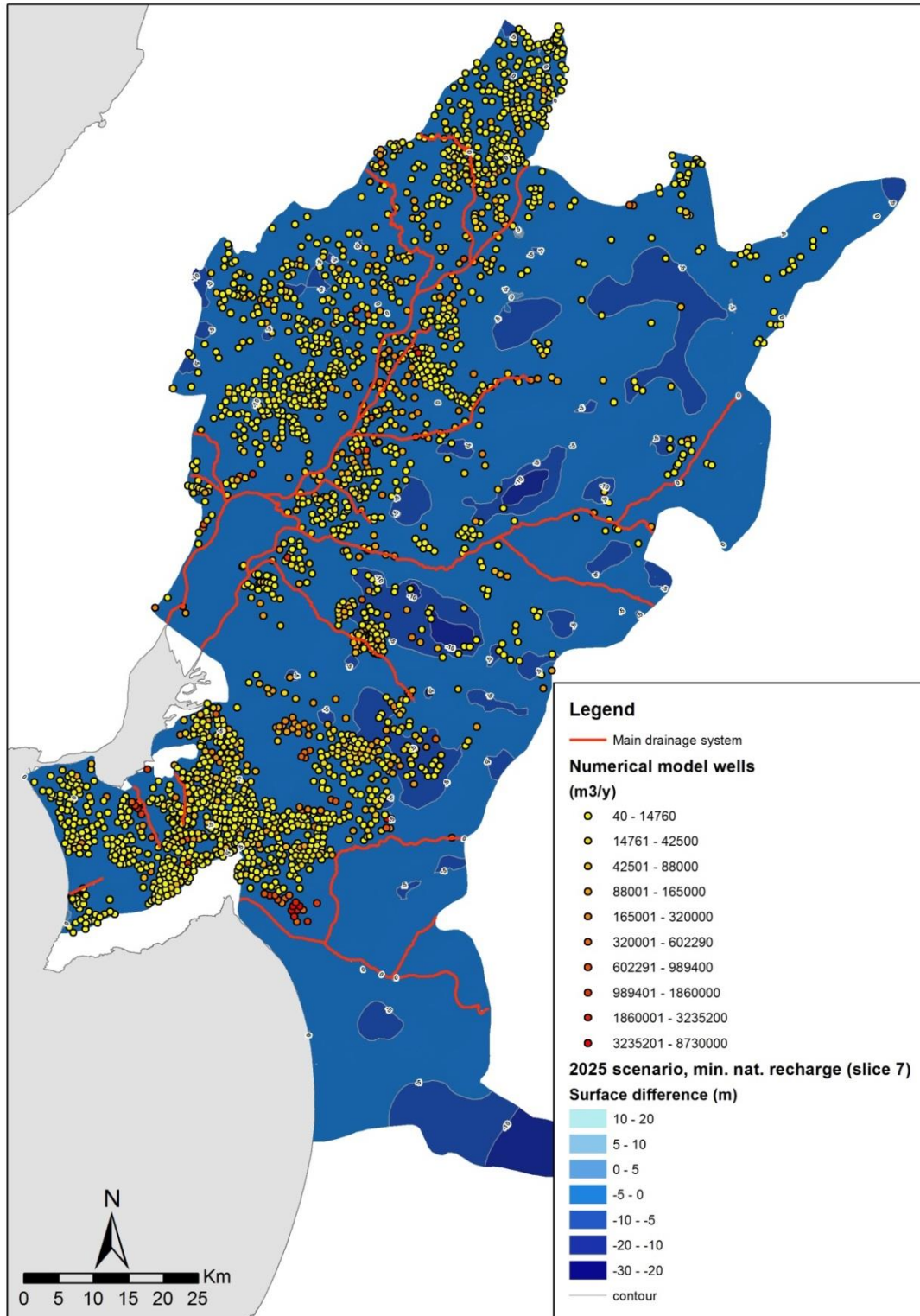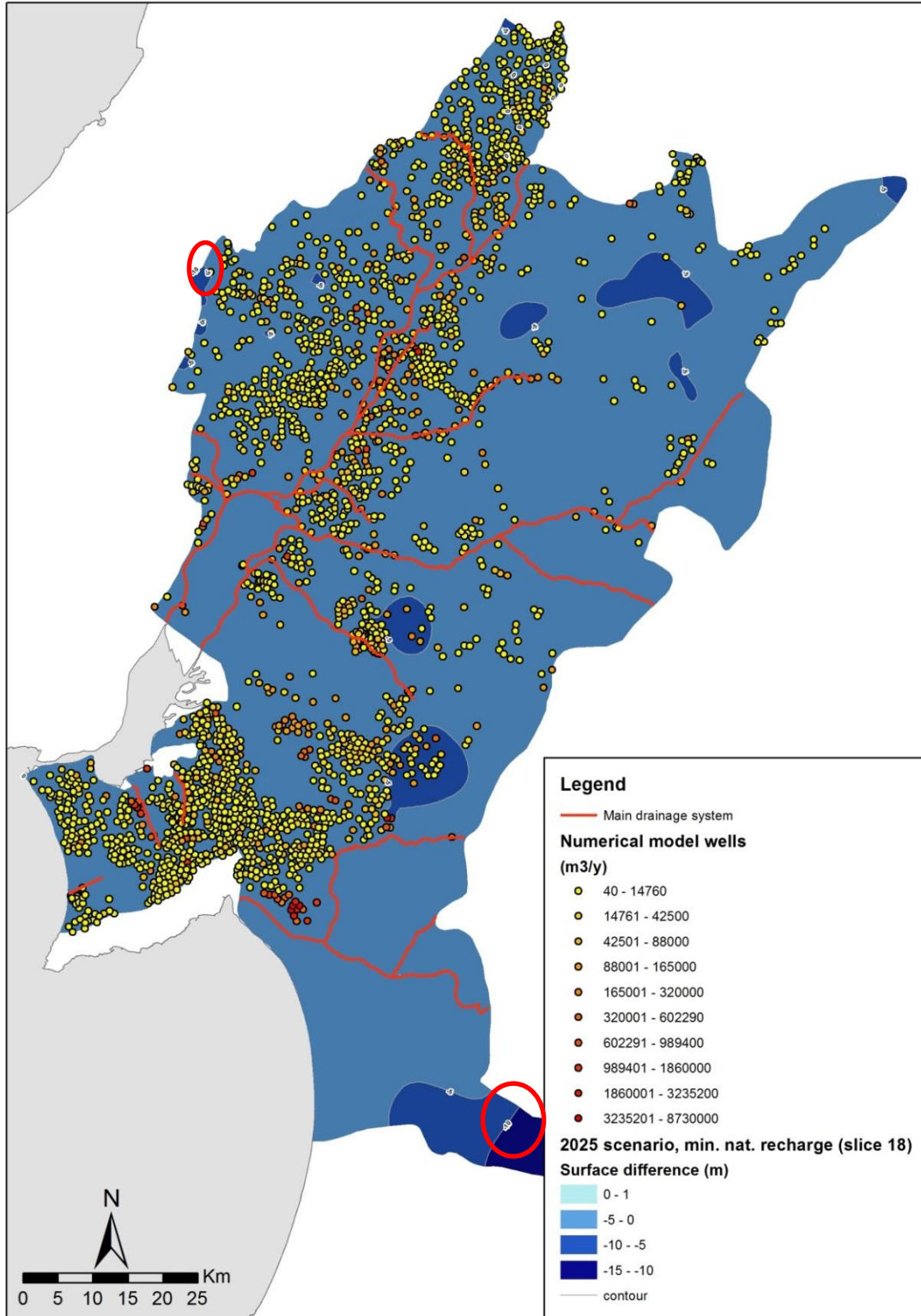- 0 - 10
- -10 - 0
- -20 - -10
- -30 - -20
- -40 - -30
- -50 - -40
- contour
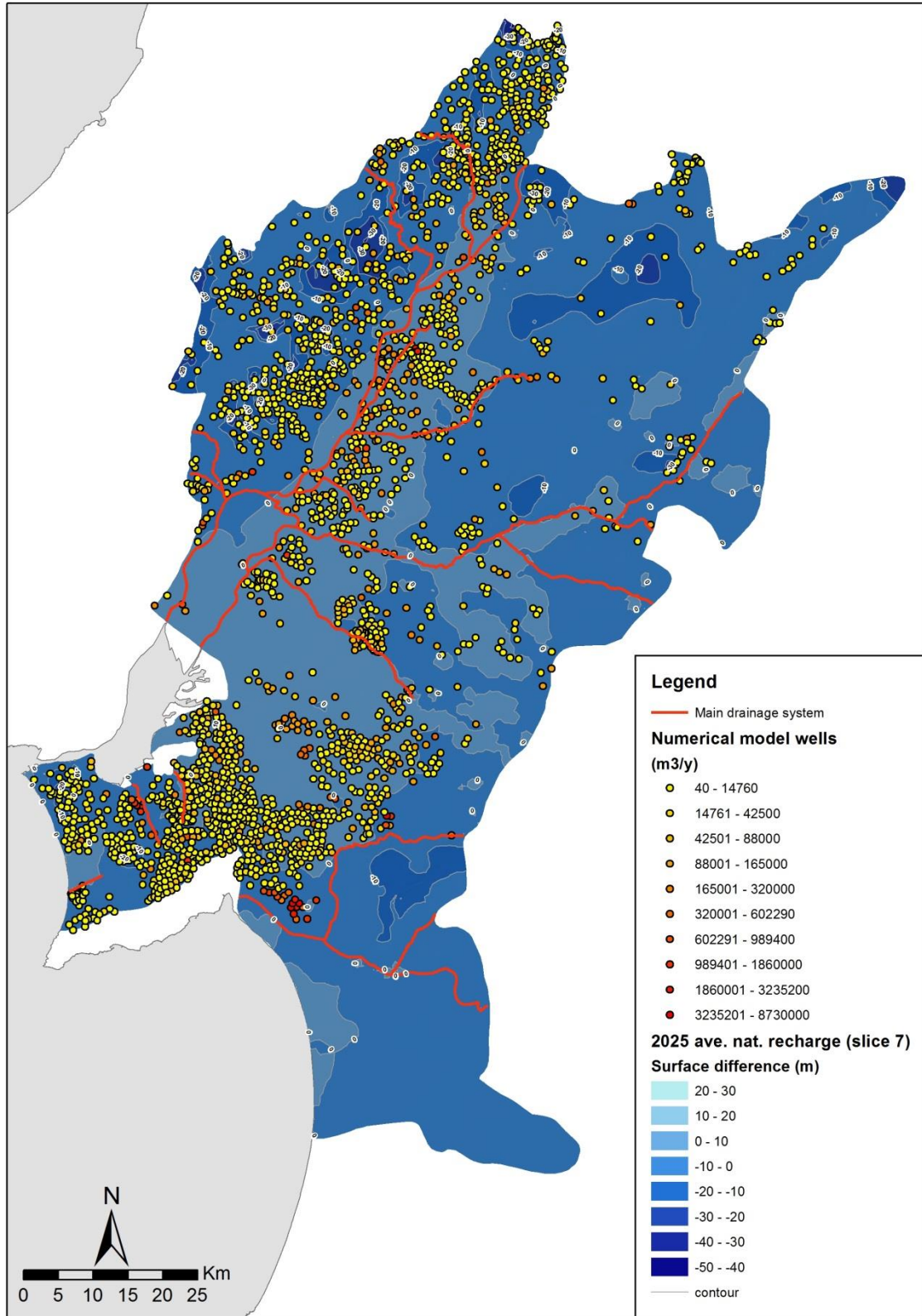
Figure 6.29 – Head differences (annual mean values) between historical period (1979-2009) pumping conditions and ensembles scenario (average of the 10 MiKlip realizations' recharges) in Slice 7

Figure 6.30 – Head differences (annual mean values) between historical period (1979-2009) pumping conditions and under ensembles scenario (average of the 10 MiKlip realizations' recharges) in Slice 18

6.1.1.3.3 High recharge scenario

High recharge scenario's (R1) head surfaces are shown in Figure 6.31, Figure 6.32 and Figure 6.33 for Slice 1, Slice 7 and Slice 18, respectively. Head differences from the historical period are shown in Figure 6.34, Figure 6.36 and Figure 6.37, for Slice 1, Slice 7 and Slice 18, respectively.

In **Slice 1**, heads rise from the historical values are less than 2 m, in valley areas, and 2 to more than 5 m, upstream and away from the river network; rises up to 10 m occur in high conductivity gradient's areas (Figure 6.34). Due to this head rise, topography and conductivity characteristics, **several areas are flooded** (Figure 6.35). Local areas of heads' drawdown (Figure 6.34, red circles) result from local instabilities of the model.

In **Slice 7**, head rises are more attenuated, ranging from 0.5 m up to 2 m for almost the whole area of the model (Figure 6.36). Head rises ≥ 5 m areas are smaller than in Slice 1. This reduction is particularly significant for the 10 m head rises' areas (Figure 6.34 vs. Figure 6.36).

In **Slice 18**, head rises are even more attenuated, with areas of > 5 m head rise strongly reduced when compared with Slices 1 and 7 (Figure 6.34 vs. Figure 6.37 vs. Figure 6.36). The same sharp reduction is observed for > 10 m head rise's areas, which almost disappear, exception being the central W, NE and SE tips of the model when compared with Slices 1 and 7 (Figure 6.34 vs. Figure 6.36 vs. Figure 6.37).

As to be expected in this scenario, there is a general head's rise from the historical period's heads for the whole model area, due to the sharp recharge increases associated with the R3 realisation. This recharge and ensuing head rises prompt flooding in several topographically depressed areas of the model (Figure 6.35).
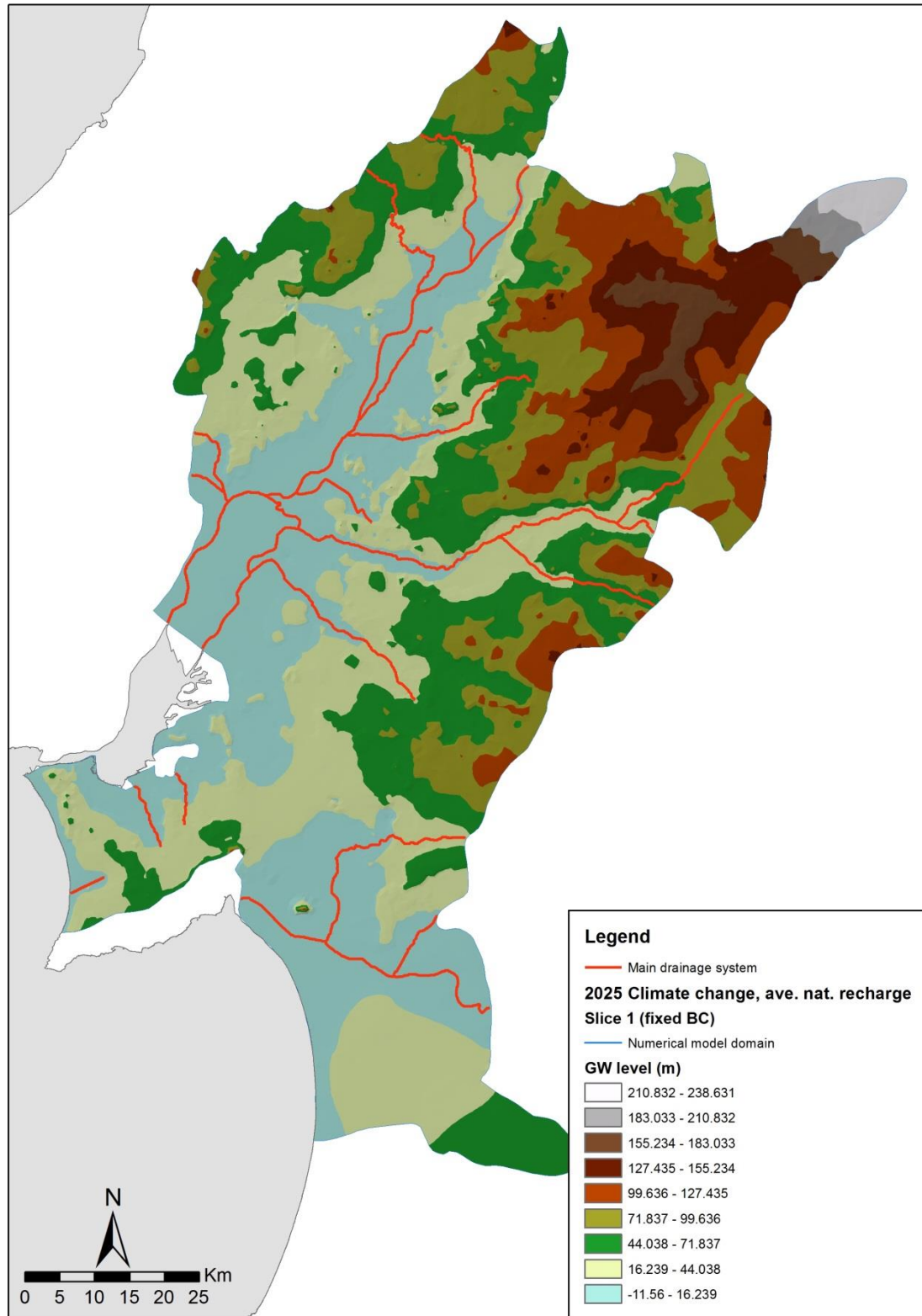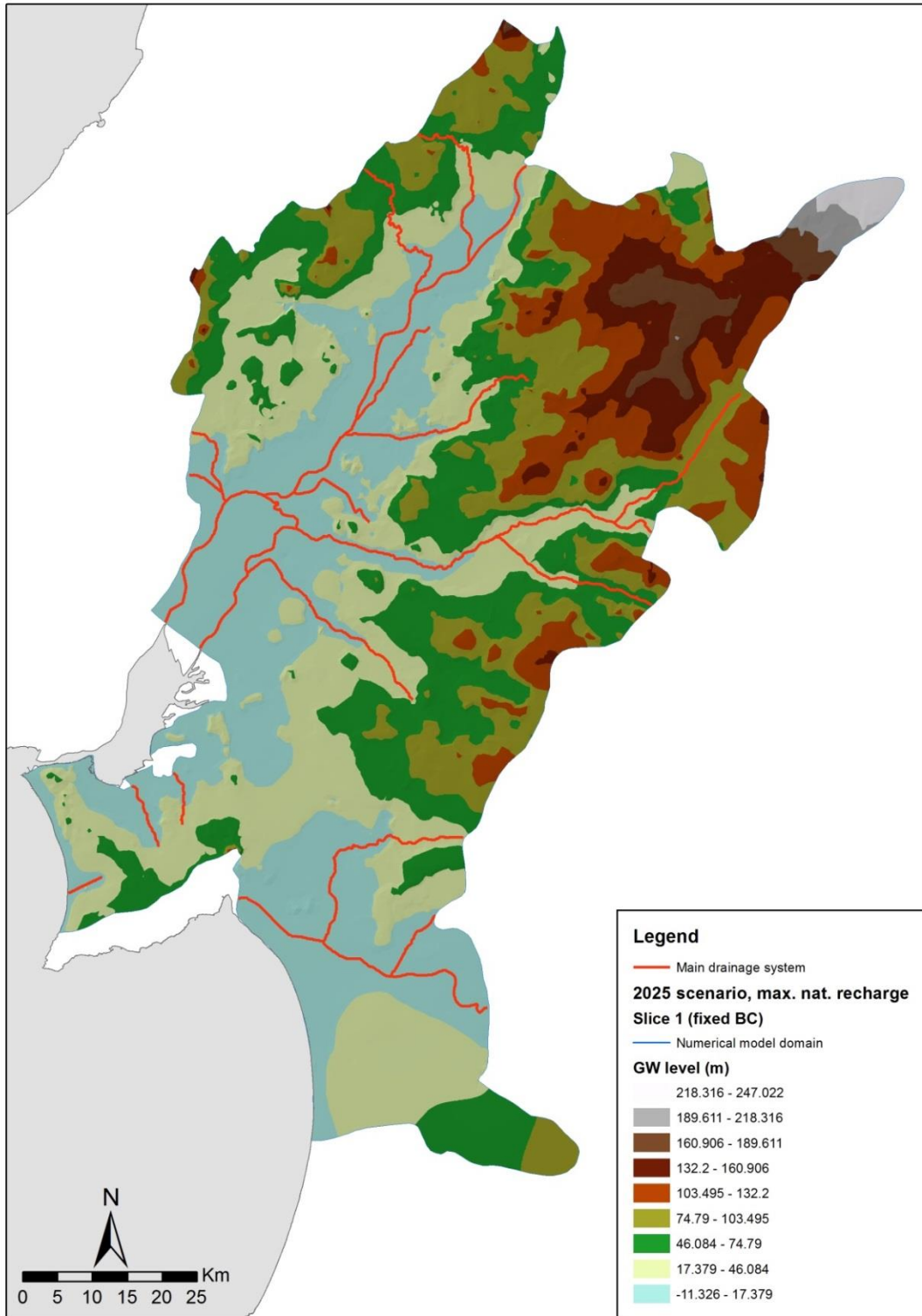
Figure 6.31 – Heads surfaces for alluvial deposits and topmost Pliocene + Miocene water bearing units (Slice 1) under high recharge scenario (R1 climate realisation's recharge)
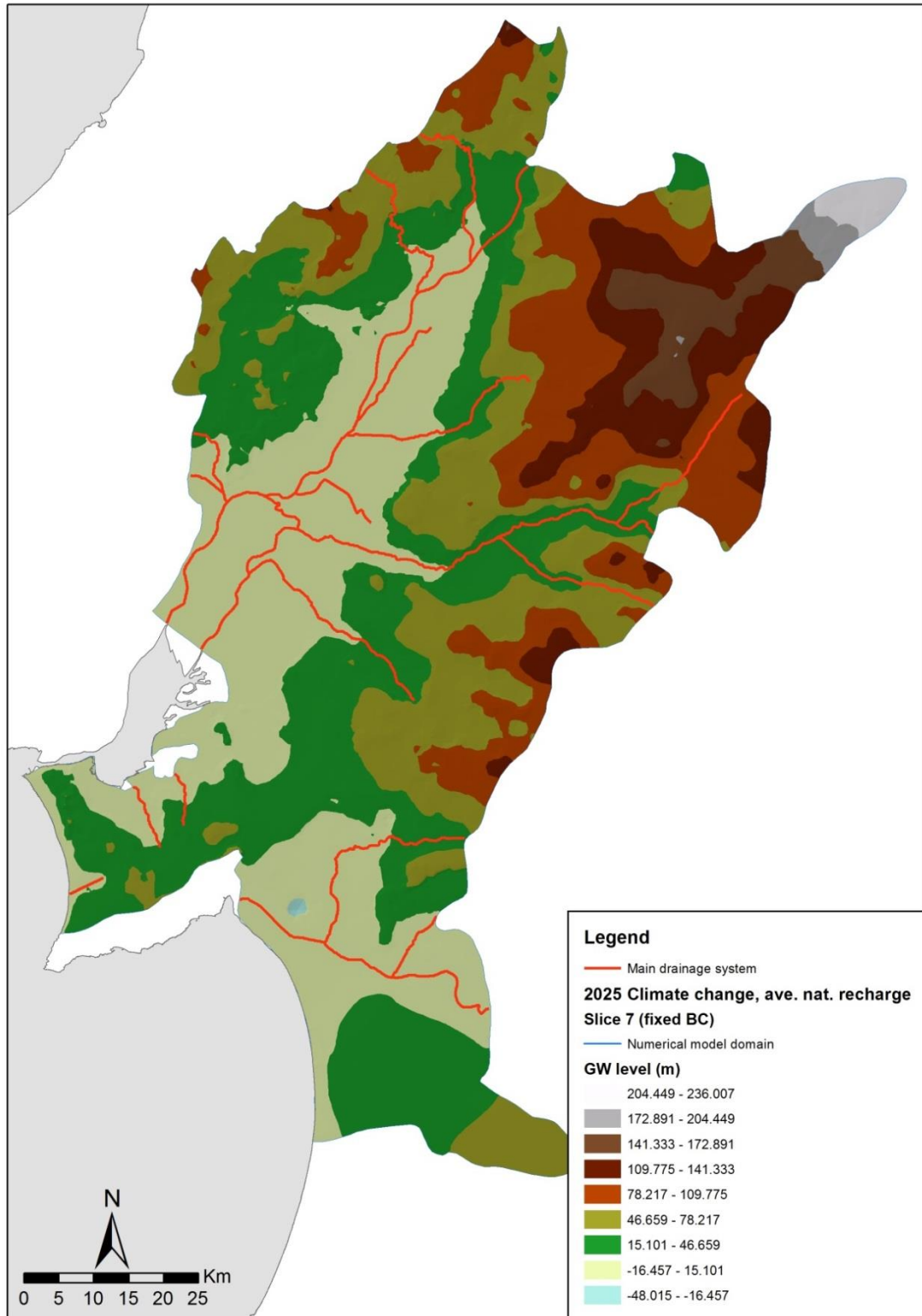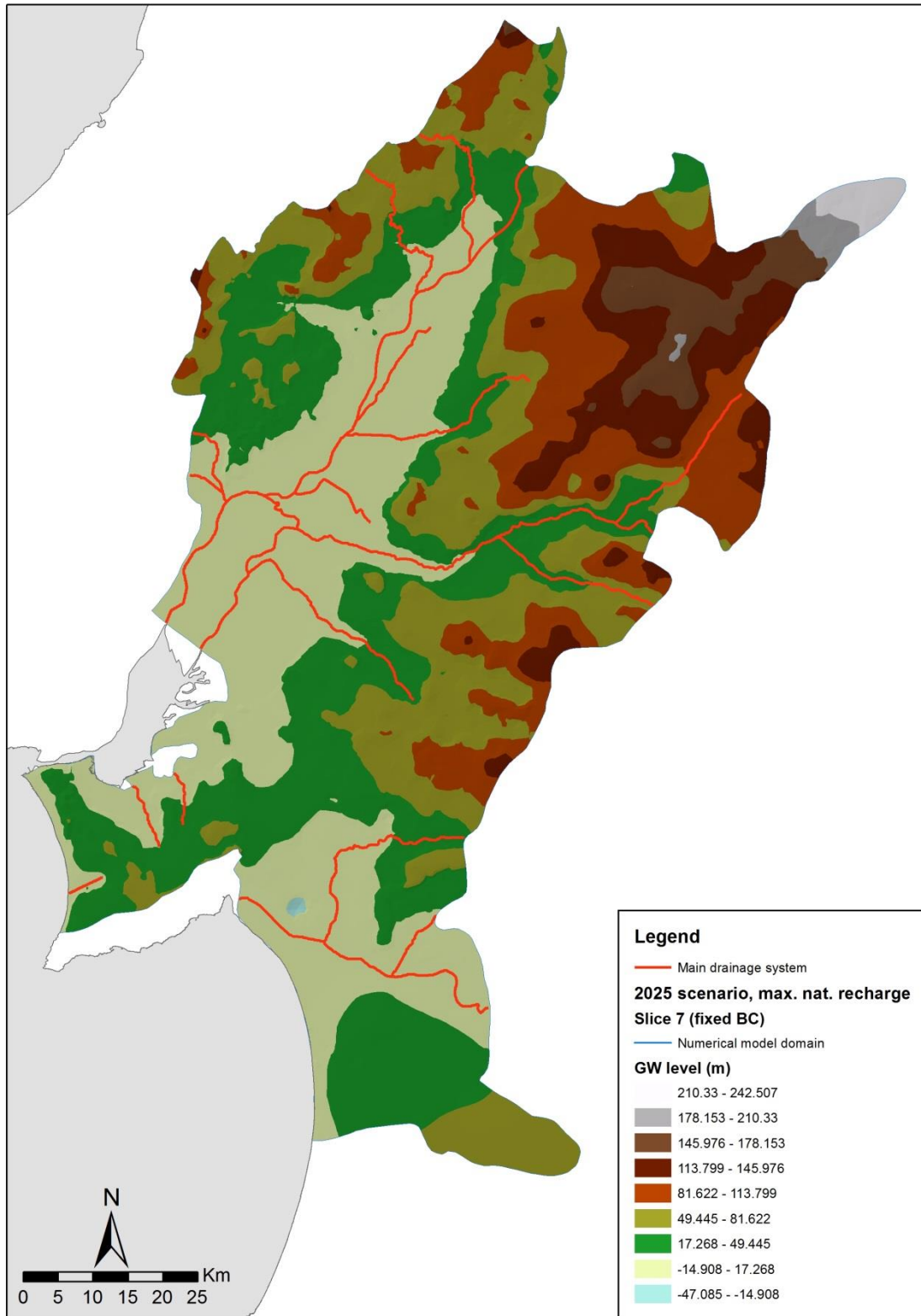
Figure 6.32 – Heads surface for Pliocene formations and topmost Miocene water bearing units (Slice 7) under high recharge scenario (R1 climate realisation's recharge)
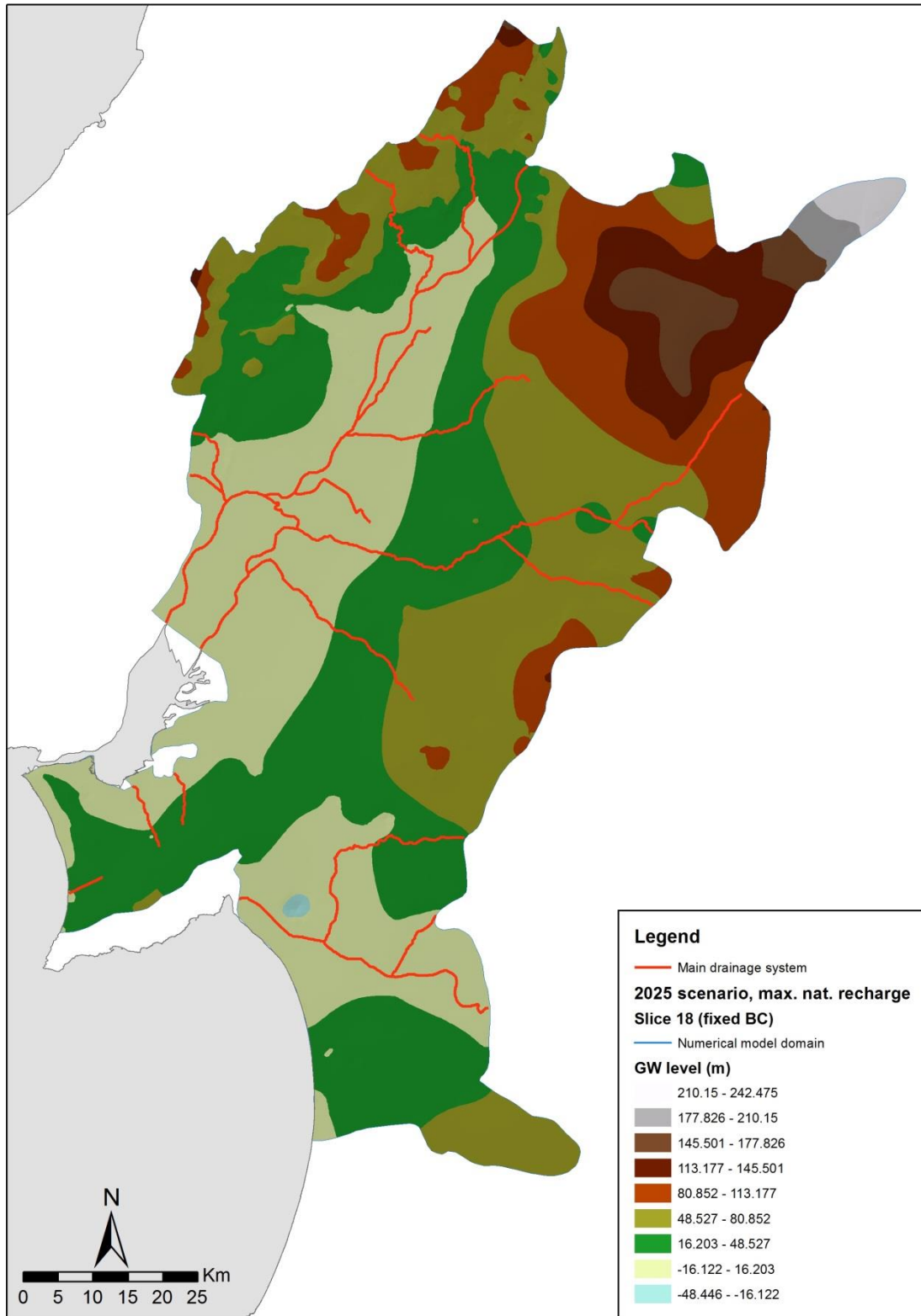
Figure 6.33 – Heads surface for Miocene formations (Slice 18) under high recharge scenario (R1 climate realisation's recharge)
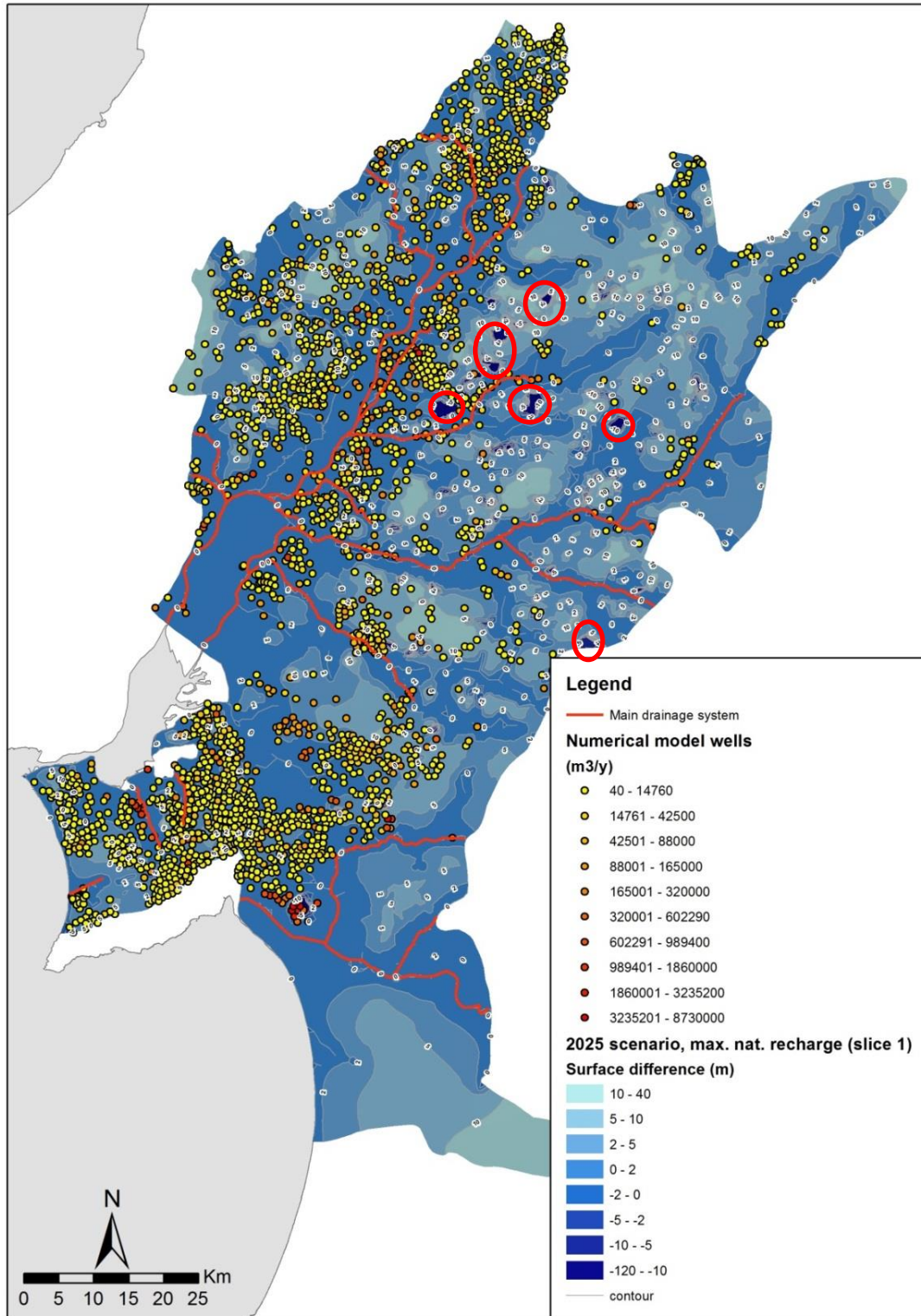
Figure 6.34 – Head differences (annual mean values) between historical period (1979-2009) pumping conditions and R1 realization (minimum recharge scenario) in Slice 1

Figure 6.35 – Flooded areas (orange) in the high recharge scenario (Slice 1)
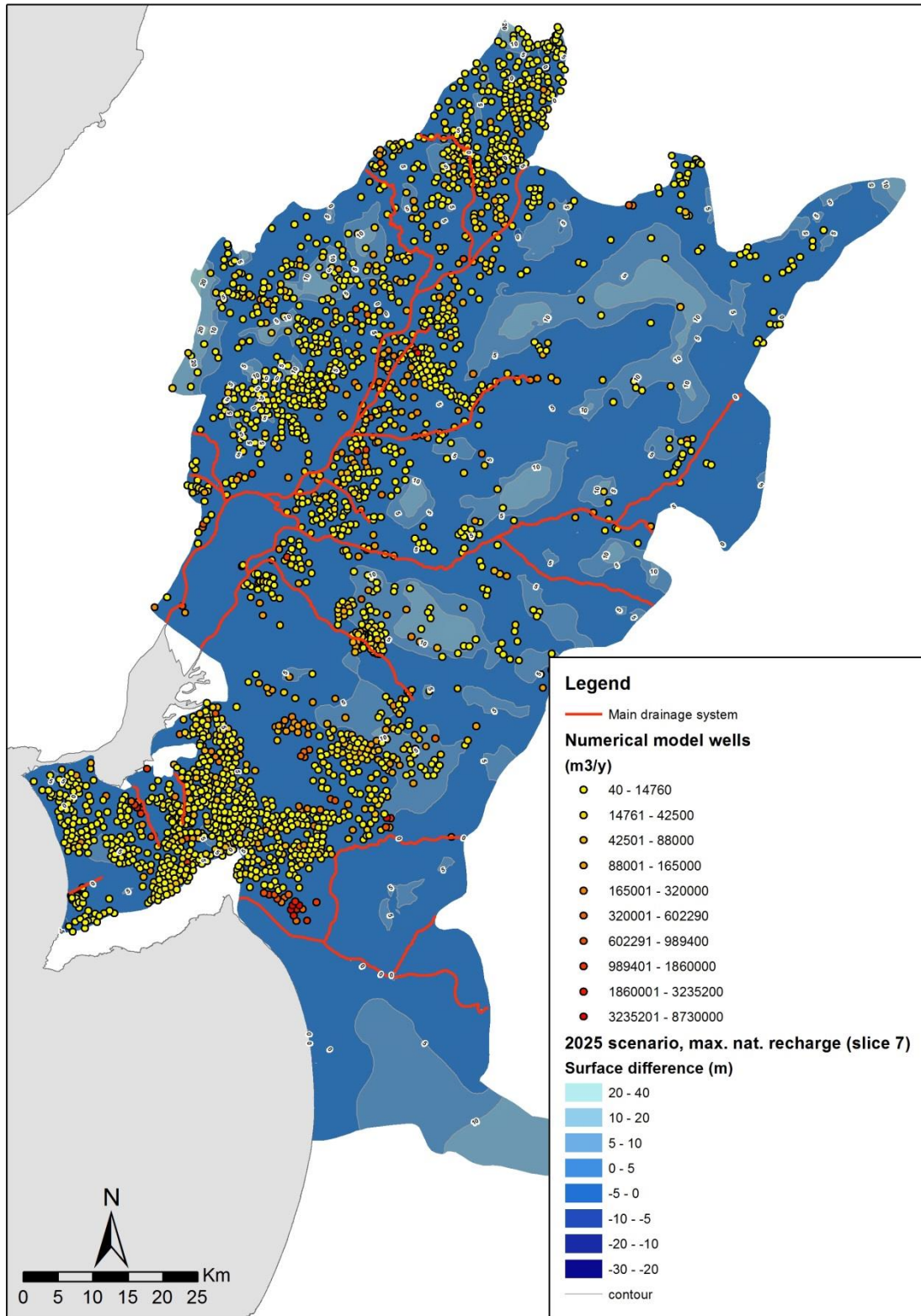
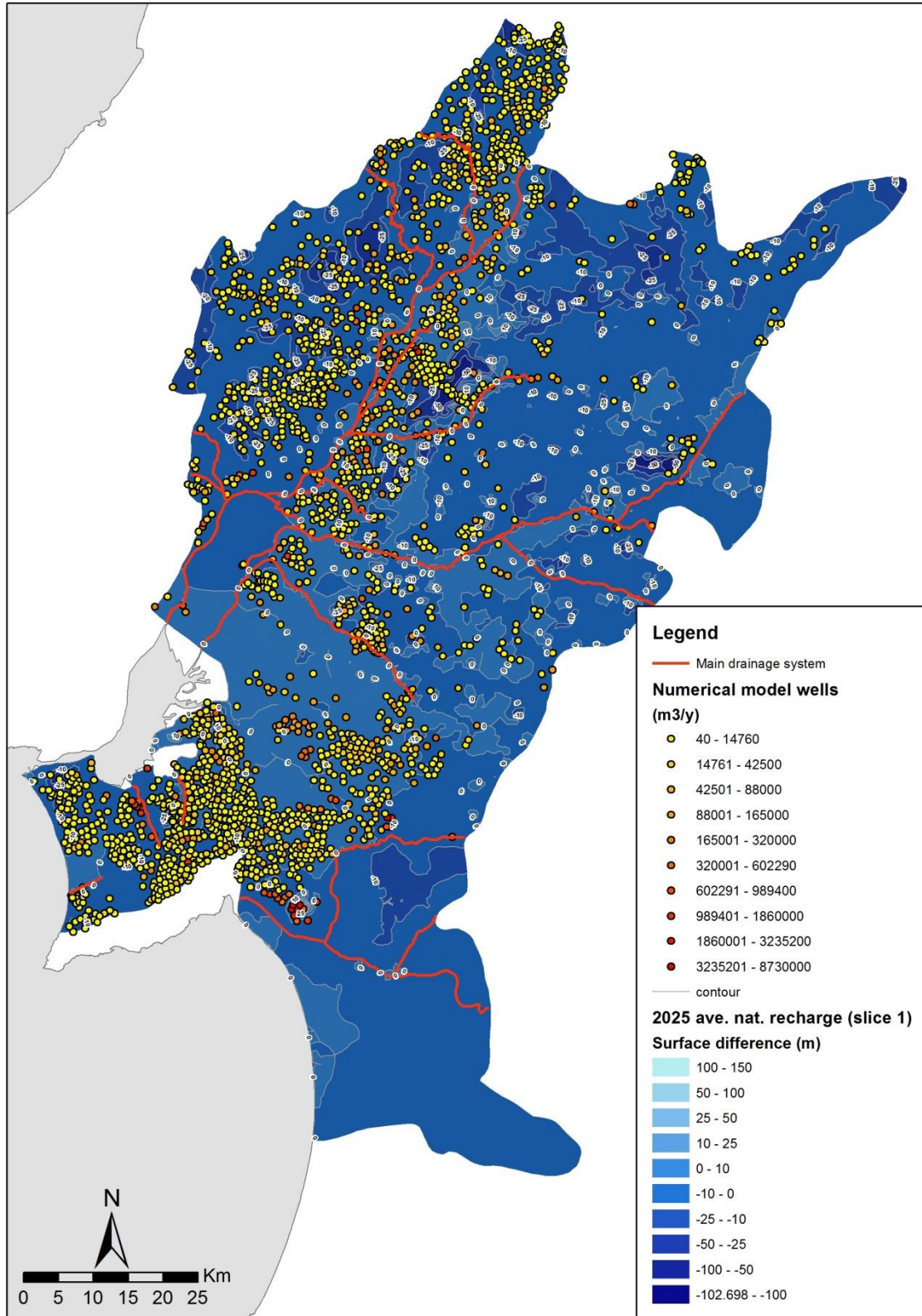**Figure 6.36 – Head differences (annual mean values) between historical period (1979-2009) pumping conditions and R1 realization (minimum recharge scenario) in Slice 7**
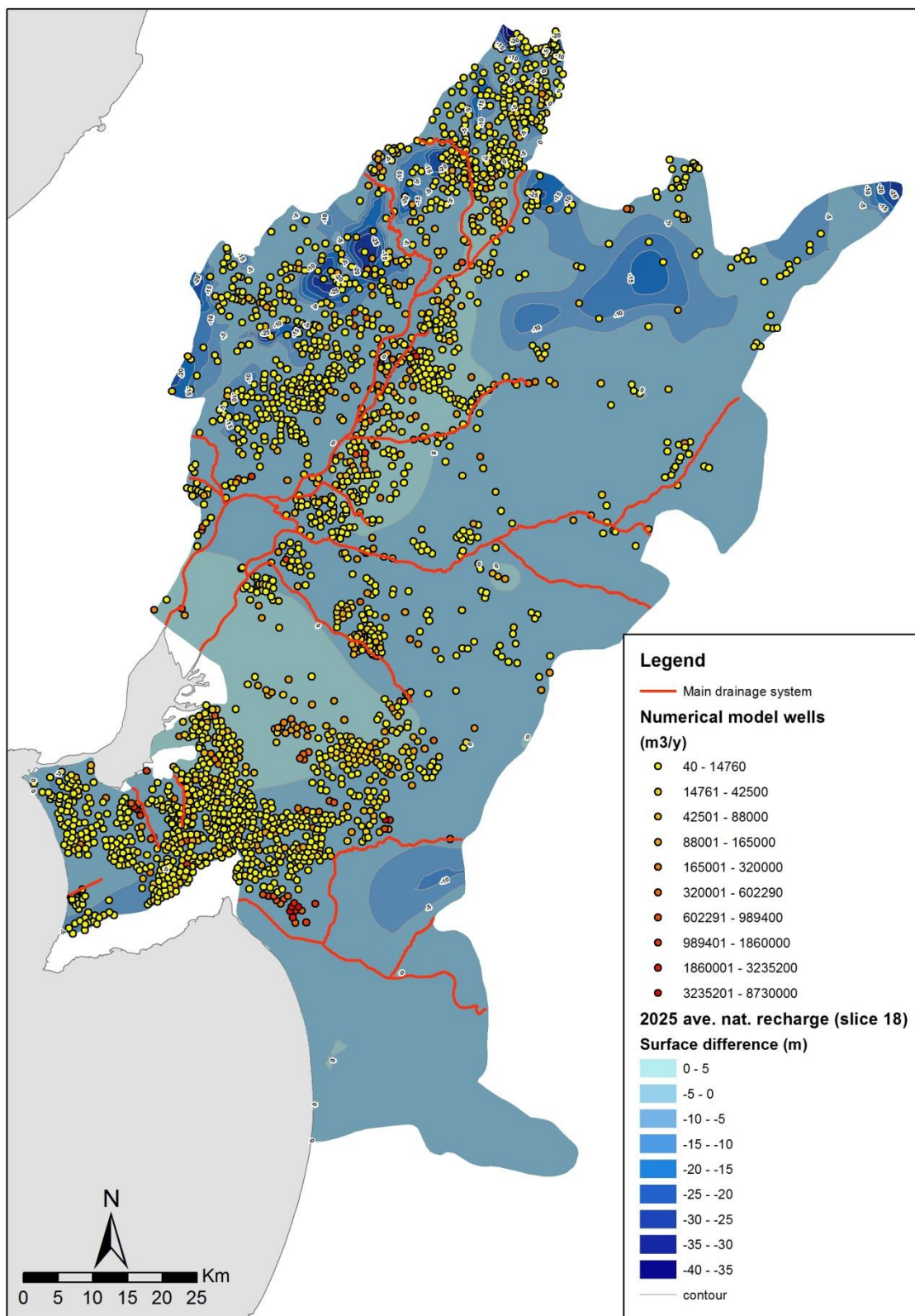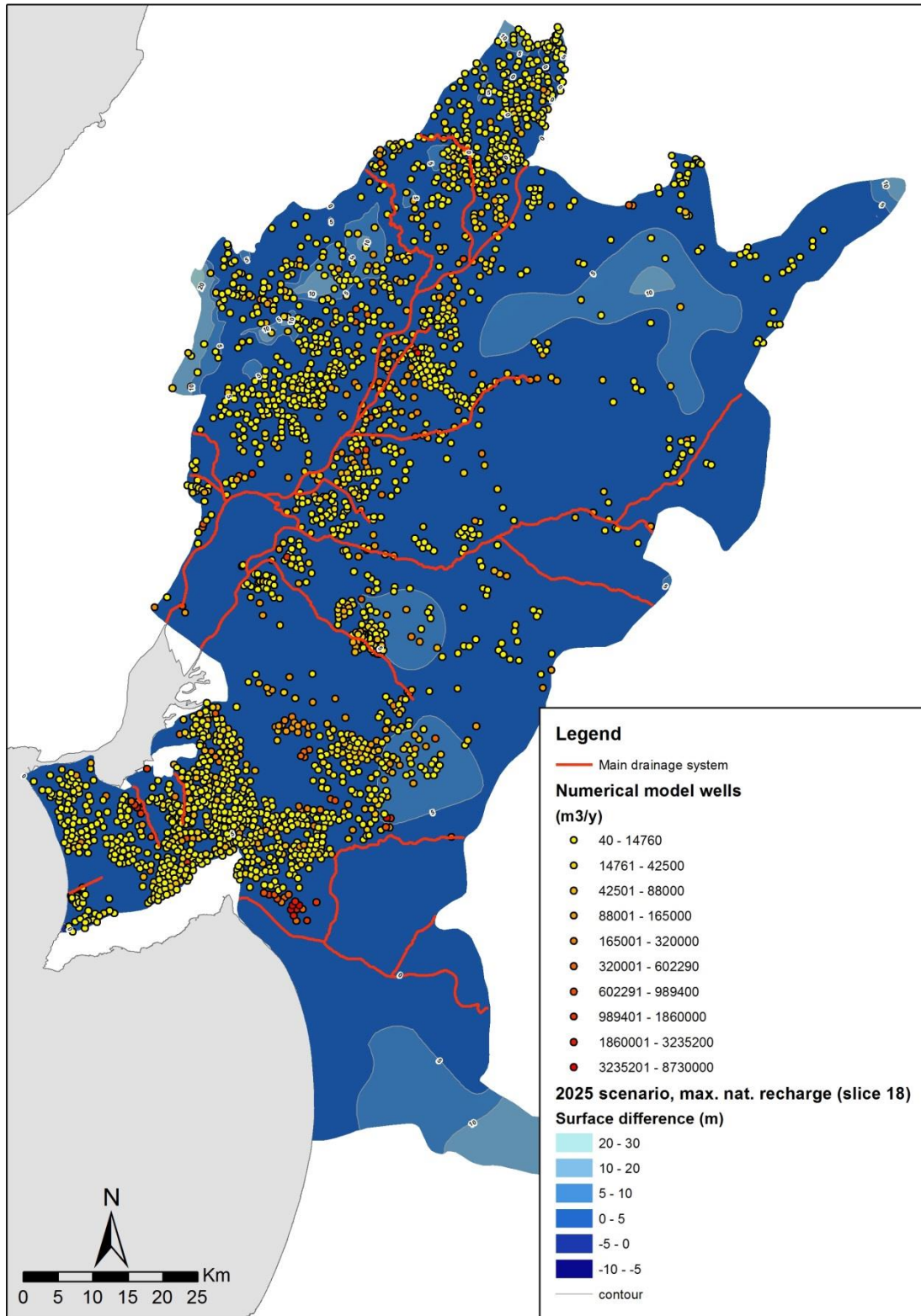
Figure 6.37 – Head differences (annual mean values) between historical period (1979-2009) pumping conditions and R1 realization (minimum recharge scenario) in Slice 18

6.1.2   Semi-transient runs

The semi-transient simulations were performed for the 2024 horizon to analyse head changes under a multi-year drought assuming as average climate/recharge that of ensembles scenario. The 3 drought scenarios developed were:

- 1 year drought length
- 3 years drought length
- 5 years drought length.

The reason to simulate multi-year droughts stems from the possibility that these might become more usual in the long term future (Guerreiro et al., 2017). In the historical period only 1 and 2-year drought have occurred and for the whole XX century only one 3-year, one 2,5-year and two 2-year droughts have occurred (https://www.ipma.pt/pt/educativa/tempo.clima/index.jsp?page=seca.pt.xml&print=true; https://www.ipma.pt/pt/oclima/observatorio.secas/pdsi/apresentacao/evolu.historica/index_link.html?page=os_series_longas_matriz.xml). Once for 2024 the ensembles scenario suggests a climate similar to that of the historical period, multi-year droughts have a low possibility of occurrence up to 2024, particularly the 5-year droughts. The latter can then be viewed as a threshold scenario. Nevertheless, MiKlip results show high climate variability and quite severe drought years can occur even under high recharge scenario (realization R1) although not necessarily on a 5-year stretch.

The annual drought recharge values used in 1, 3 and 5-year drought scenarios are those of 2005[12] (cf. chapter 6.1.1.2). All semi-transient runs for these scenarios start with the heads' results of the ensembles scenario (R1_10). Pumping rates remain equal to present-day rates. Starting from the results of the ensembles scenario, ensembles recharge is replaced for the 2005 recharge and the model is set to run for 1, 3 and 5 years. The transient simulations run on a varying time-step lengths. A 1 year simulation (365 days) is run and the results saved. Then starting from these results, the model is kept running for 730 days more, simulating a total 3-year drought. The results are saved and used to run the model others 730 days more, so accounting for a 5-years drought. The results for each drought scenario are presented as head surfaces for Slice 1, Slice 7 and Slice 18 and as the differences between these surfaces and those of the historical period (1979-2009).

After testing several combinations of initial time step and error tolerance, the smallest budget imbalance and fit errors are achieved with an initial time step = 0.001 and error tolerance = 2.3×10^{-3} for the initial 1 year run (Table 6.3). This error tolerance is in agreement with the value for steady state runs (cf. sub-chapter 6.1.1).

Due to data constraints – no time-series data for pumping rates; very incomplete heads' time-series; only average annual recharge values available – simulation of full transient conditions is not possible. The alternative semi-transient approach has however some shortcomings: once monthly time series for pumping rates are not available, monthly head changes under drought cannot be analysed. Also, to

---

[12] 2005 drought conditions generated a 79% lower average recharge than that of the historical period.

simulate droughts using present-day average pumping rates is optimistic because under protracted droughts groundwater abstraction increases. This hinders the analysis of supply contingency options under droughts and the simulated heads should be viewed as optimistic.

Table 6.3 – Errors on semi- transient simulations for different error tolerances (1 year run)

Initial time step	Error tolerance	Errors	
		Imbalance	Fit errors
0.0005	$2.28x10^{-3}$	-65797 m^3/day	E= 3.667; RMS = 5.145; σ = 5.1497
	$3x10^{-3}$	-66986 m^3/day	E= 3.649; RMS = 5.138; σ = 5.144
	$3.3x10^{-3}$	-55518 m^3/day	E= 3.692; RMS = 5.252; σ = 5.257
0.001	$0.8x10^{-3}$	-93011 m^3/day	E= 3.672; RMS = 5.205; σ = 5.210
	$1x10^{-3}$	-67251 m^3/day	E= 3.647; RMS = 5.133; σ = 5.138
	$1.5x10^{-3}$	-58685 m^3/day	E= 3.696; RMS = 5.334; σ = 5.3396
	$2x10^{-3}$	-45850 m^3/day	E= 3.663; RMS = 5.2198; σ = 5.225
	$2.28x10^{-3}$	-45020 m^3/day	E= 3.626; RMS = 5.059; σ = 5.064
	$2.3x10^{-3}$	-31974 m^3/day	E= 3.618; RMS = 5.017; σ = 5.022
	$2.5x10^{-3}$	-77288 m^3/day	E =3.632; RMS = 5.0496; σ = 5.047
	$3x10^{-3}$	-31918 m^3/day	E= 3.653; RMS = 5.130; σ = 5.135
	$3.3x10^{-3}$	-46565 m^3/day	E= 3.715; RMS = 5.357; σ = 5.362
0.365	$2.28x10^{-3}$	-31842 m^3/day	E= 3.684; RMS = 5.2709; σ = 5.276
	$3.3x10^{-3}$	-53443 m^3/day	E = 3.72; RMS = 5.476; σ = 5.48

6.1.2.1   1-year drought scenario

Figure 6.38, Figure 6.39 and Figure 6.40 show heads surfaces for Slices 1, 7 and 18 respectively. Figure 6.41, Figure 6.42 and Figure 6.43 show the difference between historical period (1979-2009) heads and 1 year drought heads' scenario for Slice 1, Slice 7 and Slice 18, respectively.

Slice 1 shows a general small head drawdown, lying between <0.5 m to 1 m, for most part of the model, while drawdowns up to 5 m occur in areas with sharp conductivity gradients (Figure 6.41).Head

drawdowns also occur in **Slice 7** and **Slice 18,** ranging between 0.5 and 1 m in Slice 7 for most of the model area (Figure 6.42) and between 0 m to 0.5 m for most part of the model for Slice 18 (Figure 6.43). In Slice 18, the 1 m head drawdown areas are strongly reduced at Left Margin. Anomalous head rise areas (light blue) occur in Slice 7 (Figure 6.42) and residually in Slice 18, which are probably due to the influence of error_norm_flow zones occurring nearby.

Figure 6.38 – Heads surface for alluvial aquifer and topmost Pliocene + Miocene water bearing units (Slice 1) under 1 year 2005 drought scenario

Figure 6.39 – Heads surface for Pliocene formations and topmost Miocene water bearing units (Slice 7) under 1 year 2005 drought scenario
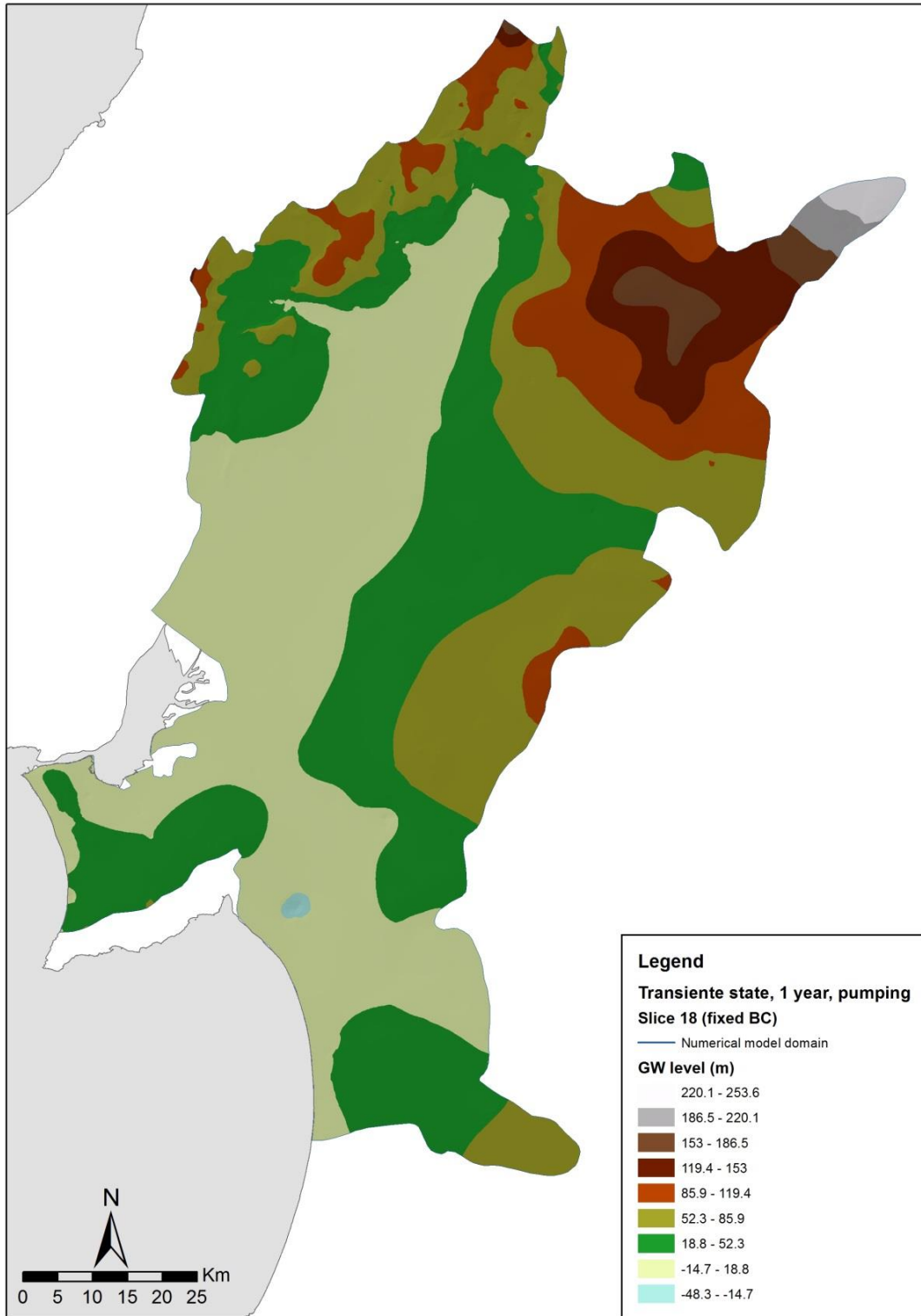
Figure 6.40 – Heads surface for Miocene formations (Slice 18) under 1 year 2005 drought scenario

Figure 6.41 – Head differences (annual mean values) between historical period (1979-2009) pumping conditions and 1 year drought scenario in Slice 1

Figure 6.42 – Head differences (annual mean values) between historical period (1979-2009) pumping conditions and 1 year drought scenario in Slice 1
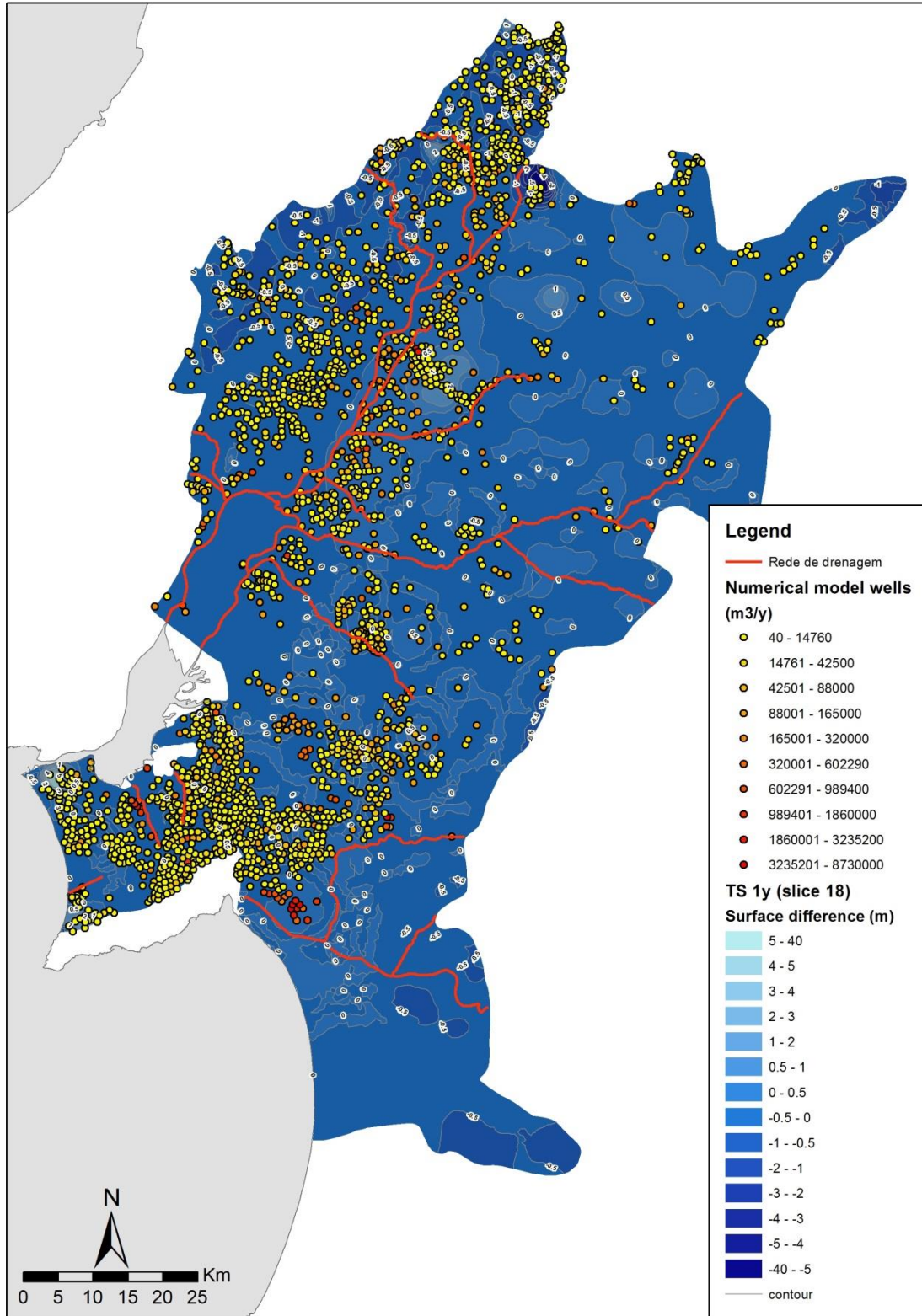
Figure 6.43 – Head differences (annual mean values) between historical period (1979-2009) pumping conditions and 1 year drought scenario in Slice 1

6.1.2.2   3-years drought scenario

Figure 6.44, Figure 6.45 and Figure 6.46 show heads surfaces for Slices 1, 7 and 18 respectively. Figure 6.47, Figure 6.48 and Figure 6.49 show the difference between historical period heads and 3 year drought heads' scenario, for Slice 1, Slice 7 and Slice 18, respectively.

Head drawdowns are larger than for 1 year drought scenario, as is to be expected. In **Slice 1**, drawdowns range from 1 to 2 m for large part of the model (Figure 6.47). 3 to 5 m drawdowns typically occur in areas with sharp conductivity gradients or important abstractions. Drawdown areas of < 0.5 to 1 m are strongly reduced from the 1 year drought scenario (Figure 6.47 vs. Figure 6.41).

In **Slice 7** (Figure 6.48) drawdown > 1 m areas show a strong increase from the 1 year drought scenario and this is done at the expense of the lower drawdown areas (Figure 6.48 vs. Figure 6.42). The difference is especially relevant on the SE tip of the model. As in 1 year drought scenario, anomalous heads rise areas occur (light blue), which, due to its similar location with those of 1 year drought scenario, are assumed as due to the same reasons (ct. chapter 6.1.2.1).

In **Slice 18**, drawdowns between 0 and 0.5 m occur in most part of the model. 1 m (or larger) drawdown areas, although important, occur mainly in Right Margin and SE tip of the model (Figure 6.49). These drawdown > 1 m areas increased from those of 1 year drought scenario, (Figure 6.49 vs. Figure 6.43). As seen already for the 1 year drought scenario, drawdowns become smaller as slices get deeper, due to the same reasons explained in chapter 6.1.1.2.
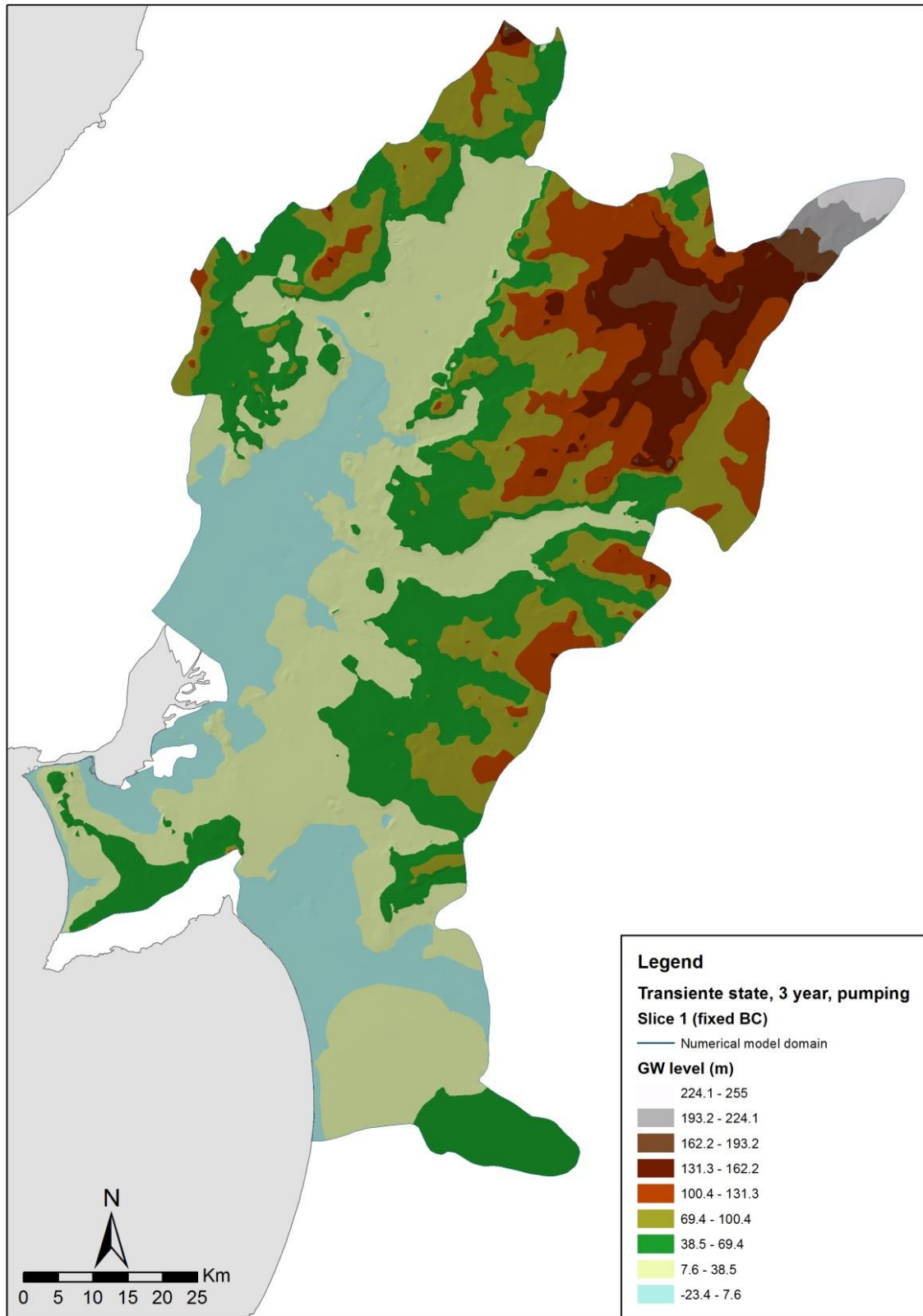
Figure 6.44 – Heads surface for alluvial aquifer and topmost Pliocene + Miocene water bearing units (Slice 1) under 3 years 2005 drought scenario

Legend

Transiente state, 3 year, pumping Slice 7 (fixed BC)
— Numerical model domain

GW level (m)
- 218.3 - 251.7
- 185 - 218.3
- 151.7 - 185
- 118.3 - 151.7
- 85 - 118.3
- 51.6 - 85
- 18.3 - 51.6
- -15.1 - 18.3
- -48.4 - -15.1
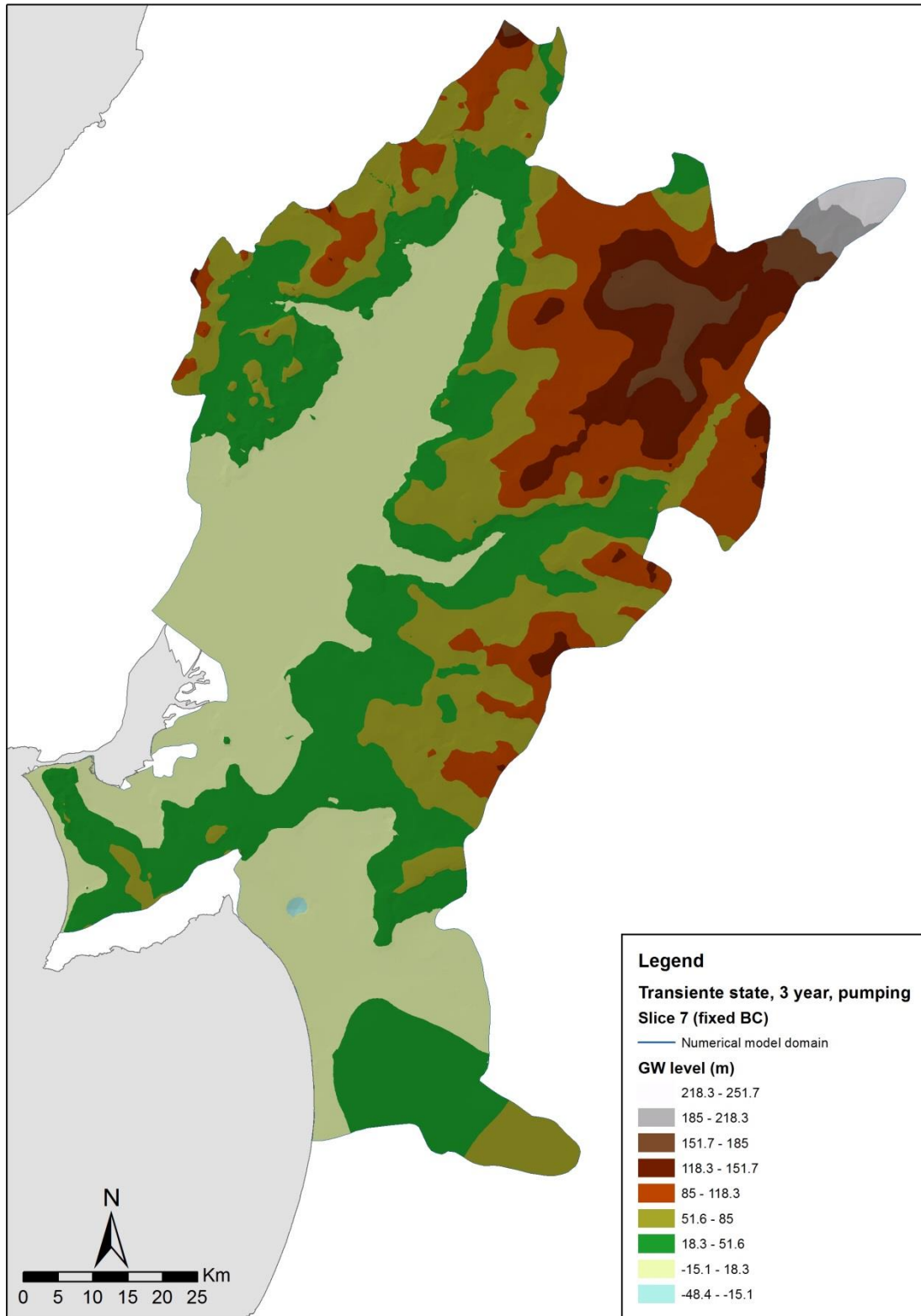
Figure 6.45 – Heads surface for Pliocene formations and topmost Miocene water bearing units (Slice 7) under 3 years 2005 drought scenario
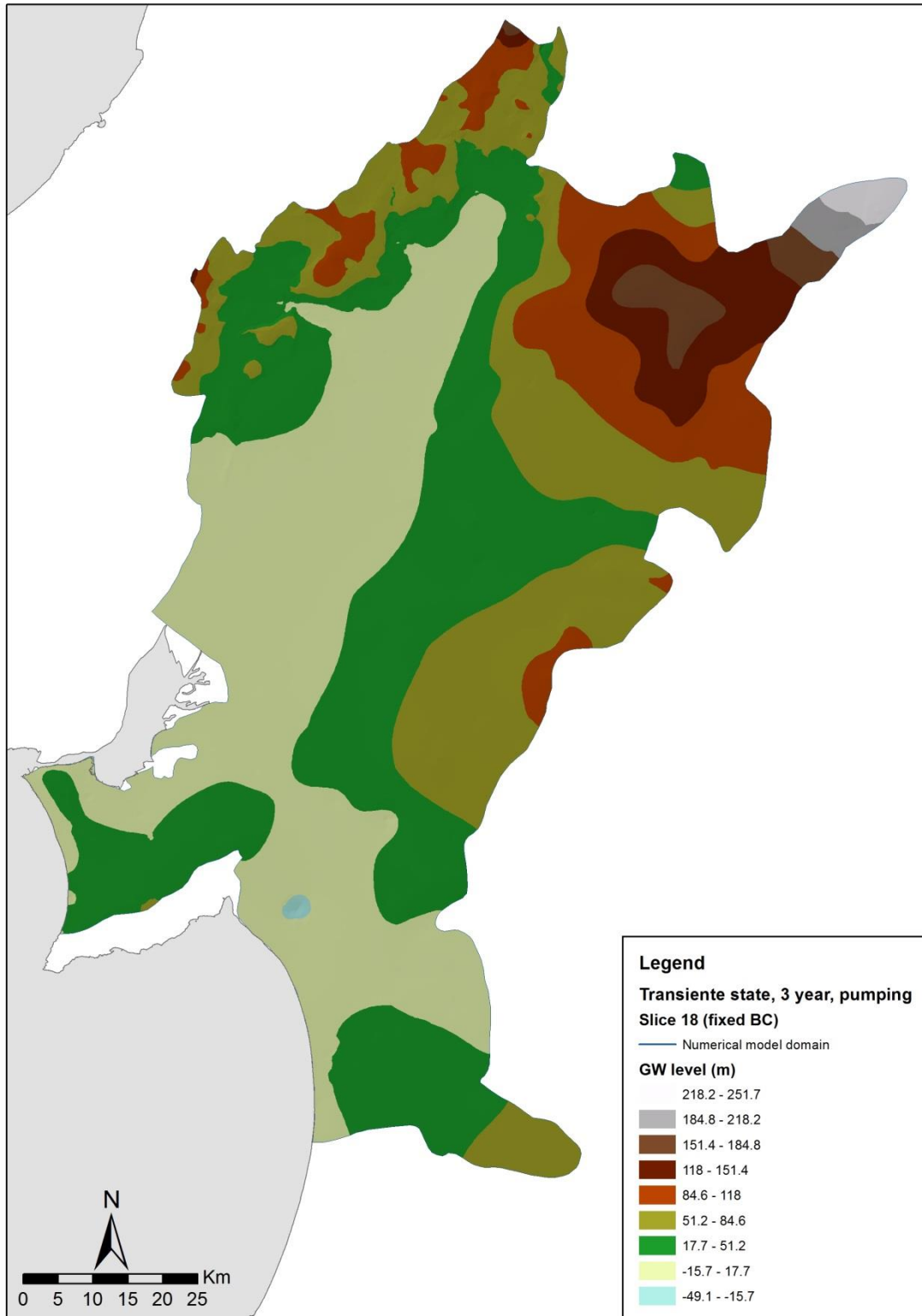
Figure 6.46 – Heads surface for Miocene formations (Slice 18) under 3 years 2005 drought scenario
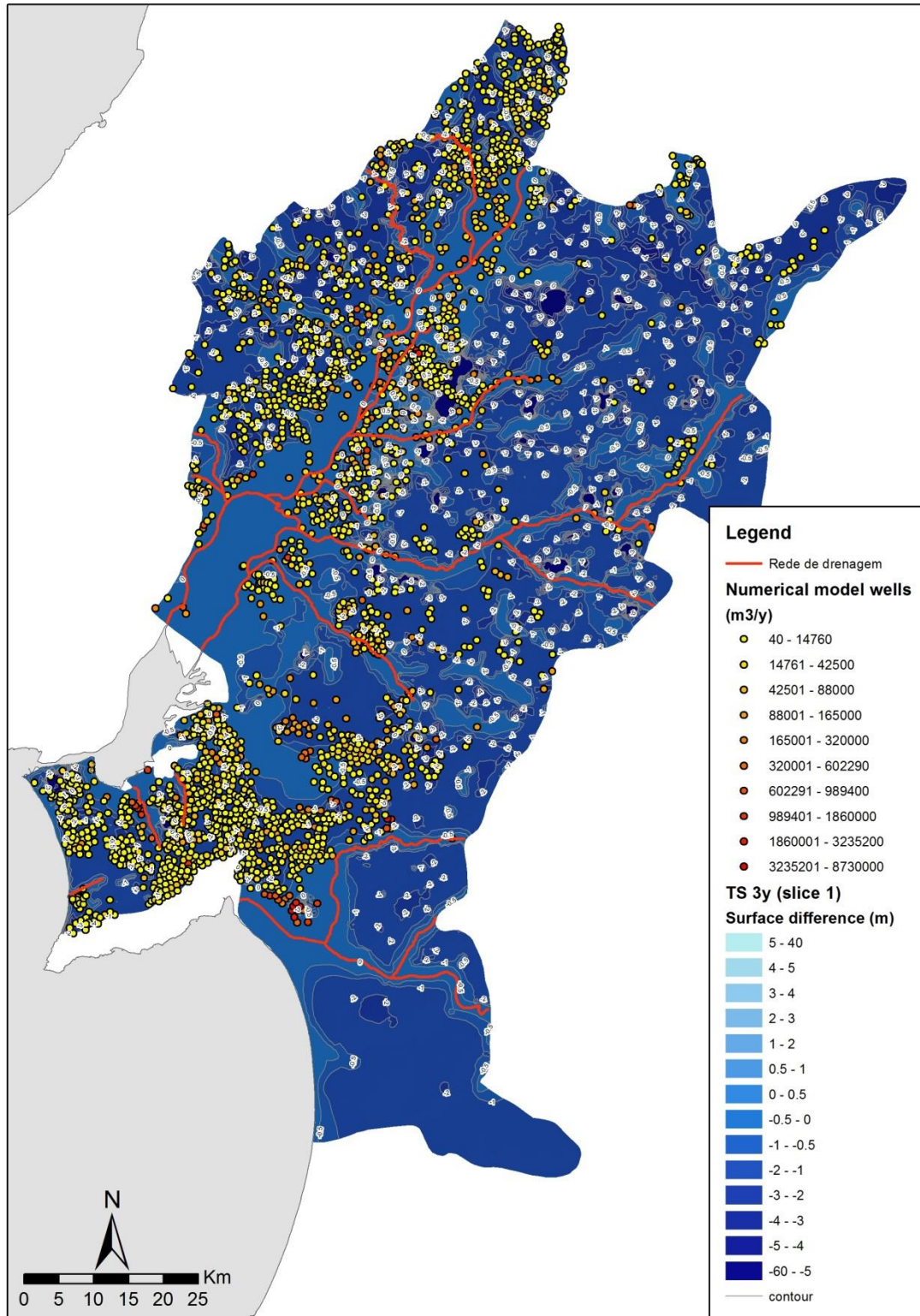
Figure 6.47 – Head differences (annual mean values) between the historical period (1979-2009) pumping conditions and 3 years drought scenario in Slice 1
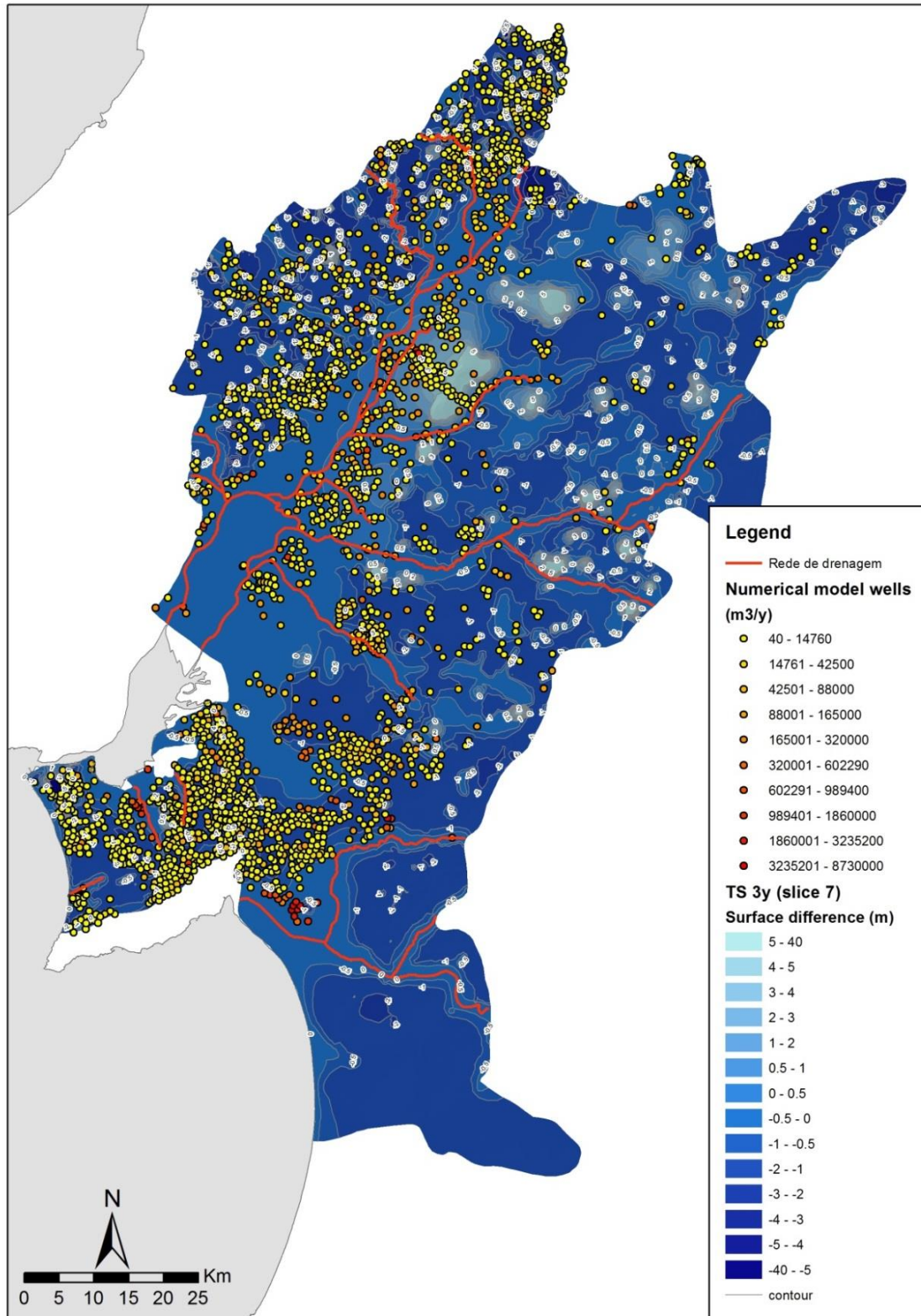
Figure 6.48 – Head differences (annual mean values) between the historical period (1979-2009) pumping conditions and 3 years drought scenario in Slice 7
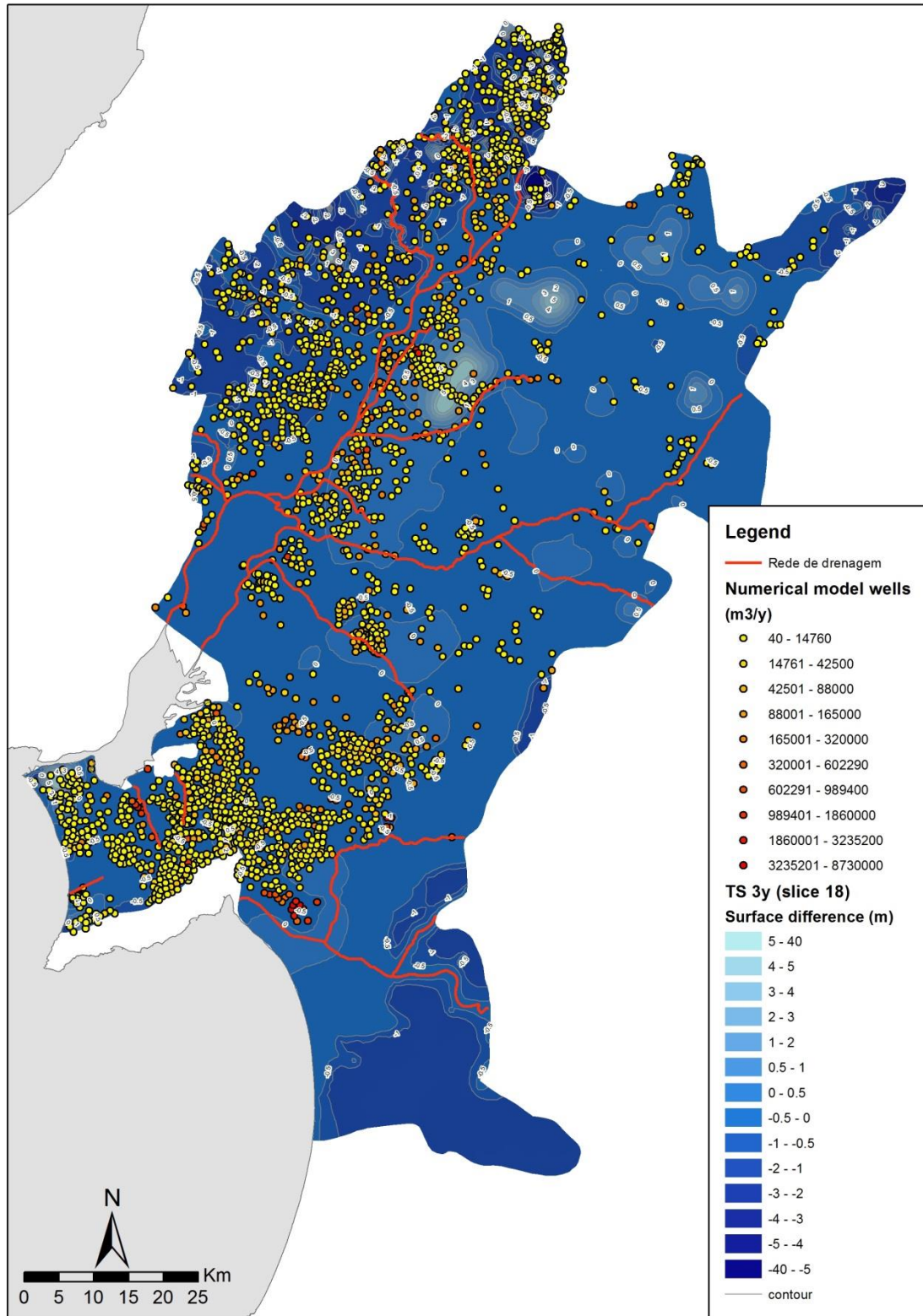
Figure 6.49 – Head differences (annual mean values) between the historical period (1979-2009) pumping conditions and 3 years drought scenario in Slice 18

6.1.2.3   5-years drought scenario

Figure 6.50, Figure 6.51 and Figure 6.52 show heads surfaces for Slices 1, 7 and 18 respectively. Figure 6.53, Figure 6.54 and Figure 6.55 show the difference between the historical period heads and this scenario's heads for Slice 1, Slice 7 and Slice 18, respectively.
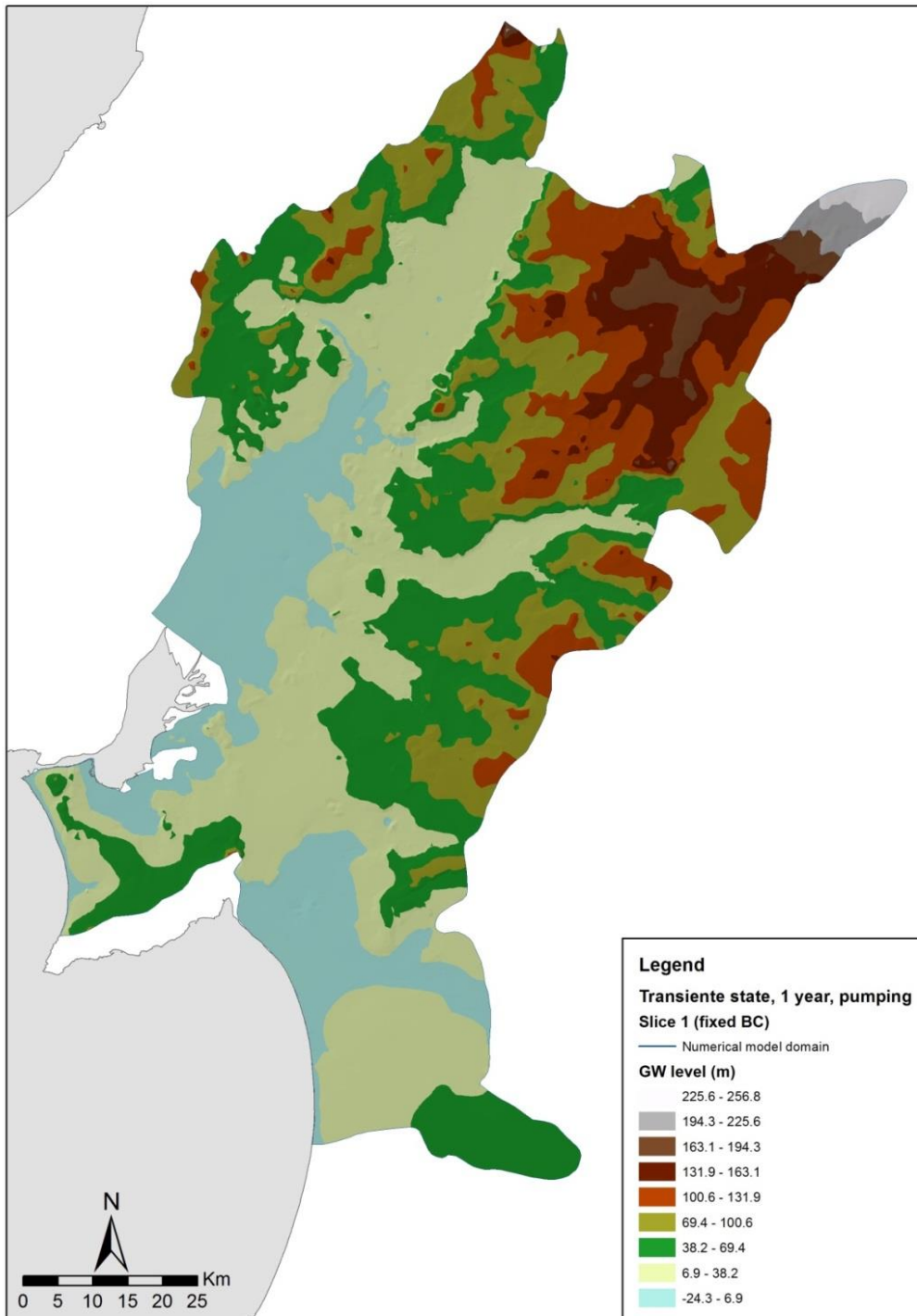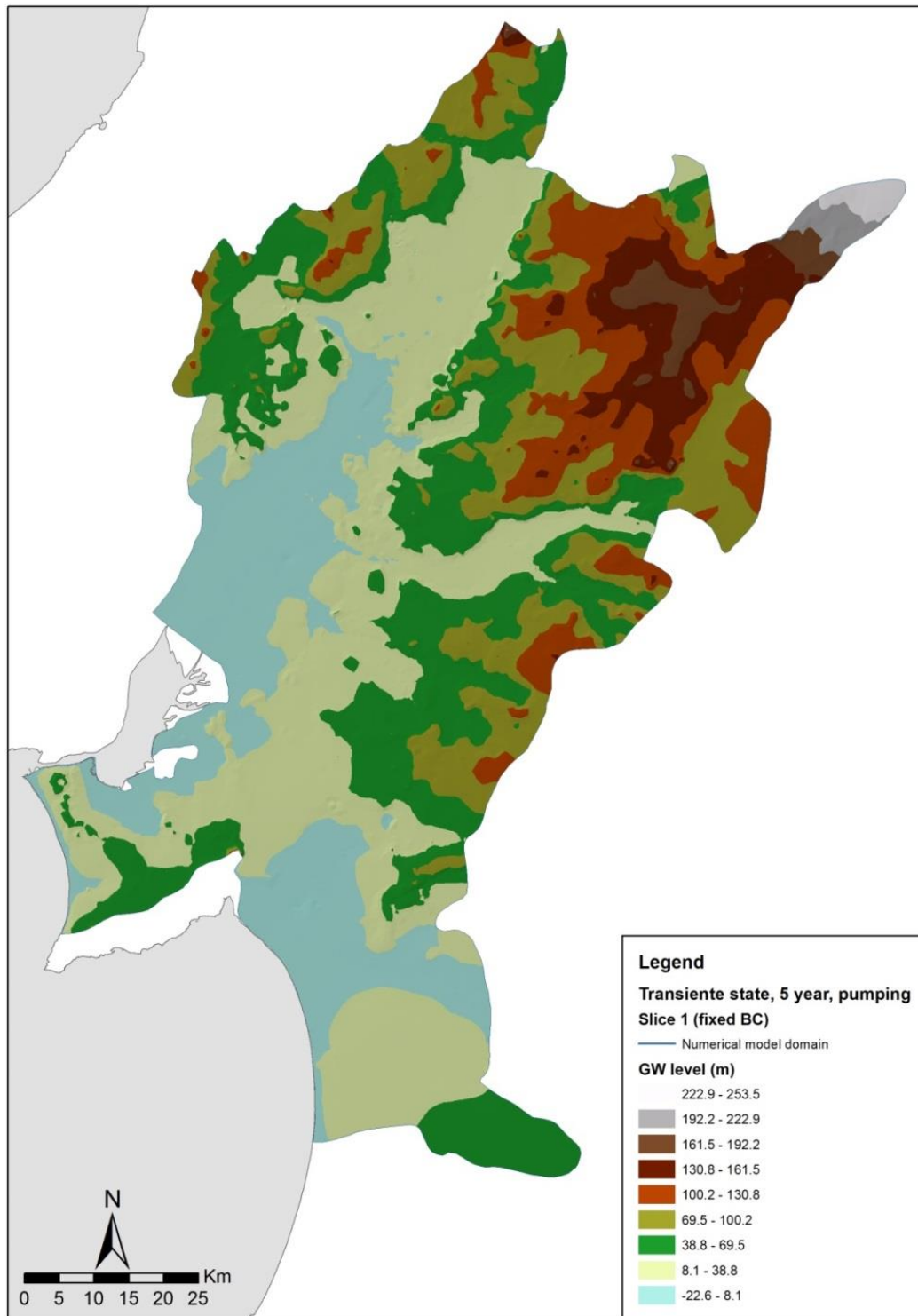

Figure 6.50 – Heads surface for alluvial aquifer and topmost Pliocene + Miocene water bearing units (Slice 1) under 5 years 2005 drought scenario
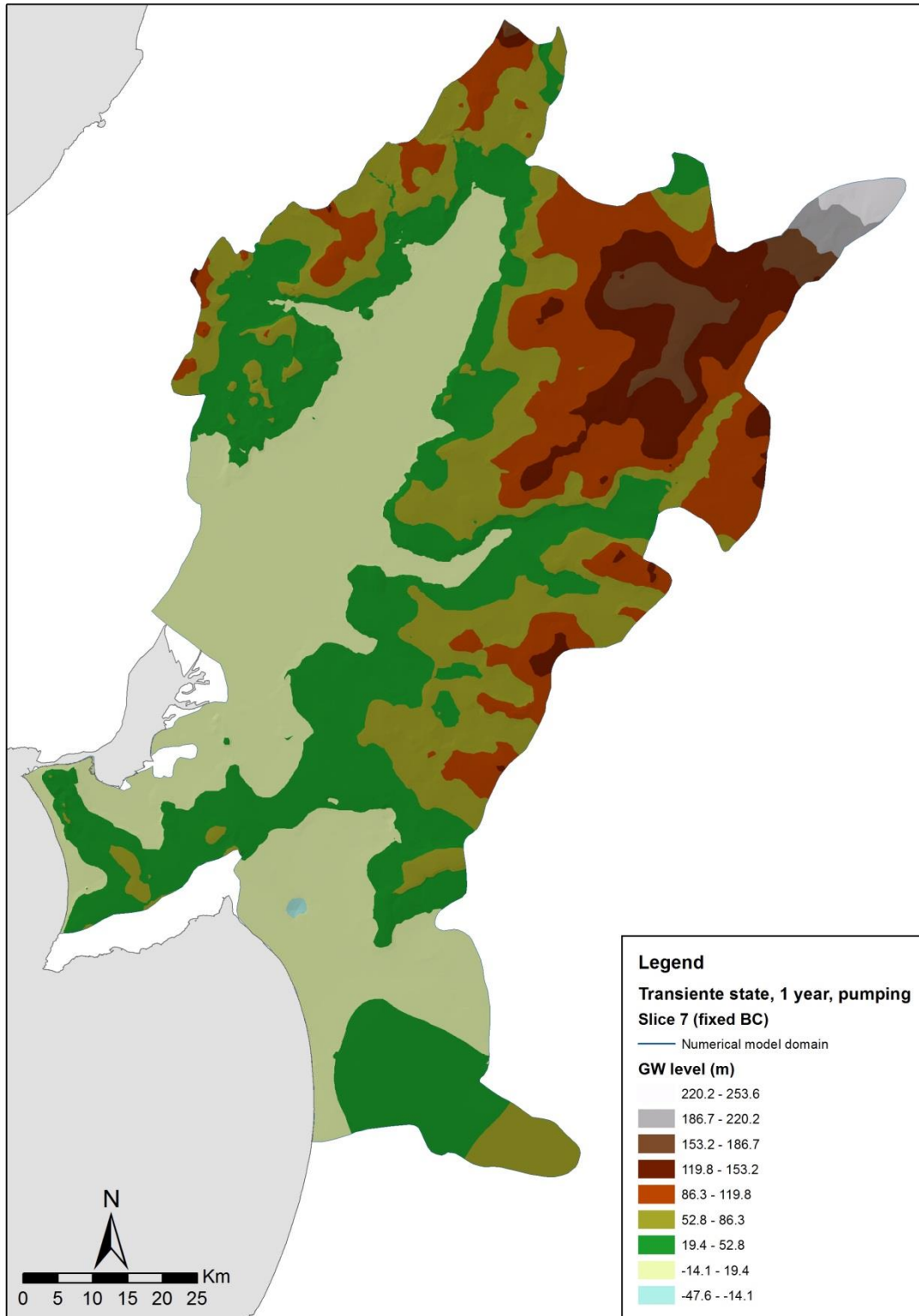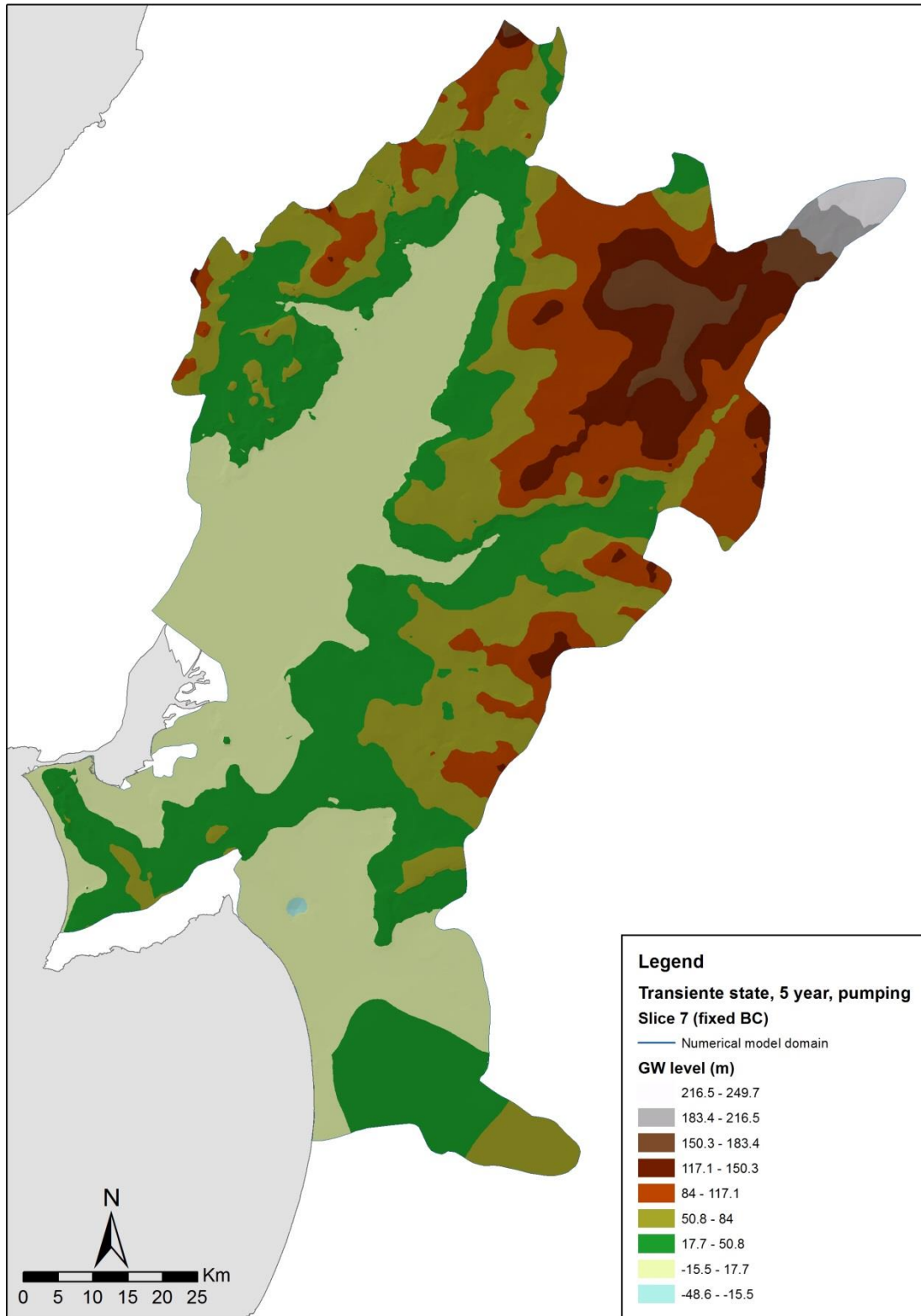
Figure 6.51 – Heads surface for Pliocene formations and topmost Miocene water bearing units (Slice 7) under 5 years 2005 drought scenario

Legend

Transiente state, 5 year, pumping Slice 18 (fixed BC)
—— Numerical model domain
GW level (m)
216.4 - 249.7
183.2 - 216.4
150 - 183.2
116.8 - 150
83.6 - 116.8
50.4 - 83.6
17.1 - 50.4
-16.1 - 17.1
-49.3 - -16.1
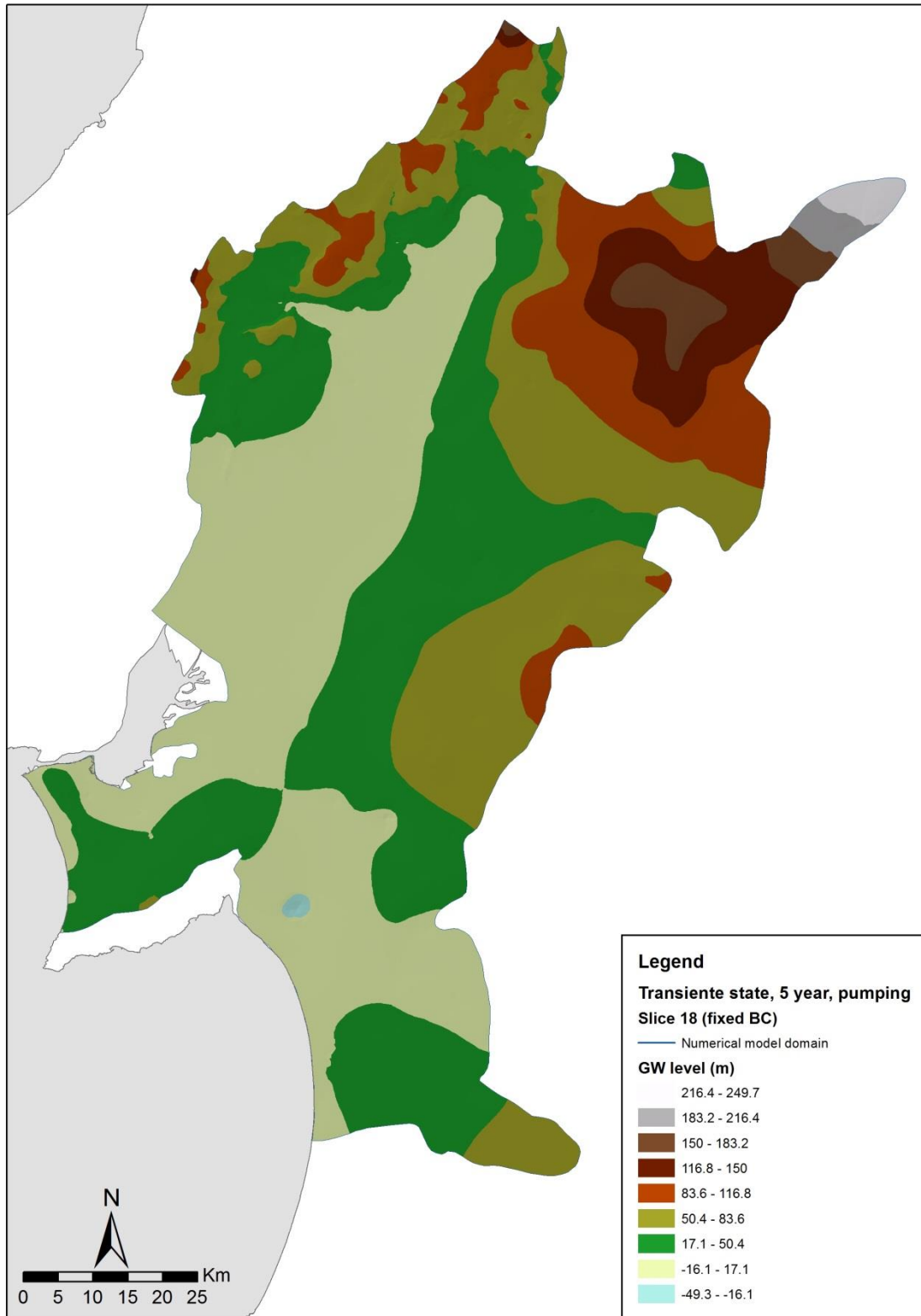
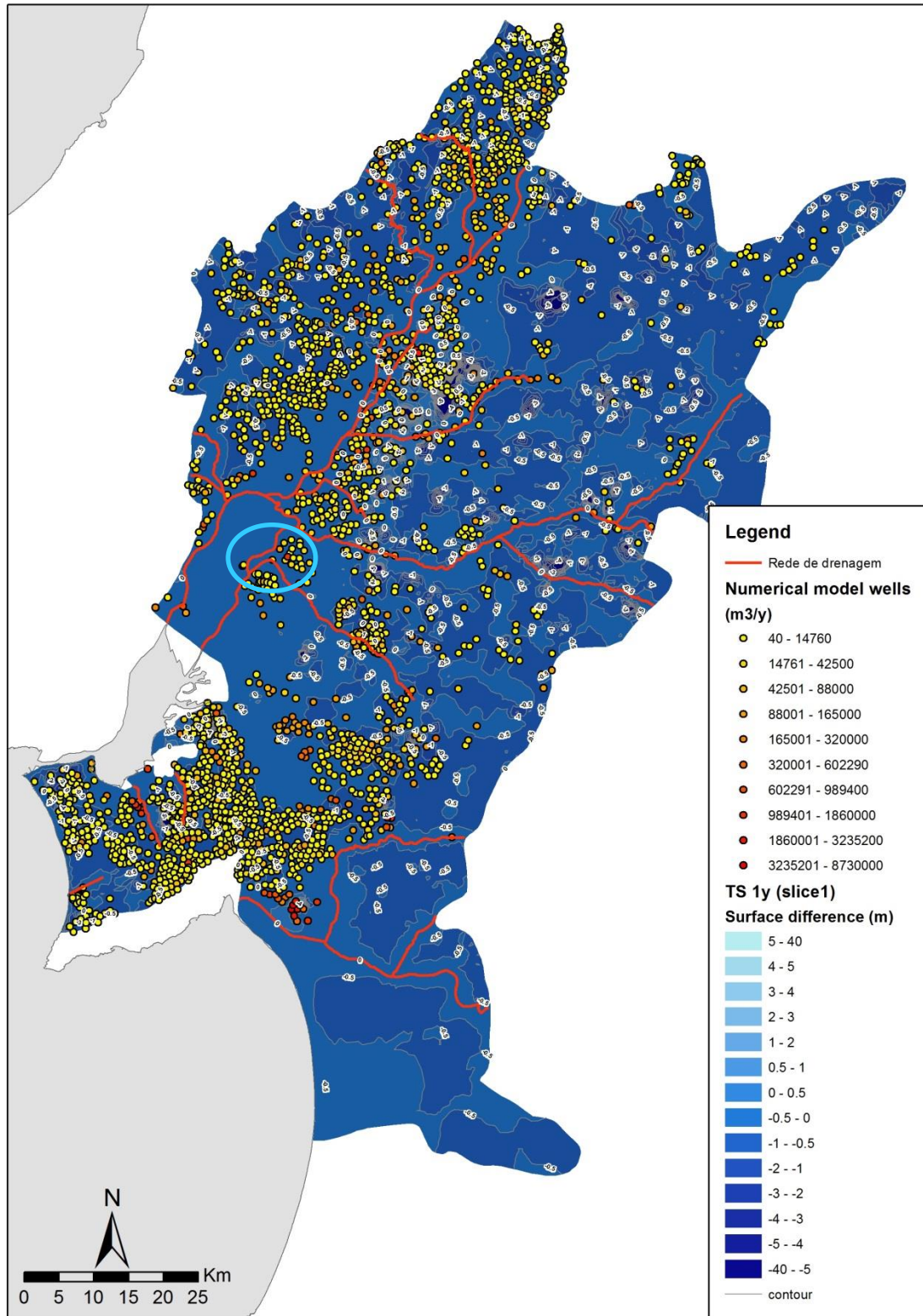**Figure 6.52 – Heads surface for Miocene formations (Slice 18) under 5 years 2005 drought scenario**
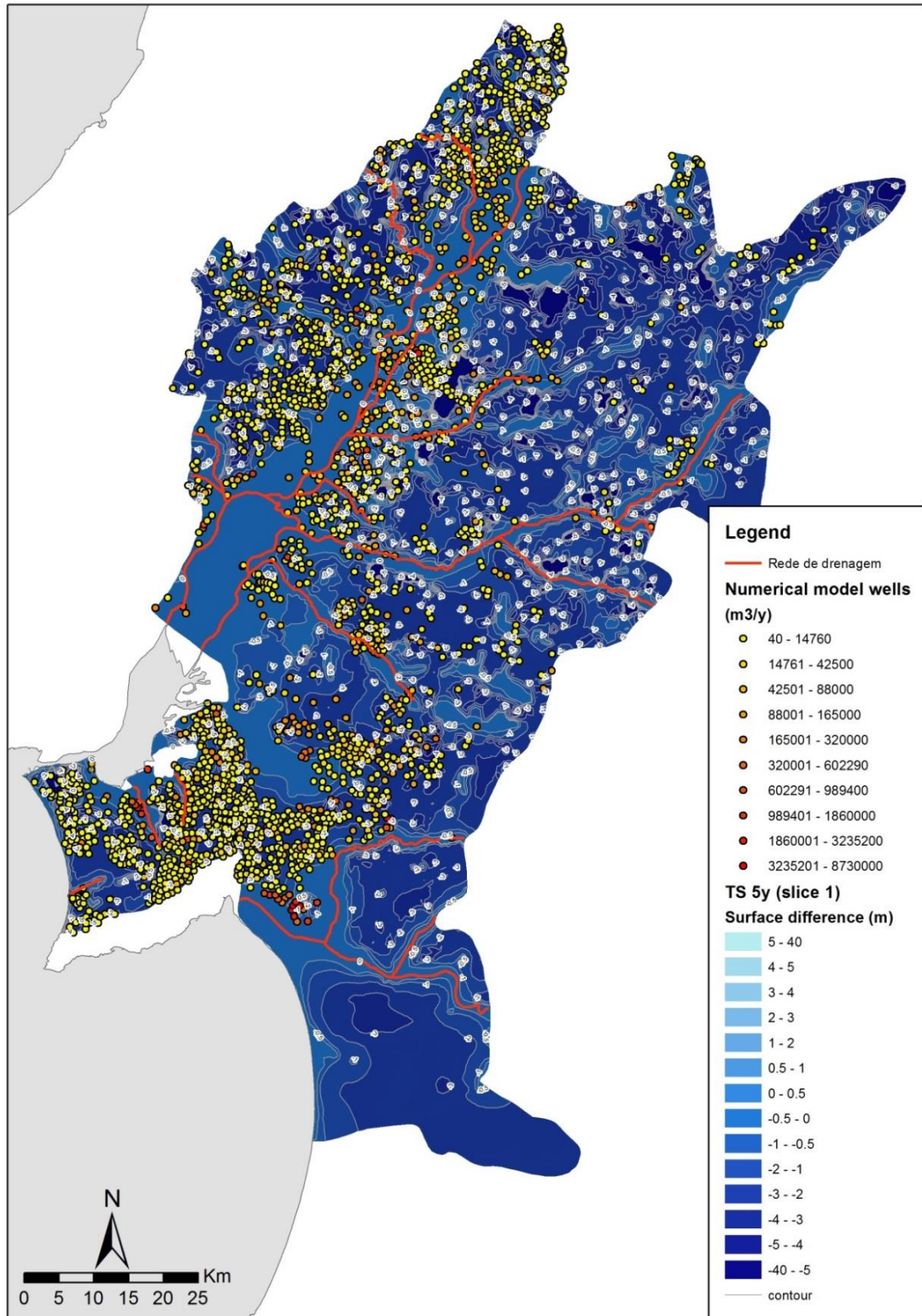
Figure 6.53 – Head differences (annual mean values) between historical period (1979-2009) pumping conditions and 5 years drought scenario in Slice 1
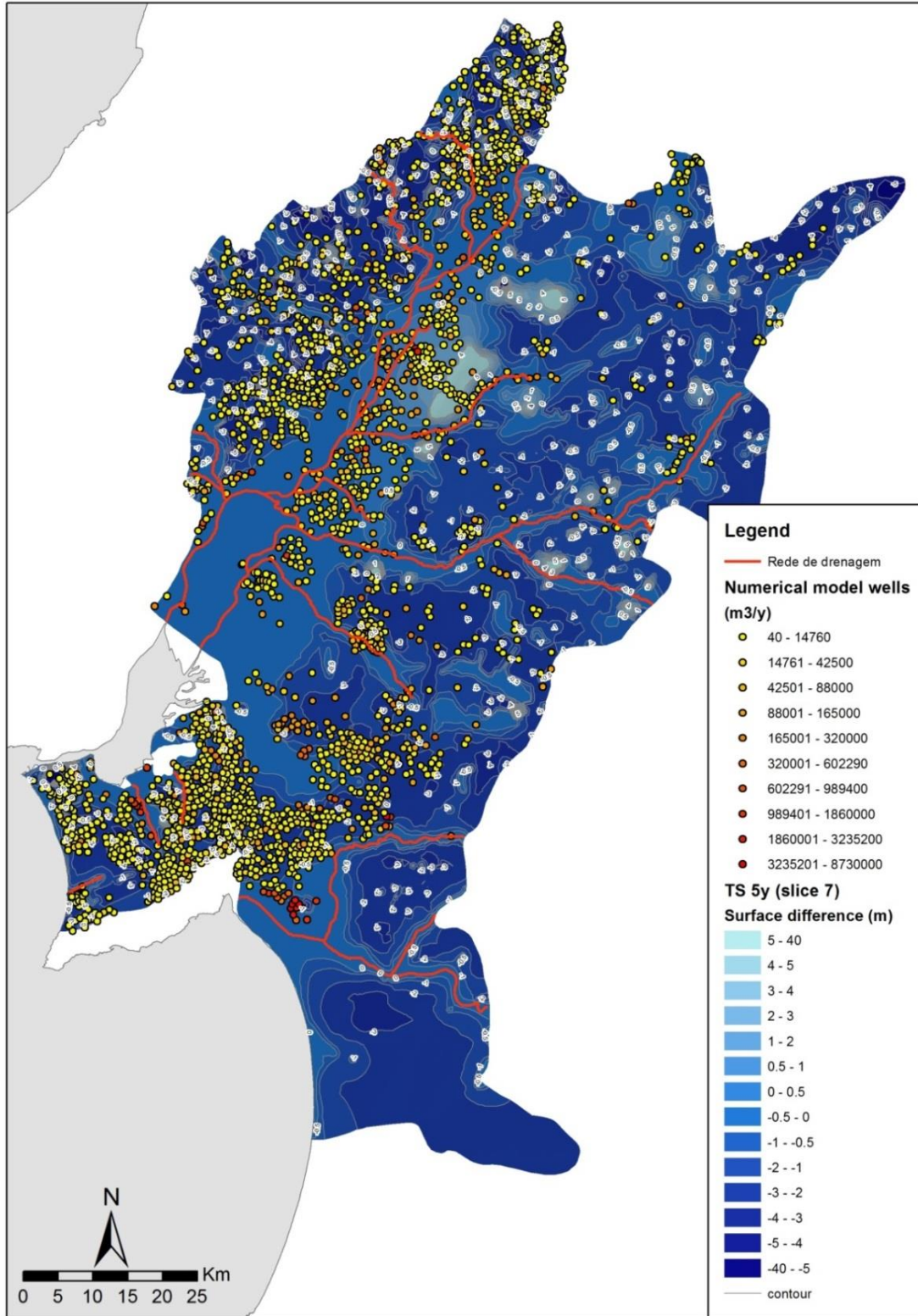
Figure 6.54 – Head differences (annual mean values) between historical period (1979-2009) pumping conditions and 5 years drought scenario in Slice 7
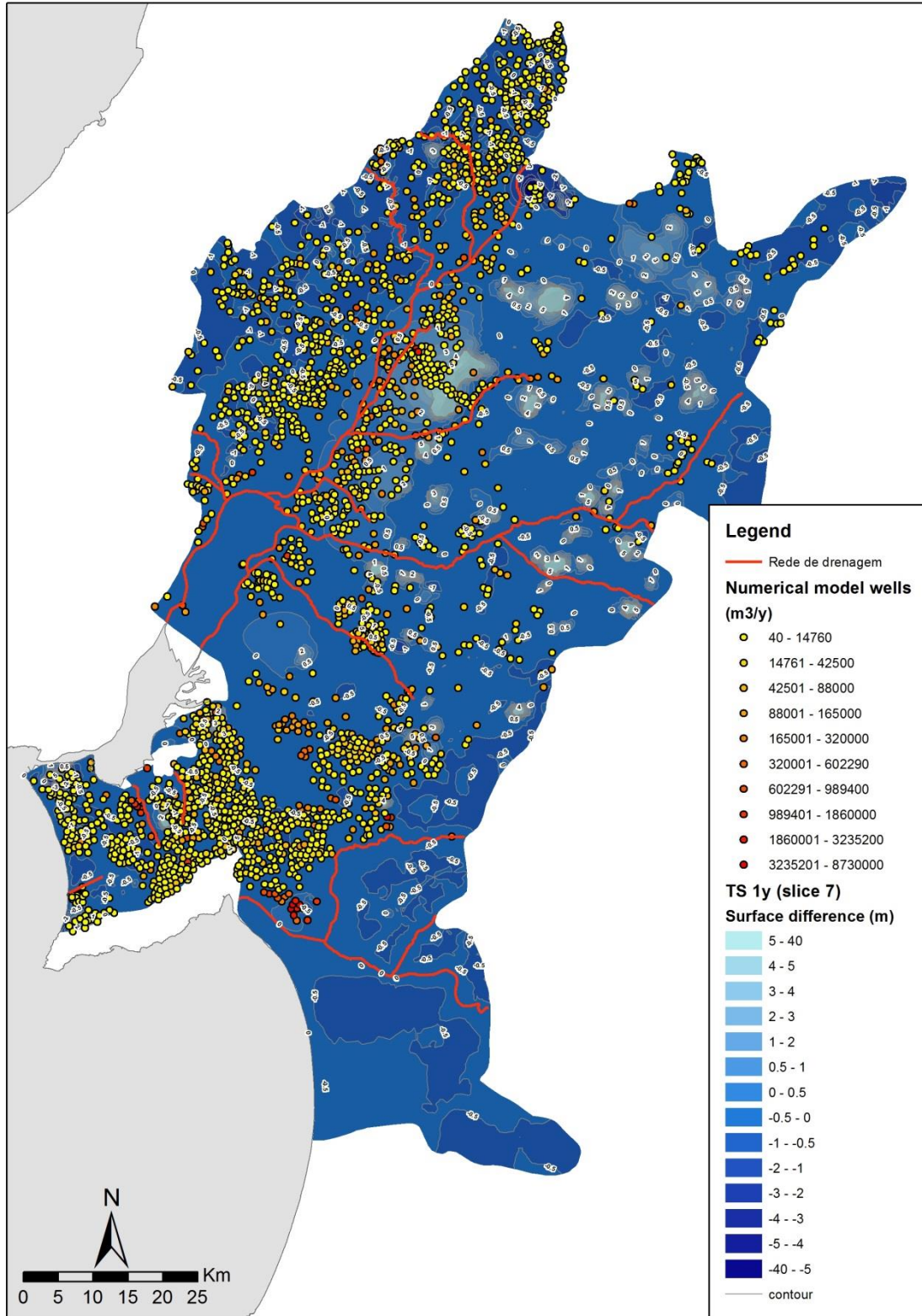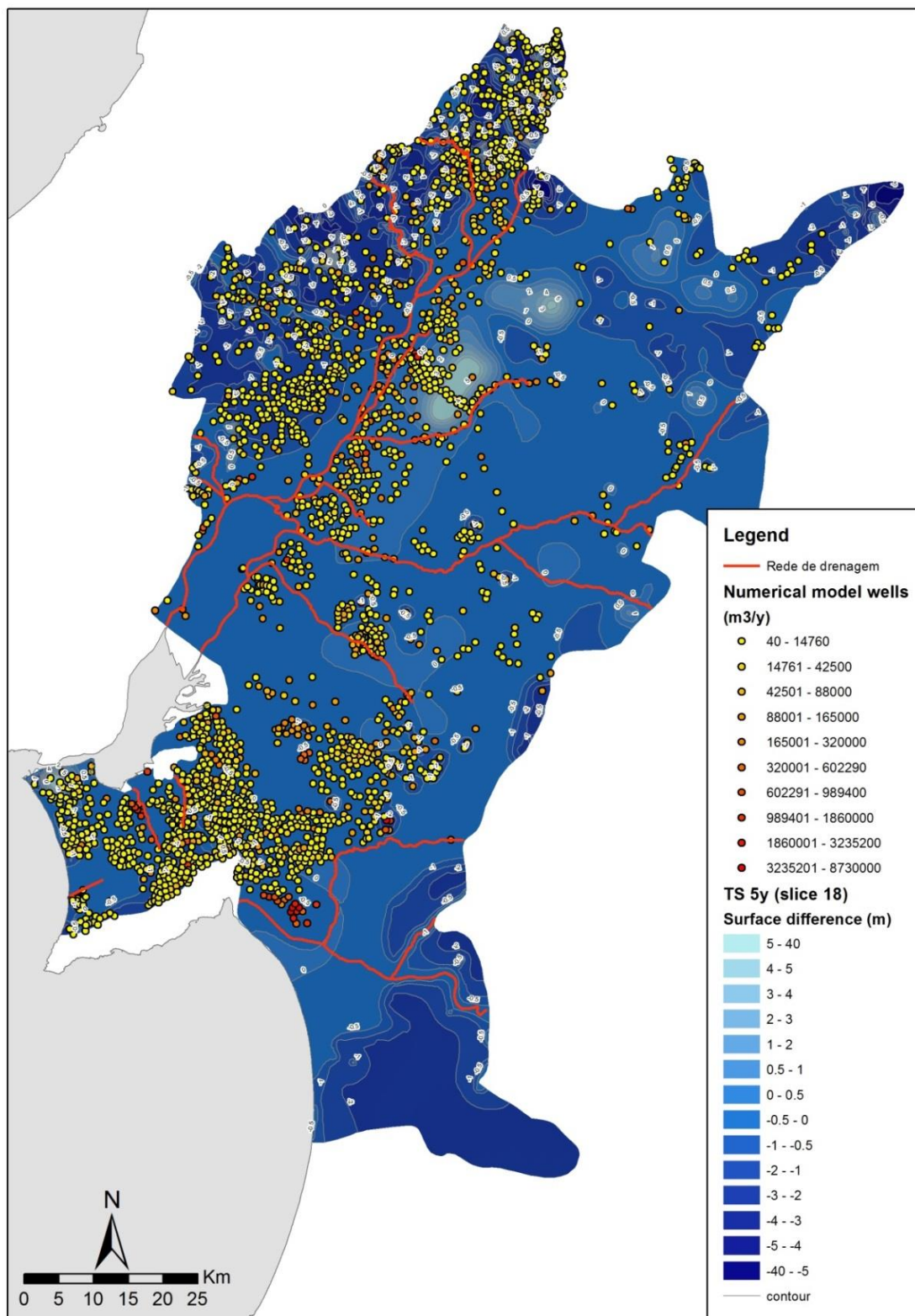
Figure 6.55 – Head differences (annual mean values) between historical period (1979-2009) pumping conditions and 5 years drought scenario in Slice 18

In **Slice 1**, 2 to > 3 m head drawdown areas have a large expansion, at expanse of 1 m drawdown areas of 3 year drought scenario (Figure 6.53 vs. Figure 6.47). The change is particularly striking in model's

SE zone (Figure 6.53). Areas with large conductivity gradients show drawdowns > 5 m (Figure 6.53 dark blue areas). The exception is Aluviões do Tejo and river valleys areas, where drawdowns remain < 0.5 m, most likely due to boundary conditions' influence.

In **Slice 7** (Figure 6.54), head drawdowns are smaller than for Slice 1, suggesting a shielding effect from natural water losses. For instance, a sharp reduction of > 5 m drawdown areas is observed when compared with Slice 1 (Figure 6.54 vs. Figure 6.53). When comparing with 3 year drought scenario, a sharp increase in ≥ 2 m drawdown areas is observed, being very relevant in the model's SE tip (Figure 6.54 vs. Figure 6.48).

In **Slice 18**, drawdowns are between 0 and 0.5 m in most part of the model (Figure 6.55). A large 0.5 to 1 m drawdown area's increase from the 3 years drought scenario, mainly in SE tip of the model, is observed. 2 m drawdown areas show up, unlike what happened in previous drought scenarios (Figure 6.55 vs. Figure 6.49 and Figure 6.43).

6.2   Transport model – Saltwater intrusion

Saltwater intrusion occurs at the coastal areas under natural conditions but becomes relevant under aquifer exploitation. The seawater/groundwater interface might be located at the coastal line, a bit inland from it or in the sub-tidal zone if there are coastal or submarine groundwater discharges. This location is controlled by the difference between groundwater heads and sea level. When aquifers are over-exploited, this interface moves significantly inland and it is this process that usually is labelled as saltwater intrusion (Figure 6.56).
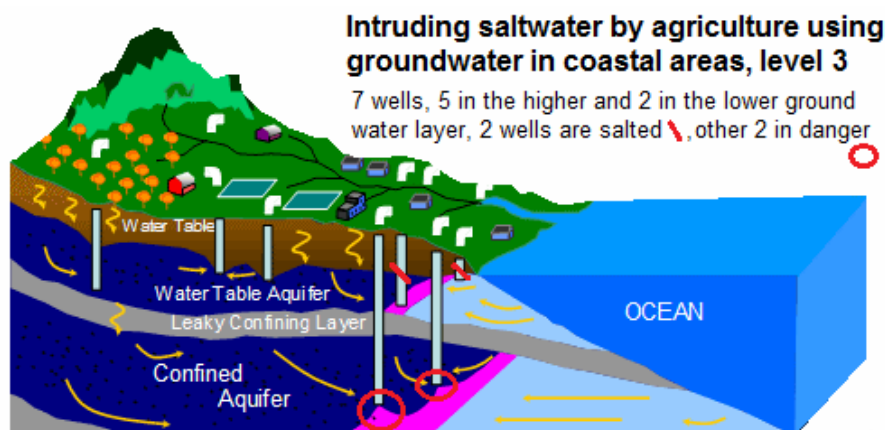
Figure 6.56 – Saltwater intrusion in a multilayer aquifer, due to saltwater/groundwater interface's inland progression and upwelling of this interface (red circles) bellow exploitation wells

Source: http://www.geschichteinchronologie.com/welt/wasser-u-grundwasser03-groundwater-salinization-ENGL.html

Saltwater intrusion is then mainly a water management issue controlled by:

- ▪ **Sea level and groundwater heads difference** at sea/aquifer interface. Heads are strongly influenced by *recharge* and *water abstraction* while sea level is controlled by *tectonic activity* and *sea level rise*.

▪ **Characteristics of the aquifers**, such as conductivity, layering, thickness and topography.

Under climate change, saltwater intrusion will be affected not only by the expected increase of water abstraction to supply demand, but by all the following processes:

- **Recharge changes**, due to precipitation/runoff regimes and land cover changes. Leads to head changes and consequently influences seawater/groundwater interface's location.
- **Sea level changes**, due to polar caps and glaciers' melting coupled with oceans' thermal expansion and, at regional/local level, subsidence (often due to aquifer over-exploitation and/or isostatic movements) or tectonic movements. Seawater/groundwater interface is driven inland if sea level rises but its advance is controlled by aquifer's conductivity and structural characteristics (homogeneous or multi-layer; coastal zone's low conductivity barriers, etc.). Most important, this advance increases if recharge decreases and/or over-exploitation occur. Besides sea level rise, other factors impact saltwater intrusion:
  - o **Coastal area topography**: low lying coastal areas, are at higher risk of submersion, which will further increase seawater/ groundwater interface inland encroachment (Figure 6.57). If the area is also suffering subsidence, this encroachment becomes even larger.
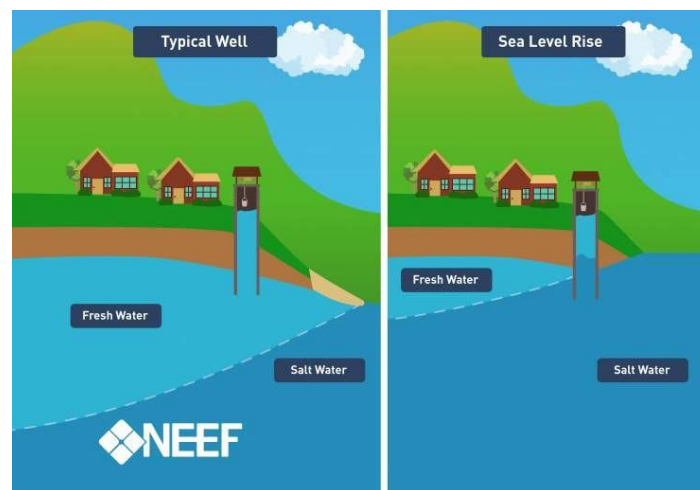
Figure 6.57 – Saltwater intrusion advance inland under sea level rise

Adapted from: https://blogs.egu.eu/network/gfgd/tag/saltwater-intrusion/

  - o **Salinity changes on transition environments**: the salinity distribution in an estuary can change due to sea-level rise induced water currents shifts. If a river flow reduction also occurs due to precipitation changes, estuarine waters can reach farther upstream more permanently, leading to an upstream advance of the "seawater"[13]/groundwater interface.

---

[13] Estuarine water, in this case.

- **Abstraction changes:** influenced by socio-economic development but also by adaptation practices and new water demands due to climate change (e.g. increased irrigation needs).

To develop the saltwater intrusion model, the above-cited processes under the climate/recharge scenarios R1, R3 and R1_10[14] would be defined as:

1. **Recharge** – recharges obtained for MiKlip realisations R1, R3 and R1_10. The benchmark recharge is that of the historical period (1979-2009).
2. **Sea level changes** – between 2000 e 2022 sea-level rise was estimated between 8.8 and 11 cm[15] (Taborda et al., 2009; Fortunato et al., 2018). So, for 2015-2024, sea level rise is estimated at 4 to 5 cm. As such, present day sea level + 5 cm is assumed as the new sea level in saltwater intrusion simulations.
3. **Land lost to the sea** – once the ocean rise is quite small (5 cm), the amount of land lost to the sea in 2024, is assumed negligible. Present-day shoreline is then unchanged for 2024.
4. **Salinity changes** – these are dependent of both (1) sea level rise and (2) Tagus flow changes due to precipitation and groundwater discharges changes. A Tagus' lower flow regime allows an upstream advance of brackish estuarine water. This will push the saltwater/groundwater interface upstream along the river margins. An illustration of the interplay between Tagus flows and upstream advance of estuarine waters is shown in Figure 6.58 for distinct drought events under present-day climate conditions. Similar salinity distributions for R1, R3 and R1-10 scenarios should be used to analyse saltwater intrusion associated with those scenarios.
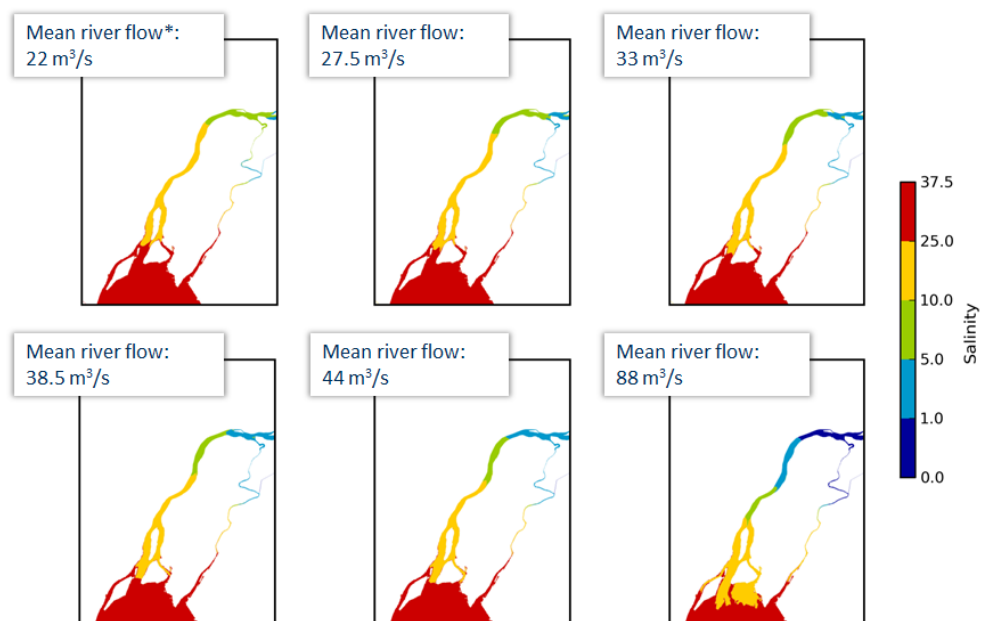
Figure 6.58 – Salinity distributions in Tagus estuary for present day distinct river flow conditions

Source: Fortunato et al. (2018)

---

[14] High, low and ensembles scenarios respectively.

[15] A sea level rise of 4 mm/year is observed from Cascais gauge station's data.

5. **Water abstraction changes** – abstraction rates are the main driver of saltwater intrusion. They change due to socio-economic evolution and new water demands due to climate change and climate change adaptation policies. Water demands up to 2024 are not expected to increase once the most likely climate outcome (ensembles scenario) will be similar to today's climate, meaning similar water demands. Water demands' changes due to socio-economic evolution are also not expected to change significantly (cf. Iacovides et al., 2016) in agriculture and forestry. Tagus Watershed Management Plan (APA, 2011) socio-economic scenarios also suggest a demographic stabilization and minor changes in agriculture and industry. Due to this, water abstractions are assumed as similar to those of present-day.

The saltwater intrusion model was not developed due to lack of salinity data in the aquifers surrounding the estuary, including temporal salinity series, and the mismatch between aquifers' official limits set by Almeida et al. (2000) and the real Tagus estuary's coastline (Figure 6.59; cf. chapter 5.5). From the aquifer's definition – which implies a potential for economic exploitation – the limits set by Almeida et al. (2000) are correct, once they exclude areas of swampy low permeability zones. However, in depth, those low permeability deposits do not exist and the lower aquifer units may be connected with the estuary and ensuing effects of an increased saltwater column due to sea-level rise, which promotes saltwater intrusion in those units (cf. Figure 6.56). These excluded areas are then important to simulate saltwater intrusion but the complete lack of information (groundwater levels, hydraulic properties) for the units immediately below these marshy deposits hinders any saltwater modelling attempt. It is hoped that this issue can be further investigated in future projects.

Although saltwater intrusion is a transient problem, the lack of temporal data could be overcome by simulating the initial state of the system (= the historical period saltwater intrusion) and the final state (saltwater intrusion in 2025) for each of the recharge scenarios presented in chapter 6 |. Comparing the chlorides spatial distribution between the historical conditions and those of each climate scenario in 2024 would give the saltwater intrusion evolution for each of these scenarios.
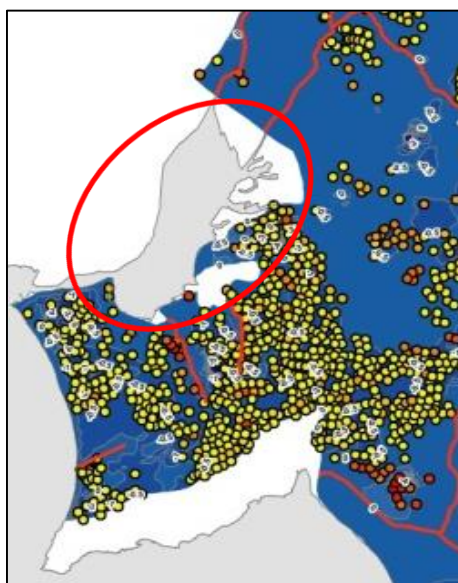
Figure 6.59 – Differences between estuarine coastline and aquifer limits (white area inside red circle)

6.3   Results' discussion

Climate change impacts analysis for the period 20115-2024 was performed for steady state and transient conditions. **Steady state conditions** were applied to a "permanent" drought scenario (year 2005's recharge conditions) and 3 MiKlip climate realisations (cf. Rust et al., 2017). The **semi-transient conditions** simulated the impacts of 1, 3 and 5 years-long droughts with 2005 recharge conditions. The 3 MiKlip scenarios, chosen to encompass the whole spectrum of climate/recharge variations of the 10 MiKlip realisations, were:

- *Lowest recharge scenario* (stems from realisation R3),
- *Highest recharge scenario* (stems from realisation R1)
- *Average recharge scenario* (stems from ensembles of the 10 climate realisations R1_R10).

The steady state *permanent drought scenario* is a threshold scenario, where climate change would be so dramatic that the average climate would be a permanent severe drought.

Semi-transient scenarios for multi-annual severe droughts were also studied because some studies for Tagus basin suggest such extreme phenomena might be frequent by the end of the century (Guerreiro et al., 2017). However, and because climate change realisations for 2024 time horizon do not suggest such multi-year droughts will become more common (and in the last century 5-years droughts did not happen while 3-years droughts just happened once) they should be also viewed as threshold scenarios for the 2024 horizon.

6.3.1   Steady state results

Steady state simulations show water levels' evolution for average climate/recharge conditions. The evolution variations under different scenarios illustrates water levels' evolution uncertainty under climate change, providing and interval of possible water level's outcomes in the near future. Such evolution is obtained by comparing the climate change (and drought) scenarios' results with those of the historical period under pumping conditions.

In the *historical period*, changes between natural and pumping conditions were analysed to understand the impact of pumping activities. Those last bring about an expected water level's (= heads) decrease but this decrease is minor (drawdowns < 0.5 m) for Pliocene and Miocene aquifer units when compared with Alluvial unit (represented by Slices 1 to 3), as illustrated by Figure 6.10, Figure 6.11, Figure 6.12). As such, pumping impacted the artesian relationships between these units and potential circulation inversions between these 3 units may occur in some areas of the model, in agreement with the reality. In Peninsula de Setúbal, however, Miocene water levels drawdowns can be important, which is probably due to the significant abstraction rates occurring there. As such the model adequately simulates, in general, the impacts of water abstractions throughout the aquifers.

Nevertheless, there are some areas were the model is less sensitive to pumping than it should be, as is the case of its central area between the 2 head constant boundary conditions simulating rivers (cf. Figure 5.4, red circle), where drawdowns remain almost null. This is a consequence of the boundary condition type used to simulate rivers, the choice of which was explained in sub-chapter 5.3.5. So, in spite of

being well calibrated overall, the model is probably not adequately simulating Alluvial aquifer's responses to recharge/abstraction rates' changes. If better data on river stages will be provided, then the model can be improved and better simulate what happens in this area.

In **climate change scenarios**, water levels' evolution is due to recharge modifications (cf. Table 6.4 under **Δ RAQ**[16]; Oliveira, 2019). Recharge variations between present day conditions and recharge scenarios, although being quite large for some of these scenarios, are translated into relatively attenuated water levels' changes (Table 6.4). This is partly due to the large aquifer system's dimensions and its ensuing high inertial response. For large head changes to occur with wide spatial significance, recharge should shift dramatically as in permanent drought scenario (Table 6.4). The occurrence likelihood of these scenarios in 2024 is given in Table 6.5.

Table 6.4 – Recharge and water levels' variation from present day conditions in Slice 1 (steady state)

Aquifer	High recharge scenario		Low recharge scenario		Ensemble of realisations scenario	
	Δ RAQ	*Δ water levels*	*Δ RAQ*	*Δ water levels*	*Δ RAQ*	*Δ water levels*
Aluviões do Tejo	29.39%	0.5 to 2 m	-11.62%	-0.5 m	0.19%	0 m
Margem Direita	49.07%	0.5 to > 10 m	-10.40%	-0.5 to -5 m	5.36%	≈ 0 m

Aquifer	Permanent drought scenario	
	Δ RAQ	*Δ water levels*
Aluviões do Tejo	-74.01%	≤ -20 m
Margem Esquerda	-86.38%	≤ -20 m to > -60 m
Margem Direita	-77.08%	≤ -20 m to > - 40 m

RAQ = recharge

For the ***ensemble of realisations (R1_R10) scenario***, and once recharge is similar to the historical period's recharge (cf. Table 6.2, chapter 6.1.1.3.2), water levels remain very similar to those of the historical period. This suggests that, if this scenario holds true in 2024, no significant water levels' changes are to be expected, at least if no significant abstraction increase occur.

In the ***high recharge scenario***, which shows a significant increase from present day recharge, a general water levels' rise occurs across the model, leading to flooding of several small depressed areas where strong topographic and conductivity gradients occur (cf. Figure 6.35). Such rises tend to be smaller and

---

[16] ΔRAQ = variação entre a recarga do período de referência e a recarga do cenário em análise.

smoother as the slices' depth increases. For instance, in **Slice 1**, water level rises lower than 2 m occur in the low lying areas (e.g. Aluviões do Tejo) but upstream they range from 5 to 10 m, with the areas of 10 m rise being quite significant (Figure 6.34). In **Slice 7**, this rise is from < 0.5 m up to 5 m (Figure 6.36) for most part of the model, with a sharp reduction of the 5 to 10 m rise areas. In **Slice 18**, 5 to 10 m heads rise areas are strongly reduced (Figure 6.37) when compared with slices above. The exceptions are NE and SE model borders, where fluid-flux boundary conditions were defined at Slice 1 and 2, which show no significant drawdown differences between slices.

Table 6.5 – Scenario occurrence likelihood for 2024

Scenario	Likelihood
High recharge	Likely
Ensembles recharge	Most likely
Low recharge	Likely
Permanent drought recharge	Extremely unlikely

For the ***low recharge scenario***, which has lower recharges than those of present day, flooded areas disappear and a general water levels' drawdown occurs across the model. Such drawdowns are smaller and smoother as slice depth increases. In **Slice 1**, drawdowns from 0.5 to 2 m occur across the model while 5 to > 10 m drawdowns occur in sharp conductivity and topographic gradients' areas (Figure 6.22). In **Slice 7**, > 5 m drawdown areas are strongly reduced from Slice 1, being located beneath the largest drawdown areas of that slice (Figure 6.23). In **Slice 18**, > 5 m drawdown areas are reduced when compared with the slices above (Figure 6.24).

The **permanent drought scenario** simulates a climate whose average conditions are those of a severe drought, which is translated by a 79% average recharge reduction[17] from the historical period. Due to such strong recharge reduction, a sharp water levels' drawdown occurs across the model. As in former scenarios, drawdowns are smaller as the slice depths increase. In **Slice 1,** up to 20 m drawdowns occur in the most part of the model and Alluvial deposits show drawdowns of 10 to 15 m, when in the other scenarios drawdowns were quite mild; areas of sharp conductivity gradients or fluid-flux boundary condition borders show > 40 m drawdowns (Figure 6.16). In **Slice 7**, the most important changes in comparison with Slice 1, is the large reduction of ≥ 60 m drawdown areas and the disappearance in Peninsula de Setubal of ≥ 40 m drawdown areas (Figure 6.17). In **Slice 18**, < 20 m drawdowns occur across the model, other larger drawdowns' areas are strongly reduced and ≥ 60 m drawdowns almost disappear (Figure 6.18).

---

[17] Such reduction corresponds to recharge conditions of year 2005, a real drought occurred during the time frame of the historical period

As seen from the above results, the model behaves as should be expected: when recharge increases, the water levels increase and when recharge decreases, the water levels decrease. However, water levels depend also on water abstraction rates and their respective changes under socio-economic and climate changes and these data are strongly lacking, particularly on what concerns climate change adaptation. If the socio-economic projections hold true to 2024, abstraction rates will not increase significantly and then the pumping conditions set in the model are correct, at least for the ensembles and high recharge scenario, and water levels will mainly be controlled by recharge changes. Under _low recharge and drought scenarios_ this assumption might lead to **optimistic results** once reduced precipitation will prompt water demands and water abstractions rises.

Model's sensitivity to recharge changes is translated by the heads surfaces rise or drawdown in accordance with recharge rises (high recharge scenario) and decreases, being particularly illustrated by the permanent drought scenario, where head surfaces drawdowns are particularly striking.

Nevertheless, and in spite of model's sensitivity to recharge changes, these are translated by **heads variations being much more attenuated when compared with recharge variations**. For instance, a recharge reduction of 20% is translated to much less than 20% heads drawdowns (cf. Table 6.4) and wide areas of the model show small heads' variations. This is most likely due to the very large aquifer system's dimensions and large storage capacity, giving the system a strong inertial response. Also not to be discarded is the influence of boundary conditions that simulate rivers once they strongly influence their neighbouring areas, leading to large low heads' change zones along the valleys.

In all scenarios there is a **heads' change reduction as the slices depth increases**. This might be due to the combined effect of shielding from evapotranspiration losses and progressively smaller disturbance due to pumping, once fewer wells are abstracting at larger depths. Nevertheless, in some areas were several deep wells are pumping, disturbances can override evapotranspiration absence, so significant heads' drawdowns may occur in deeper slices.

In the **permanent drought scenario, large heads drawdown occurs at all slices**, becoming a bit smaller as slices' depth increases. Being a radical change from present day climate, these large heads drawdowns are expected (cf. Table 6.4), leading to a large number of superficial wells dry-outs. From the ensemble of realisations, it is expected that the climate will not change significantly up to 2024 and this permanent drought scenario is extremely unlikely. However, it might become more likely by the end of the century, once the Paris Agreement goals of curbing GGEs emissions to avoid atmospheric temperature increase beyond 2ºC are not being met by most signing countries and one of the largest emitters – the USA – is out of the agreement.

Further analysis shows that **some model issues are not yet fully solved**. They are basically related with _localized error-norm-flow_ issues impacting heads evolution and are usually located in or near areas of strong conductivity gradients. So far changes in the model hadn't been effective in eliminating such issues. This leads to abnormal heads' drawdowns as those observed in all slices in all scenarios but this is especially odd under high recharge scenario (cf. Figure 6.34). Although occurring at all slices, these abnormal drawdowns' areas decrease in number and extension as depth increases. This seems to follow the decrease in size and number of the error-norm-flow areas from Slice 4 (inclusive)

downwards. Such change might be related with the strong conductivity differences between the first 3 slices and the following 3 low conductivity slices.

Error-norm-flow areas might also be behind the erroneously high water levels in 3 nodes of Slices 5 and 6 (in all scenarios) associated with the large conductivities' changes between 2 adjacent slices (in this case Slice 3, has K = 100 m/day and Slice 4 has K = 10^{-6} m/day in the immediate neighbourhood of the main error-norm-flow zone). In spite of being small, error-norm-flow areas influence results in larger areas, in particular if conductivities range from high to small in very short horizontal or vertical distances.

In _ensembles scenario_ such abnormal head drawdowns' areas show up mainly in Margem Direita region, where larger recharge increases occur (cf. Figure 6.28) when compared with historical period. This is the opposite of what would be expected. However, this area has the largest density of low conductivity zones in Slices 1 to 3, promoting sharp horizontal conductivity gradients and abnormal heads' zones seem spatially related to these (and the large vertical gradients between slices). In _high recharge scenario_, these abnormal drawdown areas virtually disappear in Margem Direita (Figure 6.34). Margem Esquerda abnormal drawdown areas occur in all scenarios.

The **fluid-flux boundary conditions** also strongly influence heads' changes in its neighbouring areas, as illustrated in the model's NE, NW, SE and westernmost tips, leading to very large drawdowns. This suggests these boundary conditions require further calibration/validation, which is bound to be difficult due to the absence of observation data in those regions.

Large heads variations are also related with **high topography gradients**. Model calibration in these areas demanded large conductivity reductions in slices 1 to 3, which translated into the above cited sharp conductivity gradients with neighbouring regions. Most likely, such areas have small suspended water-bearing layers but lack of data and the scale of the model does not allow for the identification, characterization and simulation of such small structures. Due to this lack of data, it was assumed that one unique water level surface occurs in the superficial aquifer, which almost surely does not, and the large conductivity reductions had to be performed. The model is then calibrated but almost surely does not properly simulate aquifer's behaviour in those specific areas.

6.3.2   Transient state results

Transient simulations were performed for drought conditions of year 2005's recharge but, unlike the permanent drought scenario which simulated a permanent shift in average climate conditions, transient simulations picture droughts of protracted duration under ensembles recharge scenario. The choice the ensembles scenario as the drought starting point is due to its higher occurrence probability (Table 6.5; cf. Rust et al., 2017) in 2024. Three transient scenarios were simulated and their assumed occurrence likelihood is shown in Table 6.6. _The simulation results are **optimistic**_ once historical period's average pumping rates were used while during droughts groundwater abstraction increases. The reason to keep average historical pumping rates in these scenarios was due to lack of pumping rates' information during droughts.

In **1 year drought scenario** _small heads' drawdowns occur_, becoming smaller as slices depths increase. Areas with larger drawdowns are associated with regions of sharp conductivity gradients. The results are optimistic once drawdowns are smaller than those provided from some field reports. These small heads variations at the end of 1 year severe drought may be due to the large dimensions and storage capacity of the aquifer system, generating its strong inertial response but other reasons may also be at play.

Boundary conditions can strongly impact model results and this is particularly expressive along valley areas, where the very small head changes must be due to the boundary conditions used to simulate river network. Reliable data on river' water stages (which are very incomplete) could help set a more realistic boundary condition and so allowing better simulation of flow and water level's changes in valley areas. Insufficient spatial discretization of hydraulic properties, due to lack of detailed data (and large scale of the model), may also be an influencing factor.

Table 6.6 – Likelihood of scenario occurrence in 2024

Scenario	Likelihood
1 year drought	Most likely
3 years drought	Less likely
5 years drought	Unlikely

In **3 years drought scenario** _drawdowns are larger than in 1 year scenario_, as expected, ranging from 1 to 2 m in Slice 1 in a large area. Drawdowns become smaller as slice depths increase, due to the same reasons underlined in previous scenarios. Larger drawdowns (3 to > 5 m) show up in sharp conductivity gradients' areas and sometimes in significant wells' concentration zones. In valley areas, water levels remain essentially equal to those of 1-year drought scenario. This suggests that again the model is giving optimistic results. However, having no data concerning the only 3 years drought occurred in the 20th century it is difficult to assess if the results are optimistic or not.

In **5 years drought scenario**, _drawdowns are larger than in 3 year drought scenario_, as expected, with exception of the valley areas, where heads drawdowns remain basically the same as in 1-year and 3-years drought scenarios. As in above scenarios, heads drawdowns become smaller as slices depths increase, but are nevertheless larger than in those scenarios, showing the impact of protracted droughts in lower aquifers. This may compound the operability of the wells and higher risk of pumping equipment's damage. From the results, it seems the model is giving optimistic projections but once a 5 years drought has never occurred in the 20th century, it is impossible to evaluate if this is so. Taking the precautionary approach, it should be assumed the reality would be more serious than what the model projections, in spite of the large stored water volumes and aquifer's ensuing regulation capacity. One way to overcome such optimistic results would be a better knowledge of the hydraulic properties and its spatial variations, which are not presently available or known.

On the whole, increasing drought duration generates heads drawdowns' increase (Table 6.7) but they are, as expected, not as extreme as in drought permanent scenario. Head drawdowns decrease at increasing slice's depth shows the combined effect of lower abstraction and shielding from water losses. This is also observed in permanent state drought and low recharge scenarios.

Table 6.7 – Sorraia valley's groundwater level variations from present day average conditions in Slice 1

Observation point	Differences between observed and simulated heads (m)			
	Present average conditions	Drought scenarios		
		1 year	3 years	5 years
231	-7.11	-8.23	-9.42	-9.89
232	-2.08	-2.53	-3.36	-4.04
234	-0.79	-1.44	-2.55	-3.34
198	-0.23	-0.74	-1.38	-1.73
191	-2.67	-3.68	-5.16	-6.18
200	-0.59	-0.81	-1.84	-1.89
201	-2.80	-3.11	-3.68	-4.22
202	-0.73	-0.96	-1.45	-2.00
185	-3.08	-3.45	-4.16	-4.79
186	-3.47	-3.74	-4.24	-4.71
195	3.39	3.14	3.03	2.94
219	-1.90	-1.65	-1.70	-2.00
190	0.80	0.45	0.02	-0.27
193	-4.68	-5.19	-5.88	-6.32
189	-3.98	-4.30	-4.52	-4.60
216	-4.08	-4.52	-5.25	-5.83
188	-0.27	-0.54	-0.72	-0.81

Observation point	Differences between observed and simulated heads (m)			
	Present average conditions	Drought scenarios		
		1 year	3 years	5 years
214	-1.53	-1.93	-2.71	-3.32
215	1.25	0.69	0.18	-0.52
184	-7.99	-8.10	-8.30	-8.50
187	1.48	1.28	1.07	0.93
211	-2.66	-2.87	-3.02	-3.07
212	-4.01	-4.27	-4.59	-4.75
210	1.16	0.98	0.85	0.81
209	-3.33	-3.49	-3.64	-3.70
208	1.66	-1.77	-1.83	-1.85
207	2.11	2.03	1.99	1.98
303	-3.59	-6.7	-9.01	-10.72
295	-2.68	-3.14	-3.88	-4.55
296	-3.47	-3.84	-4.35	-4.70

Although if general heads decreases are relatively small, in some areas of the model they can be quite large. These areas, as in all scenarios, are related to zones of higher conductivity gradients and are usually located in the vicinity of hilly areas. Such strong head changes might be larger than reality and this is due to the lack of sufficient data on conductivity and head variations as well as upper water bearing units' depth in these specific areas. Overhanging aquifers most likely occur there, instead of a continuous heads' surface following the topography. In such cases, conductivities might be different from those in the model, but data to correct them is lacking.

Boundary conditions also play a role in these optimistic results. Head constant boundary conditions were used to simulate rivers and fluid-flux defined the aquifer discharge areas into neighbouring formations (NE, NW and SE tips of the model and Arrábida region). Simulating rivers with _head constant boundary conditions_ doesn't properly simulates the river/aquifer interactions both temporal and spatially. This is illustrated by the very small water level's changes around the rivers, in transient and steady state

simulations, in particular along model's central area, where Aluviões do Tejo aquifer is located. As said previously, lack of sufficient and reliable data concerning river's heads along the river network, both spatial and temporally, prevented the use of the more adequate fluid-transfer boundary condition. *Fluid-flux boundary conditions* strongly impact the heads of their surrounding areas and this is particularly striking at model's SE tip, although head variations are less significant than in steady state simulations. This again highlights the need of more stringent calibration, which is difficult to achieve due to the lack of heads data in the area.

Some abnormal **water level rises** for all transient state scenarios occur in very specific locations, downward from Slice 7. These occurrences might be related with error_norm_flow areas which albeit small, seem to strongly impact the local behaviour of the model. It is however interesting to notice that such problems do not occur in low, ensembles and permanent drought steady state scenarios.

Multiannual droughts are unlikely on present-day climate conditions and the same should hold true in 2024, if the climate evolution until then will follow the ensembles scenario. However, their occurrence likelihood will increase by the end of the century (Guerreiro et al., 2017), so analysing multiannual droughts make sense on a precautionary perspective to inform on adaptation strategies.

7 | Conclusions

The case-study area encompasses 3 large aquifers: *Tejo/Sado – Margem Direita, Tejo/Sado – Margem Esquerda* and *Aluviões do Tejo*. Tejo/Sado – Margem Esquerda is the largest aquifer in Portugal. These three aquifers are intergranular porosity reservoirs with large storage capacity, able to regulate episodic events of low or large recharge and even extreme events, with the exception of severe and protracted droughts with duration ≥ 1 year. This is illustrated by the dim heads' changes either in lower or higher recharge conditions (R1, R3 and drought scenarios), the exception being the steady state drought which, from the climate projections for 2024, seems to have a very low occurrence probability.

The results presented in this chapter refer to Slice 1 in all scenarios. For the remaining slices, head changes are similar, but more attenuated as slices' depths increases, which also leads to smoother heads surfaces. This is to be expected due to lesser water abstraction with increased depth and shielding from evapotranspiration losses. In slice 1, water losses are also due to discharges into the river network.

Three non-drought climate recharge scenarios were analysed: R1 (high recharge), R3 (low recharge) and R1_10 (ensembles recharge). Recharge values for each scenario are presented in Beek et al. (2018), Oliveira (2019), Novo et al. (2018; 2018a) and in Table 7.1. These are average scenarios for 2015-2024 and do not illustrate any possible changes in droughts frequency, length or severity.

Table 7.1 – Recharge changes from historical conditions (%)

Realizations	Aquifers			Average of change per realisation (%)
	Margem Direita	Margem Esquerda	Aluviões do Tejo	
R1	+49.1	+37.6	+29.4	+38.6
R3	-10.4	-20.6	-11.6	-17.9
Ensembles	+5.4	+4.2	+0.2	+4.0

Ensembles recharge scenario shows heads' distribution similar to historical period's distribution (cf. sub-chapter 6.1.1.3.2), which is due to the small recharge rise in this scenario (cf. Table 6.4). *R3 (low recharge) scenario*, in average, shows a mild heads drawdown, usually less than 1 m for low lying areas (average drawdowns in Aluviões do Tejo aquifer are < 0.5 m) up to 2 to 10 m in inter-fluvial zones. This is due to 10 to 20% recharge reductions from the historical period values. *R1 (high recharge) scenario* shows heads' rises, with some low-lying areas being flooded due to this. Water level's rises up to 2 m occur in low lying areas (e.g. Aluviões do Tejo) while rises from 2 m up to > 10 m occur in

inter-fluvial areas. This is due to this scenario's larger recharge variation from the historical values (cf. Table 6.4). Head results for these scenarios are shown in Table 7.2.

Table 7.2 – Water level's changes from the historical period for the 3 climate change scenarios

Areas in the model		Realisation R1	Realisation R3	Ensembles
Low lying areas (e.g. Aluviões do Tejo aquifer)		Rise < 2 m	Drop < 2 m	
Upstream areas	Margem Esquerda & Margem Direita aquifers	Rise > 5 m	Drop from 2 m to ≥ 10 m	≈ 0 m
Sensitive areas		Rise > 10 m	Drop > 10 m	

The model has a large inertial response, translated by small water level's (= heads) changes in spite of sometimes significant recharge changes (e.g. scenario R1). In low lying areas this is also due to the boundary conditions used to simulate the river network (cf. chapter 6.3). As such, head changes in Aluviões do Tejo (central area of the model) are most likely larger as it is shown by the model.

Relatively small areas of large heads variation (> 10 m) are most likely due to erroneous conductivity values and/or the presence of small suspended aquifers which were impossible to simulate at the model's scale. So the conductivities adopted after model calibration (assuming a continuous aquifer instead of a set of unknown suspended aquifers in the inter-fluvial areas of the top slices), may be quite different from reality, leading to unrealistic values there. Error_norm_flow issues may also play a role in this.

In spite of the fact that areas of large density of wells might not show wide heads variations because they are located in large conductivity zones and/or near head constant boundary conditions simulating rivers (e.g. Aluviões do Tejo aquifer), they should be viewed as vulnerable areas. In fact, under low recharge conditions, abstraction increases lead to larger drawdowns than if just due to recharge. The larger the amount of abstraction, the more vulnerable becomes the abstraction area.

Although any of the 10 climate model MiKlip's realisations may occur in 2024, the most likely to occur is the ensembles scenario (Rust et al., 2017). This scenario shows a small recharge increase from the historical values (cf. Table 6.2), suggesting a future a little bit more wet that the present days and leading to small water level's rises. However, for impact analysis it is necessary to have the full range of possible scenarios and ensuing aquifer system's response. Simulating for R1 (high recharge) and R3 (low recharge) scenarios provides such response range. Besides, if in the near future tipping points are reached, the climate evolution may lead to much more dramatic recharge changes. And even if ensembles scenario will occur, the expected higher climatic variability will bring frequent years of very high precipitation and years of severe droughts. The best way to adapt to this larger climatic variability is to be prepared for drier and wetter conditions.

The **steady state drought scenario** is an extreme scenario where a severe dry climate (2005 conditions) is the new normal. As far as MiKlip realisations suggest, such drastic change is very unlikely

up to 2024, suggesting instead a climate not much different from the historical period. But because climate observations suggest climate is changing faster than models' predictions (https://www.sciencedaily.com/releases/2015/03/150309134642.htm; https://phys.org/news/2018-10-climate-faster.html) and an upper limit of drought impacted heads' changes was required to set a framework for drought simulations, this scenario was simulated. Under such severe recharge reductions (ranging from 74 to 86%; cf. Table 6.4) there is a sharp heads' drawdown of 10 m up to > 60 m (10 to 15 m in Aluviões do Tejo aquifer; cf. Table 7.3). This could lead to the dry-out of many superficial wells and severely impact the exploitation of the superficial water bearing units. The most affected areas are inter-fluvial with significant topographic gradients, which might in reality correspond to small suspended water bearing units, which due to their size are particularly sensitive to drought.

The **transient drought scenarios** simulate protracted drought events under ensembles scenario. This means the initial conditions at the droughts' start are the results obtained by running the ensembles scenario. These are theoretical scenarios loosely based on drought projections for the end of the century in the Iberian Peninsula (Guerreiro et al., 2017). Assuming the increasing possibility of multi-year droughts, 3 scenarios were considered: a) 1 year; b) 3 years; c) 5 years droughts. 1-year drought is a very likely scenario in 2015-2024's period once such lengthy droughts already occur in the historical period. A 3-year drought is less likely and a 5-year drought is a quite unlikely worst-case scenario, once 5-year drought events have not been recorded in the 20th century.

As to be expected, heads drawdowns increase in tandem with the length of the drought. They are however less dramatic than field anedotical reports would lead to expect, at least as far as 1 year-drought is concerned. Simulated drawdowns in most part of the model range between 0.5 to 1 m in a *1-year drought*, from 1 to 2 m in a *3-years drought*, and 2 to 3 m in a *5-year drought* (except in Aluviões do Tejo, where drawdowns remain < 0.5 m, most likely due to the boundary condition used to simulate rivers); the change is particularly striking in SE zone. The results for the 4 drought scenarios are presented in Table 7.3.

Table 7.3 – Head changes from the historical period for drought scenarios

| Model zones | Water levels (= heads) variations from 2005 drought heads | | | |
| | Transient simulations | | | Permanent state simulation |
	1 year	3 years	5 years	
Low lying areas	Drop < 0.5 m	Drop ≤ 1 m	Drop ≤ 2 m	Drop 10 to 15 m
Upstream areas	Drop < 1 m	Drop 1 to 2 m	Drop ≥ 2 to 3 m	Drop ≈ 20 m
Sensitive areas	Drop 1 to 5 m	Drop 3 up to 5 m	Drop 3 to > 5 m	Drop 40 to 60 m

These results should be assumed as optimistic. Not only general information has described larger drawdowns than those simulated for 1 year drought scenario but also pumping rates increase under severe drought. Such pumping abstraction increase (which gets larger to meet water demand increases as the drought gets longer) leads to increasing larger drawdowns. However, such abstraction increases were not simulated due to lack of sufficient reliable pumping data under droughts. This adds to the issue of using head constant boundary conditions adopted to simulate rivers, which generate suspiciously small drawdowns in model's central area.

Droughts are a particularly relevant problem in Mediterranean countries and adaptation to such extreme events is required once, regardless of the scenario that might occur, the wider climatic variation will make these events more frequent. For instance, in ensembles scenario, year 2020-2021 is predicted to have an average precipitation of less than 50 mm/year (Oliveira, 2019). If instead there will be a drier future (realization R3), droughts are likely to have more severe impacts. Once simulation results are optimistic, due to the simplified nature of the model which does not capture local head variations, the best approach is to use the historical period severest droughts' observational water level's data to tailor drought adaptation measures, at least until the model will give better results.

Being climate change somewhat incremental – if no tipping points are surpassed – it is not a surprise that the models for near future give small to mild changes in climate, recharge and water levels. So, if adaptation measures are based on just short term predictions, there is a chance they will be too mild and will not prepare for longer term impacts or if tipping points are reached. Under financial budget constraints, decision makers might be tempted to not act once the simulation results point to small changes.

Climate change is a problem requiring actions now to minimize impacts on the long term, as well as unpredicted impacts due to tipping points. If we assume no significant changes occur up to 2024 and then do a new study for 2034 and so forth, change trends (which are more expressive under larger time frames) might go undetected due to the short time span of the studies. And if they are detected, they might not be large enough for decision makers to implement the required adaptation measures. So, societies risk to reach a point where changes are already large when compared with the past, while managing water resources as if little change has happened. Long trend analysis is important to understand the change expected in a foreseeable future and help shield societies from the risk of non-efficient adaptation.

This means that, to efficiently deal with adaptation to climate change, a paradigm change must occur. **Decisions-makers must give up thinking on short time frameworks but instead act for the long term, using long term projections**. Short term projections are useful to understand the first impacts but do not show the larger impacts for which societies must be prepared in the long term. Short term projections can identify the sectors first affected and for which adaptation must be priority but to really cope with climate change without running the risk of non-efficient adaptation, long range projections must be used. Besides, latest years' observational data suggest a speeding of climate change impacts evolution, as for instance the Greenland ice sheet melting (http://science.sciencemag.org/content/313/

5795/1958) or the progressive increase of severe drought events in the North Hemisphere (https://www.pnas.org/content/early/2011/01/05/1010070108.short). Societies must be prepared for this.

8 | Further Advances on Research

Following BINGO Project, further studies are here suggested, either for model improvement, climate change impact studies on saltwater intrusion and better knowledge of the groundwater/surface water interactions (quantity and quality) under climate change. For **model improvement**, the following studies are required:

- *Monitoring wells along aquifers' coastal areas*, to monitor groundwater levels and chemistry, in particular chlorides and TDS. *Periodical monitoring campaigns* must be performed to obtain time series for heads and hydrochemical data, as well as the location of present-day interface sea water/groundwater and its evolution. In some areas, namely the estuary's upstream region, where no observation wells exists, *setting up new observation points* is advisable. The data provided by these campaigns are required for good calibration of flow and saltwater intrusion models. The data will also improve the knowledge on aquifers' estuarine areas.

- *Monitoring new network in inland areas with no data,* to improve model calibration in those areas. This network should provide data on heads and water chemistry, the latest to simulate impacts of land cover and climate changes on water quality. Monitoring should be periodical, with no observation hiatus, to allow model calibration improvements in those areas. Correlation between heads and water quality with precipitations series are also required to validate the model under changing conditions.

- *Studies to identify and characterise superficial water bearing units*, in model areas where calibration lead to very small conductivity values. This field work should also gather data on their thickness and hydraulic conductivity, to better represent them in the model and achieve better calibration.

- *Overcoming time series hiatus*, to reduce several hiatus on heads and water quality data in 1980-2009. This could be done by generating heads and quality surfaces, using data from nearby wells. Geostatistical analysis should be used (e.g. krigging) to generate these surfaces for the time series missing data in the points were that missing occurs.

- *Studies on groundwater/surface-water (quantity and quality) interactions with the river network*, to improve the simulation of such interactions and better understanding of aquifers/river dynamics. This demands reliable water levels along the river network and nearby observation wells. Once these are very scarce, a monitoring network along the riverine areas should be set up and data periodically obtained, without hiatuses. These surveys should also monitor water quality in the rivers and aquifer's neighbouring areas, coupled with field experiments to assess hydraulic conductivities of the riverbed and its vertical and horizontal variations. The use of surface water models to obtain rivers' water levels would be another approach. These models would then give water levels' averages and time series for 1980-2009, at each FEFLOW node. An in-depth analysis of the existing data could also be done but may be hindered due to the lack of heads in the riverine area and data scarcity along much of the

river network). The data series from field surveys can help identify river/aquifer interaction changes in summer/winter and wet/dry years, which would allow for transient flow and transport models' validation.

- ***Studies on inflows/outflows along the borders of the aquifers***, to address the lack of knowledge in such areas, in particular flows with surrounding areas. These are expected to be important to/from Arrábida Hills, Sines and Bacia de Alvalade (south border of the model). To understand and quantify these flows, monitoring campaigns and other field work is required to obtain head series and hydraulic parameters.

- ***Improving hydraulic parameters data***, to achieve a more accurate representation of these parameters in the model. At present stage of model development, general bibliographic data were used due to the lack of reliable field data. Pumping tests and well logging should be used to gather hydraulic properties' (horizontal and vertical values), as well as (for well logging) location and thickness of water bearing units, particularly for the areas with calibration/error-norm-flow issues. Experiments *in situ* and lab to quantify transport parameters could also be used to improve transport model's calibration in coastal areas.

- ***Geophysical surveys*** are useful to map saltwater intrusion affected areas. Periodical surveys, coupled with sea level time series, can identify saltwater intrusion expansion and correlate it with sea level rise and weather variations. Water sampling at different depths and locations can give information about the saltwater/groundwater interface's shape.

- ***Improving pumping data***, to obtain actual real pumping rates (averages and time series). To do this, remote and/or field monitoring should be carried out. Such surveys could also establish the rate variations for different crop rotations. These data are important to better calibrate the model. They could also be used to generate pumping series for 1980-2009, using geostatistics and comparison with the climate conditions of the season they were collected.

- ***Improving data on well screening***, to improve knowledge on well screening locations and water bearing units exploited. This is mostly done by well logging, and the information gathered would identify which wells exploit the most superficial water bearing units (these wells may be simulated through *wells boundary condition*), which exploit one or more deeper units and their respective depths and thicknesses (they would be simulated through *multi-layer wells boundary condition*). This would lead to a better simulation of flow and transport.

- ***Unstructured modelling***, could be performed to obtain more realistic simulations, namely on the leaking flows between Alluvial deposits, Pliocene and Miocene. This would mean Pliocene and Miocene should be confined just in certain areas of the model but under present structured mesh model that is not allowed. The development of a new unstructured mesh model would allow the simulation of distributed confined/unconfined behaviours on the same layer as well as the hydraulic behaviour of existing tectonic systems.

The **development of saltwater intrusion model**, can rely on 2 distinct approaches: (1) transient simulation – sea level is not fixed by a boundary condition but changes over time, (2) steady state simulation – requires 2 distinct simulations (A) saltwater/freshwater interface under present day sea

level and (B) under sea level at final time horizon; comparing interface changes between (A) and (B) would give the saltwater intrusion's evolution.

For the steady state approach, just the actual and the final sea levels are required. For the transient approach, series of sea level values from present day to final time horizon are required. To generate such series, sea level rise projections for distinct climate change scenarios coupled with observation trends should be used. Geophysical surveys can assess summer/winter, dry/humid years' interface fluctuations, which would allow the model validation. Once validated, the model could be used to identify the most vulnerable saltwater intrusion areas under distinct climate scenarios, taking into account the coupled effects of recharge, pumping rates and sea level changes, including variations from summer/winter and wet/dry years.

The knowledge of **climate change impacts on groundwater quality** is less developed in comparison with quantity impacts. Although they seem less important than quantity impacts, they are relevant in some cases, namely limestone aquifers (Oliveira, 2011)[18]. Climate change indirectly impact ground water quality thorough recharge chemistry, volume changes and river water quality changes (cf. Goldscheider et al., 2006). These indirect impacts are even less studied and under BINGO, ground water quality issues were not simulated.

Nevertheless, they are important issues and developing a transport model to analyse such impacts is relevant. A first step is to analyse existing data in SNIRH, and other databases, and try to correlate the data evolution with dry/wet seasons and distribution + loads of pollution sources to identify any possible patterns. This analysis could provide water quality series for model calibration and validation. Once data hiatuses are frequent and often for large periods, geostatistics should be used to generate the missing data. These generated data must be critically assessed before being input into the model. Such assessment can be carried out with hydrochemical models or series analysis.

Periodical surveys (which demand the setup of monitoring networks) should be carried in areas with scarce data, to get reliable quality data and identify possible correlations with seasonal and multi-annual weather variations. These correlations, if possible, will allow the generation of past quality series. Field work could also assess transport parameters. This would give more solid, albeit local, variation ranges of such parameters and help improve model calibration.

Due to largely unknown hydraulic linkages between aquifers and rivers and its impacts on pollutants transport, such field work is most relevant along riverine areas. Besides using the calibrated transport model for projections of pollution evolution under climate change (and socio-economic) scenarios, it would be important to investigate possible changes in aquifers' hydrogeochemical behaviour under climate change. Using hydrochemical models to identify present hydrogeochemical processes at work, with data surveys and then change the conditions to simulate the hydrogeochimical conditions under climate change may help identify possible changes in these processes.

---

[18] Amongst them, increased hardness, higher content of dissolved bicarbonates and larger dissolved solids

9 | Acknowledgments

Lisboa, LNEC, June 2020

APPROVED

AUTHORS

The Head of the Water resources and hydraulic
structures unit

Maria Teresa Viseu

Maria Emília Novo

Assistant Researcher

The Director of the Hydraulics and Environment
Department

Helena Alegre

Tiago Martins

Research Fellow

Maria José Henriques

Senior Technician

Bibliographic references

Internet sources:

https://apambiente.pt/index.php?ref=16&subref=81&sub2ref=118&sub3ref=393. (consulted 18/12/2019).

http://aquiferural.ist.utl.pt/es/node/109. (consulted 3/10/2011).

https://blogs.egu.eu/network/gfgd/tag/saltwater-intrusion/. (consulted12/12/2018)

http://climadapt-local.pt/wp-content/uploads/2016/09/ficha_lisboa.pdf. (consulted 12/12/ 2017)

https://dre.pt/application/file/a/611853. (consulted 25/6/2018).

https://earthzine.org/2013/05/07/how-weather-stations-can-be-used-to-measure-evaporation/. (consulted 21/11/2017)

https://phys.org/news/2018-10-climate-faster.html. (consulted 19/12/2018)

http://portaldoclima.pt/en/. (consulted 8/2/2018)

http://science.sciencemag.org/content/313/5795/1958. (consulted 4/1/2019)

https://snirh.apambiente.pt/index.php?idMain=4&idItem=3&idISubtem=link4d. (consulted 7/1/2019)

http://snirh.pt/ snirh/download/relatorios/redes_agsub_oeste.pdf. (consulted 21/11/2017)

https://water.usgs.gov/edu/rivers-contain-groundwater.html. (consulted 21/11/2017)

http://www.arhtejo.pt/c/document_library/get_file?uuid=e5a4e269-88f5-440c-88d3-28cf40c218b7&groupId=10225. (consulted 3/10/2011)

http://www.aqtesolv.com/aquifer-tests/aquifer_properties.htm. (last consulted 16/01/2018)

http://www.draplvt.mamaot.pt/Ordenamento/Ambiente/Zona-Vulneravel-Nitratos/Docu-ments/Zona%20VulneravelA3.pdf. (consulted 24/11/2017)

http://www.geschichteinchronologie.com/welt/wasser-u-grundwasser03-groundwater-salinization-ENGL.html. (consulted 12/12/2018)

http://www.ipma.pt/pt/oclima/observatorio.secas/pdsi/apresentacao/evolu.historica/. (consulted 11/12/ 2017)

https://www.ipma.pt/resources.www/docs/im.publicacoes/edicoes.online/20081014/KZcwnQrfVHeUZOaTzIth/cli_20050101_20051231_pcl_aa_co_pt.pdf. (consulted 7/2/2018)

https://www.ipma.pt/pt/educativa/tempo.clima/index.jsp?page=seca.pt.xml&print=true. (consulted 30/1/2020).

https://www.ipma.pt/pt/oclima/observatorio.secas/pdsi/apresentacao/evolu.historica/index_link.html?page=os_series_longas_matriz.xml. (consulted 30/1/2020).

http://www.ipma.pt/pt/oclima/observatorio.secas/pdsi/apresentacao/evolu.historica/index_link.html?page=os_series_longas.xml. (consulted 11/12/2017)

http://www.mae.gov.nl.ca/waterres/training/adww/2015/04_Lynn_Pilgrim.pdf. (consulted 22/12/2017)

https://www.pnas.org/content/early/2011/01/05/1010070108.short. (consulted 4/1/2019)

https://www.sciencedaily.com/releases/2015/03/150309134642.htm. (consulted 19/12/2018)

http://www2.icnf.pt/portal/pn/biodiversidade/ei/ramsar. (consulted 23/2/2018)

http://www2.nau.edu/~doetqp-p/courses/env303a/lec36/lec36.htm. (consulted 26/2/2018)

http://zebu.uoregon.edu/1999/es202/l2.html. (consulted 21/11/2017)

Articles, books and journals:

ALMEIDA, C.; MENDONÇA, J.; JESUS, M.; GOMES, A., 2000 – **Sistemas Aquíferos de Portugal Continental**. Instituto da Água, Portugal. In: www.academia.edu/35471890/_Sistemas_Aquiferos_de_Portugal_Continental_Volume_III.

ALPHEN, H.-J.v.; ALVES, E.; BEEK, T.a.d.; BRUGGEMAN, A.; CAMERA, C.; FOHRMANN, R.; FORTUNATO, A.; FREIRE, P.; IACOVIDES, A.; IACOVIDES, I.; KRISTVIK, E.; KÜBECK, C.; LORZA, P.; MUTHANNA, T.; NOVO, E.; ROCHA, F.; RODRIGUES, M.; RODRIGUES, R.; RUSSO, B.; SÁNCHEZ, P.; SCHEIBEL, M.; SPEK, T.; WITTE, F.; ZOUMIDES, C., 2016 – **Project BINGO: Bringing Innovation to Ongoing Water Management. Deliverable D3.1. Characterization of the catchments and the water systems**. February, 2016, pp. 98. In: http://www.projectbingo.eu/downloads/BINGO_Deliverable3.1_EC.pdf.

AMARAL, H.I.F.; FERNANDES, J.; BERG. M.; SCHWARZENBACH, R.P.; KIPFER, R.; 2009 – **A Contaminação por TNT e DNT nas Águas Subterrâneas do Seixal**. Seminário sobre os sistemas aquíferos da Bacia do Baixo Tejo: o maior recurso hídrico subterrâneo em Portugal, Lisboa, 27 de Novembro de 2009, pp. 7.

ANTUNES, C.; TABORDA, R., 2009 – **Sea level at Cascais tide gauge: data, analysis and results**. Journal of Coastal Research, SI 56, Lisbon, Portugal, pp. 218 – 222. In: http://e-geo.fcsh.unl.pt/ics2009/_docs/ICS2009_Volume_I/218.222_C.Antunes_ICS2009.pdf (consulted 22/12/2017).

APA, 2012a – **Plano de Gestão da Bacia Hidrográfica do Tejo. Relatório Técnico. Versão Extensa. Parte 2 – Caracterização e Diagnóstico da Região Hidrográfica**. APA, Lisboa, pp. 376. In https://sniambgeoviewer.apambiente.pt/Geodocs/geoportaldocs/Planos/PGRH5-TEJO /RB%5Cpgrhtejo_p2.pdf (consulted 4/12/2017).

APA, 2012b – **Plano de Gestão da Bacia Hidrográfica do Tejo. Fichas de Diagnóstico**. APA, Lisboa, pp. 94. In: https://sniambgeoviewer.apambiente.pt/Geodocs/geoportaldocs/Planos/

PGRH5-TEJO/RelatorioTecnico_CE%5C2_PGRHTejo_Rel_CE_FD.pdf (consulted   5/12/
2017).

BACHAND, P.A.M.; ROY, S.B.; CHOPERENA, J.; CAMERON, D.; HORWATH, W.R., 2014 –
**Implications of using on-farm flood flow capture to recharge groundwater and mitigate
flood risks along the King River, CA**. Environ. Sci. Technol. 2014, Vol. 48, pp. 13601 –
13609.

BARREIRAS, N.; MEDEIROS, A.; ALMEIDA, J.A., 2009 – **Contribuição para o Conhecimento
da Hidrogeologia do Concelho do Seixal através da Construção de um Modelo
Hidrogeológico: Cenários de Exploração**. Seminário sobre os sistemas aquíferos da
Bacia do Baixo Tejo: o maior recurso hídrico subterrâneo em Portugal, Lisboa, 27 de
Novembro de 2009, pp. 7.

BEEK, T.a.d.; ALVES, E.; BRUGGEMAN, A.; CAMERA, C.; FORTUNATO, A.; FREIRE, P.;
GRANGE, A.S.; IACOVIDES, I.; KRISTVIK, E.; LORZA, P.; MONTES, J.; MOUSKOUNDUS,
M.; MUTHANNA, T.M.; NOTTEBOHM, M.; NOVO, E.; OLIVEIRA, M.; RIJPKEMA, S.;
RODRIGUES, M.; RODRIGUES, R.; RUSSO, B.; SÁNCHEZ, P.; SCHEIBEL, M.; SUNYER,
D.; VISEU, T.; VOORTMAN, B.; WITTE, F.; ZITTIS, G., 2017 – **Project BINGO: Bringing
Innovation to Ongoing Water Management. Deliverable D3.3. Calibrated water
resources models for past conditions**. December, 2016, pp. 181. In: http://www.project
bingo.eu/ downloads/BINGO_Deliverable3.3.pdf.

BEEK, T.a.d.; ALVES, E.; BECKER, R.; BRUGGEMAN, A.; FORTUNATO, A.B.; FREIRE, P.;
GRAGNE, A.; VAN HUIJGEVOORT, M.H.J.; IACOVIDES, A.; IACOVIDES, I.; KRISTVIK, E.;
LOCATELLI, L.; LORZA, P.; MOUSKOUNDIS, M.; MUTHANNA, T.; NOTTEBOHM, M.;
NOVO, E.; OLIVEIRA, M.; RIJPKEMA, S.; RODRIGUES, M.; RUSSO, B.; SCHEIBEL, M.;
SUNYER, D.; TENEKETZI, E.; VAYANOU, P.; VISEU, T.; VOORTMAN, B.R.; WITTE,
J.P.M., 2018 – **Project BINGO: Bringing Innovation to Ongoing Water Management.
Deliverable D3.4 Model results for water and land use scenarios completed and
analysed**. June, 2018, pp. 233. In: http://www.projectbingo.eu/downloads/BINGO_Delivera
ble3.4_final.pdf.

BJERG, P.L., 2008 – Note A5: Dispersion in aquifers. Version 1.1. DTU Environment, pp. 6: In:
file:///C:/Users/enovo/Downloads/dispersivity-in-aquifers-1-1.pdf (consulted 22/01/2018).

CAO, Y.J.; TANG, C.Y.; SONG, X.F.; LIU, C.M.; ZHANG, Y.H., 2012 – **Characteristics of nitrate
in major rivers and aquifers of the Sanjiang Plain, China**. J. Environ. Monit. 2012, Vol.
14, pp. 2624 – 2633.

CAVACO, M.A.; BENOLIEL, M.J., 1997 – **Qualidade Físico-Química das Águas Subterrâneas
Utilizadas pela EPAL**. Anais do Seminário Qualidade de Sistemas de Abastecimento.
Lisboa, 24 a 26 Novembro, pp. 24-26.

CHATURONGKASUMRIT, Y.; TECHARUVICHIT, P.; TAKAHASHI, H.; KIMURA, B.;
KEERATIPIBUL, S., 2013 – **Microbiological evaluation of water during the 2011 flood
crisis in Thailand**. Science of the Total Environment, vols. 463-464, 2013, pp. 959 – 967.

In: https://www.sciencedirect.com/science/article/pii/S0048969713007237 (consulted 14/12 /2017).

CRUCES, A.; LOPES, I.; FREITAS, M.C.; ANDRADE, C., 2002 – **A Geologia Litoral – Parte I: Do Tejo à Lagoa de Albufeira**. Geologia no Verão 2002 – Guia de Excursão. pp.34.

DELGADO RODRIGUES; J., LOBO FERREIRA, J.P.; SANTOS, J.B.; MIGUÉNS, N., 1989 – **Caracterização Sumária dos Recursos Hídricos Subterrâneos de Portugal**. Lisboa, Laboratório Nacional de Engenharia Civil, Memória n.º 735.

DIAMANTINO, C., 2001 – **Intrusão Salina: Caracterização da Situação na Faixa Costeira de Portugal Continental e Aplicação de um Modelo matemático a uma Região a Norte de Sines**. Informação Científica Hidráulica, INCH 6, LNEC, pp. 143.

DUARTE, A.S., 2012 – **Estudo da interacção água subterrânea/água superficial nos sistemas associados à Lagoa de Albufeira**. Universidade de Lisboa, Tese de Mestrado. In: http://hdl.handle.net/10451/9252 (consulted 29/11/2017).

EEA, 2012 – **Climate change, impacts and vulnerability in Europe 2012**. An indicator-based report. EEA Report Nº 12/2012, pp. 300. ISSN 1725-9177.

EEA, 2017 – **Climate change poses increasingly severe risks for ecosystems, human health and the economy in Europe**. EEA News, pp. 8.

EEA, 2019 – **Heavy precipitation in Europe**. EEA Indicator Assessment/Data and Maps, pp. 24.

DHI, 2014 – **Training Manual FEFLOW 6.2. Groundwater Modelling with FEFLOW 6.2**. DHI – WASY GmbH, Groundwater Modelling Centre, FEFLOW services, February 2014.

FERREIRA, F., 2012 – **Avaliação dos Impactes das Alterações Climáticas nos Aquíferos Costeiros do Concelho de Almada**. Mestrado em Geologia Aplicada. Faculdade de Ciências, Universidade de Lisboa, pp. 89.

FEYEN, L.; DANKERS, R.; BÓDIS, K.; SALAMON, P.; BARREDO, J.I., 2011 – **Fluvial flood risk in Europe in present and future climates**. Climatic Change 112(1), 47–62. doi: 10.1007/s10584-011-0339-7 In: https://link.springer.com/article/10.1007/s10584-011-339-7 (consulted 18/12/2017).

FIALHO, R.G., 2009 – **Caracterização dos Parâmetros Hidráulicos do Sistema Aquífero da Bacia do Tejo-Sado/Margem Esquerda na Área do Concelho do Seixal**. Dissertação para a obtenção do grau de de Mestre em Hidráulica e Recursos Hídricos. Lisboa, IST, pp. 113.

FORTUNATO, A.B.; FREIRE, P.; BERTIN, X.; RODRIGUES, M.; FERREIRA, J.; LIBERATO, M.L., 2017 – **A numerical study of the February 15, 1941 storm in the Tagus estuary**. Continental Shelf Research, vol. 144, pp. 50-64.

FORTUNATO, A.B.; MEREDITH, E.P.; RODRIGUES, M.; FREIRE, P.; FELDMANN, H., 2018 – **Near-future changes in storm surges along the Atlantic Iberian coast**. Natural Hazards, pp. 18. In: https://doi.org/10.1007/s11069-018-3375-z (consulted 12/12/2018).

FREITAS, M.C.; ANDRADE, C.; PINTO, C., 1993 – **Dispersão da glaucónia no arco litoral Caparica – Cabo Espichel – 1ᵒˢ Resultados**. 3ª Reunião do Quaternário Ibérico. Coimbra. pp. 257-265. In: https://core.ac.uk/download/pdf/12427664.pdf (consulted 6/12/ 2017).

FREEZE, A.; CHERRY, J., 1997 – **Groundwater**. Prentice Hall, ISNB 0-13-365312-9, pp. 604.

GHAZAVI, R.; VALI, A.B.; ESLAMIAN, S., 2021 – **Impact of flood spreading on groundwater level variation and groundwater quality in an arid environment**. Water Resources Management, April 2012, Volume 26, Issue 6, pp. 1651 – 1663. In: https://link.springer.com/article/10.1007/ s11269-012-9977-4 (consulted 14/12/2017).

GOLDSCHEIDER, N.; MUDRY, J.; SAVOY, L.; ZWAHLEN, F., 2006 – **Climate change and water resources in limestone and mountain areas: the case of Firenzuola Lake (Umbria, Italy)**. Proceedings of the 8th conference on limestone hydrogeology, Neuchâtel, Switzerland, 21 – 23 September 2006. Presses universitaires de Franche-Comté, Université de Franche-Comté. ISBN: 2-84867-143-2

GUERREIRO, M. ; FORTUNATO, A.B. ; FREIRE, P.; RILO, A. ; TABORDA, R. ; FREITAS, M.C.; ANDRADE, C. ; SILVA, T.; RODRIGUES, M., BERTIN, X.; AZEVEDO, A., 2015 – **Evolution of the hydrodynamics of the Tagus estuary (Portugal) in the 21st century**. Journal of Integrated Coastal Zone Management, Vol. 15, Issue 1, pp. 65-80, DOI: 10.5894. In: http://www.aprh.pt/rgci/pdf/rgci-515_Guerreiro.pdf. (consulted 22/12/2017).

GUERREIRO, S.B.; KILSBY, C.; FOWLER, H.J., 2017 – **Assessing the threat of future megadrought in Iberia**. International Journal of Climatology Volume 37, Issue 15, December 2017, pp. 5024–5034, DOI: 10.1002/joc.5140. In: http://onlinelibrary.wiley.com/doi/10.1002/joc.5140/full (consulted 12/12/2017).

HEATH, R.C., 1983 – **Basic ground-water hydrology**. U.S. Geological Survey Water-Supply Paper 2220, pp. 86. In: http://www.aqtesolv.com/aquifer-tests/aquifer_properties.htm (acedido a 13/2/2017).

HP, 1994 – **Estudo de Caracterização dos Aquíferos e Consumos de água na Península de Setúbal**. Hidrotécnica Portuguesa, estudo efectuado para Empresa Portuguesa de Águas Livres, S.A. (EPAL), Lisboa.

IACOVIDES, A.; MOUSKOUNDIS, M.; IACOVIDES, I.; RUSSO, B.; SÁNCHEZ, P.; CARRETERO, J.-A.M.; GRAGNE, A.S.; ERLE KRISTVIK; LORZA, P.; SCHEIBEL, M.; RODRIGUES, R.; HENRIQUES, M.J.; ALVES, E.; RODRIGUES, M.; SPEK, T.; AUS DER BEEK, T., 2016 – **Project BINGO – D3.2 Future Land and Water Use Scenarios**. October, 2016, pp. 65 In: http://www.projectbingo.eu/downloads/BINGO_Deliverable3.2.pdf (consulted 23/11/2018)

INAG, 1997 – **Definição, Caracterização e Cartografia dos Sistemas Aquíferos de Portugal Continental**. Estudo coordenado pelo Prof. Costa Almeida, Faculdade de Ciências de Lisboa, para o Instituto da Água, Direcção de Serviços de Recursos Hídricos, Divisão de Recursos Subterrâneos, pp. 236.

IPCC, 2013 – **Climate Change 2013: The Physical Science Basis. Contribution of Working Group I to the Fifth Assessment Report of the Intergovernmental Panel on Climate Change**. Cambridge University Press, Cambridge, United Kingdom & New York, USA, pp. 1535.

KOENIGER, P.; LEIBUNDGUT, C., 2000 – **Study of river water impacts on groundwater during floods in a dry flood plain of the upper Rhine Valley**. Institute of Hydrology, Freiburg

University, pp. 6. In: http://www.hydrology.uni-freiburg.de/forsch/hartheim/Koe__gwecol.pdf
(consulted 14/12/2017)

KUNDZEWICZ, Z.W.; LUGERI, N.; DANKERS, R.; HIRABAYASHI, Y.; DÖLL, P.; PIŃSKWAR, I.;
DYSARZ, T.; HOCHRAINER, S.; MATCZAK, P., 2010 – **Assessing river flood risk and
adaptation in Europe — review of projections for the future**. Mitigation and Adaptation
Strategies for Global Change 15(7), 641–656. doi: 10.1007/s11027-010-9213-6. In:
https://link.springer.com/article/ 10.1007/s11027-010-9213-6 (consulted 18/12/2017).

LOBO FERREIRA, J.P.; OLIVEIRA, M.M.; LEITÃO, T.E., 2008 – **Análise Técnica Comparada
das Alternativas de Localização do Novo Aeroporto de Lisboa na Zona da Ota e na
Zona do Campo de Tiro de Alcochete. 2.ª Fase: Avaliação comparada das duas
localizações – Componente Águas Subterrâneas**. LNEC - Proc. 0607/541/5606. Relatório
28/2008 – NAS.

LOBO FERREIRA, J.P., (Coord.); NOVO, M.E.; OLIVEIRA, M.M.; LARANJEIRA, I.; LEITÃO, T.E.;
MARTINHO, N.; QUINTA-NOVA, L.; FERNANDEZ, P.; LOPES, M.H.; PARALTA, E.;
TUJEIRA, R.; ROQUE. N.; DIAS, S.; MESTRE, S.; FREIRE, M.; GALHETAS, M.; GOMES,
S.; MATOS, C.; GAMBOA, M., 2009 – **Avaliação do Impacte de Fogos Florestais nos
Recursos Hídricos Subterrâneos**. Relatório Final de Execução Material. LNEC - Proc.
0607/14/15798. Relatório 351/2009 – NAS.

LOBO FERREIRA, J.P.; VAZ PINTO, I.; MONTEIRO, J.P.; OLIVEIRA, M.M.; LEITÃO, T.E.;
NUNES, L.; NOVO, M.E.; SALVADOR, N.; NUNES, J.F.; POMBO, S.; SILVA, M.F.; IGREJA,
A.; HENRIQUES, M.J.; SILVA, D.; OLIVEIRA, L.; MARTINS, T.; MARTINS, J.; BRACEIRO,
A.; HENRIQUES, R.S.; MONTE, M.; QUARESMA, M.; MARTINS, R., 2011 – **Plano de
Gestão da Região Hidrográfica do Tejo. Lote 2: Recursos Hídricos Subterrâneos, 1.ª
FASE, Segunda Versão dos Conteúdos do PGRH Tejo. Versão 2.** Relatório
Hidroprojecto-LNEC-ICCE, PGRH Tejo. Lisboa, Maio 2011, pp. 938.

LOUREIRO, J.M., 2009 – **Rio Tejo. As grandes cheias 1800 – 2007**. Série Tágides, ARH Tejo,
pp. 80. In: https://www.apambiente.pt/_zdata/Divulgacao/Publicacoes/Tagides/TAGIDES_
01.pdf (consulted 18/12/2017).

MAGALHÃES, P.; MADUREIRA, N.; RUSSO, C.; PAIS, G.; BORGES, C.; CASTANHEIRA, M.;
MESTRE, P.; NOGUEIRA, L.; MESTRE, A.C.; BATISTA, A.L.; FONSECA, T.; MOREIRA, I.;
FIGUEIREDO, J.; CHANOCA, J., 2013 – **Plano Director Municipal do Seixal. Revisão –
Proposta de Plano. Proposta de Delimitação da Reserva Ecológica Nacional.** Seixal,
CM Seixal, pp. 124.

MAIA, R.; OLIVEIRA, B.; RAMOS, V., 2014 – **Avaliação dos impactos das alterações climáticas
na bacia hidrográfica do Guadiana**. 9as Jornadas de Hidráulica, Recursos Hídricos e
Ambiente, FEUP, ISBN 978-989-99439-0-2, pp. 10. In: https://paginas.fe.up.pt/
shrha/publicacoes/pdf/JHRHA_9as/16_BOliveira_Avalia%C3%A7%C3%A3oDosImpacto_2
.pdf (consulted 19/12/2017)

MENDES, M.P.; RIBEIRO, L.; PARALTA, L.; BATISTA, S.; SILVA, E.; CEREJEIRA, M.J.; LEÃO
DE SOUSA, P., 2006 – **Vulnerabilidade, Monitorização e Risco na Zona Vulnerável do**

Tejo. 8º Congresso da Água, "Água, Sede de Sustentabilidade", Figueira da Foz, 13 a 17 de Março, pp. 15.

MENDONÇA, J.J.L., 1990 – **Sistema Aquífero Aluvionar do Vale do Tejo (V.N. Barquinha a Alverca): Características e Fundamento Hidráulico**. Dissertação de Doutoramento em Geologia, Universidade de Coimbra, Centro de Geociências da Universidade de Coimbra.

MENDONÇA, J.J., 1993 – **Identificação e Estudo da Propagação de Contaminações Salinas no Sistema Aquífero Terciário do Tejo e do Sado**. Lisboa, Revista da Associação Portuguesa dos Recursos Hídricos, Vol. 14, n°s 2 e 3, pp. 61-66.

MENDONÇA, J.J.L., 1996 – **Síntese das Características Hidráulicas e Hidroquímicas do Aquífero Terciário do Tejo e Sado na Região da Lezíria de Vila Franca de Xira**. Lisboa, 3º Congresso da Água "A Água em Portugal – Por uma Política de Excelência", Comunicações, Vol. III, pp. 105-113.

MENDONÇA, D.; CHAVES, J.A.; CARVALHO, J.M.; LOPO MENDONÇA, J.J., 1982 – **As Águas Subterrâneas da Bacia Terciária do Tejo e o Abastecimento de Água a Lisboa: Alguns Exemplos de Trabalhos de Pesquisa e Captação**. Lisboa, Simpósio "A Bacia Hidrográfica Portuguesa do Rio Tejo. Perspectivas para o seu Desenvolvimento e para a Gestão dos seus Recursos Hídricos", Sondagens e Fundações A. Cavaco.

MENDONÇA, J.L.; MEDEIROS, A. C.; AZEVEDO, J.C.C., 2004 – **Considerações sobre a Hidrogeoquímica do Sistema Aquífero Terciário Tejo-Sado na Região Central da Bacia do Baixo Tejo**. 7º Congresso da Água, Lisboa, LNEC, 8 a 12 de Março, pp. 12.

MENDONÇA, J.L., 2009 – **Caracterização Geológica e Hidrogeológica da Bacia Terciária do Tejo-Sado**. Os aquíferos das bacias hidrográficas do Rio Tejo e das Ribeiras do Oeste. Saberes e Reflexões. Série Tágides, ARH Tejo. In: https://www.researchgate.net/publicati on/307205223_Caracterizacao_geologica_e_hidrogeologica_da_bacia_terciaria_do_Tejo_ Sado (consulted 5/11/2018).

NOVO, M.E.; OLIVEIRA, M.M.; MARTINS, T.; HENRIQUES. M.J., 2018 – **Projecto Bingo: O Impacto das Alterações Climáticas na Componente Subterrânea do Ciclo Hidrológico**. Revista Recursos Hídricos da APRH, Vol. 39, nº 2, pp. 59 – 74, Outubro 2018, pp. 65-80. DOI: 10.5894/rh39n2-cti3. In: http://www.aprh.pt/rh/v39n2_cti-3.html.

NOVO, M.E.; OLIVEIRA, M.M.; MARTINS, T., 2018 – **BINGO PROJECT: Impacts of Climate Change on Lower Tagus Aquifers**. Poster to the International Conference on Natural Hazards and Risks in a Changing World, University of Potsdam, Germany, 4-5 October 2018.

OLIVEIRA, J., 2011 – **Impacto das Alterações Climáticas na qualidade das águas subterrâneas de aquíferos carbonatados em Portugal**. Dissertação para obtenção do Grau de Mestre em Engenharia Geológica e de Minas, IST – Universidade Técnica de Lisboa, pp. 170.

OLIVEIRA, J.M., 2011 – **Impacto das Alterações Climáticas na Qualidade das Águas Subterrâneas de Aquíferos Carbonatados em Portugal**. Dissertação para a Obtenção do Grau de Mestre em Engenharia Geológica e de Minas. IST, Lisboa, Abril, pp. 170.

OLIVEIRA, M.M., 2009a – **Sistema Tejo-Sado: Recarga de Águas Subterrâneas. Os aquíferos das bacias hidrográficas do Rio Tejo e das Ribeiras do Oeste**. Saberes e Reflexões. Série Tágides, ARH Tejo.

OLIVEIRA, M.M., 2009b – **Aspectos Quantitativos dos Sistemas Aquíferos do Baixo Tejo**. Seminário sobre os sistemas aquíferos da Bacia do Baixo Tejo: o maior recurso hídrico subterrâneo em Portugal, Lisboa, 27 de Novembro de 2009, pp. 10.

OLIVEIRA, M.M., 2019 – **BINGO Project: Impact of Climate Change for the Period 2015-2024 on the Recharge of Margem Direita, Margem Esquerda, Aluviões do Tejo and Ota-Alenquer Aquifer Systems**. Relatório DHA/NRE (in press).

OLIVEIRA, M.M.; MOINANTE, M.J.; LOBO FERREIRA, J.P., 1994 – **Estudo de Caracterização dos Aquíferos e dos Consumos de Água na Península de Setúbal: Contribuição do LNEC para o Relatório da HP a Entregar à EPAL em Fevereiro de 1994**. Relatório Final. LNEC - Proc. 0607/1/11376. Relatório 37/94 – GIAS.

OLIVEIRA, M.M.; NOVO, M.E.; MOINANTE, M.J., LOBO FERREIRA, J.P.C., 2000a – **Plano de Bacia Hidrográfica do Rio Tejo. 1.ª Fase - Análise e Diagnóstico da Situação Actual. Anexo Temático 4 - Recursos Hídricos Subterrâneos. Tomo A - Caracterização Hidrogeológica. Revisão 2**. Estudo realizado para a Hidrotécnica Portuguesa – Consultores para Estudos e Projectos Lda, LNEC.

OLIVEIRA, M.M.; NOVO, M.E.; MOINANTE, M.J.; LOBO FERREIRA, J.P.C., 2000b – **Plano de Bacia Hidrográfica do Rio Tejo. 1.ª Fase - Análise e Diagnóstico da Situação Actual. Parte A: Síntese e Métodos**. Estudo realizado para a Hidrotécnica Portuguesa – Consultores para Estudos e Projectos Lda, LNEC.

PARADELA, P.L.; ZBYSZEWSKI, G., 1971 – **Hidrogeologia Geral do Centro e Sul de Portugal**. Lisboa, Direcção Geral de Geologia e Minas e Serviços Geológicos de Portugal, I Congresso Hispano-Luso-Americano de Geologia Económica.

PARALTA, E.A.; OLIVEIRA, M.M.; BATISTA, S.B.; FRANCÊS, A.P.; RIBEIRO, L.F.; CEREJEIRA, M.J., 2001 – **A Aplicação de SIG na Avaliação da Vulnerabilidade Aquífera e Cartografia da Contaminação Agrícola por Pesticidas e Nitratos na Região do Ribatejo**. Seminário "A Hidroinformática em Portugal", Lisboa, 13-16 Novembro, pp. 16.

PARALTA, E.A.; DOMINGUES, S.; MIMOSO, P.; BASTOS, M., 2009 – **Prospecção Hidrogeológica no Sistema Aquífero do Tejo-Sado para o Novo Aeroporto de Lisboa**. Seminário sobre os sistemas aquíferos da Bacia do Baixo Tejo: o maior recurso hídrico subterrâneo em Portugal, Lisboa, 27 de Novembro de 2009, pp. 7.

PINTO, C.; TABORDA, R.; ANDRADE, C., 2007 – **Evolução Recente da Linha de Costa no Troço Cova do Vapor – S. J. da Caparica**. 5as Jornadas Portuguesas de Engenharia Costeira. PIANC. AIPCN. Lisboa. pp. 13.

PMAAC-AML, 2018 – **PMAAC: Plano metropolitano de adaptação às alterações climáticas. Volume II - Avaliação de impactes e de vulnerabilidades**. Lisboa, 21 Dezembro 2018, pp. 244.

PNUD, 1980 – **Étude des Eaux Souterraines de la Péninsule de Setúbal (Système Aquifère Mio-Pliocène du Tejo et du Sado). Rapport final sur les résultats du project, conclusions et recommendations.** Programme des Nations Unies pour le Developpement, Direcção-Geral dos Recursos e Aproveitamentos Hidráulicos, Lisboa.

RODRIGUES, M.; FORTUNATO, A.B., 2017 – **Assessment of a three-dimensional baroclinic circulation model of the Tagus estuary (Portugal)**. AIMS Environmental Science, Issue 4/6, pp. 763-787.

RUST, H.W.; RICHLING, A.; MEREDITH, E.; FISCHER, M.; VAGENAS, C.; KPOGO-NUWOKLO, K.A.; KADOW, C.; ULBRICH, U., 2017. DECO – **A plug-in for data extraction and conversion developed within and for BINGO**. Freie Universität Berlin, Version from December 8, 2017.

SANTOS, F.D.; MIRANDA, P. (eds.), 2006 – **Alterações Climáticas em Portugal. Cenários, Impactos e Medidas de Adaptação**. Projecto SIAM II. ISBN 989-616-081-3, Editora Gradiva, Lisboa, pp. 504.

SANTOS, F.D.; FORBES, K.; MOITA, R. (eds), 2002 – **Climate Change in Portugal. Scenarios, Impacts and Adaptation Measures – SIAM Project**. Editora Gradiva, Lisboa, pp. 454.

SCHULZE-MAKUCH, D., 2005 – **Longitudinal Dispersivity Data and Implications for Scaling Behavior**. Gorund Water, Vol. 43, No. 3, May–June 2005, pp. 443–456. In: http://online library.wiley.com/doi/10.1111/j.1745-6584.2005.0051.x/pdf (consulted 22/01/2018).

SHAKESBY, R.; DOERR, S., 2006 – Wildfire as a hydrological and geomorphological agent. Earth Science Reviews. Vol. 74, pp. 269-307.

SILVA, M.O.; 2009 – **Recursos Hídricos Subterrâneos nas bacias do Tejo e das Ribeiras do Oeste**. Conselho de Região Hidrográfica, Golegã, 17 Dezembro 2009, Power Point, 27 slides.

SIMÕES, M.M.M., 1998 – **Contribuição para o Conhecimento Hidrogeológico do Cenozóico na Bacia do Baixo Tejo**. Dissertação apresentada à Universidade Nova de Lisboa para obtenção do grau de Doutor em Geologia, na especialidade de Hidrogeologia. Monte da Caparica.

SCOCCIMARRO, E.; VILLARINI, G.; VICHI, M.; ZAMPIERI, M.; FOGLI, P.G.; BELLUCCI, A.; GUALDI, S., 2015 – **Projected changes in intense precipitation over Europe 2 at the daily and sub-daily time scales**. Journal of Climate, doi: 10.1175/JCLI-D-14-00779.1, pp. 11. In: https://journals.ametsoc.org/doi/pdf/10.1175/JCLI-D-14-00779.1 (consulted 27/12/2019).

SUN, R.; AN, D.; LU, W.; SHI, Y.; WANG, L.; ZHANG, C.; ZHANG, P.; QI, H.; WANG, Q., 2016 – **Impacts of a flash flood on drinking water quality: case study of areas most affected by the 2012 Beijing flood**. Heliyon, Volume 2, Issue 2, February 2016, pp. 14. doi.org/10.1016/j.heliyon.2016.e00071. In: https://www.sciencedirect.com/science/article/pii/S2405844015305259 (consulted 13/12/2017).

VICTOR, L.A.; HIRN, A.; VEINANTE, J.L., 1980 – **A Seismic Section across the Tagus Valley, Portugal: Possible Evolution of the Crust**. Annals Géophysics, Tomo 36, fasc., N.º 4, pp. 469-476.

WADA, Y.; VAN BEEK, L.P.H.; VAN KEMPT, C.M.; RECKMAN, J.W.T.M.; VASAK, S.; BIERKENS, M.F.P., 2010 – **Global Depletions of Groundwater Resources**. Geophysical research Letters, Vol. 37, pp. 5, doi: 10.1029/2010GL044571.

WADA, Y.; Lo MH; YEH, P.J.F.; REAGER, J.T.; FAMIGLIETTI, J.S.; WU, R.J.; TSENG, Y.H., 2016 – **Fate of water pumped from underground and contributions to sea-level rise. Nature Climate Change**, Vol. 6, pp. 777–780. doi: 10.1038/NCLIMATE3001.

WANG, X.; ZHANG, G.; XU, Y.J., 2015 – **Impacts of the 2013 Extreme Flood in Northeast China on Regional Groundwater Depth and Quality**. Water, 2015, Vol., 7, pp. 4575 – 4592. doi: 10.3390/w7084575. In: https://pdfs.semanticscholar.org/f468/8a6d86ed74c4050 25c81117e5524fedde1a0.pdf (consulted 13/12/2017).

WANG, L.; STUART, M.E.; LEWIS, M.A.; WARD, R.S.; SKIRVIN, D.; NADEN, P.S.; COLLINS, A.L.; ASCOTT, M.J., 2016 – **The changing trend in nitrate concentrations in major aquifers due to historical nitrate loading from agricultural land across England and Wales from 1925 to 2150**. Science of the Total Environment, Vol. 542, Part A, pg. 694-705.

WISCONTEXT, 2016 – **How Heavy Flooding Can Damage Drinking Water Quality. Northwest Wisconsin Deluge Should Put Well Owners On Alert For Contamination**. Series: Drinking Water Quality, July 14, 2016. In: https://www.wiscontext.org/how-heavy-flooding-can-damage-drinking-water-quality (consulted 13/12/2017).

ZBYSZEWSKI, G., 1953 – **Carta Geológica de Portugal, 1:50 000, Notícia Explicativa da Folha 31-A: Santarém**. Serviços Geológicos de Portugal.

ZBYSZEWSKI, G.; ASSUNÇÃO, T., 1965 – **Carta Geológica de Portugal, 1:50 000, Notícia Explicativa da Folha 30-D: Alenquer**. Serviços Geológicos de Portugal.

ZBYSZEWSKI, G.; MANUPPELLA, G.; VEIGA FERREIRA, O., 1971 – **Carta Geológica de Portugal, 1:50 000, Notícia Explicativa da Folha 27-C: Torres Novas**. Serviços Geológicos de Portugal.

ZEFERINO, J.F.C., 2016 – **Modelação numérica (FEFLOW) e contaminação por intrusão salina do sistema aquífero Mio-Pliocénico do Tejo, na frente ribeirinha do Barreiro**. Dissertação para obtenção do Grau de Mestre em Engenharia Geológica. Universidade Nova de Lisboa, Faculdade de Ciências e Tecnologia, Monte da Caparica, pp. 82.